Evolution of the distribution of high energy nuclei and induced collective modes in plasmas

by

Gregory Evan Penn

Submitted to the Department of Physics
in partial fulfillment of the requirements for the degree of

Doctor of Philosophy

at the

MASSACHUSETTS INSTITUTE OF TECHNOLOGY

September 1998

Author .....
Department of Physics
August 11, 1998

Certified by .....
Bruno Coppi
Professor
Thesis Supervisor

Accepted by .....
Professor Thomas J. Greytak
Associate Department Head for Education

Evolution of the distribution of high energy nuclei and induced collective modes in plasmas

by

Gregory Evan Penn

Submitted to the Department of Physics
on August 11, 1998, in partial fulfillment of the
requirements for the degree of
Doctor of Philosophy

Abstract

Recent experiments in plasmas undergoing fusion have shown evidence of novel processes which are correlated with the onset of fusion reactions. In view of such evidence and observed effects of the injection of high energy neutral beams in laboratory plasmas, as well as the existence of subpopulations of high energy particles in astrophysical plasmas, there is a rich variety in the possible interactions of energetic nuclei within a plasma. This thesis examines the effects of the He nuclei produced by fusion in a magnetically confined plasma. Both single-particle effects and interactions with collective modes in the plasma will be considered.

Part of this research will focus on the distribution of high energy nuclei undergoing motion in unperturbed orbits. This work utilizes appropriate symmetry properties and conservation laws, including the conservation of angular momentum in a toroidally symmetric configuration. Considering the various time scales involved in the evolution of the distribution function, a reasonable form for the distribution function of fusion products is derived. With this distribution function, basic properties such as the first-orbit losses out of the plasma chamber and geometric effects on the distribution function can be deduced. A major role is played by magnetically trapped particles, which can undergo wide excursions away from magnetic field surfaces due to their high energy. The resulting distribution function displays a strong contrast between the central region of the plasma, where the fusion reaction rate for the production of α-particles is greatest, and the outermost regions of the plasma. In particular, at the outer edge particles are concentrated furthest away from the symmetry axis of the toroidal configuration, where the magnetic field is at its lowest. The velocity-space distribution function is dominated by trapped particles which undergo large radial excursions; these particles are not deeply trapped and have pitch angles close to those of passing particles.

Another topic examined is the resonant interactions of fusion products with an internal mode of the plasma referred to as the "contained mode", whose local properties are analogous to those of a magnetosonic-whistler wave. The resonance occurs for modes whose frequency lies at multiples of the cyclotron frequency of the ener-

getic particles. The contained mode has been shown to be localized in a thin radial shell towards the edge of the plasma column. Key features examined are the mode frequency, localization and radial extent of the mode, and how these properties are affected by the direction of mode propagation. As these modes can have frequencies larger than the fusion product cyclotron frequency, they can undergo resonant interactions with the small population of particles formed by fusion processes. Such interactions can lead to an instability of the collective mode which draws energy from the fusion products.

The induced growth rates are calculated for parameters typical of recent experiments in burning plasmas resulting in the formation of α-particles. These experiments have observed enhanced radiation emission at harmonics of the fusion product cyclotron frequencies and it is argued that this anomalous ion cyclotron emission (ICE) is associated with the excitation of the contained modes by α-particles. According to this model, this emission can yield information about the α-particle distribution. In addition, these modes will modify the distribution of α-particles, offering an alternative to collisional processes for the exchange of energy with the background plasma of which slowing down of α-particles on electrons predominates. Such a mechanism would impart energy from fusion to the plasma ions without having to first heat the electron population. The effects of the eventual loss of energy of α-particles to this collective mode are illustrated and compared to collisions.

Thesis Supervisor: Bruno Coppi
Title: Professor

To my mother

Acknowledgments

I would like to thank Professor Bruno Coppi for his insight and guidance, and for his fatherly interest in me. I greatly benefited from his intensive and far-reaching courses on high-energy plasma physics and plasma astrophysics. I learned a tremendous amount from his courses, from our discussions, and from the distinctive and powerful way of doing physics which is his specialty. I am also thankful for the productive summer collaborations at UCLA and Princeton which he helped to arrange.

I am grateful to the entire research group for listening to my ideas and sharing their knowledge and experience. I owe a special debt to Dr. Stephano Migliuolo, whose patience and personal interest in my work springs from a true generosity of heart.

During our extensive collaboration, which I greatly enjoyed, Dr. Caterina Riconda significantly strengthened both the creative and analytical aspects of my research through her own work and as a result of our discussions. She also pushed me to write my research in a more readable style. In addition, I would like to thank her for her companionship and for her circle of friends to whom she introduced me.

Dr. Neer Asherie made significant, early contributions on the topic of ion cyclotron emission. His initial insights left me with a strong foundation from which to build. In addition, my association with him led to many interesting experiences, including but not limited to a complete overdose on physics during my second year at MIT.

I wish to express my appreciation to Professor Richard Sydora for an enjoyable and educational period of collaboration on the topic of sawteeth. His subsequent interest in my research and my career has been extremely gratifying.

There are many other excellent scientists whom I have had the privilege to learn from or to work with. I wish to thank Professor Peter Catto for his lucid teaching style, for his friendly advice, and for encouraging me to interact with the researchers at the PSFC. I learned a great deal from Professor Abraham Bers, who elegantly explained many complicated aspects of plasma physics and who revealed the complexity to what I thought was simple. I am also grateful to Dr. Sergei Krashnennikov for his

penetrating and difficult questions.

Peggy Berkovitz has been a constant source of comfort for me at MIT through her effectiveness and kindness. I greatly appreciate her willingness to help me navigate through the numerous administrative complexities which I encountered.

I owe a personal debt to Bonnie Souter for encouraging my participation in the Graduate Student Council, which made my stay at MIT much richer in experiences. Through this organization, I got involved with student issues and with broader issues besides science. I would also like to commend Maria Raposo for her continued hospitality long after I overstayed my welcome at the GSC, allowing me a place to de-stress.

I would like to thank Professor Shamit Kachru for the inspiration of his rocketing career in physics, for the basketball games, and for his patience in responding to my constant scientific questions.

I am grateful to Marc, Ruth, and Courtney Cannava for welcoming me in their home, and for many enjoyable gatherings.

I would like to thank my mother Carol, and my siblings Laurence, Jonathan, and Valerie, for their comfort and sympathy during hard times, and for sharing in my happiness at graduating. I would also like to recall my father, who passed away during my studies at MIT.

Finally, I would like to thank the National Science Foundation for financial support during my first three years at MIT.

Contents

1 Introduction **10**

2 The alpha-particle distribution function **15**

2.1 Constants of the motion 18

2.2 Model for the transient distribution function 22

2.3 Collisional effects 24

3 Dynamics of alpha-particles **32**

3.1 Adiabatic invariants and the magnetic moment 32

3.2 Distribution function in guiding center coordinates 34

3.3 Alpha-particle orbits 36

3.4 Numerical results 39

4 Characteristic equation for the contained mode **46**

4.1 Magnetosonic-whistler wave in a homogeneous plasma 47

4.2 Contained mode equation 53

4.3 Analytical solution with purely perpendicular propagation 57

5 Properties of the contained mode **62**

5.1 Numerical results 62

5.2 General analytical solution 67

6 Ion cyclotron emission driven by alpha-particles **82**

6.1 ICE observations 83

6.2 Homogeneous magnetosonic-cyclotron instability 88
6.3 Interaction of energetic ions with contained modes 94

7 Induced growth rate of contained modes **98**
7.1 Magnetic field geometry and drifts 99
7.2 Gyrokinetic calculation of linear response 101
7.3 Radial mode structure effects on gyrokinetic calculations 103
7.4 Growth rate in the local approximation 114
7.5 Discussion of the mode-particle resonance 117
7.6 Numerical calculations 122

8 Comparison of resonant interactions and collisions **128**

9 Model for toroidal rotation generated by ICRF **134**
9.1 Torque generated by balanced inputs 135
9.2 Estimate for rotation induced by contained modes in Alcator C-Mod 140
9.3 Angular momentum transport 141
9.4 Experimental considerations 154
9.5 ICRF heating and mode conversion 159
9.5.1 Linear mode conversion 163
9.5.2 Nonlinear mode coupling 164

10 Conclusions **169**

Chapter 1

Introduction

Energetic particles produced from fusion have begun to be formed in significant quantities in recent experiments on the Joint European Torus (JET)[1] and Tokamak Fusion Test Reactor (TFTR)[2]. Subpopulations of ions with superthermal speeds can also be present in experiments with injected beams. Fusion products are expected to have quite significant effects on plasma confinement properties for burning plasmas. A study of the dynamics of energetic ions is also applicable to astrophysical phenomena such as cometary tails and accretion disks.

In a magnetized plasma, the motion of the ions is primarily determined by the action of the magnetic fields, which conserve the particle energy and, for slowly varying fields, also conserve the magnetic moment $\mu = m|\vec{v} \times \vec{B}|^2/2B^3$ as an adiabatic invariant. Other interactions can occur either through collisions, predominantly between pairs of particles, or through collective modes. For energetic ions the strongest collisional effect is slowing down against the electrons. This thesis will focus on interactions of energetic ions with one particular class of modes, termed "contained modes", at frequencies in resonance with multiples of the cyclotron frequency of the energetic ions. Experimental observations of ion cyclotron emission (ICE) provide evidence of α-particle interactions with the background plasma[3]. Analytical calculations of the destabilization of contained modes by α-particles are consistent with experimental results. An understanding of these interactions has implications for observing and influencing α-particle dynamics, and suggests a signature for energetic

particle subpopulations in magnetized space plasmas.

The significance of these contained modes lies in their radial confinement which allows them, in contrast to convective modes, to be driven to large amplitudes by weak interactions. In particular, these modes can be driven unstable by a subpopulation of energetic ions for mode frequencies resonating with their cyclotron frequency even when the fraction of energetic ions is small, as in fusing plasmas[4]. For these modes the energy can only be convected out by coupling with other modes or by interacting with the plasma. For fusing plasmas we expect α-particle interactions with these modes to play a role in α-particle detection and the study of α-particle dynamics[5, 6]. Observed ion cyclotron emission (ICE) correlated with neutron production from fusion[3] may be the result of such interactions. Furthermore, ion cyclotron range of frequency (ICRF) waves, typically injected into the plasma to heat ions, can also drive contained modes to significant amplitudes. Besides offering a means to directly observe these modes in non-fusing plasmas, the ability to excite selected contained modes in fusing plasmas would provide the choice of either adding energy to or removing energy from α-particles, depending on the choice of mode. In particular, externally driven contained modes which damp against α-particles produced by fusion would mediate the transfer of energy from α-particles to the background ions.

Considering the wide range of plasma profiles which are achieved in different operating regimes in fusing plasma experiments, these results are suggestive of a means of identifying specific experimental observations as being a consequence of the existence of contained modes in the plasma. In current fusing plasma experiments regimes such as hot-ion mode and optimized shear are characterized by very different density profiles[7] leading to different regions within the plasma where the contained modes are found. As the contained mode can be driven to large amplitudes in the presence of an energetic particle subpopulation, we expect enhanced cyclotron emission related to this interaction to exhibit different spectra in different regimes. Effects of ICRF related to the excitation of contained modes should be observable even when the injected wave frequency is not in resonance with the ion cyclotron frequency, as con-

tained modes can be found at multiple intermediate frequencies between resonances.

The dynamics of energetic ions produced by fusion are examined by first considering the effect of the magnetic field on the ions, as well as other "fast" effects such as losses to the plasma chamber walls. This leads to the introduction of an orbit-averaged source function for the α-particles which is a function only of constants of the motion, i.e., energy, magnetic moment and toroidal angular momentum, when expressed in guiding center co-ordinates. This new source function provides an accurate description of the energetic ions so long as the equilibrium time scales are longer than the ion orbit period and the equilibrium scale lengths are larger than the ion gyroradius.

From the orbit-averaged source function one can then obtain a description of basic dynamic effects such as first-orbit losses to the wall and the characteristics of those energetic particles which can interact with contained modes. Influences such as the geometry of the plasma configuration and the form of the plasma profiles are then considered for their impact on the α-particle dynamics.

It is then proposed that the distribution function for those α-particles which have not yet experienced significant slowing down or interaction with collective modes is simply proportional to this orbit-averaged source function. The resulting distribution function is calculated for parameters appropriate to the JET experiment. The main features of these results are discussed, and used to develop an appropriate model for the distribution function to be used in subsequent calculations. In particular, velocity-space anisotropy is seen to be substantial towards the plasma edge because of magnetic confinement effects and the concentration of α-particle production in the plasma core.

The properties of the contained modes, which are a special case of the extension of magnetosonic-whistler waves for an inhomogeneous plasma, are evaluated. These contained modes exhibit sharp localization determined by the density profile. The role of the Hall effect is shown to be an important factor in the properties of contained solutions. In particular, for realistic plasma parameters contained modes generally have poloidal phase velocities in the direction of the ion cyclotron motion; exceptions,

where contained solutions may have the opposite phase velocity, are restricted to cases where there is a large component of propagation parallel to the equilibrium magnetic field. Expressions are obtained for the mode layer, outside of which the amplitude of the mode rapidly falls off, and for the mode frequency. The interaction between these energetic ions and the contained mode is analyzed in a gyrokinetic formalism[8, 9] and growth rates of these modes induced by resonant interactions are obtained. The results are then compared to ICE observations.

The format of this thesis is as follows: the dynamics of α-particles produced by fusion are evaluated in Chapter 2. Noting that any distribution function which varies slowly compared to the orbit period can be expressed in terms of the constants of the motion, which are the particle energy, magnetic moment, and toroidal angular momentum, a modified source function is defined by taking the average of the source function over particle orbits. An argument is presented for identifying this function with the distribution function for recently produced α-particles.

In Chapter 3 key aspects of the α-particle dynamics, such as the first orbit losses and the edge distribution function are analyzed for a range of plasma parameters. A model distribution function is adopted for the edge of the plasma.

In Chapter 4 the equation governing the contained mode is derived and compared to the homogeneous magnetosonic-whistler mode. Methods for the analytical solution to the contained mode are presented, and applied to the limit of purely perpendicular propagation. While there is no whistler contribution to the mode, the Hall term still affects the mode structure through the density inhomogeneity, an effect which is characterized by the quantity d_{i0}/a, where $d_{i0} = c/\omega_{pi}$ evaluated at the magnetic axis.

In Chapter 5 the general contained mode structure is analyzed, allowing for a small component of propagation parallel to the magnetic field. Numerical calculations of the radial profile of the contained mode are described and presented. It is shown how the limit of perpendicular propagation examined in Chapter 4 corresponds to taking specific choices of mode numbers for the full mode equation. The analytical model is then extended to arbitrary mode numbers, and compared with numerical results.

In Chapter 6 the observations of ICE in D-T plasma experiments are discussed, and the motivation for explaining this radiation as an effect of α-particles is given. The instability of fast magnetosonic-whistler waves resulting from the presence of α-particles is calculated for a homogeneous plasma. Reasons are given for focussing on the contained mode as the mediator between the energetic ions produced by fusion and the observed radiation emission.

In Chapter 7 the growth rate of contained modes driven by resonant interactions with α-particles is evaluated, using the model distribution function from Chapter 3. The resulting instabilities are compared with observations of ICE.

In Chapter 8 the effect of these mode-particle interactions on the α-particles is compared with collisional processes. The implications are considered for the development of diagnostics and the potential for selectively altering the dynamics of those particles which interact with contained modes.

In Chapter 9 the effect of contained modes in ICRF-heated plasmas is considered for the potential to explain experimental observations of toroidal rotation of the plasma driven by balanced inputs of ICRF.

In Chapter 10 the conclusions of this research are presented, with a summary of the significance of these results. After presenting an overview of the α-particle interactions with the background plasma, unresolved issues are examined. Finally, future applications and further areas of study are discussed.

Chapter 2

The alpha-particle distribution function

We are interested in the interaction of energetic ions with the background plasma, in particular through collective modes. To characterize these interactions it is necessary to evaluate the distribution function of energetic ions. The time evolution of the distribution function F, normalized to the canonical phase space volume, is governed by

$$\frac{d}{dt}F = F_s + \left(\frac{\delta F}{\delta t}\right)_{\text{coll}}, \tag{2.1}$$

where F_s is the source function representing the creation of energetic particles in phase space, $(\delta F/\delta t)_{\text{coll}}$ characterizes the effect of collisions (or collective modes), and

$$\frac{d}{dt} \equiv \frac{\partial}{\partial t} + \vec{v}\cdot\nabla + \frac{q_\alpha}{m_\alpha}\left(\vec{E} + \vec{v}\times\vec{B}\right)\cdot\nabla_v \tag{2.2}$$

is the convective derivative in phase space. We take the equilibrium electric field to be zero.

Fusion products are created at a rate determined by the local values of the plasma density and temperature, which are roughly constant over time and on flux surfaces, which in this case are taken to be surfaces of constant (minor) radius. For the range of temperatures attained in existing experiments, the rate of α-particle production as

determined by $S_\alpha = n_D n_T \langle \sigma v \rangle$ can be approximated as[10]

$$S_\alpha \ [\mathrm{m}^{-3}\mathrm{s}^{-1}] \simeq 3.68 \times 10^{-18} n_D n_T T_i^{-2/3} \exp\left(-20 T_i^{-1/3}\right),$$

where T_i is in units of keV and the densities are in units of m^{-3}. The quantity S_α is the local density of α-particles created per unit time.

In considering the case of α-particles produced by fusion, we assume for simplicity that all α-particles are born with exactly the same energy $\mathcal{E}_\alpha \simeq 3.5$ MeV. We also take the distribution of α-particle velocities at birth to be isotropic. Thus the production of α-particles through fusion can be characterized in phase space by

$$F_b \equiv S_\alpha(\vec{x}) \ \delta(\mathcal{E} - \mathcal{E}_\alpha) \frac{1}{4\pi\sqrt{2\mathcal{E}_\alpha / m_\alpha^3}}. \tag{2.3}$$

When the width of the energy distribution of the α-particles at birth is the result mainly of thermal effects, the delta function in energy would be more accurately replaced by

$$\frac{1}{\mathcal{E}_W \sqrt{2\pi}} \exp\left[-\frac{(\mathcal{E} - \mathcal{E}_\alpha)^2}{2\mathcal{E}_W^2}\right],$$

where $\mathcal{E}_W \simeq (1.6 \ T_i \mathcal{E}_\alpha)^{1/2}$ is of the order of the geometric mean between the deuteron thermal energy and α-particle energy[11]. For experiments where the tritium for fusion reactions comes from neutral beam injection (NBI), the spread in energy will be much greater. For example, in experiments on JET where 78 keV tritium beams were injected into the plasma[3], the range of energies of the fusion products was determined to be between 2.9 MeV and 4.4 MeV, with a strong dependence on the direction of motion along the beam axis.

When collision rates and the variation in equilibrium quantities are much slower than the orbit period, the convective derivative defined in Eq. (2.2) is dominated by gradient terms, and the partial derivative with respect to time can be neglected. The convective derivative can be rewritten in terms of the parametric time τ as

$$\frac{d}{dt} \equiv \frac{\partial}{\partial t} + \frac{\partial}{\partial \tau},$$

where $\tau(\vec{x},\vec{v})$ characterizes position along a particle orbit through the differential equation

$$\vec{v}\cdot\nabla_x\tau+\frac{q_\alpha}{m_\alpha}(\vec{v}\times\vec{B})\cdot\nabla_v\tau=1.$$

Thus, neglecting the partial derivative with respect to time in Eq. (2.1) yields

$$\frac{\partial}{\partial\tau}F=F_s+\left(\frac{\delta F}{\delta t}\right)_{\text{coll}}. \tag{2.4}$$

Here we focus on the transient distribution function of α-particles which have been produced by fusion within a time period that is short compared with the characteristic times for collisions and other effects such as drift losses, but much longer than the orbit period. These conditions should be sufficient to model certain of the novel processes seen in recent experiments in fusing plasmas, where the α-particles are not well confined and where effects such as ion cyclotron emission are observed promptly after neutrons produced by fusion are observed in significant quantities. The further evolution of the distribution function can be calculated in terms of changes to the particle orbits rather than by following individual particles. The resulting transient distribution function will depend only upon the fusion production rate of α-particles and the particle orbits. Because the dominant effect of collisions is the slowing down of α-particles, all of the high-energy α-particles must have been recently produced by fusion. Thus, the transient distribution function calculated here is expected to mimic the form of the high-energy portion of the distribution function except for its dependence on particle energy. The effect of collisions and α-particle losses will primarily be to determine the saturation level at which the addition of new, energetic α-particles from fusion is balanced by particle and energy losses.

For these reasons we expect the solution to Eq. (2.4) to have the form

$$F=\int^{t_0}d\tau\ F_s(\tau)\simeq\frac{t_0}{\tau_b}\oint d\tau\ F_s(\vec{x}(\tau),\vec{v}(\tau)), \tag{2.5}$$

where $\tau_b=\oint d\tau$ is the orbit period and t_0 is a time scale reflecting losses and the time history of the source function. The time-dependence of the source function arises

only from changes in density and temperature profiles and is suppressed. Replacing $(1/t_0)\int^{t_0} d\tau$ with an average over a complete orbit neglects terms only of the order of $\tau_b/t_0 \ll 1$. The result is a distribution function which does not change significantly over the course of an orbit period. The parameter t_0 can represent either the buildup of α-particles immediately after the onset of significant fusion reaction rates, or the saturated value after the high-energy portion of the distribution function has reached a steady state. This procedure is analogous to the "method of characteristics" used to evaluate linear responses to perturbations by integrating over unperturbed orbits. Here the "frequency" for collisional effects and changes in the profile is approximated as zero and the "wave vector" is replaced by gradients in the equilibrium quantities. In this case the dominant perturbation, the production of α-particles through fusion, does not affect particle orbits and so this methodology is not restricted to small reaction rates.

The dominant collisional processes affecting α-particles having high energies near 3.5 MeV is slowing down against electrons. This process is characterized by a time scale $\tau_{\rm sl}$ such that the average rate of change in velocity for particles having a velocity v is $v/\tau_{\rm sl}$. For parameters corresponding to the JET experiment[1] $\tau_{\rm sl} \simeq 1.03$ s in the core of the plasma[3], while equilibrium quantities evolve on a time scale $\tau_{\rm equilib} \sim 0.5$ s. Because the rate of slowing down from collisions depends on the local electron density and temperature as $n_e T_e^{-3/2}$, α-particles born in the core but which undergo large radial excursions, so that they pass through the plasma edge as well, have an effective slowing down time of roughly 1.2 s. This result is obtained by averaging $1/\tau_{\rm sl}$, as given by Ref. [12], over a typical orbit of this type. The typical orbit period for α-particles which undergo large radial excursions away from the core is $\tau_b \simeq 6\times10^{-5}$ s.

2.1 Constants of the motion

The consequence of approximating the distribution function F through Eq. (2.5) is that F depends only on constants of the motion of the α-particles and a dependence on time which is slow compared to the orbit period. When the characteristic time for

collisions is much slower than the orbit period, so that particles undergo similar orbits many times before being significantly affected by collisions, the effects of slowing down can be represented as an operator which acts only on the constants of the motion. This operator will be related to the average over a particle orbit of the change of the constants of the motion resulting from collisions. Thus the distribution function is a solution of Vlasov's equation, $dF/dt = 0$. At the same time, however, F preserves detailed information about the α-particle production rate and also contains an estimate of the effectiveness of collisions and the time history of the production of α-particles. For an axisymmetric system, the constants of the motion are given by $\mathcal{E}$, $\mathcal{M}$, and $\mathcal{L}_\zeta$, where

$$\mathcal{E} = m_\alpha v^2/2$$

is the particle energy,

$$\mathcal{M} \simeq \mu = m_\alpha v_\perp^2/2B$$

is the adiabatic invariant related to the magnetic moment of the particle in its cyclotron motion about magnetic field lines, and

$$\mathcal{L}_\zeta = q_\alpha R A_\zeta + mRv_\zeta$$

is the toroidal component of the canonical angular momentum. The magnetic potential A_ζ is defined by

$$RA_\zeta = -\int_0^r RB_\vartheta \, dr,$$

where $(\hat{e}_r, \hat{e}_\vartheta, \hat{e}_\zeta)$ form an orthonormal coordinate system.

These constants of the motion are first treated as identical to the constants of the motion as determined by the initial conditions of the α-particles at birth. This procedure does not incorporate the effects of slowing down of α-particles against electrons nor of collective modes. The primary processes which are represented by this model are radial drifts and first-orbit losses out of the plasma. The radial drifts are quite large because of the high energies of the α-particles and cannot be adequately described in terms of "banana orbits". When the slowing down time is much greater

than the orbit period, the effect of collisions can be represented as an operator which acts only on the constants of the motion because of the difference in time scales between collisions and particle orbits, allowing for an evaluation of the changes in F due to collisions averaged over many orbit periods.

To simplify the calculation of F, we note that the integral over particle orbits includes at its shortest time scale an integral over gyroorbits, effectively averaging out gyrophase-dependent quantities. Thus, we first change to guiding center coordinates given by $\mathcal{E}$, $\mathcal{M}$, $\vec{X}_g$ and φ_g where φ_g is the generalized gyrophase and $\vec{X}_g$ is the location of the guiding center. We also perform an expansion in the parameter $\lambda \equiv \rho_\alpha / L_B$ where $\rho_\alpha = v_\alpha / \Omega_\alpha$ is the α-particle gyroradius and L_B is the scale length for the magnetic field. The integral over gyroorbits is roughly equivalent to an average in gyrophase, as the other quantities are slowly varying on the time scale of the cyclotron motion. The canonical angular momentum can be expressed in terms of guiding center coordinates as

$$\mathcal{L}_\zeta = q_\alpha R_g A_\zeta(\vec{X}_g) + m_\alpha R_g U \frac{B_\zeta(\vec{X}_g)}{B(\vec{X}_g)} + \mathcal{L}_2,$$

where $U = \hat{e}_{||} \cdot d\vec{X}_g/dt$ is roughly the velocity parallel to the magnetic field and satisfies

$$\frac{1}{2} m_\alpha U^2 + \mathcal{M} B(\vec{X}_g) = \mathcal{E},$$

and $\mathcal{L}_2$ is an order λ^2 correction to $\mathcal{L}_\zeta$ which in general includes a dependence on φ_g. If we only consider $\mathcal{O}(\lambda)$ corrections, however, $\mathcal{L}_\zeta$ is independent of gyrophase and can be expressed in terms of $\mathcal{E}$, $\mathcal{M}$ and $\vec{X}_g$ alone. To this order, the particle orbits for fixed $\mathcal{E}$ and $\mathcal{M}$ can be characterized by curves in space and do not vary with gyrophase, thus the orbit integral can be reduced to an average over gyrophase and an independent integral along curves in space. Here, $\hat{e}_{||} \equiv \vec{B}/B$ and the parallel velocity $v_{||} = \vec{v} \cdot \hat{e}_{||}$.

The integral over a single gyroorbit results in average quantities which correspond to gyrocenter coordinates if $\mathcal{O}(\lambda^2)$ terms are neglected. For example, defining the gyrophase φ through $\vec{v}_\perp = v_\perp(\hat{e}_1 \cos\varphi + \hat{e}_2 \sin\varphi)$, where $\hat{e}_1 \times \hat{e}_2 = \hat{e}_{||}$, the gyroorbit

is determined by $d\varphi/d\tau \simeq -\Omega_\alpha$ and to first order the position is given by

$$\vec{x}(\tau) = \vec{X}_g(\tau) - \rho\left[\hat{e}_1 \sin\varphi(\tau) - \hat{e}_2 \cos\varphi(\tau)\right].$$

Thus gyroradius-scale corrections average out to zero over a gyroorbit. For a source function F_s which is isotropic in velocity,

$$F(\mathcal{E}, \mathcal{M}, \mathcal{L}_\zeta) \propto \oint F_s(\vec{x}(\tau), \mathcal{E}) d\tau = \oint F_s(\vec{X}_g(\tau), \mathcal{E}) d\tau, \tag{2.6}$$

which is an integral over much simpler curves in space than the actual particle orbits. It is particularly significant that even though F_s is independent of pitch angle, the final distribution function will acquire a dependence on $\mathcal{M}$ because both $\mathcal{L}_\zeta$ and the source function vary with position, and this dependence can be quite strong. In addition we note that the switch to guiding center coordinates would be valid even if F_s depended upon pitch angle, with the pitch angle replaced by its average over a gyroorbit, so long as there was no explicit dependence on gyrophase. Together with the assumption that all quantities are symmetric in the toroidal angle ζ, the averaging over fast time scales to eliminate dependences on φ_g and the parametric time τ account for the remaining degrees of freedom of the α-particles. Because of the toroidal symmetry, the orbits can be considered in their projections on the (r_g, ϑ_g) cross-section; the orbits are all periodic in this perspective.

Finally, we note that because of the large size of the α-particle gyroradius, we cannot evaluate the orbit integral for trapped particles using the usual "banana orbit" approximation, and even for passing particles the radial excursion of particles orbits is significant. Such orbits have been termed "potato orbits" and are the typical case for α-particles in current experiments where the toroidal currents are insufficient to constrain the α-particles to closely follow their initial magnetic surface. The banana orbit approximation requires instead a high current, and also breaks down for particles that are very close to the magnetic axis.

2.2 Model for the transient distribution function

Returning to a specific calculation of the distribution function for a monoenergetic source of α-particles as defined by Eq. (2.3), it is convenient to define an orbit average of the source function after the delta function has been factored out,

$$\mathcal{F}(\mathcal{E}_\alpha, \mathcal{M}, \mathcal{L}_\zeta) \propto \oint d\tau \; S_\alpha(\vec{x}(\tau)),$$

where $\mathcal{F}$ is dimensionless. Our distribution function will have the general form

$$F = \mathcal{F}(\mathcal{E}, \mathcal{M}, \mathcal{L}_\zeta)\delta(\mathcal{E} - \mathcal{E}_\alpha)\frac{n_{\alpha 0}}{4\pi\sqrt{2\mathcal{E}_\alpha/m_\alpha^3}}, \tag{2.7}$$

where $n_{\alpha 0}$ is the density of α-particles created at the center of the plasma. Note that the local density of α-particles at the center of the plasma will be somewhat smaller because of the magnetic drifts which carry some particles towards the edge of the plasma. The normalized distribution function $\mathcal{F}$ is defined so that at a fixed position,

$$\frac{1}{2v_\alpha}\int_{-v_\alpha}^{v_\alpha} dv_\parallel \; \mathcal{F} = \frac{n_\alpha}{n_{\alpha 0}}.$$

We consider n_α to be roughly constant during an orbit period. The quantities $\mathcal{E}$, $\mathcal{M}$ and $\mathcal{L}_\zeta$ are the constants of the motion defined by $\mathcal{E} = m_\alpha v^2/2$, $\mathcal{M} \simeq \mu + \mu_1$, $\mathcal{L}_\zeta = R\,(m_\alpha v_\zeta - q_\alpha A_\zeta)$. Here $\mu = m_\alpha v_\perp^2/2B$ and μ_1 is the next term in the adiabatic invariant when expressed as an expansion in $\lambda \equiv \rho_\alpha/L_B$.

Considering the source function of α-particles and their motion in some given magnetic configuration, we can obtain a reasonable form for the distribution function. Let us first consider the dynamics of the α-particles. We consider a region near the edge of the plasma column, so that the α-particles which reach this region will typically be trapped particles with large radial excursions, because fusion occurs primarily in the core of the plasma column. These particles have pitch angles close to those characteristic of passing particles, and are in a very different regime from "deeply trapped particles" as characterized in the banana orbit approximation. The

trapping condition restricts the distribution at the mode layer to a narrow range of values of $\mathcal{M}B(\vartheta)/\mathcal{E}$, whose width we denote by Σ; the value about which this range is centered is denoted by Λ_0. The distribution will thus be a strongly anisotropic function.

The single-particle drifts are the result of the axial magnetic field configuration. These drifts carry positively charged ions in the same direction as the current which produces the axial magnetic field. The simplest form for the particle drift velocity is

$$\vec{v}_d \simeq -\frac{2\mathcal{E} - \mu B}{m_\alpha \Omega_\alpha}(\hat{e}_{||} \cdot \nabla \hat{e}_{||}) \times \hat{e}_{||}. \tag{2.8}$$

In addition to magnetic drifts, the motion along the field line carries the ions in the poloidal direction because of the poloidal component to the magnetic field created by toroidal currents. The result of the combination of magnetic drifts and motion along the field lines is that particles in the core of the plasma which are moving opposite to the toroidal current are carried further inwards towards the magnetic axis until they are reflected by mirror forces. Thus trapped particles move counter to the toroidal current in the plasma core, and tend to undergo larger radial excursions than passing particles. After these particles pass their turning points, they move in the same direction as the toroidal current and are carried towards the outboard edge of the plasma. Particles originating in the core of the plasma tend not to reach the inboard side of the plasma where the magnetic field is highest, because of the magnetic forces.

Here, we assume that the toroidal current and magnetic field have the same orientation, so the particles that can reach the mode layer are restricted to having $v_{||} > 0$ at the mode layer. For a plasma configuration where the toroidal current is directed opposite to the toroidal magnetic field, the sign of $v_{||}$ must be reversed everywhere below.

From these considerations an appropriate model for the function $\mathcal{F}$ introduced in Eq. (2.7) is

$$\mathcal{F} \simeq AH(\vartheta_{cr} - |\vartheta|) \exp\left[-\frac{(\mathcal{M}B(R)/\mathcal{E}_\alpha - \Lambda_0)^2}{2\Sigma^2}\right], \tag{2.9}$$

where we only consider particles with $v_{||} > 0$, as explained above. Here A is a constant

(for fixed radius near the edge) of order unity which corresponds to the peak of the normalized distribution function, and H is the step function which vanishes for negative argument. In order to discard from the distribution function those particles which suffer first orbit losses, we set the distribution function to zero along orbits which extend beyond the plasma edge. This is the significance of the cutoff angle ϑ_{cr}.

The magnetic field B is of the form

$$B \simeq \frac{B_0}{1 + r\cos\vartheta/R_0}.$$

The ratio $\mathcal{M}B(\vartheta)/\mathcal{E}_\alpha \simeq \Lambda_0$ corresponds to trapped particles whose orbits extend from well into the plasma core to the mode layer. At $r = r_{\text{mode}}$ and for $\vartheta > \vartheta_{cr}$, $\mathcal{M}B(\vartheta)/\mathcal{E}_\alpha = \Lambda_0$ characterizes orbits which extend beyond the plasma edge. We keep only first order corrections in the inverse aspect ratio, which leaves $B(\vartheta)$ as the only remaining ϑ-dependent term.

The local density for the particles of interest is approximately given by

$$n_\alpha \simeq A n_{\alpha 0} H(\vartheta_{cr} - |\vartheta|) \left[\frac{\pi}{8(1-\Lambda_0)}\right]^{1/2} \Sigma. \tag{2.10}$$

The actual local density will be slightly greater because the model does not account for the small contribution of those particles that are created far from the center of the plasma column. In experiments on the JET machine, local α-particle densities rapidly drop off from the central value[3], and at $r = 0.5\ a$ the local density is already reduced by a factor of 10.

2.3 Collisional effects

When the characteristic time for collisions is much longer than the orbit period, the effects of slowing down can be represented as an operator which acts only on the constants of the motion. This operator describes the average over a particle orbit of changes of the constants of the motion resulting from collisions. Evaluating these effects for $\mathcal{E} \gtrsim 0.7$ MeV is made simpler by the fact that the dominant collisional

process is slowing down against electrons and velocity space diffusion can be neglected, allowing the time evolution of particles to be treated as deterministic. In addition, the energy decay dominates any effects from thermal spread of the α-particle energy at birth except for the fact that the distribution function does not exactly vanish for $\mathcal{E} > 3.5$ MeV, and instead falls off as a narrow Gaussian distribution. This approximation is valid except immediately after α-particle production begins when the distribution function is a Gaussian in energy growing linearly in time, which is only relevant for times less than $\tau_{\rm sl}\sqrt{T_i/\mathcal{E}_\alpha}$.

If we assume that the background particles (e, D, and T) have Maxwellian distributions, the effect of collisions on F_0 can be represented as a Fokker-Planck type of operator[11, 13]:

$$\left(\frac{\delta F}{\delta t}\right)_{\rm coll} \simeq \sum_{\beta=e,D,T} \frac{3\sqrt{\pi}}{4}\frac{1}{\tau_{\rm sl}}\frac{Z_\beta^2 n_\beta}{n_e}\frac{m_e}{m_\beta}v_e^3\nabla_v\cdot\left[\frac{\Psi_\beta\vec{v}}{v^3}F_0+\frac{T_\beta}{m_\alpha}\frac{\Psi_\beta}{v^3}\nabla_v F_0\right], \qquad (2.11)$$

where $v_\beta^2 \equiv 2T_\beta/m_\beta$, $\Psi_\beta = \Psi(v^2/v_\beta^2)$, and

$$\Psi(x) \equiv \frac{2}{\sqrt{\pi}}\int_0^x y^{1/2}\exp(-y)\,dy$$

characterizes the dependence of collisions on the relative velocity of the particles. In the limit $x \ll 1$, $\Psi(x) \simeq 4x^3/3\sqrt{\pi}$, while for $x \gg 1$, $\Psi(x) \simeq 1$. The slowing down time $\tau_{\rm sl}$, for electrons with thermal velocity much greater than the α-particle velocity ($T_e \gg 0.5$ keV), satisfies[12, 14]

$$\frac{1}{\tau_{\rm sl}} \equiv \frac{1}{3(2\pi)^{3/2}}Z_\alpha^2 n_e\frac{e^4 m_e^{1/2} ln\Lambda}{\epsilon_0^2 m_\alpha T_e^{3/2}} = \frac{1}{3(2\pi)^{3/2}}\frac{Z_\alpha^2 m_e}{m_\alpha}\frac{\ln\Lambda}{n_e\lambda_{De}^3}\omega_{pe},$$

where $\omega_{pe}^2 = n_e e^2/\epsilon_0 m_e$ and $\lambda_{De}^2 \equiv T_e/m_e\omega_{pe}^2$. The quantity $\ln\Lambda$ is the Coulomb logarithm. More explicitly,

$$\tau_{\rm sl}[{\rm s}] \simeq 0.42\frac{15}{\ln\Lambda}\left(\frac{T_e}{10\ {\rm keV}}\right)^{3/2}\left(\frac{n_e}{10^{20}\ {\rm m}^{-3}}\right)^{-1},$$

$$\ln\Lambda \simeq 17.1 - \frac{1}{2}\ln\left(\frac{n_e}{10^{20}\ {\rm m}^{-3}}\right) + \ln\left(\frac{T_e}{10\ {\rm keV}}\right).$$

Because the slowing down is the dominant effect and does not affect pitch angles, it is convenient to rewrite Eq. (2.11) in terms of the velocity space variables $\mathcal{E}$, $\Lambda \equiv \mu B/\mathcal{E} = v_\perp^2/v^2$, and φ, where φ is the gyrophase. Then the collision operator for a general distribution function $F_0(\mathcal{E}, \Lambda, \varphi)$ is

$$\left(\frac{\delta F}{\delta t}\right)_{\rm coll} \simeq \sum_{\beta=e,D,T} \frac{3\sqrt{\pi}}{4}\frac{1}{\tau_{\rm sl}}\frac{Z_\beta^2 n_\beta}{n_e}\frac{m_e}{m_\beta}v_e^3\frac{1}{\sqrt{2\mathcal{E}/m_\alpha^3}}\left[\frac{\partial}{\partial\mathcal{E}}\left(\Psi_\beta F_0\right) + T_\beta\frac{\partial}{\partial\mathcal{E}}\left(\Psi_\beta\frac{\partial F_0}{\partial\mathcal{E}}\right)\right.$$

$$\left. + \frac{T_\beta}{\mathcal{E}^2}\Psi_\beta\sqrt{1-\Lambda}\,\frac{\partial}{\partial\Lambda}\left(\Lambda\sqrt{1-\Lambda}\,\frac{\partial F_0}{\partial\Lambda}\right) + \frac{T_\beta}{4\mathcal{E}^2}\Psi_\beta\frac{1}{\Lambda}\frac{\partial^2 F_0}{\partial\varphi^2}\right] \qquad (2.12)$$

The terms in Eq. (2.12) respectively represent slowing down, energy diffusion, pitch angle scattering and gyrophase scattering. Every process but slowing down is diffusive and has a characteristic time scale at least $\mathcal{E}/T_e$ longer than the time scale for slowing down. Thus, we can considerably simplify the above equation. First, because the variations in gyrophase only occur to order $\lambda = \rho_\alpha/L_B$, the gyrophase operators can be neglected. However, the velocity space anisotropy (in pitch angle or Λ) is extremely strong at the edge, so these terms must be kept. For the ion terms, all of the operators have a small effect and $v_{D,T} \ll v$ so we can set $\Psi_{D,T} \simeq 1$. For electrons, $\Psi_e \simeq 4v^3(1 - 3v^2/v_e^2)/(3\sqrt{\pi}v_e^3)$. The first order correction to Ψ_e has a negligible effect everywhere except in the slowing down operator, where the correction is in fact greater than the energy diffusion term.

We first consider the effects of slowing down alone, because the collision operator is dominated by slowing down against electrons. The diffusive terms are much slower than the slowing-down term by a factor of m_e/m_α for electrons and $(T_i/\mathcal{E}_\alpha)^{5/2}$ for ions. If we treat these collisions as if they were uniformly slowing down α-particles[14], the resulting change in energy is $d\mathcal{E}/dt \simeq -2\mathcal{E}/\tau_{\rm sl}$. Then conservation of particle number implies that $F_{\rm slow}(\mathcal{E})v d\mathcal{E}/dt$ is constant and the delta function in energy in Eq. (2.7) can be replaced by $1/2\mathcal{E}$ for energies slower than $\mathcal{E}_\alpha$. The saturated density is determined by the slowing-down time. There is no acceleration of particles at energies much greater than the background thermal energies, so the high-energy part

of the distribution function then becomes

$$F_{\rm slow} \simeq H(\mathcal{E}_\alpha - \mathcal{E})\mathcal{F}(\mathcal{E}_b, \mathcal{M}_b, \mathcal{L}_{\zeta_b})\frac{\bar{\tau}_{\rm sl} S_{\alpha 0}}{4\pi}\left(\frac{2\mathcal{E}}{m_\alpha}\right)^{-3/2}, \tag{2.13}$$

where H is a step function which vanishes for negative argument and $S_{\alpha 0}$ is the central rate of production of α-particles from fusion (to remain consistent with the normalization of $\mathcal{F}$). The arguments of $\mathcal{F}$ are the constants of the motion of the α-particles at birth. Note that the average value of $\mathcal{F}$ over parallel velocity is still a close approximation to the local density if only particles with $\mathcal{E} \gtrsim 0.7$ MeV are considered.

The quantity $\bar{\tau}_{\rm sl}$ is the effective slowing down time defined by the orbit average

$$\frac{1}{\bar{\tau}_{\rm sl}} \equiv \frac{1}{\tau_b}\oint d\tau \frac{1}{\tau_{\rm sl}}.$$

Corrections for slowing down by ions[11] can be included by replacing $\mathcal{E}^{-3/2}$ with

$$\left[\mathcal{E}^{3/2} + \frac{5\sqrt{\pi}}{4}\left(\frac{m_\alpha}{m_e}\right)^{1/2} T_e^{3/2}\right]^{-1}.$$

This form for the distribution function treats background ions as motionless compared to the α-particles, and breaks down when the two terms above become comparable to each other. For a D-T plasma, the energy at which slowing down by ions rapidly decelerates the α-particles is given by D. Pfirsch in Ref. [14] as $\mathcal{E} \simeq 67\ T_e$. Typical electron temperatures in current fusion experiments are 10 keV.

When particles undergo many orbits before being significantly affected by collisions, the effect of collisions should be independent of where along an orbit a particle is at any particular time. The evolution of the distribution function due to collisions can be described in terms of changes in particle orbits and thus as an operator acting on the constants of the motion. This operator will be related to the average over a particle orbit of the change of the constants of the motion resulting from collisions. As indicated above, the slowing-down rate has to be averaged over particle orbits to give the long term time average of the rate of energy change $\bar{\tau}_{\rm sl}$. For long time scales

the smoothed out time evolution of the energy is roughly given by

$$\frac{d\mathcal{E}}{dt} \simeq -\frac{2\mathcal{E}}{\bar{\tau}_{\rm sl}}.$$

Only constants of the motion can be effectively treated in this way, because other quantities change much more rapidly due to the motion along an orbit than due to collisions. Because the gyroradius is larger than the Debye length, which is the longest scale length for collisions, collisional processes are independent of the magnetic field. Thus, besides $d\mathcal{E}/dt \simeq -2\mathcal{E}/\bar{\tau}_{\rm sl}$ governing the long-term time evolution of the particle energy, the magnetic moment μ changes in the short term according to $d\mu/dt \simeq -2\mu/\tau_{\rm sl}$. Because μ is a first order approximation to the adiabatic invariant $\mathcal{M}$, this implies that the ratio $\mathcal{M}/\mathcal{E}$ remains roughly constant under the action of collisions up to order $\lambda = \rho_\alpha/L_B$, in other words the smoothed out time evolution of $\mathcal{M}$ is given by $d\mathcal{M}/dt \simeq -2\mathcal{M}/\bar{\tau}_{\rm sl}$. Thus, it is convenient to evaluate Eq. (2.13) in terms of $\mathcal{F}(\mathcal{E}_b, \mathcal{M}_b, r_b, \vartheta_b)$ as defined in Eq. (2.9).

Because slowing down can be treated as a deterministic process which monotonically changes the particle energy, we can express the original constants of the motion as approximate functions of the actual constants of the motion. We know that $\mathcal{E}_b \simeq \mathcal{E}_\alpha$, and because of the similar effects of collisions on $\mathcal{E}$ and $\mathcal{M}$ this implies that $\mathcal{M}_b \simeq \mathcal{M}\mathcal{E}_\alpha/\mathcal{E}$. The original angular momentum at birth is more difficult to evaluate, but as a rough approximation changes to angular momentum can be ignored for trapped particles. Canonical angular momentum is only affected by collisions through changes in the parallel velocity U, and as this quantity reverses sign the net effect tends to average out. However, this approximation has only about the same accuracy as the banana-orbit approximation, because it relies on the two halves of the particle orbit being roughly symmetric and on the magnetic potential being the dominant term in the canonical momentum. A more detailed calculation will be performed in Chapter 8. Nevertheless, as a first attempt at accounting for collisions we assume that collisions do not cause loss of confinement of the particles and consider the evolution of single particle orbits due to slowing down. We begin by considering

only $r_b = r$, which is allowable because there is an extra degree of freedom in guiding center coordinates; in this case we can approximate $R_b \simeq R(1-\eta)$ for η small, where $\eta = (1-\mathcal{E}/\mathcal{E}_\alpha)(1-\Lambda)/(2-\Lambda)$ and $\Lambda \equiv \mathcal{M}B(R)/\mathcal{E} = v_\perp^2/v^2$. Equivalently,

$$\cos\vartheta_b \simeq (1-\eta)\cos\vartheta - \eta\frac{R_0}{r}.$$

The turning points of the orbits remain unchanged but as the energy decreases the radial excursion becomes smaller and the crossing point of the orbit with a fixed radial shell moves towards $\vartheta = 0$. Thus,

$$\mathcal{F}(\mathcal{E}_\alpha, \mathcal{M}\mathcal{E}_\alpha/\mathcal{E}, r, \vartheta_b) \simeq AH((1-\eta)R - R_{cr}) \exp\left[-\frac{((1+\eta)\mathcal{M}B(R)/\mathcal{E} - \Lambda_0)^2}{2\Sigma^2}\right],$$

and the steady-state distribution function is roughly given by

$$\begin{aligned} F \;\simeq\; & AH(\mathcal{E}_\alpha - \mathcal{E})H(R - (1+\eta_0)R_{cr})\frac{\bar{\tau}_{sl}S_{\alpha 0}}{4\pi}\left(\frac{2\mathcal{E}}{m_\alpha}\right)^{-3/2} \\ & \times \exp\left[-\frac{(\mathcal{M}B(R)/\mathcal{E} - (1-\eta_0)\Lambda_0)^2}{2(1-\eta_0)^2\Sigma^2}\right], \end{aligned} \tag{2.14}$$

where η_0 is η evaluated at $\Lambda = \Lambda_0$. The net result is very similar to the distribution at $\mathcal{E} = \mathcal{E}_\alpha$ except that the cutoff occurs at higher values of R (lower values of $|\vartheta|$) and the peak of the distribution in pitch angle is shifted from Λ_0 to $(1-\eta_0)\Lambda_0$. The change in the width of the distribution function cannot be taken seriously as a small amount of pitch angle scatter will significantly reduce the velocity-space anisotropy.

The effects of pitch angle scatter are more complicated to evaluate than for slowing down because it is a diffusive process and cannot be approximated as a deterministic operator. Two general statements can be made with confidence, however. In the core of the plasma, the velocity space anisotropy is weak and the main effect is to move a few extra particles into trapped orbits with wide excursions. This process acts as an additional source term, and although it scatter particles with energies lower than $\mathcal{E}_\alpha$ towards the edge, the scattered particles are subject to the same constraints on pitch angle at the plasma edge and so their anisotropy mimics that of unscattered particles.

The net effect is only a small change in the amplitude of the distribution function. However, pitch angle scatter at the plasma edge will flatten out the anisotropy at the edge, and as the original anisotropy is very large the distribution will broaden on time scales comparable to the slowing down time. In addition, pitch angle scatter will cause some losses of particles out of the plasma altogether. Because the relevant collisions only take place away from the plasma core and the effect is reduced in regions where the velocity space anisotropy is less strong, the effective rate of broadening of the anisotropy will be reduced. The long-term time evolution of the parameter Σ due to electron collisions can be described by

$$\frac{d}{dt}\Sigma^2 \simeq \frac{4\alpha_0}{\bar{\tau}_{\rm sl}}\frac{T_e}{\mathcal{E}}\left[\Lambda(1-\Lambda) - 5\Sigma^2/2\right], \tag{2.15}$$

where α_0 is a dimensionless parameter describing the relative importance of pitch angle scatter near the edge, where collisions broaden the distribution function. Here α_0 is taken to be roughly equal to unity, because the fraction of the orbit which passes through the core is partially made up for by the fact that collisions are more effective near the plasma edge due to the lower electron temperature. The ion contribution to pitch angle scatter is smaller by a factor of $v_e v_i^2/v^3$. When $\Sigma \ll 1$, we can approximate the solution to Eq. (2.15) at a time $t - t_b$ after the particles are born as

$$\Sigma(t-t_b) \simeq \left[\Sigma_0^2 + 4\alpha_0\Lambda_0(1-\Lambda_0)\frac{T_e}{\mathcal{E}}\frac{t-t_b}{\bar{\tau}_{\rm sl}}\right]^{1/2}.$$

Of course, there is no single time at which particles were born, but the energy of a specific particle is a function of $t - t_b$ due to slowing down and thus the anisotropy can be expressed as a function of particle energy. Using $\mathcal{E} \simeq \mathcal{E}_\alpha \exp[-2(t-t_b)/\bar{\tau}_{\rm sl}]$, this yields

$$\Sigma(\mathcal{E}) \simeq \left[\Sigma_0^2 + 2\alpha_0\Lambda_0(1-\Lambda_0)\frac{T_e}{\mathcal{E}}\ln\left(\frac{\mathcal{E}_\alpha}{\mathcal{E}}\right)\right]^{1/2}. \tag{2.16}$$

To keep the local density roughly constant, the distribution function should scale as

$1/\Sigma$. Thus Eq. (2.14) should be replaced by

$$F \simeq AH(\mathcal{E}_\alpha - \mathcal{E})H(R - (1+\eta_0)R_{cr})\frac{\bar{\tau}_{\rm sl}S_{\alpha 0}}{4\pi}\left(\frac{2\mathcal{E}}{m_\alpha}\right)^{-3/2} \times\frac{\Sigma_0}{\Sigma(\mathcal{E})}\exp\left[-\frac{(\mathcal{M}B(R)/\mathcal{E} - (1-\eta_0)\Lambda_0)^2}{2(1-\eta_0)^2\Sigma^2(\mathcal{E})}\right], \tag{2.17}$$

with $\Sigma(\mathcal{E})$ as defined in Eq. (2.16).

Chapter 3

Dynamics of alpha-particles

We now consider specific examples of fusing plasma in order to calculate aspects of α-particle dynamics such as the fraction of particles which are not confined by the magnetic fields in the plasma, and also to establish a model distribution function. From general considerations the distribution can be written as a function of the constants of the motion. Before going into detailed calculations of the distribution function, we return to notion of $\mathcal{M}$ as a constant of the motion and describe its relationship to the usual definition of the magnetic moment as $\mu = mv_\perp^2/2B$.

3.1 Adiabatic invariants and the magnetic moment

In general, if there is periodic motion whose parameters are slowly varying, we can define an adiabatic invariant as the action associated with the motion, $I = \int pdq/2\pi$. In our case, for cyclotron motion in a slowly changing magnetic field and approximating $\vec{p} = m\vec{v}$,

$$I_\mu = \int_0^{2\pi} mv_\perp r_\perp d\varphi/2\pi = \frac{2m}{q}\mu.$$

If the magnetic field is constant in time, then this is a real constant of the motion, but only to lowest order in the expansion parameter ρ/L_B. For a time-varying magnetic

field, μ is slowly changing so long as $|\Omega| \gg |(1/B)\partial B/\partial t|$

We can explicitly calculate $d\mu/dt$ for μ defined as above, in order to show that it is not an exact constant of the motion, even for $\partial B/\partial t \equiv 0$. We obtain

$$\frac{d\mu}{dt} = -\frac{\mu}{B}\left(\frac{\partial B}{\partial t} + \vec{v}\cdot\vec{\nabla}_x B\right) - \frac{v_{||}}{B}\left(\frac{\partial}{\partial t}\hat{e}_{||} + \vec{v}\cdot\vec{\nabla}_x \hat{e}_{||}\right)\cdot\vec{v}_{\perp}. \tag{3.1}$$

However, averaging over the gyrophase φ defined by $\vec{v}_{\perp} = v_{\perp}(\hat{e}_1\cos\varphi + \hat{e}_2\sin\varphi)$ yields $\langle d\mu/dt\rangle_{\varphi} = -(\mu/B)\partial B/\partial t$.

This suggests the existence of a quantity $\mathcal{M}$ which is always close in value to μ and which is the true adiabatic invariant: $\mathcal{M}$ varies only on the time scale of the magnetic field variations, and $d\mathcal{M}/dt$ is small to all orders of perturbation in the quantity $|(1/\Omega B)\partial B/\partial t|$.

Also, note that despite the fact that

$$\left\langle \frac{d\mu}{dt} \right\rangle_{\varphi} = 0,$$

$\mathcal{M}$ is not equal to $\langle\mu\rangle_{\varphi}$. In most textbook derivations of the invariance of μ, the average over gyromotion and the approximation that variations in space and time are neglected in a single gyroorbit are taken implicitly, by considering the motion of the guiding center. Coordinates of the guiding center are used even if not explicitly described as such, or only referred to as the "average position" of the particle. For example, in the case of $\partial B/\partial t = 0$, the force (written as if acting on the guiding center) may be expressed as $F_{||} = -\mu\partial B/\partial s$. Thus,

$$m\frac{dv_{||}}{dt} = -\mu\frac{\partial B}{\partial s} \qquad \Rightarrow \qquad \frac{d}{dt}\left(\frac{1}{2}mv_{||}^2\right) = -\mu\frac{dB}{dt},$$

and energy conservation yields

$$0 = \frac{d}{dt}(\mu B) + \frac{d}{dt}\left(\frac{1}{2}mv_{||}^2\right) = B\frac{d\mu}{dt}$$

if the difference between $\mathcal{M}$ and μ is neglected.

We see from Eq. (3.1) that the relevant expansion parameter is ρ/L_B, and we can calculate the first order correction μ_1 to the adiabatic invariant by using this equation perturbatively. The dominant term in the LHS arises from $\Omega\partial\mu/\partial\varphi$, and thus the correction to μ is determined up to a constant by integrating the RHS of this equation over φ, yielding the rapidly varying term $\tilde{\mu}_1$. Then $\bar{\mu}_1 = \mu_1 - \tilde{\mu}_1$ can be determined from the constraint

$$\langle \vec{v} \cdot \nabla \mu_1 \rangle_\varphi = 0,$$

yielding

$$\begin{aligned} \tilde{\mu}_1 &= -\frac{1}{B}\vec{v}_\perp \cdot \vec{v}_d - \frac{v_\parallel}{4\Omega B}\left\{(\vec{v}_\perp \cdot \nabla \hat{e}_\parallel) \cdot (\vec{v}_\perp \times \hat{e}_\parallel) + [(\vec{v}_\perp \times \hat{e}_\parallel) \cdot \nabla \hat{e}_\parallel] \cdot \vec{v}_\perp\right\}, \\ \bar{\mu}_1 &= -\frac{v_\parallel v_\perp^2}{2B\Omega}\, \hat{e}_\parallel \cdot \nabla \times \hat{e}_\parallel, \end{aligned} \tag{3.2}$$

with $\vec{v}_d$ defined as before. For first order corrections this can be evaluated at the physical particle coordinates. Because the average of μ over an orbit is not exactly equal to $\mathcal{M}$, the average pitch angle is also not simply related to U. Thus for a more general $F_s(\vec{x}, \mathcal{E}, v_\parallel)$, the proper integral equation for the distribution function to $\mathcal{O}(\lambda^2)$ would be

$$F(\mathcal{E}, \mathcal{M}, \mathcal{L}_\zeta) \propto \oint F_s(\vec{X}_g(\tau), \mathcal{E}, U(\tau) - (1/q_\alpha)\mathcal{M}\hat{e}_\parallel(\tau) \cdot \nabla \times \hat{e}_\parallel(\tau))d\tau.$$

3.2 Distribution function in guiding center coordinates

Because we are primarily interested in the interaction of α-particles with high frequency modes ($\omega \gtrsim \Omega_\alpha$) that require a microscopic treatment, we shall incorporate corrections to Eq. (2.7) of the order of λ as derived in Refs.[8] and [9] in the so-called gyrokinetic approximation. In this formalism a distribution function of the form of Eq. (2.7) is expanded in the parameter λ by first taking $\mathcal{M} \simeq \mu$ as the lowest order distribution function F_0. Corrections arising from the difference between $\mathcal{M}$ and μ

are then taken into account by Taylor expanding about $\mathcal{M}$. In terms of the guiding center variables $\vec{X} = \vec{x} + \vec{v} \times \hat{e}_{||}/\Omega_\alpha$, $\mathcal{E}$, μ, and φ we have

$$F(\mathcal{E}, \mathcal{M}, \mathcal{L}_\zeta) \simeq F(\vec{X}, \mathcal{E}, \mu) + \mu_1(\vec{X}, \mathcal{E}, \mu, \varphi)\frac{\partial}{\partial \mu}F(\vec{X}, \mathcal{E}, \mu) + \mathcal{O}\left(\lambda^2\right) \equiv F_0 + F_1, \quad (3.3)$$

where F_0 is gyrophase-independent when expressed using guiding center variables, and $F_1 \equiv \mu_1 \partial F_0 \partial \mu$ is the $\mathcal{O}(\lambda)$ correction which arises from the fact that μ is only an approximation to the magnetic moment. Corrections to the guiding center position, on the other hand, do not come in until second order in λ. In order simplify the notation and avoid complicated expressions for $\mathcal{M}$ and $\mathcal{L}_\zeta$, we will consider only F_0 which is a function of the magnetic moment μ and the guiding center location, and obtain the final form for F by adding the correction F_1. This is convenient because the guiding center coordinates perpendicular to the magnetic field only change due to the magnetic drifts which are smaller by order λ. The functional form of F and F_0, however, are the same and so we have

$$F_0 = \mathcal{F}_0(\mathcal{E}, \mu, r, \vartheta)\delta(\mathcal{E} - \mathcal{E}_\alpha)\frac{n_\alpha}{4\pi\sqrt{2\mathcal{E}_\alpha/m_\alpha^3}}, \quad (3.4)$$

where ϑ and r are the coordinates of the guiding centers. All spatial coordinates below will refer to the location of the guiding center $\vec{X}$ unless otherwise indicated.

To understand the nature of the relevant α-particle orbits, we distinguish between the effects of the guiding center drifts and the rotational transform of the magnetic field. In the following we take $B_\zeta > 0$ as the main component of the magnetic field and approximate $B_\zeta \simeq B \simeq B_0 R_0/R$, where R is the major radius or distance from the axis of symmetry and R_0 is the major radius at the magnetic axis. Because this quantity only appears in $\mathcal{O}(\lambda)$ corrections to the expression for the distribution function, this approximation neglects terms of the order of $\lambda r^2/q^2 R_0^2$ where r is the minor radius and $q = rB_\zeta/R_0 B_\vartheta$ is the inverse rotational transform. Thus $\mathcal{L}_\zeta \simeq q_\alpha R_g A_\zeta(\vec{X}) + m_\alpha R v_{||}$, where U has similarly been approximated by $v_{||}$. The resulting particle orbits correspond to a guiding center equation of motion $d\vec{X}/dt \simeq v_{||}\hat{e}_{||} + \vec{v}_d$.

where

$$\vec{v}_d \simeq -\frac{1}{m_\alpha R\Omega_\alpha(\vec{X})}\left[2\mathcal{E} - \mu B(\vec{X})\right](\hat{e}_\vartheta \cos\vartheta + \hat{e}_r \sin\vartheta)\,.$$

A small component of the guiding center drift in the toroidal direction has been neglected. This quantity $\vec{v}_d$ corresponds to the drift from the toroidal magnetic field alone, and for $B_\zeta > 0$ lies in the $-\hat{e}_z$ direction where $z = r\sin\vartheta$.

3.3 Alpha-particle orbits

We choose experimental parameters typical of JET[1] where $B \simeq 2.8$ T, $R_0 \simeq 3.5$ m, and $\epsilon \equiv a/R_0 \sim 0.3$, and we consider a magnetic field configuration where $q(r) \simeq 1{+}2.5r^2/a^2$. To note the importance of the particle drift for α-particles in these experimental configurations, we observe that for a particle at the edge of the plasma column ($r \simeq a$) with $|v_{||}| = v_\alpha$ the ratio of the toroidal velocity component of the canonical angular momentum to the magnetic field component (which ties particles to magnetic flux surfaces) is given by $4\rho_\alpha R/a^2 \simeq 1.2$ so large radial excursions are possible which would take particles at the edge into the core of the plasma.

In addition, at the plasma edge stationary orbits, analogous to very deeply trapped particles because of the small poloidal angle encompassed, occur when

$$\frac{v_{||}}{v_\perp} \simeq \frac{\rho_\alpha q(a)}{2a} \simeq 0.16,$$

which is a small change in pitch angle from $v_{||} = 0$ but represents a significant departure from the banana-orbit approximation where the radial excursion is independent of the sign of $v_{||}$.

The production of α-particles through fusion is concentrated mainly in the core of the plasma and the peak of the distribution function at the mode layer corresponds to trapped particles whose orbits span a wide range in radius and intersect with the mode at the outer edge. If in particular we consider particles at the origin, characterizing the particle velocity at the origin as $v_{||0}$ for the component along the field line and $v_{\perp 0}$ for the perpendicular velocity, one of the trapping conditions is $v_{||0} < 0$, that is only

particles whose velocities at the origin are oriented opposite the magnetic field (and thus the toroidal current) can be trapped, and also their pitch angle has to be such that $|v_{\|0}/v_{\perp 0}| \leq (2\rho_\alpha/R_0)^{1/3} \simeq 0.73\,[R_0(\mathrm{m})B_0(\mathrm{T})]^{-1/3} \simeq 0.34$, with parameters taken as above. This expression is still approximately valid for orbits that originate close to the magnetic axis. An example of the projection on the (r, ϑ) plane of such an orbit is shown in Fig. 3-1, where the direction of motion of the particle is indicated. At the point of the largest radial excursion from the core of the plasma[15], the corresponding value of the pitch angle for the given form of $q(r)$ is given by

$$\frac{v_\|}{v_\perp} \simeq \left(\frac{2\rho_\alpha}{R_0}\right)^{1/3} \left[1 + \frac{r}{(2\rho_\alpha)^{2/3} R_0^{1/3}}\right]^{1/2}. \tag{3.5}$$

With $\mathcal{E} = \mathcal{E}_\alpha$, this trapping condition determines the quantity Λ_0 in Eq. (2.9).

To obtain the above condition on $v_{\|0}/v_{\perp 0}$, we combine the constancy of $\mathcal{L}_\zeta$ with the limiting case for a trapped orbit, that is defined by the fact that the turning point occurs at $\vartheta \simeq \pi$, this gives the value of the pitch angle corresponding to the largest characteristic trapped orbit. This pitch angle can be rewritten in terms of the radius of the turning point r_t using $v_\|(r_t, \vartheta = \pi) \simeq 0$ which yields

$$\frac{v_{\|0}}{v_{\perp 0}} \simeq -\sqrt{\frac{r_t}{R_0}}.$$

The radius r_t must satisfy the condition of constancy of toroidal angular momentum so that $\mathcal{L}_\zeta(r = 0) \simeq \mathcal{L}_\zeta(r_t, \vartheta = \pi)$, which for the profile considered can be expressed as

$$R_0 v_{\|0} \simeq -\frac{q_\alpha B_0}{m_\alpha} \frac{a^2}{5} \ln\left(1 + 2.5\frac{r_t^2}{a^2}\right),$$

using the approximation $B_\vartheta(r_t, \vartheta = \pi) \simeq r_t B_0/q(r_t)R_0$. By combining these two equations, we finally obtain the condition on the pitch angle given above. Note that for the parameters considered the radial excursion of the orbit is significantly greater than that obtained for the limit of a deeply trapped banana orbit[15]. Another difference from this limit is that in the case of large radial excursion the range of parallel velocities corresponding to trapped orbits is not symmetric about $v_{\|0} = 0$.

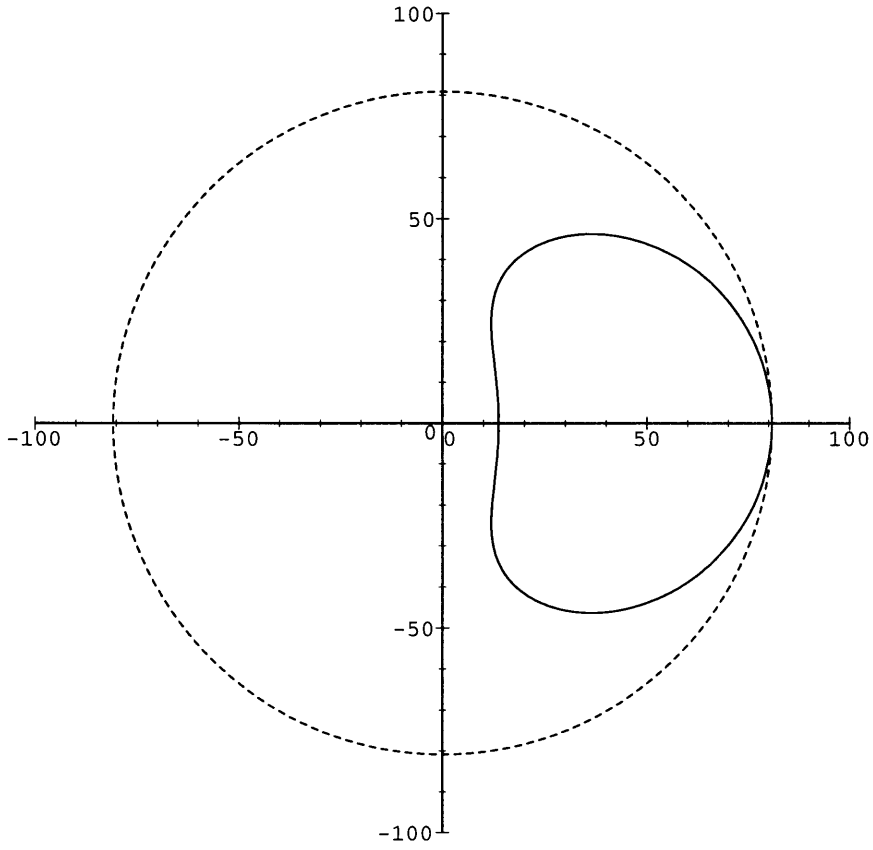

Figure 3-1: Typical orbit of a fusion-produced α-particle which is magnetically trapped, transits close to the center of the plasma column and undergoes a large radial excursion. The dashed line indicates the outermost flux surface reached by the particle.

3.4 Numerical results

For a numerical evaluations of $\mathcal{F}_0$ and other aspects of the α-particle dynamics we adopt the following two density, temperature and q profiles:
Standard profile:

$$\begin{aligned} n &= n_0(1 - r^2/a^2)^{1/2} \\ T_i &= T_{i0}\left(1 - \frac{6r^2/a^2}{1 + 8r^2/a^2}\right) \\ q(r) &= (1 + 2.5r^2/a^2); \end{aligned} \tag{3.6}$$

Peaked profile:

$$\begin{aligned} n &= n_0(1 - r^2/a^2) \\ T_i &= T_{i0}\exp\left(-3r^2/a^2\right) \\ q(r) &= (1 + 2.5r^2/a^2), \end{aligned} \tag{3.7}$$

where $q(r)$ is the magnetic field unwinding function. We choose n_0 and T_{i0} to model the measurements of peak density and temperature from Ref.[1]. The corresponding physical dimensions are $R_0 \simeq 3.50$ m and $\epsilon \equiv a/R_0 \simeq 0.3$, although effects of different experimental geometries are considered as well. The form for the distribution function used in Eq. (2.9) is sufficiently robust to model a wide variety of profiles, as long as the density and temperature are peaked at the center of the plasma. The values of the numerical constants used in this model are weakly dependent on the shape of the background profiles.

Our numerical calculations with a "standard" profile and neglecting collisions are consistent with the following values for the constants previously introduced at $r \simeq 0.75\ a$: $\Lambda_0 \simeq 0.8$, $\Sigma \simeq 5 \times 10^{-2}$, $\vartheta_{cr} \simeq \pi/3$, $A \simeq 1/3$. The density according to the model is roughly given by $n_\alpha \simeq 0.03\ n_{\alpha 0}$, and if the contribution of passing particles is included then $n_\alpha \simeq 0.07\ n_{\alpha 0}$. The core density is roughly $0.6\ n_{\alpha 0}$.

In Figs. 3-2 and 3-3, the normalized distribution function $\mathcal{F}$ at $r = 0.75\ a$ is shown for poloidal angles $\vartheta = 0$ and $\vartheta = \pi/4$ as a function of $v_{\|}/v_{\alpha}$. The distribution function at the center of the plasma is shown in Fig. 3-4. These calculations are for the "normal" plasma profiles characteristic of experiments on the JET machine. At larger poloidal angles, first orbit losses becomes increasingly important; thus, at $\vartheta = \pi/2$, there are no orbits for 3.5 MeV α-particles which are confined.

In Fig. 3-5, the total fraction of α-particles whose orbits are not confined within the plasma is shown versus the quantity ρ_{α}/a. This fraction is only weakly dependent on aspect ratio, especially when $\rho_{\alpha}/a \gtrsim 0.1$, and inverse aspect ratios in the range $0.25 \leq \epsilon \leq 0.4$ are shown. The two cases of the standard and peaked profiles as given by Eqs. (3.6) and (3.7) are compared with each other. In addition, the fraction of α-particles which pass the flux surface defined by $r = 0.75\ a$ but which are not lost is shown in Fig. 3-6. Note that the calculations are for a fixed $q(r)$ profile; in general, the dependence on the magnetic field geometry is included by considering the "poloidal gyroradius"

$$\rho_{\vartheta} \equiv \rho_{\alpha} \left| \frac{B_{\vartheta}}{B} \right| \simeq \frac{\rho_{\alpha} r}{R_0 q(r)}.$$

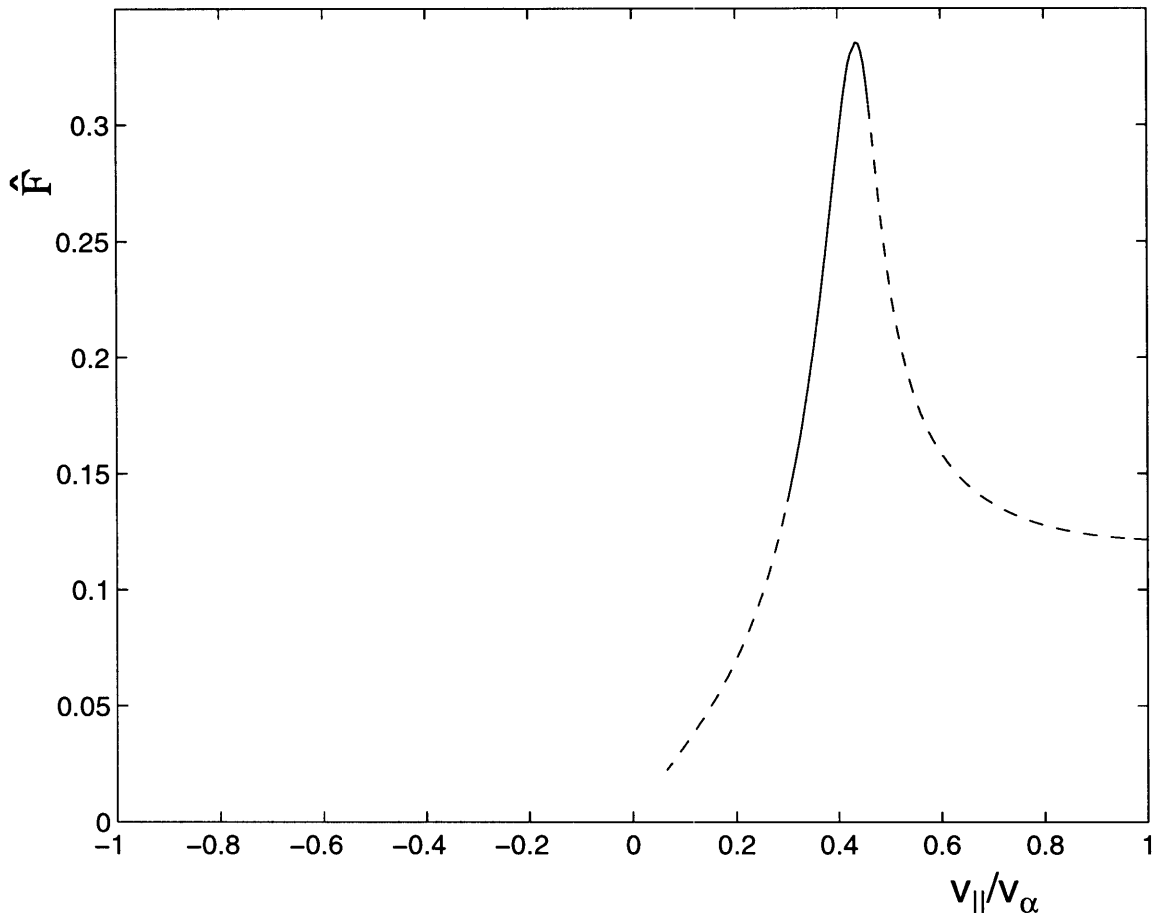

Figure 3-2: Normalized distribution function at $r = 0.75\ a$, $\vartheta = 0$, shown as a function of $v_{||}/v_\alpha$. The solid line corresponds to trapped particles, and the dashed line corresponds to passing particles.

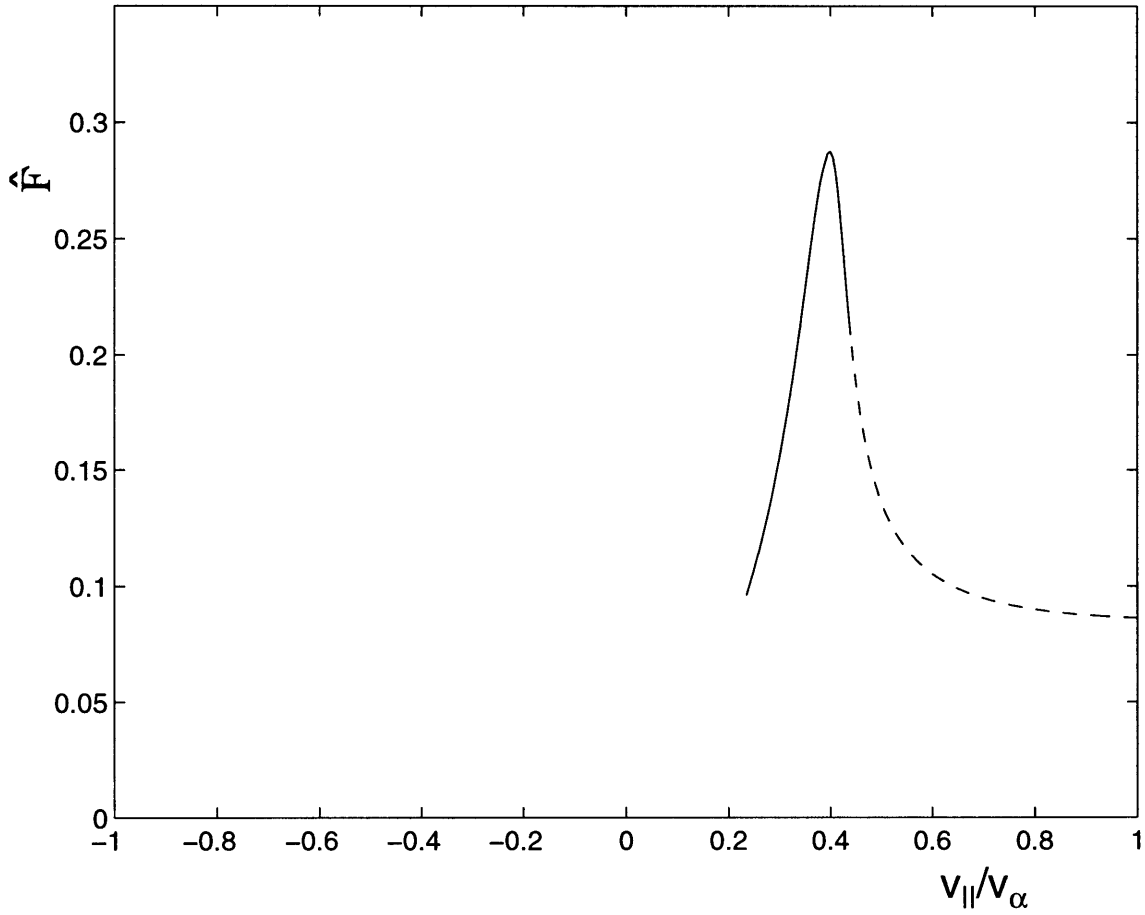

Figure 3-3: Normalized α-particle distribution function at $r = 0.75\ a$, $\vartheta = \pi/4$, shown as a function of $v_{||}/v_\alpha$. The solid line corresponds to trapped particles, and the dashed line corresponds to passing particles.

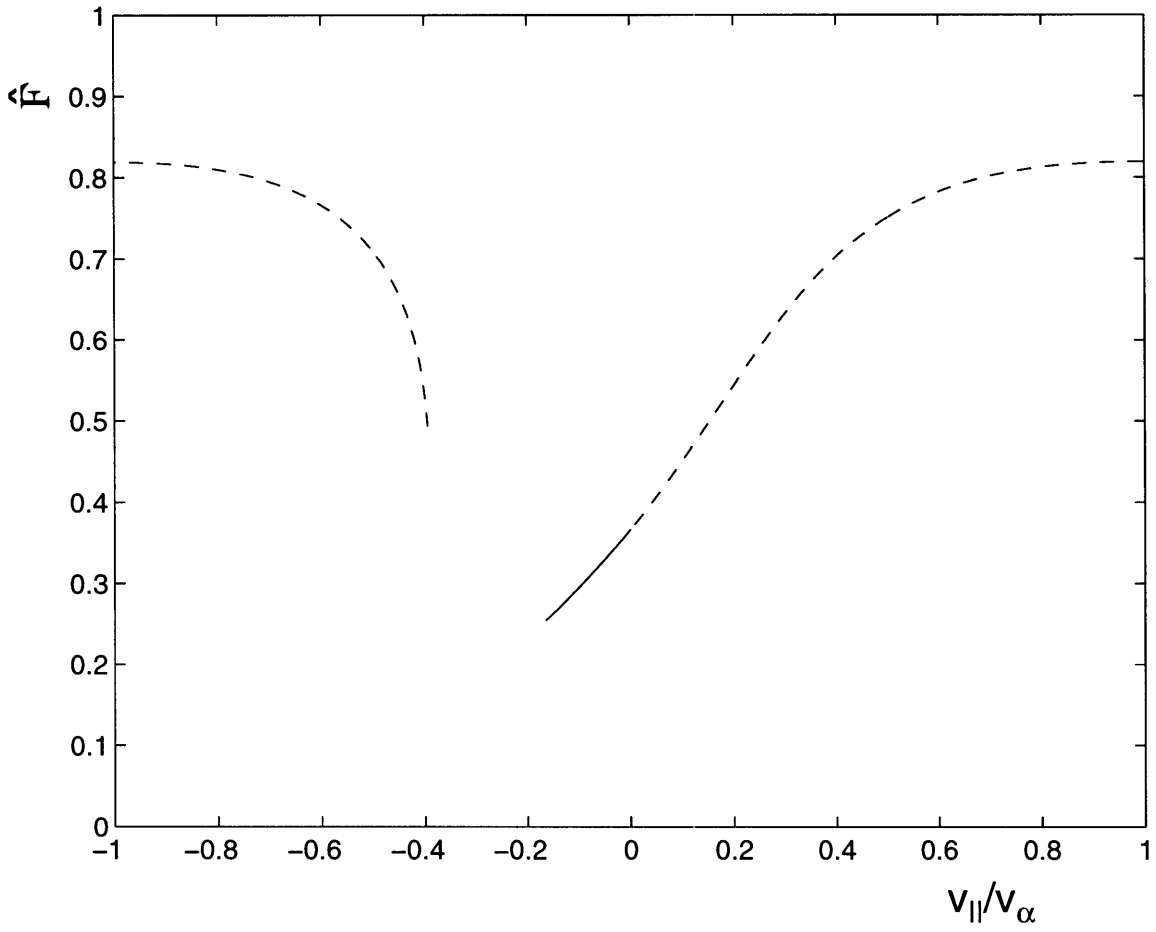

Figure 3-4: Normalized α-particle distribution function at $r = 0$, shown as a function of $v_{\|}/v_{\alpha}$. The solid line corresponds to trapped particles, and the dashed line corresponds to passing particles.

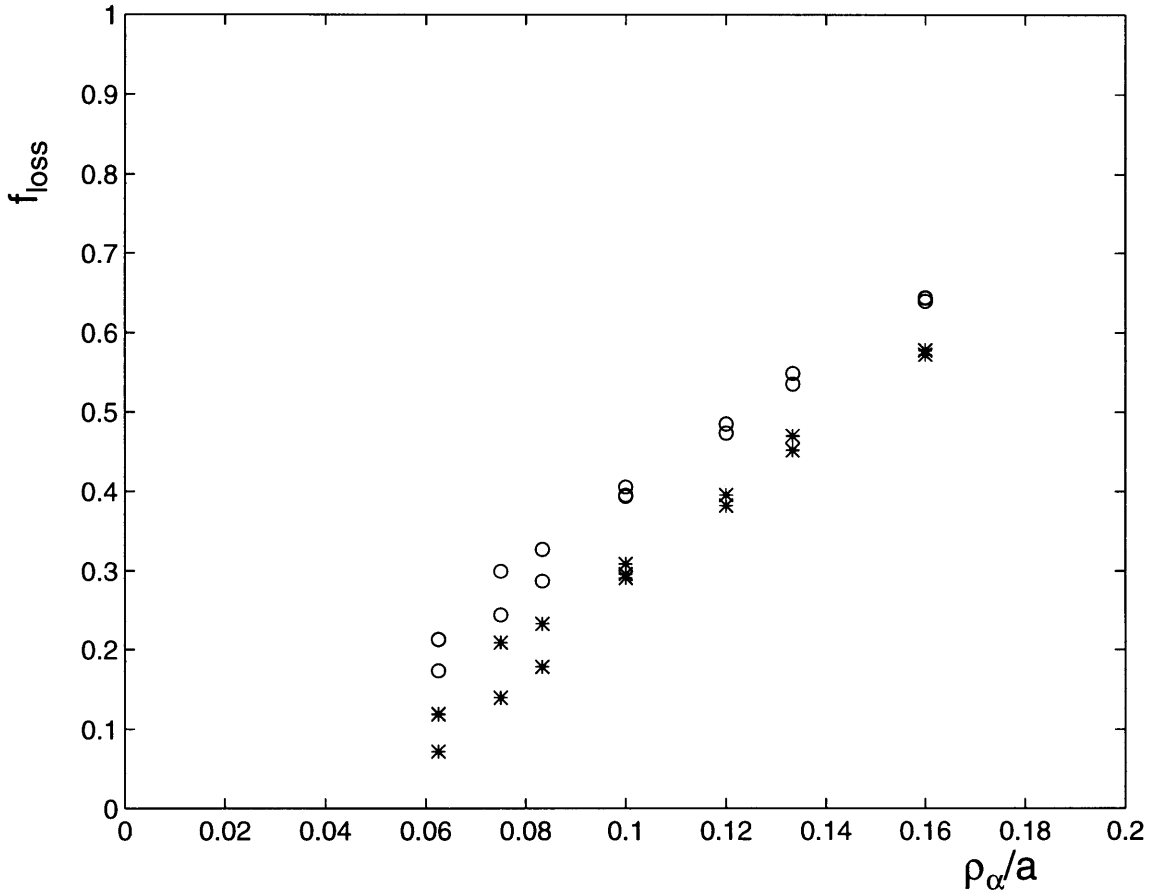

Figure 3-5: Fraction of α-particles created by fusion which suffer first orbit losses out of the plasma. Results are plotted against ρ_α/a, with ρ_α measured on the magnetic axis and a the minor radius. Values of the aspect ratio ranging from 2.5 to 4 are included. The open circles are for the standard density profile, the asterisks are for the peaked density profile.

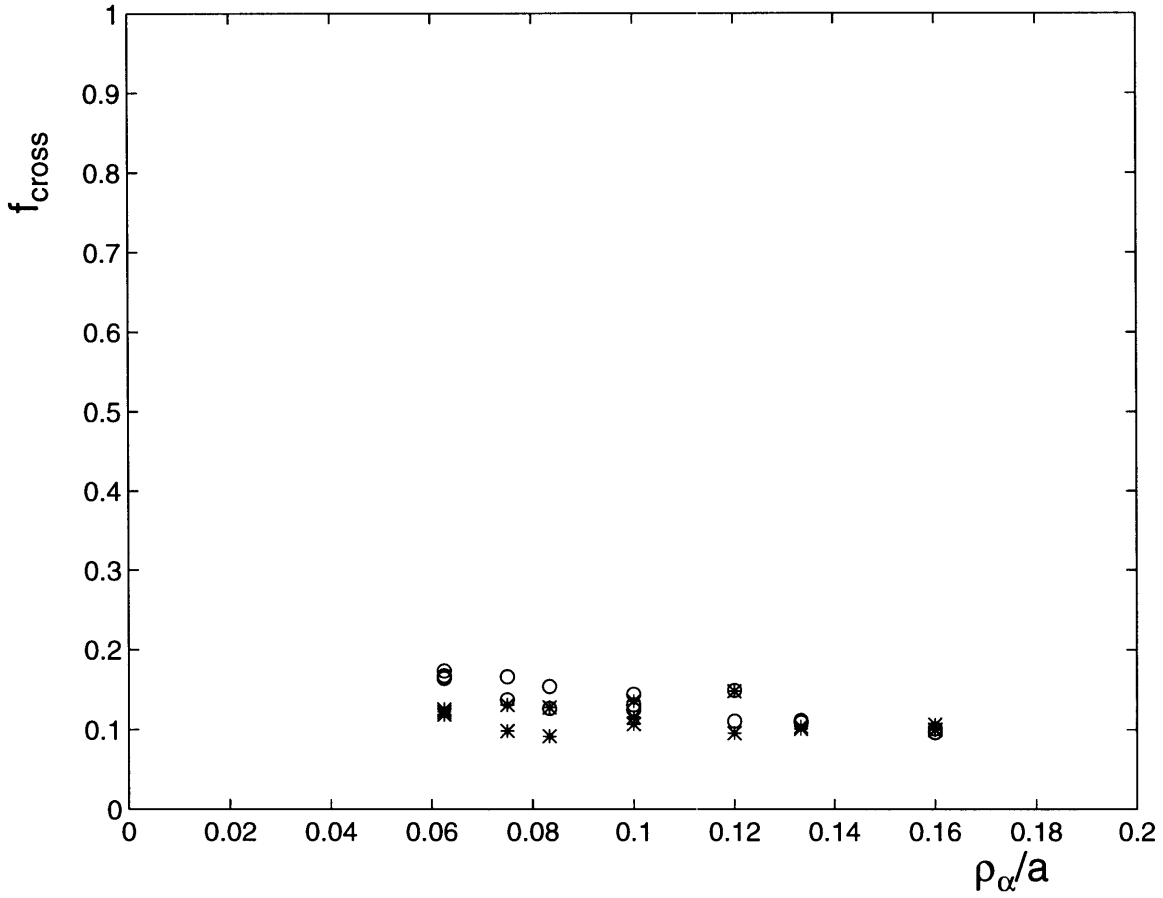

Figure 3-6: Fraction of α-particles created by fusion whose orbits intersect the flux surface defined by $r = 0.75\ a$ and which do not suffer first orbit losses. Results are plotted against ρ_α/a, with ρ_α measured on the magnetic axis and a the minor radius. Values of the aspect ratio ranging from 2.5 to 4 are included. The open circles are for the standard density profile, the asterisks are for the peaked density profile.

Chapter 4

Characteristic equation for the contained mode

In this chapter the mode equation defining the contained mode is derived in a cold inhomogeneous magnetized plasma with one ion species, for waves that have frequencies in the range $\Omega_i < \omega \ll \Omega_e$ and in the limit of high poloidal mode numbers. Here, Ω_i and Ω_e are the cyclotron frequencies of the main ion species and of the electrons. We also consider the limit where the mode propagates nearly perpendicular to the equilibrium magnetic field. In the homogeneous case, this mode is reduces to the magnetosonic-whistler wave. First, the dynamics of the magnetosonic-whistler wave in a homogeneous plasma are analyzed in detail, in particular noting the contribution of the Hall term in Ohm's law. The magnetosonic-whistler wave which is found by this analysis is a generalization of the magnetosonic wave, also referred to as the compressional Alfvén wave, to include effects that become particularly important when $\omega \gtrsim \Omega_i$. The magnetosonic wave has the dispersion relation $\omega^2 = k_\perp^2 v_A^2$, where v_A is the Alfvén velocity. The effects of inhomogeneity are then examined by considering a cylindrical plasma. This is used as an approximation to a toroidal configuration. The mode equation for this type of wave in a cylindrical plasma is derived, and we show analytically that there exist solutions which are localized within a radial shell in the plasma. The Hall term is shown to have significant effects on the mode solutions beyond what was found for the homogeneous case.

4.1 Magnetosonic-whistler wave in a homogeneous plasma

We summarize the magnetosonic-whistler wave equations for a homogeneous plasma and evaluate the polarization of the fields and the dynamics of the plasma, as this information can be related to the local properties of the contained mode. We orient our coordinate system so that the equilibrium magnetic field is $\vec{B}_0 = B_0\hat{e}_z$ and the perturbation has wave vector $\vec{k} = k_{||}\hat{e}_z + k_\perp\hat{e}_y$, where $\hat{e}_y$ is used to represent directions perpendicular to the equilibrium magnetic field. The perturbed magnetic field lies mainly in the direction parallel to the unperturbed magnetic field and is taken to have the form

$$B_{1||}(y,z,t) = B_{1||}\exp(-i\omega t + ik_{||}z + ik_\perp y)$$

We consider all field perturbations to have an analogous form. The magnetosonic-whistler mode is here derived for a hydrogenic plasma in terms of the plasma density $n \equiv n_e \simeq n_i$, current $\vec{J}$, and (ion) fluid velocity $\vec{V}$.

The electromagnetic equations are:

$$\nabla \times \vec{E}_1 = -\frac{\partial}{\partial t}\vec{B}_1, \tag{4.1}$$

$$\nabla \times \vec{B}_1 \simeq \mu_0 \vec{J}_1. \tag{4.2}$$

Combining these equations yields

$$\frac{\partial}{\partial t}\vec{J}_1 \simeq \frac{1}{\mu_0}\left[\nabla^2\vec{E}_1 - \nabla(\nabla\cdot\vec{E}_1)\right]. \tag{4.3}$$

Ohm's law is given by

$$\vec{E}_1 + \vec{V}_1 \times \vec{B} \simeq \frac{1}{en}\vec{J}_1 \times \vec{B}, \tag{4.4}$$

where the right-hand side is the Hall term, being the most significant correction to ideal magnetohydrodynamics (MHD) high-temperature plasmas at low β and for

$k^2 d_e^2 \ll 1$ so that electron inertia can be neglected. Here

$$\beta \equiv 2\mu_0 n(T_i + T_e)/B^2$$

and

$$d_e^2 \equiv c^2/\omega_{pe}^2.$$

The total momentum balance equation can be written in the following form:

$$m_i n \frac{\partial}{\partial t}\vec{V}_1 \simeq en(\vec{E}_1 + \vec{V}_1 \times \vec{B}) \simeq \vec{J}_1 \times \vec{B}. \tag{4.5}$$

In terms of the perturbed electron velocity $\vec{u}_{e1}$, the current is given by $\vec{J}_1 = en(\vec{V}_1 - \vec{u}_{e1})$ and so Eq. (4.4) can be rewritten as the electron force balance equation

$$-en(\vec{E}_1 + \vec{u}_{e1} \times \vec{B}) \simeq 0.$$

Here we use the cold plasma approximation which neglects pressure forces. For magnetosonic-whistler modes, and for the class of modes to be considered below, this approximation is valid in the regime $v_A \gg v_{\mathrm{th}i}$ where v_A is the Alfvén velocity defined by $v_A^2 = B^2/\mu_0 n m_i$ and $v_{\mathrm{th}i}$ is the ion thermal velocity $(2T_i/m_i)^{1/2}$. The ratio

$$\frac{v_{\mathrm{th}i}}{v_A} = \left(\frac{2\mu_0 n T_i}{B^2}\right)^{1/2} \equiv \beta_i^{1/2} \simeq 0.21 \left(\frac{n}{10^{20}\ \mathrm{m}^{-3}}\right)^{1/2} \left(\frac{T_i}{10\ \mathrm{keV}}\right)^{1/2} \left(\frac{B}{3\ \mathrm{T}}\right)^{-1},$$

where β_i is the contribution of the ion thermal energy to the plasma β. Note that we immediately have $E_{1z} = 0$ and $V_{1z} = 0$. Equation (4.4) is a more accurate description of the plasma dynamics than the usual frozen-in law in ideal MHD.

The x-component of Eq. (4.5) combined with the y-component of Eq. (4.3) gives

$$V_{1x} = \frac{Bk_\parallel^2}{\mu_0 m_i n \omega^2} E_{1y} = \frac{k_\parallel^2 v_A^2}{\omega^2} \frac{1}{B} E_{1y}. \tag{4.6}$$

Combining this with the y-component of Eq. (4.4) yields

$$E_{1y}\left(1-\frac{k_{\|}^2 v_A^2}{\omega^2}\right)=-\frac{B}{en}J_{1x}. \tag{4.7}$$

For a mode that propagates nearly perpendicular to the equilibrium magnetic field, $k_{\|}^2 \ll k_{\perp}^2$, this is similar to a magnetosonic wave and so $\omega^2 \sim k_{\perp}^2 v_A^2 \gg k_{\|}^2 v_A^2$. Thus $enV_{1x} \ll J_{1x}$, and the current in the x direction is carried by the electrons. In this case $J_{1x} \simeq -enE_{1y}/B$, indicating that this component of the current is driven by the $\vec{E}\times\vec{B}$ drift of the electrons.

The polarization of the wave can be evaluated by looking at the x-component of Ohm's law combined with the y-component of Eq. (4.5):

$$E_{1x}=\frac{B}{en}J_{1y}+i\frac{B^2}{\omega n m_i}J_{1x}=\mu_0 D_H J_{1y}+i\mu_0\frac{v_A^2}{\omega}J_{1x}, \tag{4.8}$$

where

$$D_H \equiv \frac{B}{\mu_0 en}$$

has the dimensions of a diffusion coefficient and is related to the Hall effect. The current components can be expressed in terms of E_{1y} using Eq. (4.7) and the y-component of Eq. (4.3); noting that $\Omega_i = v_A^2/D_H$ we obtain

$$\frac{E_{1y}}{E_{1x}}=\frac{i\omega}{\Omega_i\left(1-k_{\|}^2 v_A^2/\omega^2\right)+k_{\|}^2 D_H^2}\simeq\frac{i\omega}{\Omega_i+k_{\|}^2 D_H^2}. \tag{4.9}$$

To find the dispersion relation we obtain another expression for the polarization of the wave by combining Eq. (4.7) with the x-component of Eq. (4.3) to yield

$$\frac{E_{1y}}{E_{1x}}=i\frac{k^2 D_H}{\omega}\frac{1}{1-k_{\|}^2 v_A^2/\omega^2}. \tag{4.10}$$

From the two forms of the wave polarization, Eqs. (4.9) and (4.10), we obtain

$$\left(1-\frac{k_{\|}^2 v_A^2}{\omega^2}\right)\left(1-\frac{k^2 v_A^2}{\omega^2}\right)=\frac{k_{\|}^2 k^2 D_H^2}{\omega^2}. \tag{4.11}$$

In the limit $k_{||} \ll k_{\perp}$ with $\omega^2 \sim k_{\perp}^2 v_A^2$ this reduces to

$$\omega^2 \simeq k_{\perp}^2 (v_A^2 + k_{||}^2 D_H^2) = k_{\perp}^2 v_A^2 (1 + k_{||}^2 d_i^2), \tag{4.12}$$

where

$$d_i \equiv c/\omega_{pi} = v_A/\Omega_i.$$

Note that because of this dispersion relation, the condition $k_{\perp}\rho_i \ll 1$, where ρ_i is the ion gyroradius, is satisfied when $\omega \ll \Omega_i v_A/v_{\mathrm{th}i}$, so we see that finite Larmor radius effects are negligible even for frequencies significantly higher than the ion cyclotron frequency. For frequencies much larger than the ion cyclotron frequency, the appropriate condition for neglecting finite Larmor radius effects is $k_{\perp}\rho_i \ll \omega/\Omega_i$, which is always valid if $v_A \gg v_{\mathrm{th}i}$.

In Eq. (4.12) the term involving parallel propagation represents what we call, because of the form of the dispersion relation, the "whistler" contribution to the mode. Even when this is a small correction to the frequency of the mode the Hall term in Eq. (4.4) has other significant effects for the mode solution in the inhomogeneous case.

Note that combining Eqs. (4.3), (4.7) and the y-component of (4.5) yields

$$\frac{J_{1y}}{enV_{1y}} \simeq -k_{||}^2 d_i^2 = -\frac{k_{||}^2 D_H^2}{v_A^2},$$

so that in the case $k_{||}^2 d_i^2 \ll 1$ where the dispersion relation becomes approximately $\omega^2 \simeq k_{\perp}^2 v_A^2$, which is the limit of the magnetosonic wave, then is it also true that $|J_{1y}| \ll |enV_{1y}|$.

In terms of electromagnetic potentials, defined by $\vec{B}_1 = \nabla \times \vec{A}_1$ and $\vec{E}_1 = -\nabla\Phi_1 - \partial\vec{A}_1/\partial t$, from $E_{1z} = 0$ we find that $-ik_{||}\Phi_1 + i\omega A_{1z} = 0$. Then, choosing the gauge $\nabla \cdot \vec{A}_1 = 0$, we find that $A_{1y} = -k_{||}^2\Phi_1/\omega k_{\perp}$. In addition,

$$E_{1y} = -ik_{\perp}\Phi_1 + i\omega A_{1y} = -ik_{\perp}\Phi_1 \left(1 + \frac{k_{||}^2}{k_{\perp}^2}\right) \simeq -ik_{\perp}\Phi_1,$$

that is, the y-component of the perturbed electric field is dominated by the electrostatic term $-ik_\perp\Phi_1$. We have from Eq. (4.9) that if $\omega \gtrsim \Omega_i$, the wave becomes elliptically polarized with the largest component in the y direction. The perturbed magnetic field lies mainly in the parallel direction, with the other components smaller by a factor of $k_\parallel/k_\perp$.

If we consider a two-ion species plasma (e.g., a main species i and impurity species I), the dispersion relation as given by Eq. (4.12) becomes instead[16]

$$\omega^2\frac{\omega^2-\bar{\bar{\Omega}}}{\omega^2-\Omega_{hy}} = k_\perp^2(\bar{v}_A^2 + k_\parallel^2 D_H^2), \tag{4.13}$$

where $\bar{v}_A^2 = D_H(\alpha_i\Omega_i + \alpha_I\Omega_I)$, $\Omega_{hy}^2 = \Omega_i\Omega_I(\bar{\bar{\Omega}}/\bar{\Omega})$, $\bar{\Omega} = \alpha_i\Omega_i + \alpha_I\Omega_I$, $\bar{\bar{\Omega}} = \alpha_i\Omega_I + \alpha_I\Omega_i$, $\alpha_i = n_i/n_e$, $\alpha_I = n_I/n_e$. We note that the main effect of having a second species is to introduce a cutoff ($k = 0$) and a resonance ($k \to \infty$), that we denoted by $\bar{\bar{\Omega}}$ and Ω_{hy} and that are both below Ω_i.

In terms of B_{1z}, the component of the perturbed magnetic field parallel to the equilibrium magnetic field, the other components of the magnetic field are given by

$$B_{1x} = i\frac{k_\parallel}{k_\perp}\frac{\omega}{\Omega_i}\frac{1}{1+k_\parallel^2 d_i^2 - k_\parallel^2 v_A^2/\omega^2}B_{1z},$$

$$B_{1y} = -\frac{k_\parallel}{k_\perp}B_{1z},$$

where we used the dispersion relation in the form

$$\frac{k^2 v_A^2}{\omega^2} = \frac{1-k_\parallel^2 v_A^2/\omega^2}{1+k_\parallel^2 d_i^2 - k_\parallel^2 v_A^2/\omega^2}.$$

For the case $k_\parallel^2 \ll k_\perp^2$, the frequency is roughly given by $\omega^2 \approx k_\perp^2 v_A^2(1+k_\parallel^2 d_i^2) \gg k_\parallel^2 v_A^2$, and the equation for B_{1x} can be approximated as

$$B_{1x} \simeq i\frac{k_\parallel d_i}{\sqrt{1+k_\parallel^2 d_i^2}}B_{1z}.$$

In this limit, the component of the perturbed magnetic field parallel to the equilibrium

magnetic field is always largest.

The electric field can be expressed in terms of B_{1z} as

$$E_{1x} = -\frac{\omega}{k_\perp} B_{1z},$$

$$E_{1y} = -\frac{\omega}{k_\parallel} B_{1x} = -i\frac{\omega}{k_\perp} B_{1z} \frac{\omega}{\Omega_i} \frac{1}{1 + k_\parallel^2 d_i^2 - k_\parallel^2 v_A^2/\omega^2},$$

$$E_{1z} = 0.$$

In the limit $k_\parallel^2 \ll k_\perp^2$,

$$E_{1y} \simeq -i\frac{\omega}{k_\perp} B_{1z} \frac{k_\perp d_i}{\sqrt{1 + k_\parallel^2 d_i^2}}.$$

Note than when $k_\perp^2 d_i^2 \gg 1$, which is equivalent to $\omega^2 \gg \Omega_i^2$, the y-component of the electric field is much larger than $|E_{1x}| = |\omega B_{1z}/k_\perp|$ and the mode becomes nearly electrostatic.

The electric current is given by

$$J_{1x} = ienv_A \frac{B_{1z}}{B} \frac{k^2}{k_\perp^2} k_\perp d_i,$$

$$J_{1y} = -env_A \frac{B_{1z}}{B} k_\parallel d_i \frac{k_\parallel}{k_\perp} \frac{\omega}{\Omega_i} \frac{1}{1 + k_\parallel^2 d_i^2 - k_\parallel^2 v_A^2/\omega^2},$$

$$J_{1z} = env_A \frac{B_{1z}}{B} k_\perp d_i \frac{k_\parallel}{k_\perp} \frac{\omega}{\Omega_i} \frac{1}{1 + k_\parallel^2 d_i^2 - k_\parallel^2 v_A^2/\omega^2}.$$

In the limit $k_\parallel^2 \ll k_\perp^2$, the largest component of the current is J_{1x}, while the other components are approximately given by

$$J_{1z} = -\frac{k_\perp}{k_\parallel} J_{1y} \simeq -i\frac{k_\parallel d_i}{\sqrt{1 + k_\parallel^2 d_i^2}} J_{1x}.$$

The (ion) fluid velocity lies predominantly in the y-direction. Its components are given by

$$V_{1x} = -i\frac{\omega}{k_\perp} \frac{B_{1z}}{B} k_\parallel^2 d_i^2 \frac{\Omega_i}{\omega} \frac{1}{1 + k_\parallel^2 d_i^2 - k_\parallel^2 v_A^2/\omega^2},$$

$$V_{1y} = \frac{\omega}{k_\perp}\frac{B_{1z}}{B}\frac{1 - k_\parallel^2 v_A^2/\omega^2}{1 + k_\parallel^2 d_i^2 - k_\parallel^2 v_A^2/\omega^2},$$

$$V_{1z} = 0.$$

It is also appropriate to consider the perturbed density n_1, which by quasineutrality is assumed to be similar for the ions and electrons. Using mass conservation,

$$\frac{\partial}{\partial t} n_1 + n\nabla \cdot \vec{V}_1 = 0,$$

we find that

$$n_1 \simeq n\frac{B_{1z}}{B}\frac{1 - k_\parallel^2 v_A^2/\omega^2}{1 + k_\parallel^2 d_i^2 - k_\parallel^2 v_A^2/\omega^2},$$

while from Gauss's law,

$$\nabla \cdot \vec{E}_1 = \frac{e}{\epsilon_0}(n_{i1} - n_{e1}),$$

we have

$$n_{i1} - n_{e1} \simeq n\frac{B_{1z}}{B}\frac{1}{1 + k_\parallel^2 d_i^2 - k_\parallel^2 v_A^2/\omega^2}\frac{\omega^2}{\omega_{pi}^2}.$$

Therefore, quasineutrality is valid as long as $\omega^2 \ll \omega_{pi}^2$. The combined effect of charge separation and electron inertia, which becomes important when kd_e is of order unity, produces a resonance[17] at the lower hybrid frequency, defined by

$$\Omega_{LH}^2 \equiv \frac{\omega_{pi}^2 + (k_\parallel^2/k_\perp^2)\omega_{pe}^2}{1 + \omega_{pe}^2/\Omega_e^2}.$$

For plasmas with $v_A^2 \ll c^2$, this frequency is always much larger than the ion cyclotron frequency; for plasmas with a hydrogenic ion species the ratio is given by

$$\frac{\Omega_i^2}{\Omega_{LH}^2} = \frac{v_A^2/c^2 + m_e/m_i}{1 + (k_\parallel^2/k_\perp^2)(m_i/m_e)}.$$

4.2 Contained mode equation

We now derive the differential equations that govern the radial profile of the perturbed fields in a cylindrical geometry. We focus on the frequency range $\Omega_i \lesssim \omega \ll \Omega_e$. The

cyclotron frequency for deuterium is

$$\Omega_D \text{ [rad/s]} \simeq 1.4 \times 10^8 \left(\frac{B}{3 \text{ T}}\right)$$

and the Alfvén velocity in a deuterium plasma is

$$v_A \text{ [m/s]} \simeq 4.6 \times 10^6 \left(\frac{n}{10^{20} \text{ m}^{-3}}\right)^{-1/2} \left(\frac{B}{3 \text{ T}}\right).$$

This means that for $B \sim 3$ T and $n \sim 10^{20}$ m^{-3} the poloidal wave number has to be $m \gtrsim 15$ for a minor radius $a \simeq 1$ m, looking at the dispersion relation for small $k_{||}$ and considering a mode localized near the edge of the plasma. Thus we look for modes that have large poloidal wave vectors, which correspond to the quantity $k_\perp$ introduced above. We consider an inhomogeneous, collisionless, cold plasma with one main ion species. As seen above we can easily generalize this to include more than one species.

As before, we consider the following equations:

$$nm_i \frac{\partial}{\partial t}\vec{V} = \vec{J} \times \vec{B}, \tag{4.14}$$

$$\vec{E} + \vec{V} \times \vec{B} = \frac{1}{en}(\vec{J} \times \vec{B}). \tag{4.15}$$

The right hand side of Eq. (4.15) is the Hall term. These equations will be combined with Faraday's and Ampère's laws, as given by Eqs. (4.1) and (4.2), with the constraint $\nabla \cdot \vec{B} = 0$. We look at an equilibrium situation where $\vec{V}_0 = 0$, $\vec{E}_0 = 0$ and we refer to a magnetic field configuration represented by

$$\vec{B}_0 = B_{0z}(r)\vec{e}_z + B_{0\vartheta}(r)\vec{e}_\vartheta, \tag{4.16}$$

where $(\vec{e}_r, \vec{e}_\vartheta, \vec{e}_z)$ is a right-handed coordinate system and we consider $B_{0z} > 0$. It is

convenient to introduce the following set of coordinates:

$$\vec{e}_{\|} = \frac{\vec{B}_0}{|\vec{B}_0|}, \qquad \vec{e}_r, \qquad \vec{e}_{\perp} = \frac{\vec{B}_0 \times \vec{e}_r}{|\vec{B}_0|}. \tag{4.17}$$

We solve the linearized equations for a perturbation of the form

$$\vec{B}_1(r, \vartheta, z, t) = \vec{B}_1(r) \exp(-i\omega t - im\vartheta + ik_z z).$$

We intend to use this cylindrical model as a first approximation to toroidal configurations, where corrections to the mode structure are expected to be of the order of $\epsilon \equiv a/R_0$, where a is the radius of the plasma column and R_0 is the distance from the axis of symmetry (major radius). In this case $k_z = n^0/R_0$, where n^0 is the toroidal mode number. Defining the wave vector as $\vec{k} = -(m/r)\vec{e}_\vartheta + k_z\vec{e}_z$, the appropriate components for our set of coordinates are $k_{\|} = \vec{k} \cdot \vec{e}_{\|}$ and $k_{\perp} = \vec{k} \cdot \vec{e}_{\perp}$. Without loss of generality, we consider $\omega > 0$.

Since the main component of $\vec{B}_1$ is in the parallel direction, we solve for $B_{1\|}$. It is customary to introduce $\vec{\xi}_1 = i\vec{V}_1/\omega$. We obtain, by linearizing Eq. (4.14), the following equation relating $\vec{\xi}_1$ and $\vec{B}_1$

$$\vec{\xi}_1 = \frac{1}{\mu_0 \rho_0 \omega^2}\Big[\vec{\nabla}(\vec{B}_0 \cdot \vec{B}_1) - (\vec{B}_0 \cdot \vec{\nabla})\vec{B}_1 - (\vec{B}_1 \cdot \vec{\nabla})\vec{B}_0\Big], \tag{4.18}$$

where $\rho_0 = m_i n$. The second equation for $\vec{\xi}_1$ and $\vec{B}_1$ comes from taking the curl of

$$\vec{E}_1 - i\omega\vec{\xi}_1 \times \vec{B}_0 = \frac{1}{en}\left(\vec{J}_1 \times \vec{B}_0 + \vec{J}_0 \times \vec{B}_1\right), \tag{4.19}$$

which, combined with Eq. (4.14), yields

$$\vec{B}_1 = -\vec{B}_0(\vec{\nabla} \cdot \vec{\xi}_1) + (\vec{B}_0 \cdot \vec{\nabla})\vec{\xi}_1 - (\vec{\xi}_1 \cdot \vec{\nabla})\vec{B}_0 + i\frac{\omega m_i}{e}(\vec{\nabla} \times \vec{\xi}_1), \tag{4.20}$$

where the last quantity comes from the Hall term.

By introducing the configuration of the field given by Eq. (4.16) we can solve for

$B_{1\|}$. In the limit of $k_\|^2/k_\perp^2 \ll 1$ and $B_{0\vartheta}^2/B_{0z}^2 \ll 1$, we obtain the equation

$$\frac{d}{dr}\left[r\left(v_A^2 + k_\|^2 D_H^2\right)\frac{dB_{1\|}}{dr}\right] + \left[\omega^2 + k_\vartheta \omega \frac{d}{dr}\left(D_H\right) - k_\vartheta^2(v_A^2 + k_\|^2 D_H^2)\right] rB_{1\|} = 0, \quad (4.21)$$

where $k_\vartheta = -m/r \simeq k_\perp$ and $D_H = B_0/\mu_0 en$. Because $D_H \propto B_0/n(r)$ the spatial derivative of D_H is proportional to the density gradient, taking B_0 to be roughly constant as it varies over a longer scale length. In toroidal plasmas B_0 varies on the scale of the major radius while near the plasma edge $n(r)$ varies with a length scale significantly shorter than the minor radius of the plasma column.

The Hall term is responsible for two distinct terms in Eq. (4.21) which were not considered in earliest work analysing the effect of inhomogeneity on magnetosonic modes[16, 18], but were considered in subsequent contributions[5]. The first term is the quantity $k_\|^2 D_H^2$; an analogous form was derived in the homogeneous limit and the dynamics related to this correction are basically the same for inhomogeneous plasmas, being related to the ϑ component of the current that is generated by the Hall effect. The second quantity arising from the Hall term is proportional to dD_H/dr, is intrinsically related to inhomogeneity and does not have an equivalent in the homogeneous case. This same equation was studied by G. Kamelander and Ya. I. Kolesnichenko in Ref. [19]; however, their analysis of the localized solutions relied on the constraint that the second Hall term could be neglected. At first solutions to Eq. (4.21) are analyzed analytically in the limit of purely transverse propagation, then both analytically and numerically for the more general case in Chapter 5.

In studying Eq. (4.21), we find it convenient to introduce the dimensionless quantity

$$\frac{d_{i0}}{a} = \left.\frac{D_H}{av_A}\right|_{r=0},$$

which for typical experimental parameters will be $\ll 1$. We note that for frequencies of the order of the ion cyclotron frequency and above we will have poloidal mode numbers m comparable to $a/d_{i0} \gg 1$. Thus, to study the solution analytically we can perform an expansion in $1/m$. We will find that our analytical results closely match the features of the numerical solutions presented in Chapter 5 with corrections of the

order of $1/m^2$.

4.3 Analytical solution with purely perpendicular propagation

Returning to the full mode equation

$$\frac{1}{r(v_A^2+k_\parallel^2 D_H^2)}\frac{d}{dr}\left[r(v_A^2+k_\parallel^2 D_H^2)\frac{dB_{1\parallel}}{dr}\right] + \left[\frac{\omega^2}{v_A^2+k_\parallel^2 D_H^2}+\frac{\omega}{r(v_A^2+k_\parallel^2 D_H^2)}\frac{d}{dr}(rk_\vartheta D_H)-k_\vartheta^2\right]B_{1\parallel}=0, \tag{4.22}$$

we define $b_1 \equiv B_{1\parallel}\sqrt{r(v_A^2+k_\parallel^2 D_H^2)}$ and we obtain the following equation:

$$\begin{aligned}\frac{d^2 b_1}{dr^2} + \Bigg[&\frac{\omega^2}{v_A^2+k_\parallel^2 D_H^2}+\frac{\omega}{r(v_A^2+k_\parallel^2 D_H^2)}\frac{d}{dr}(rk_\vartheta D_H)-k_\vartheta^2 \\ &-\frac{1}{4}\left(\frac{1}{r(v_A^2+k_\parallel^2 D_H^2)}\frac{d\,r(v_A^2+k_\parallel^2 D_H^2)}{dr}\right)^2 \\ &-\frac{1}{2}\frac{d}{dr}\left(\frac{1}{r(v_A^2+k_\parallel^2 D_H^2)}\frac{d\,r(v_A^2+k_\parallel^2 D_H^2)}{dr}\right)\Bigg]b_1=0.\end{aligned} \tag{4.23}$$

We introduce Δ as the typical scale of variation of b_1 in the solution to the mode equation given by Eq. (4.23). In this equation, the first term scales as b_1/Δ^2 and the last two terms as b_1/r^2. Since we look for a localized solution occupying a narrow radial interval whose width is characterized by Δ, we can consider the limit where $1/\Delta^2 \gg 1/r^2$ and neglect the last two terms. We will show that this is consistent for the case of high-frequency modes having large poloidal mode number m, where $k_\vartheta = -m/r$.

The equation for b_1 can be characterized in terms of the action of an effective potential V_{eff}, taking the form:

$$\frac{d^2 b_1}{dr^2} - V_{\text{eff}}(r,\omega)b_1 = 0, \tag{4.24}$$

where with the ordering assumed above

$$V_{\text{eff}} \simeq -\frac{\omega^2}{v_A^2 + k_\parallel^2 D_H^2} - \frac{\omega}{r(v_A^2 + k_\parallel^2 D_H^2)} \frac{d}{dr}\left(r k_\vartheta D_H\right) + k_\vartheta^2. \tag{4.25}$$

To find a localized solution, we consider the ordering $k_\vartheta^2 \gg 1/\Delta^2 \gg 1/r^2$, so that the form for V_{eff} used in Eq. (4.25) is a good approximation and the mode propagation is mainly in the poloidal direction. We Taylor expand the effective potential as given by Eq. (4.25) around its minimum, that we call r_{mode} and which we refer to as the "radius of localization"; by doing this we approximate our equation with the Hermite equation, where

$$V_{\text{eff}} \simeq V_{\text{eff}}(r_{\text{mode}}) + \frac{1}{2} V_{\text{eff}}''(r_{\text{mode}})(r - r_{\text{mode}})^2.$$

The solutions will be localized around the surface $r = r_{\text{mode}}$ and have the form:

$$b_1(r) = b_1 H_s\left(\frac{r - r_{\text{mode}}}{\Delta}\right) \exp\left(-\frac{(r - r_{\text{mode}})^2}{2\Delta^2}\right), \tag{4.26}$$

where s is the non-negative integer index of the eigenfunction and the functions H_s are Hermite polynomials. The mode localization r_{mode} may be viewed as the center of the region within which the mode has a significant amplitude. For the simplest radial structure this corresponds with the radius at which the peak amplitude of the mode occurs.

In general, for an equation having the form of Eq. (4.24), the equations determining r_{mode}, ω, and Δ are given by:

$$\frac{dV_{\text{eff}}(\omega, r_{\text{mode}})}{dr} = 0 \tag{4.27}$$

$$V_{\text{eff}}(\omega, r_{\text{mode}}) = -\frac{2s+1}{\Delta^2} \tag{4.28}$$

$$\frac{d^2 V_{\text{eff}}(\omega, r_{\text{mode}})}{dr^2} = \frac{2}{\Delta^4} \tag{4.29}$$

where s is the radial mode number characterizing the eigenfunction. In Eq. (4.28), we see that as $V_{\text{eff}} \sim k_\vartheta^2$ and $k_\vartheta^2 \gg \Delta^{-2}$, there has to be a partial cancellation among the

terms of the effective potential at $r = r_{\text{mode}}$. Thus we can solve for the lower order set of equations $V_{\text{eff}}(\omega_V, r_V) = 0$, $dV_{\text{eff}}(\omega_V, r_V)/dr = 0$; in this case we find that $\omega_V \propto |m|$ and $\Delta \propto |m|^{-1/2}$, as shown below. Thus we see that an expansion in $1/m$ for large poloidal number m is consistent with the above equations for ω_V and r_V. The actual frequency and mode localization can then be expressed in the form of an expansion $\omega = \omega_V + \delta\omega_{Vs} + \mathcal{O}(\omega/m^2)$ and $r_{\text{mode}} = r_V + \delta r_{Vs} + \mathcal{O}(r/m^2)$. The terms in V_{eff} that have been neglected, which are all independent of m, have no effect on the first order corrections in this expansion. We note that in the limit of large poloidal mode number m, $\delta r_{Vs} \ll \Delta$ and so the correction δr_{Vs} is not physically significant; thus we neglect the difference between r_{mode} and r_V in the analytical calculations, and in general we do not consider $\mathcal{O}(1/m)$ corrections to the mode localization or the mode width to have an affect on the physical properties of the mode. In performing the numerical analysis the role of this correction will be apparent in the mode solutions to Eq. (4.22). The first order correction to the frequency found by solving for Eq. (4.28) is given by

$$\delta\omega_{Vs} = -\frac{(2s+1)}{\Delta^2}\left(\frac{\partial V_{\text{eff}}(\omega_V, r_V)}{\partial \omega_V}\right)^{-1} \propto \frac{\omega}{m}. \tag{4.30}$$

Note that $\delta\omega_{Vs}$ is independent of m and leads to constant frequency intervals between different radial eigenmodes. Additional corrections would come from higher order derivatives such as $V_{\text{eff}}^{(3)}$. In analogy with the Sturm-Liouville problem, we expect these higher order terms to alter the mode shape (radial eigenfunction) more than the mode frequency (eigenvalue), so that they will not affect the solution until order $1/m^2$. Note that in the limit $k_\perp^2 \gg 1/\Delta^2$, the polarization of the contained mode will be given approximately by Eq. (4.9).

For clarity we first evaluate the simplified case where the terms $k_\parallel^2 D_H^2$ are neglected in the effective potential, denoted as V_0, so that

$$V_0 \equiv -\frac{\omega^2}{v_A^2} - \frac{\omega}{r v_A^2}\frac{d}{dr}\left(r k_\vartheta D_H\right) + k_\vartheta^2. \tag{4.31}$$

The corresponding field variable would be $b_1 \equiv B_{1\parallel}\sqrt{r v_A^2}$. Note that the effect of the Hall term still appears through the term linear in k_ϑ, that breaks the symmetry

in the poloidal direction. The mode solutions for the case of the simplified effective potential as in Eq. (4.31) in the large m limit will be denoted as r_0, Δ_0, ω_0, and $\delta\omega_{0s}$.

Considering only positive frequency modes, $\omega > 0$, we write explicitly $m = \sigma_m|m| = \pm|m|$ because the solutions can be very different for positive or negative $k_\vartheta = -m/r$. The condition $V_{\text{eff}}(\omega_0, r_0) = 0$ can be rewritten as

$$\omega_0 = \frac{|m|v_A}{r}\left[\sqrt{1 + (D'_H/2v_A)^2} + \sigma_m D'_H/2v_A\right]\Big|_{r=r_0}, \tag{4.32}$$

where $'$ denotes the derivative with respect to r. From this condition, together with $V'_{\text{eff}}(\omega_0, r_0) = 0$, r_0 is determined by the equation

$$2 + r\frac{n'}{n} + \sigma_m d_i\left(\frac{rn'}{n}\right)'\left[1 - \frac{n'}{n}\frac{2 + rn'/n}{(rn'/n)'}\right]^{1/2}\Big|_{r=r_0} = 0, \tag{4.33}$$

where $d_i = c/\omega_{pi} = D_H/v_A$ and the gradients have been written in terms of the density profile. Note from Eq. (4.33) that for the case of purely perpendicular propagation in the large m limit r_0 does not vary with the magnitude of the mode number, and only depends on d_{i0}/a, the sign of m and the density profile.

The width of the mode is given by

$$\frac{1}{\Delta_0^4} = \frac{m^2}{r^4}\left(3 - \frac{r^2}{2}\frac{1}{N}\frac{d^2N}{dr^2}\right)\Big|_{r=r_0}, \tag{4.34}$$

where $N = n\,[1 + (d_i n'/n)(mv_A/r\omega_0)]$. This shows that $\Delta \propto |m|^{-1/2}$ and so the ordering $k_\vartheta^2 \gg 1/\Delta^2 \gg 1/r^2$ is consistent with $|m| \gg 1$.

Using this result, we can express $\delta\omega_{0s}$ as

$$\delta\omega_{0s} = (2s+1)\frac{v_A}{r}\left(3 - \frac{r^2}{2}\frac{1}{N}\frac{d^2N}{dr^2}\right)^{1/2}\frac{(nN)^{1/2}}{n+N}\Big|_{r=r_0} \tag{4.35}$$

with N defined as above.

The parameter d_{i0}/a, which estimates the influence of the Hall effect on the mode structure, alters significantly the behavior of these contained modes compared with the solution to the ideal MHD equations even when it is a small quantity. We find

from Eq. (4.33) that there is some critical value $d_i^{\rm crit}$ such that when $d_{i0} > d_i^{\rm crit}$ and when $\sigma_m < 0$ there is no contained solution because no value of r exists for which the effective potential has a minimum. The disappearance of the $\sigma_m < 0$ solution for sufficiently large d_{i0} occurs for a broad range of density profiles, with some variations in the numerical value of $d_i^{\rm crit}$. In these cases there are no localized solutions to the mode equation for m negative, which means that confined solutions exist only for modes whose poloidal motion is in the same direction as the ion gyromotion in a field aligned with the z-axis. If we consider density profiles having the form $n = n_0(1 - r^2/a^2)^\nu$, where a is the minor radius of the plasma column, we find that $d_i^{\rm crit}/a = (1/4)\left[\nu/(2+\nu)\right]^{1+(\nu/2)}/\sqrt{1+\nu}$. Using as typical experimental parameters the values $d_{i0}/a = 0.05$ and $\nu = 1/2$, we find that $d_i^{\rm crit}/a \simeq 0.027$ and so $d_{i0} > d_i^{\rm crit}$ and we do not expect to find radially confined solutions for negative m. Confined solutions do occur for $m > 0$, localized in a thin shell about a radius r_0 which is independent of the magnitude of m as can be seen from Eq. (4.33), and the radial width of the mode varies inversely with the square root of m, as given by Eq. (4.34). For the parameters considered, the modes are localized close to the edge of the plasma column and we find $r_0/a \simeq 0.77$, $\omega_0/\Omega_i \simeq 0.086\ m$, $\delta\omega_{0s}/\Omega_i \simeq 0.22\ (s + 1/2)$ and $\Delta_0/a \simeq 0.49\ m^{-1/2}$, which will be compared with numerical results in the following section. For $a \simeq 1.05$ m this value of d_{i0} corresponds to a central density $n_0 \simeq 3.75 \times 10^{19}$ m^{-3}.

We find from Eq. (4.33) that the mode localization varies with the density profile while the width of the mode is essentially the same. By considering higher densities, d_{i0} decreases and we can have $d_{i0} < d_i^{\rm crit}$ in which case solutions will exist both for $m > 0$ and $m < 0$. For example, if $d_{i0}/a = 0.01$, then with the same density profile as before we find that $r_0/a \simeq 0.80$ for modes with $m > 0$ and $r_0/a \simeq 0.83$ for modes with $m < 0$. For more peaked profiles the mode localization surface r_0 moves further to the interior of the plasma given comparable values of d_{i0}/a.

Chapter 5

Properties of the contained mode

5.1 Numerical results

In this section the numerical algorithm used to solve Eq. (4.22) is described, and some examples of the solutions obtained by this method for different values of the parameters m and n^0 are presented.

For a given value of m, Eq. (4.22) has been discretized by means of standard three-points central differences on a mesh of N grid points. A non-uniform mesh has been adopted in order to properly describe the solutions that we expect to be localized around the outer edge of the plasma column. In this way a set of $N-2$ homogeneous linear equations, depending on the unknown frequency ω, has been obtained. Typically the value we take for N in our calculations is 3000.

Two equations for the boundary conditions complete this system: we assume vanishing field solutions at the center of the column and at the edge since we focus on contained modes[4]. This assumption will be discussed in some detail further on.

In order to obtain non-trivial solutions we search for the values of ω for which the characteristic polynomial (determinant) of the coefficients matrix is equal to zero. In this way a set of eigenvalues, with the corresponding eigenvectors, is found. It is worthwhile to note that we expect numerical eigenvectors to behave in a similar way to the solutions of a Sturm-Liouville problem, with the number of nodes increasing with the order of the corresponding eigenvalue. In fact Eq. (4.22) coincides with a

classical eigenvalue Sturm-Liouville equation except that the term multiplying $B_{1||}$ is a quadratic polynomial in ω rather than a linear term.

We consider first the case that corresponds to $k_{||} = 0$ in order to compare with the results of Chapter 4 before we extend our analysis to the more general case. The explicit form for the parallel component of the wave vector is

$$k_{||} = -\frac{m}{R_0 q(r)}\left[1 - \frac{n^0 q(r)}{m}\right] \tag{5.1}$$

where $q(r) = rB_z/R_0 B_\vartheta$, and we take $k_\perp \simeq k_\vartheta = -m/r$. As shown in Chapter 4, the mode equation that we derived yields contained solutions for large poloidal mode number m which become localized within an increasingly narrow radial interval as m increases. Thus, having neglected $k_{||}$ to obtain Eq. (4.31) corresponds to requiring that n^0 satisfy $n^0/m \simeq 1/q(r_0)$ where r_0 is the localization of the mode as found in Eq. (4.33). In particular, as r_0 is independent of $|m|$ this limiting case is equivalent to only considering a fixed ratio n^0/m. We will see from the numerical results that this special case does yield mode solutions centered about $r = r_0$. Furthermore, from the analysis of the full mode equation we will find that in fact setting $k_{||} = 0$ for these particular pairs of m and n^0 is a valid assumption.

The numerical analysis depends upon the dimensionless parameters

$$\frac{d_{i0}}{a} = \left.\frac{D_H}{a v_A}\right|_{r=0} \qquad \text{and} \qquad \epsilon = \frac{a}{R_0}$$

as well as on the density profile and the q profile. We model the plasma by considering $d_{i0}/a = 0.05$, $\epsilon = 0.3$, $n(r) = n_0(1 - r^2/a^2)^{1/2}$ and $q(r) = 1 + 2.5\ r^2/a^2$. We recall that for this set of parameters, the limiting case $k_{||} = 0$ as considered in Chapter 4 led to modes localized about $r_0 \simeq 0.77$ so that $1/q(r_0) \simeq 0.4$. We seek to confirm this analysis by choosing mode numbers such that $n^0/m = 0.4$ and comparing the numerical solutions with the analytical calculations.

In Figs. 5-1 and 5-2 we plot the four lowest frequency mode solutions for the cases $(m, n^0) = (50, 20)$ and $(m, n^0) = (-50, -20)$ as a function of the radius normalized to the plasma minor radius a. The corresponding frequencies normalized to Ω_i are

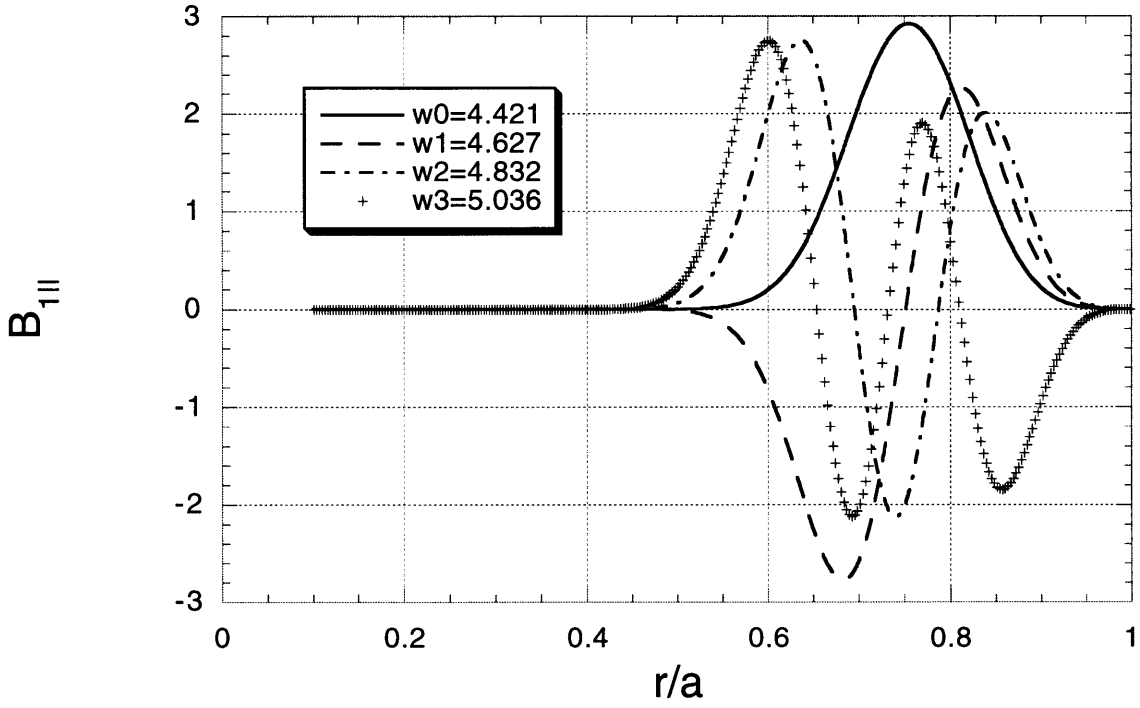

Figure 5-1: Numerical solution of Eq. (4.22). $B_{1||}(r)$ is plotted versus r/a for the first 4 radial eigenmodes $s = 0..3$, for the case $d_{i0}/a = 0.05$ with $m = 50$ and $n^0 = 20$. The corresponding frequencies are given normalized to the ion cyclotron frequency Ω_{i0}.

indicated. We see that the modes rapidly decay as the minor radius becomes small, due to the centrifugal term $k_\perp^2$ in the effective potential. When $m > 0$, the modes also decay as $r \to a$, consistent with the existence of a trapping potential located about $r = r_0$. It is also necessary for the potential well to be sufficiently deep that the mode does not extend to the plasma edge, which is equivalent to requiring that the radial extent of the mode is less than $2(a - r_0)$. What we referred to in Chapter 4 as the mode localization radius r_{mode} is the center of the region in which the mode has a significant amplitude. In the analytical model r_{mode} corresponds to either a peak or a node of the mode solution depending on the parity of the radial eigenfunction.

We see from the figures that the solutions exhibit a different behavior for negative m and in particular are no longer decaying solutions at the plasma edge, and thus can not be described as a localized or contained mode; this holds true regardless of the magnitude of m. Even if the mode satisfies the imposed boundary condition $B_{1||} = 0$ at the plasma edge, it has large higher derivatives there so we expect these waves

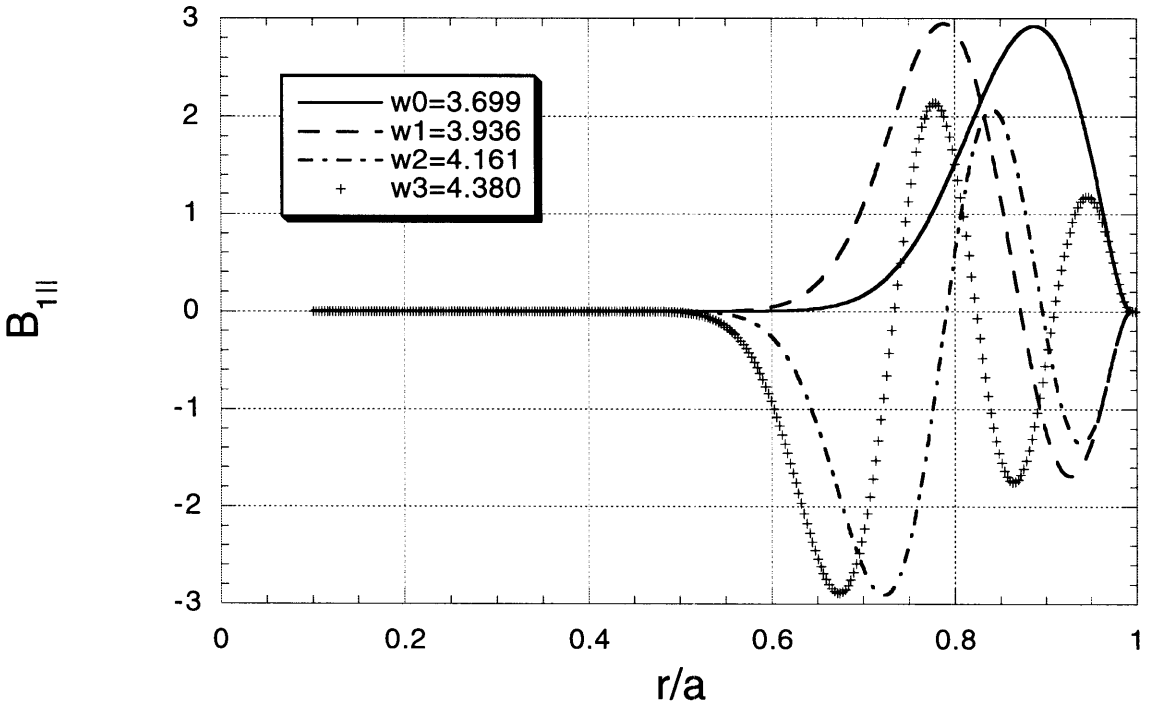

Figure 5-2: Numerical solution of Eq. (4.22). $B_{1||}(r)$ is plotted versus r/a for the first 4 radial eigenmodes $s = 0..3$, for the case $d_{i0}/a = 0.05$ with $m = -50$ and $n^0 = -20$. The corresponding frequencies are given normalized to the ion cyclotron frequency Ω_{i0}.

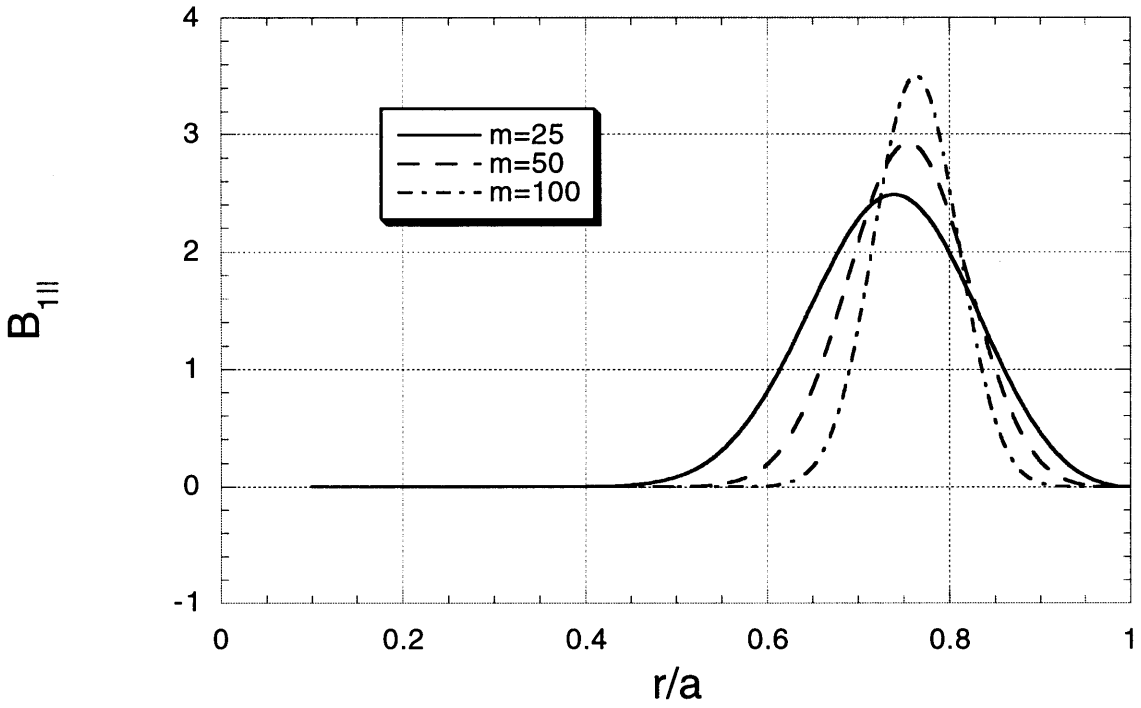

Figure 5-3: Numerical solution of Eq. (4.22). $B_{1\|}(r)$ for the lowest radial eigenmode is plotted versus r/a for the case $d_{i0}/a = 0.05$ with $m = 25$, 50, 100 and fixed ratio $n^0/m = 0.4$ that reproduces the $k_{\|} = 0$ case.

to couple with external electromagnetic waves. This dependence on the sign of the poloidal mode number comes from the Hall effect which breaks the symmetry in the poloidal direction that is found in the simplified MHD equations, and which appears in our equation through the term dD_H/dr.

In Fig. 5-3 we compare the lowest radial eigenmodes for each of $m = 25$, 50 and 100, and we observe the decrease in mode width with increasing m. We evaluate Δ by measuring the full width at half maximum, and we obtain $\Delta/a \simeq 0.092$, 0.066 and 0.046 for $m = 25$, 50 and 100 respectively. We also observe a small shift in the peak of the eigenfunction which corresponds to the correction $\delta r_{Vs} \propto 1/m$ in the analysis of Chapter 4.

The main feature of the numerical solution for the case of large positive m is that the mode is localized towards the edge of the plasma column, with the modes extending over an interval that decreases as $0.46\ m^{-1/2}a$ for increasing m as can be seen from the graphs. The localization point does not significantly change for different

values of m and is consistent with $r_0/a \simeq 0.77$. The different radial eigenmodes for a given m are separated in frequency by intervals that are roughly constant and have values in the range 0.21 — 0.22 Ω_i. The frequency of the lowest radial eigenmode scales roughly as 0.087 $m\Omega_i$. Higher radial eigenmodes tend to have a slightly broader radial extent. In addition, we observe that the higher radial eigenfunctions are not well described by Hermite polynomials except in terms of the number of nodes. In particular the absence of symmetry of the solutions reflects the strong asymmetry in the effective potential which is related to the large density gradients near the plasma edge.

5.2 General analytical solution

We have shown that the analytical results are supported by numerical calculations when terms related to $k_{||}$ are neglected. We now extend this analysis to consider the full form of V_{eff} as given by:

$$V_{\text{eff}} \simeq -\frac{\omega^2}{v_A^2 + k_{||}^2 D_H^2} - \frac{\omega}{r(v_A^2 + k_{||}^2 D_H^2)} \frac{d}{dr}\left(r k_\vartheta D_H\right) + k_\vartheta^2 \tag{5.2}$$

which incorporates terms related to $k_{||}$.

We wish to highlight the fact that $k_{||}$ as defined by Eq. (5.1) is a function of position so that in general for any particular mode the value of $k_{||}$ will vary across the radial extent of the mode. For modes having a finite width Δ the variation of $k_{||}$ across the mode layer is of the order

$$\Delta k'_{||} \sim \frac{r}{\sqrt{m}} \frac{m\hat{s}}{R_0 q} \tag{5.3}$$

where $\hat{s} = rq'/q$. Not only does the q profile determine the functional dependence of $k_{||}$ on r, but as shown below the shear parameter $\hat{s}$ explicitly appears in the condition for the surface of localization of the mode when $k_{||} \neq 0$. Thus the shear plays a significant role in determining how the $k_{||}$ effect alters the mode solutions from the $k_{||} = 0$ case and leads to a broader range of solutions compared to the limit in which

the shear is not considered[19].

The equation $V_{\text{eff}} = 0$ can be solved for the frequency to yield

$$\omega_V = \frac{|m|v_A}{r}\left\{\left[1 + k_{||}^2 d_i^2 + \left(\frac{D'_H}{2v_A}\right)^2\right]^{1/2} + \sigma_m \frac{D'_H}{2v_A}\right\}_{r=r_V} \tag{5.4}$$

and following the procedure of Chapter 4 we have

$$\delta\omega_{Vs} = \frac{(2s+1)rv_A}{2|m|\Delta^2}\left(1 + k_{||}^2 d_i^2\right)\left[1 + k_{||}^2 d_i^2 + \left(\frac{D'_H}{2v_A}\right)^2\right]^{-1/2}_{r=r_V} \tag{5.5}$$

We note that, for fixed m, ω_V is minimized at $k_{||} = 0$ and $r_V = r_0$ because there the effective potential vanishes and is a minimum in terms of both the toroidal mode number n^0 and the radial co-ordinate.

The value of the mode localization radius to lowest order in $1/m$, r_V, satisfies the equation

$$0 = 2 + r\frac{n'}{n} - \Gamma + \sigma_m \frac{d_i}{\left(1 + k_{||}^2 d_i^2\right)^{1/2}}\left(\frac{rn'}{n}\right)' \times \left[1 - \frac{n'}{n}\frac{2 + rn'/n}{(rn'/n)'}\right]^{1/2}\left[1 - \Gamma\frac{n'/n}{(rn'/n)'}\right]^{1/2}_{r=r_V} \tag{5.6}$$

where

$$\Gamma \equiv \frac{2k_{||}d_i}{1 + k_{||}^2 d_i^2}\left(-\frac{1}{2}\frac{rn'}{n}k_{||}d_i + \frac{md_i\hat{s}}{R_0 q}\right)$$

If $k_{||} = 0$ this reduces to Eq. (4.33) which was derived in Chapter 4 and defines r_0. If we compare Eq. (5.6) with Eq. (4.33) we can define as the significant parameter the quantity

$$d_i^{\text{eff}} \equiv \frac{d_{i0}}{\left(1 + k_{||}^2 d_i^2\right)^{1/2}}$$

For $k_{||}$ sufficiently large, even for $d_{i0} > d_i^{\text{crit}}$ we shall find $d_i^{\text{eff}} < d_i^{\text{crit}}$ and in this case we expect to have solutions for $m < 0$ as well as for $m > 0$. Other quantities where $k_{||}d_i$ appear modify the equation but do not prohibit solutions altogether. The physical significance of the parameter d_i^{eff} is clear from Eq. (5.2) where it can be seen that the frequency scales as $(1 + k_{||}^2 d_i^2)^{1/2}$ and so the term linear in frequency is reduced

by a factor $(1 + k_{||}^2 d_i^2)^{-1/2}$. This can be interpreted as rescaling the magnitude of the factor dD_H/dr. It is this linear term that causes $m < 0$ mode solutions to become delocalized.

When $k_{||}$ was neglected, the radius of localization of the contained modes was completely determined by the sign of m and independent of the magnitude of m (or $k_\perp$). For the full mode equation instead the radius of localization will vary with $k_{||}$. Like the magnetosonic-whistler wave, the mode frequency will depend on $k_{||}$ as well. In Figs. 5-4 to 5-7 we present the mode frequency normalized to Ω_i and the localization point as described by Eqs. (5.4), (5.5) and (5.6), for the two cases $m = 100$ and $m = -100$, shown versus different values of n^0, that is for different values of $k_{||}$. We take as before $\epsilon = 0.3$, $d_{i0}/a = 0.05$ and $n(r) = n_0(1 - r^2/a^2)^{1/2}$. As can be seen from Fig. 5-5, when $m > 0$ the maximum and minimum values of r_V occur for $n^0 \simeq 0$ and $n^0 \simeq 2m/q(r_0)$, respectively[4]. In Fig. 5-8 we show the numerical radial eigenmode solution for the lowest radial eigennumber for the cases $m = 100$ and $n^0 = 0$, 40, and 100. These values of n^0 correspond to the above mentioned extremes.

We can see in Fig. 5-7 that, since $d_{i0} > d_i^{\text{crit}}$, there is a gap in n^0 where contained mode solutions do not exist. However we see that for sufficiently large $|k_{||}|$ there are contained solutions even though $m < 0$. The fact that contained solutions are absent only for small $|k_{||}|$ can be related to the definition of d_i^{eff}, that becomes smaller than d_i^{crit} for $|k_{||}|$ sufficiently large.

If we take $d_{i0} < d_i^{\text{crit}}$ and we look at negative m, there is no gap in n^0 for the localized solution. In this case, the dependence of the mode localization on n^0, i.e. $k_{||}$, is similar to the case of positive m, taking n^0 into $-n^0$. Fig. 5-9 shows radial eigenmode solutions for $d_{i0}/a = 0.01$, $m = -250$, $n^0 = -100$, where $k_{||} \simeq 0$. We see that in this case solutions for negative m are localized.

Returning to Eq. (5.6), we find that one particular case where we can immediately verify the existence of contained solutions for $m < 0$ and $k_{||} \neq 0$ is when $d_i^{\text{eff}} < d_i^{\text{crit}}$ and $k_{||}/k_\perp$ is such that the quantity Γ defined above vanishes at $r = r_V$. In this case the equation becomes formally identical to Eq. (4.33) with d_i^{eff} instead of d_{i0} and defines mode solutions for both $m > 0$ and $m < 0$. It is clear from the definition of

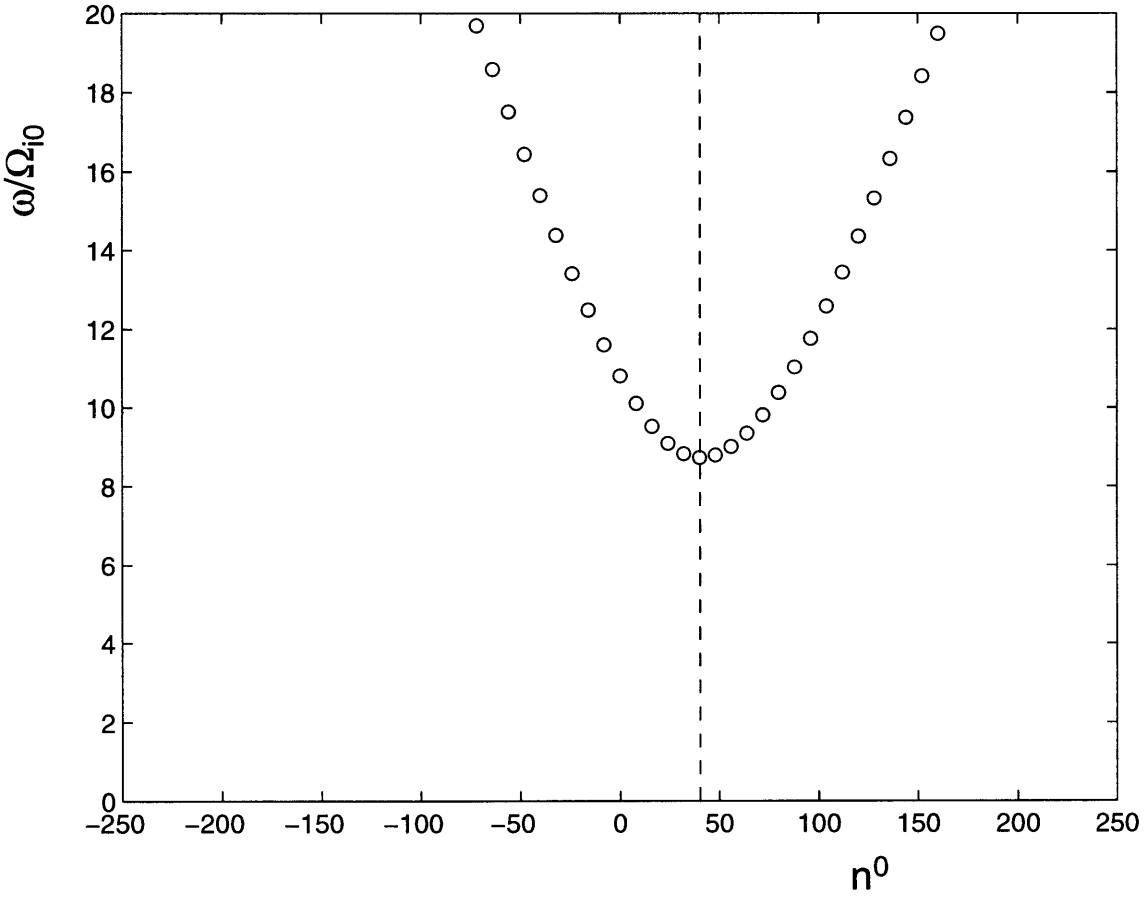

Figure 5-4: Mode frequency ω, normalized to the cyclotron frequency Ω_{i0}, of the contained mode for the effective potential as defined in Eq. (4.25) using the analytical formulas of Eqs. (5.4) and (5.5). A fixed poloidal mode number $m = 100$ is considered and the toroidal mode number n^0 is varied over a wide range. The minimum corresponds to $k_{||} = 0$, that is to propagation perpendicular to the magnetic field. Here $d_{i0}/a = 0.05$.

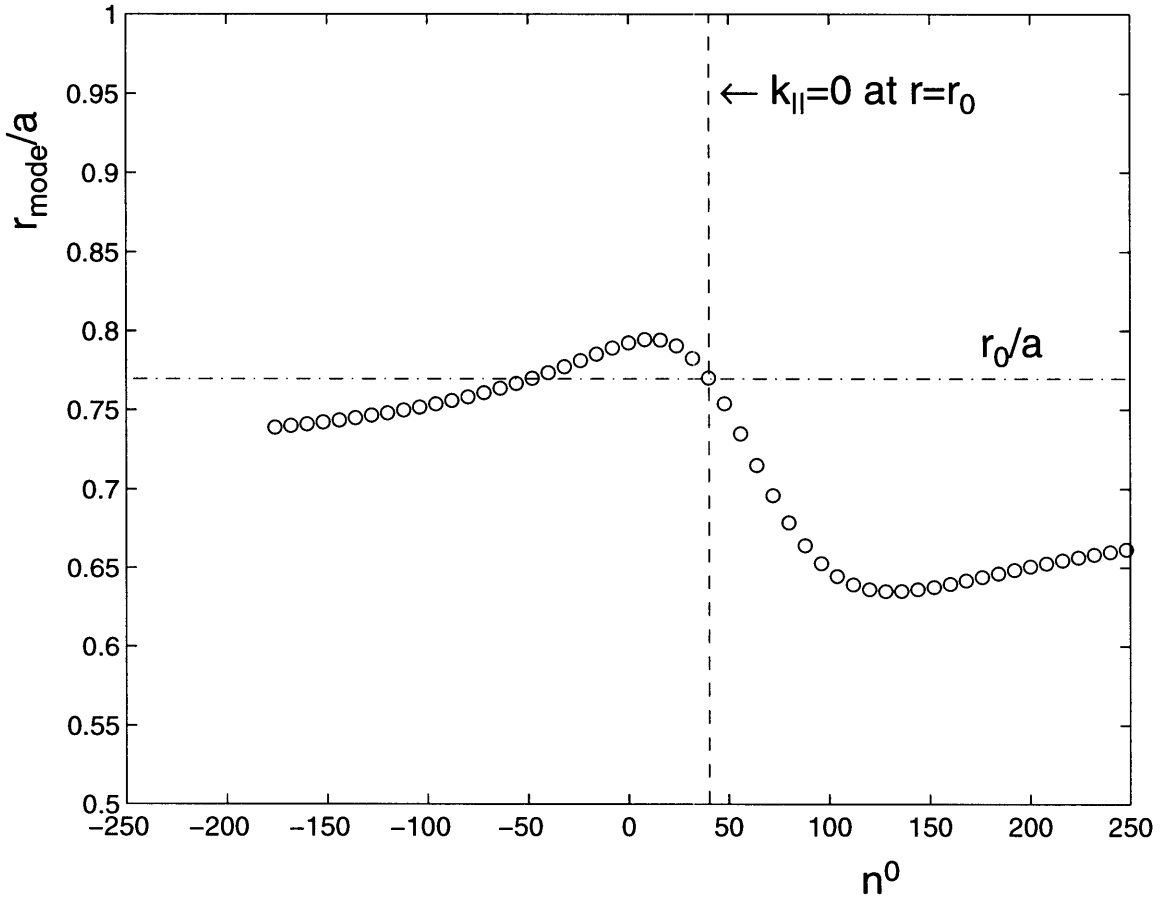

Figure 5-5: Radial localization of the contained mode, scaled to the minor radius a, determined by the effective potential as defined in Eq. (4.25), using the analytical formula Eq. (5.6). A fixed poloidal mode number $m = 100$ is considered and the toroidal mode number n^0 is varied over a wide range. The localization point r_0 as defined in Eq. (4.33) corresponds to $k_{||} = 0$ so that $n^0 \simeq m/q(r_0) \simeq 40$. Here $d_{i0}/a = 0.05$.

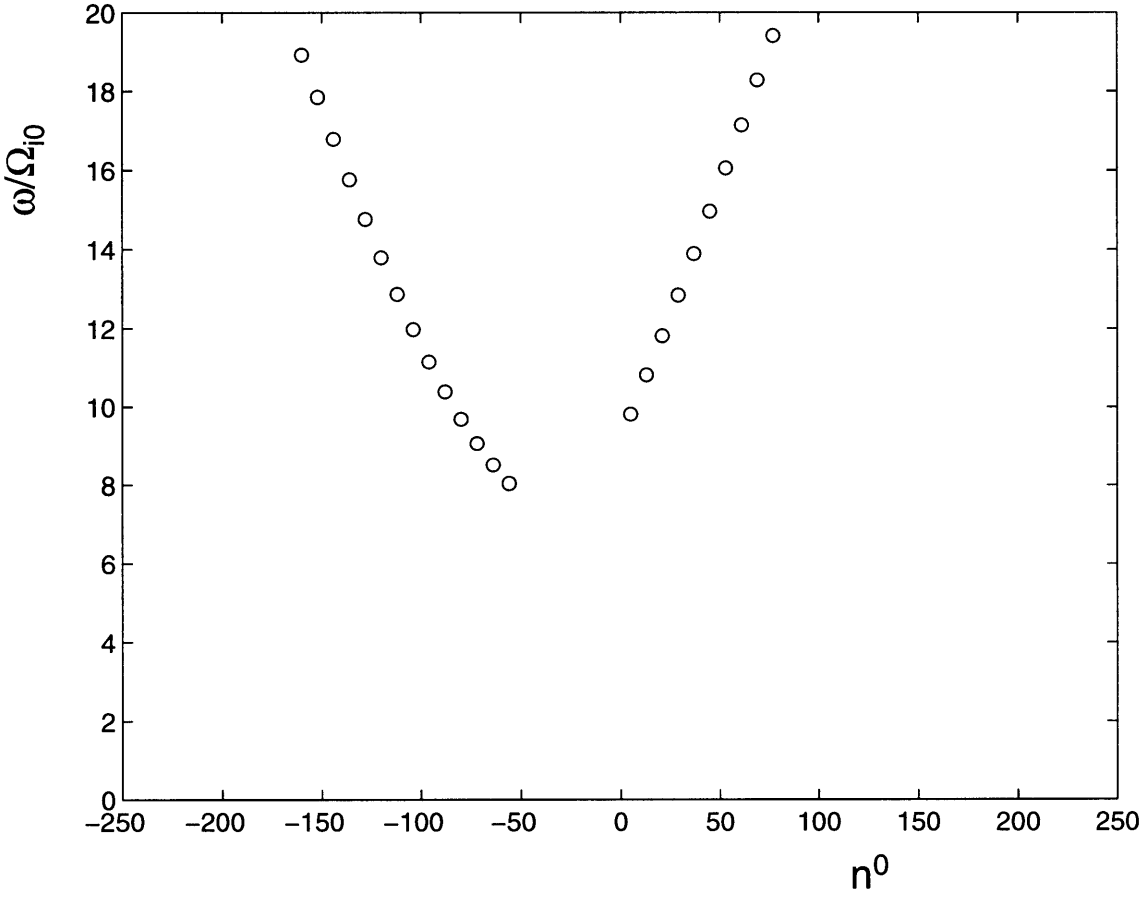

Figure 5-6: Mode frequency ω, normalized to the cyclotron frequency Ω_{i0}, of the contained mode for the effective potential as defined in Eq. (4.25) using the analytical formulas of Eqs. (5.4) and (5.5). A fixed poloidal mode number $m = -100$ is considered and the toroidal mode number n^0 is varied over a wide range. Here $d_{i0}/a = 0.05$.

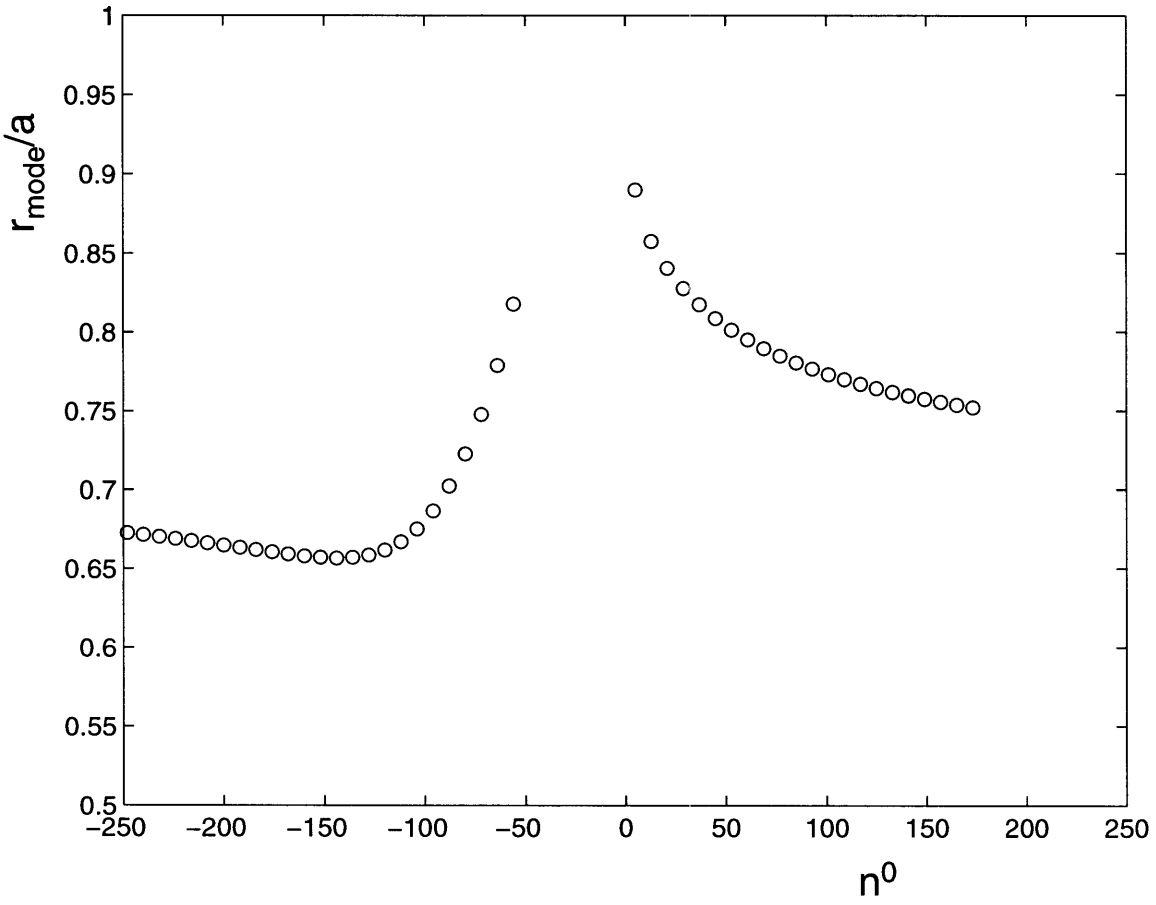

Figure 5-7: Radial localization of the contained mode, scaled to the minor radius a, determined by the effective potential as defined in Eq. (4.25), using the analytical formula Eq. (5.6). A fixed poloidal mode number $m = -100$ is considered and the toroidal mode number n^0 is varied over a wide range. Here $d_{i0}/a = 0.05$.

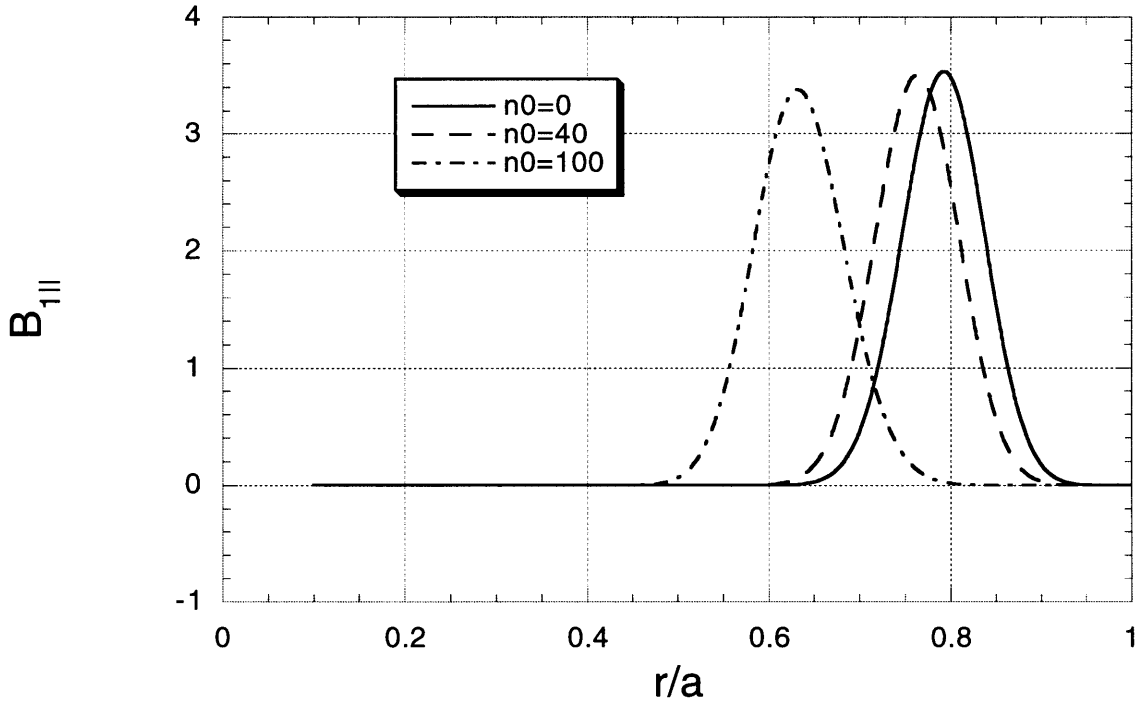

Figure 5-8: Numerical solution of Eq. (4.22). $B_{1||}(r)$ for the lowest radial eigenmode is plotted versus r/a for the case $d_{i0}/a = 0.05$ with fixed $m = 100$ and $n^0 = 0$, 40, 100, showing the variation of the localization point.

d_i^{eff} that the bigger d_{i0} is the bigger $k_{||}$ has to be to have solutions for $m < 0$. For larger m, this condition is easier to satisfy as $k_{||}^2 d_i^2 \propto m^2$.

In Figs. 5-10 to 5-12 we reproduce the eigenfrequency normalized to Ω_i, the localization of the mode and the mode width, normalized to a, for the cases $m = 25$, 50, 100, -100 shown versus $k_{||}/|k_\perp|$ evaluated at $r = r_V$. This definition of $k_{||}$ holds since, as we are considering modes which have $\Delta \ll r$, the variation of $k_{||}$ as given by Eq. (5.3) does not alter the mode propagation in the region where the modes have significant amplitude ($|r - r_0| \lesssim \Delta$). However, $k_{||}$ and the shape of the q profile are necessary for evaluating the mode solution. In particular, the shear parameter plays a large role in determining the range of mode solutions and the variation in mode localization surfaces even though the main cause of confinement of the mode is still given by the density gradient.

The frequency is minimized for $k_{||} = 0$ and increases quadratically with $k_{||}$, as expected from the magnetosonic-whistler wave. We see from Fig. 5-11 that as m

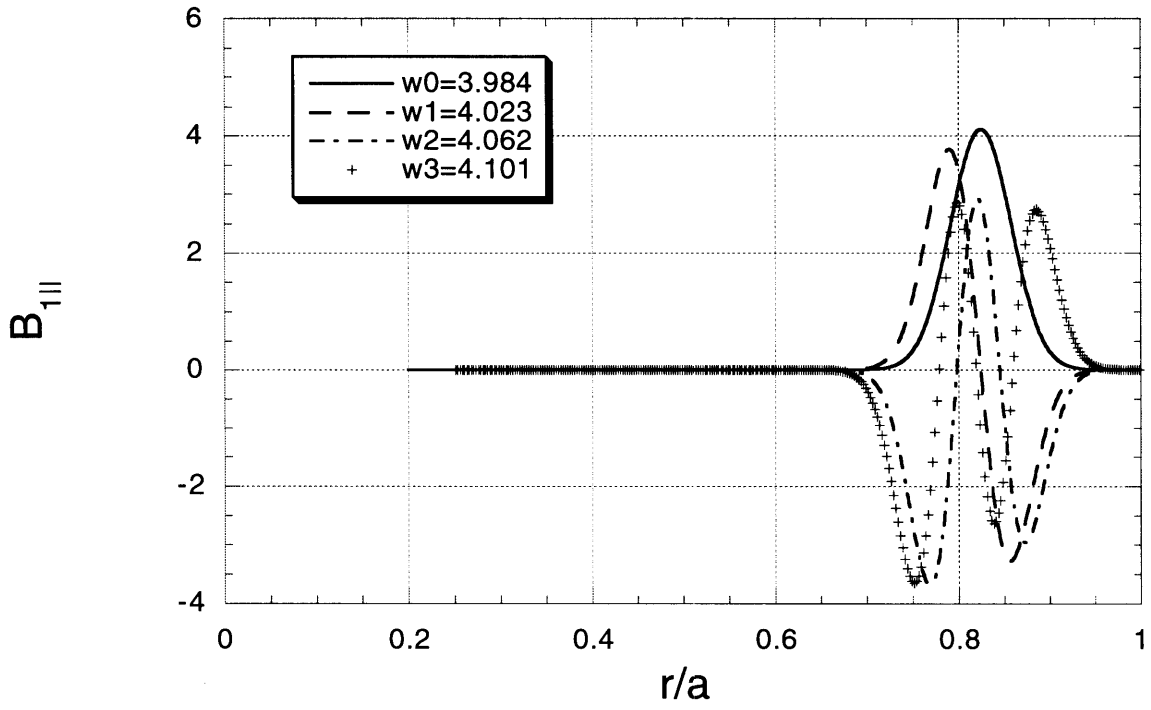

Figure 5-9: Numerical solution of Eq. (4.22). $B_{1\|}(r)$ is plotted versus r/a for the first 4 radial eigenmodes $s = 0..3$, for the case $d_{i0} = 0.01$ with $m = -250$ and $n^0 = -100$. The corresponding frequencies are given normalized to the ion cyclotron frequency Ω_{i0}.

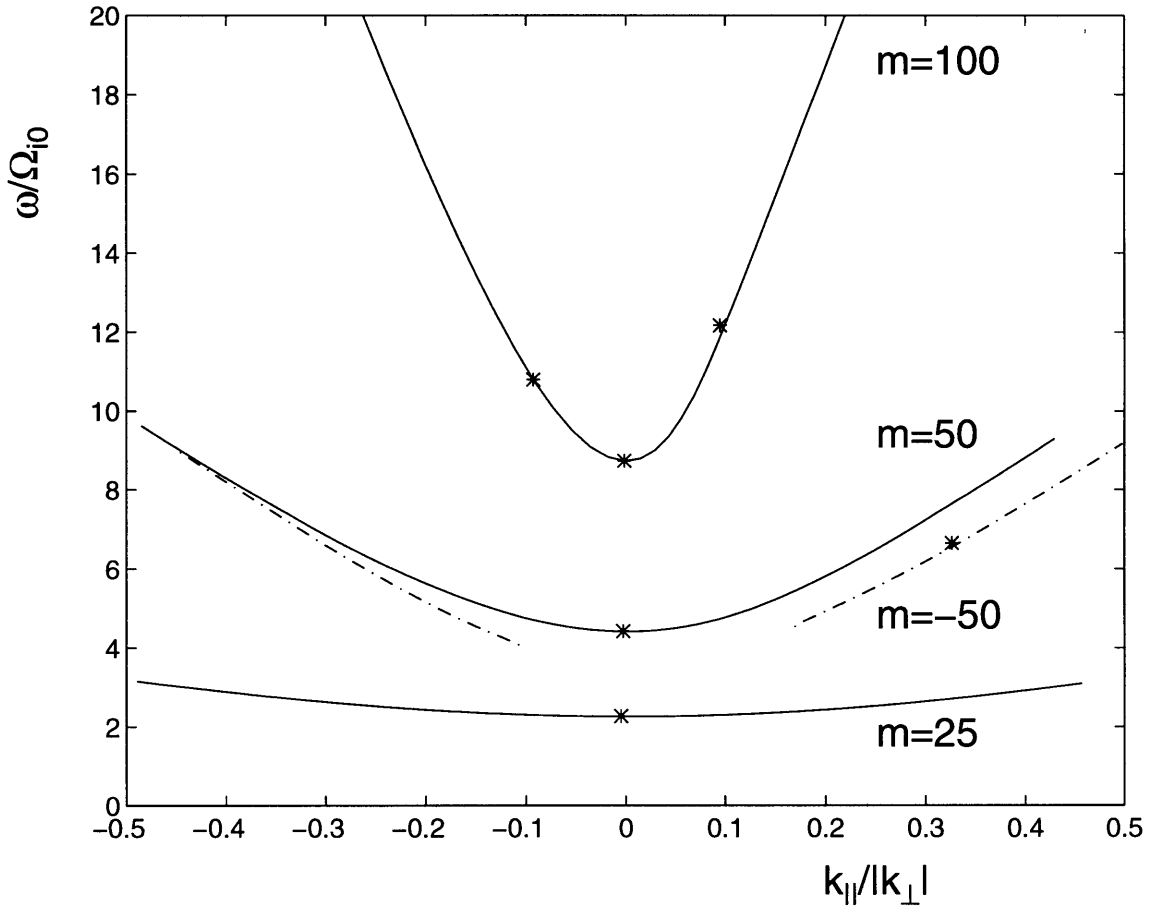

Figure 5-10: Mode frequency ω, normalized to the cyclotron frequency Ω_{i0}, of the contained mode for the effective potential as defined in Eq. (4.25) using the analytical formulas of Eqs. (5.4) and (5.5). The mode frequency is plotted versus $k_{||}/|k_{\perp}|$ for the case $d_{i0}/a = 0.05$ and $m = 25$, 50, -50, 100. Each asterisk corresponds to a numerical solution as plotted in Figs. 5-3 and 5-8, as well as the case $m = -50$, $n^0 = 50$.

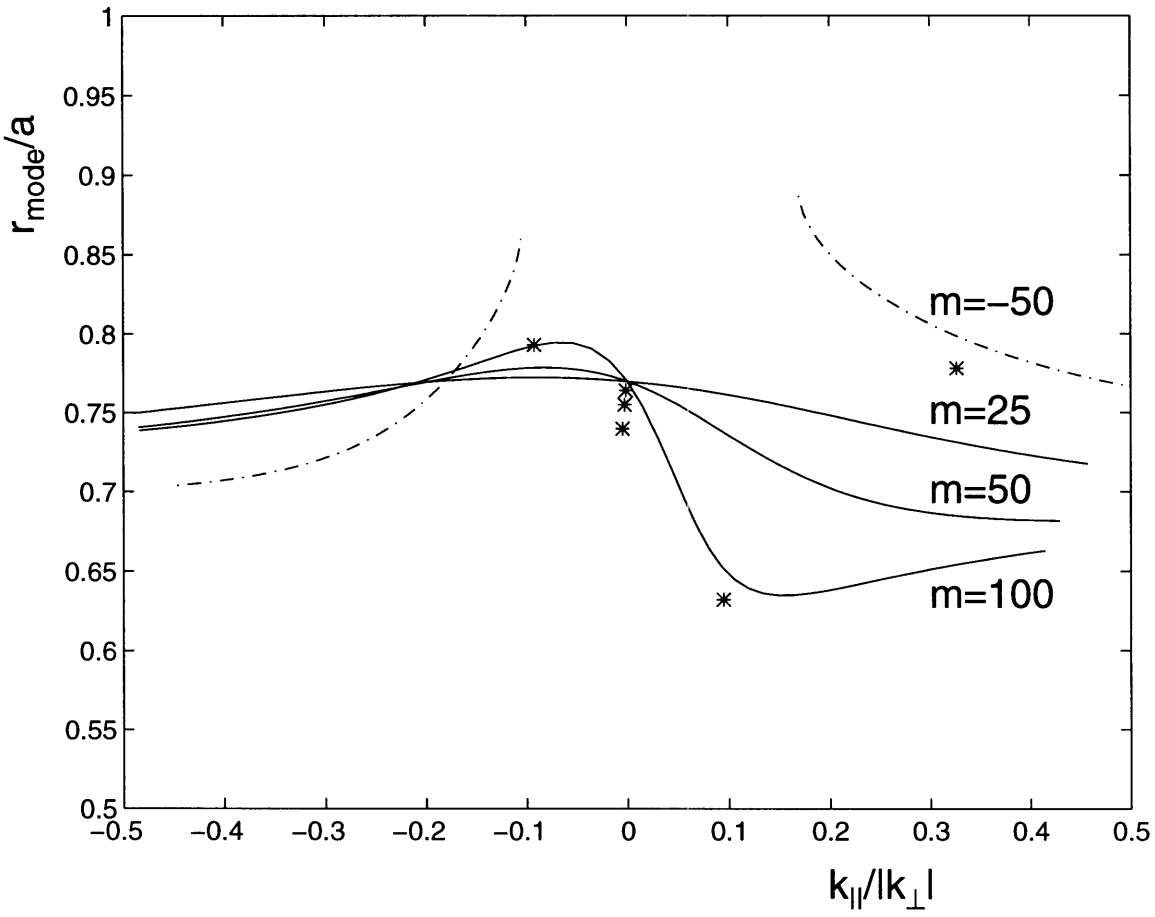

Figure 5-11: Radial localization of the contained mode, scaled to the minor radius a, determined by the effective potential as defined in Eq. (4.25), using the analytical formula Eq. (5.6). The mode localization point is plotted versus $k_{||}/|k_{\perp}|$ for the case $d_{i0}/a = 0.05$ and $m = 25$, 50, -50, 100. Each asterisk corresponds to a numerical solution as plotted in Figs. 5-3 and 5-8, as well as the case $m = -50$, $n^0 = 50$.

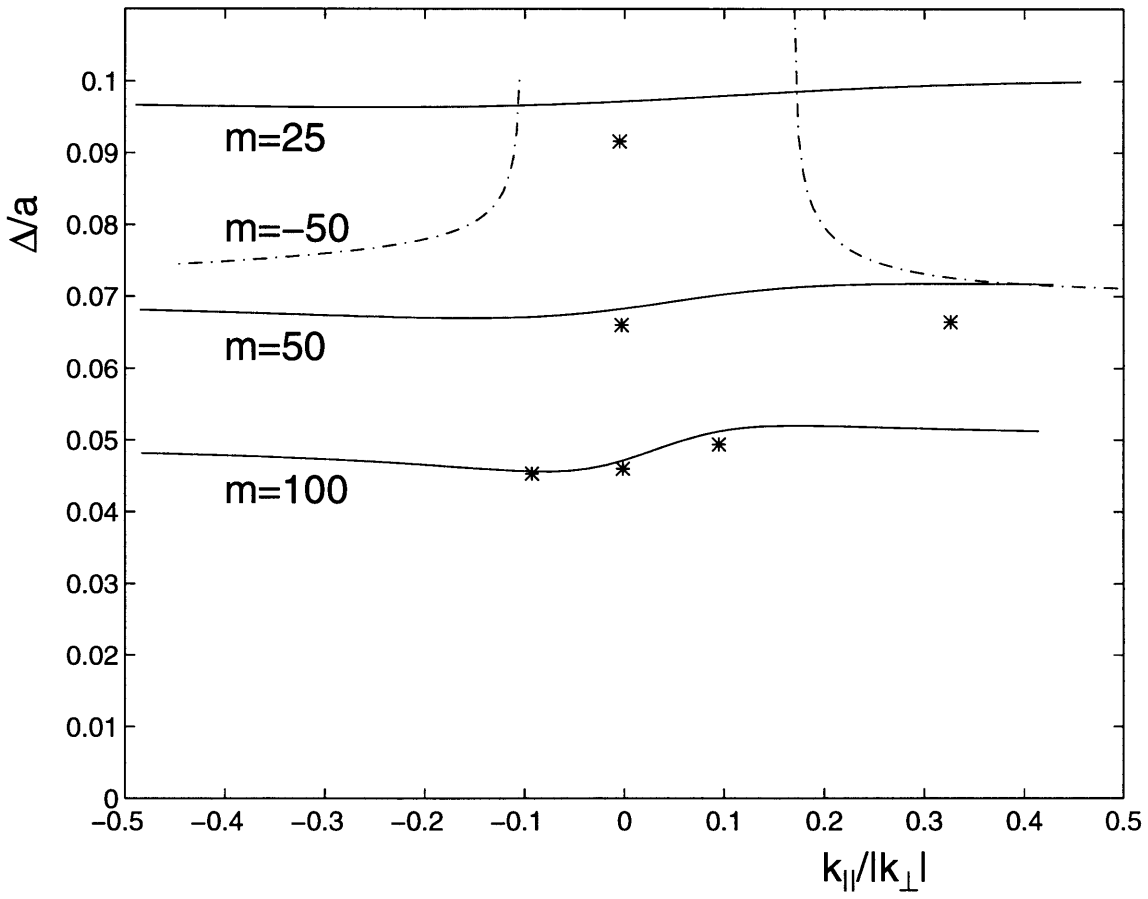

Figure 5-12: Radial mode width of the contained mode, scaled to the minor radius a, determined by the effective potential as defined in Eq. (4.25), according to the prescription given by Eq. (4.29). The mode width is plotted versus $k_{||}/|k_{\perp}|$ for the case $d_{i0}/a = 0.05$ and $m = 25$, 50, -50, 100. Each asterisk corresponds to a numerical solution as plotted in Figs. 5-3 and 5-8, as well as the case $m = -50$, $n^0 = 50$.

increases the variation of the mode localization becomes more pronounced. In particular we see that we have a significant effect when $k_{||}d_i \sim 1$, that appears[4] when $m \sim qR_0/d_i$. In Fig. 5-11 for $k_{||} = 0$ there is a unique localization point for all $m > 0$.

We have seen from Eqs. (5.4) and (5.6) that mode solutions with $k_{||} = 0$ at $r = r_V$ satisfy $r_V = r_0$ and $\omega_V = \omega_0$. This is because the parallel component of the wave vector appears in the effective potential as $k_{||}^2$. However, the mode width depends on the second derivative of the effective potential and so will have a contribution from the magnetic shear. Thus the mode width is not given by Δ_0 but instead satisfies

$$\frac{1}{\Delta^4} = \frac{1}{\Delta_0^4} + \left.\frac{m^4 \hat{s}^2 d_i^2}{q^2(r) r^4 R_0^2}\right|_{r=r_0}$$

where Δ_0 is defined by Eq. (4.34). This is equivalent to

$$\Delta = \Delta_0 \left.\left[1 + \left(\frac{m^2 \Delta_0^2 \hat{s} d_i}{q(r) r^2 R_0}\right)^2\right]^{-1/4}\right|_{r=r_0} \tag{5.7}$$

Because $\delta\omega_{Vs}$ includes a dependence on the mode width, in this case it is related to $\delta\omega_{0s}$ by

$$\delta\omega_{Vs} = \delta\omega_{0s} \left.\left[1 + \left(\frac{m^2 \Delta_0^2 \hat{s} d_i}{q(r) r^2 R_0}\right)^2\right]^{1/2}\right|_{r=r_0} \tag{5.8}$$

If we consider small values of $k_{||}d_i$, it is useful to consider the effective potential as a perturbation of the potential V_0 as given by Eq. (4.31). This will give an analytical expression[20] for the leading behavior in small $k_{||}$ of the curves in Figs. 5-10 and 5-11. Thus we write

$$V_{\text{eff}} = \frac{1}{1 + k_{||}^2 d_i^2} \left(V_0 + m^2 k_{||}^2 d_i^2 / r^2\right)$$

The eigenfrequency and mode localization, ω_V and r_V, satisfy the equations

$$V_0(\omega_V, r_V) = -m^2 k_{||}^2 d_i^2 / r^2$$

$$\frac{dV_0}{dr}(\omega_V, r_V) = -\frac{d}{dr}\left(m^2 k_{||}^2 d_i^2 / r^2\right)$$

In the limit $k_{||} \to 0$, this reduces to $r_V = r_0$ and $\omega_V = \omega_0$. However, the mode width and the frequency correction $\delta\omega_{Vs}$ are slightly different from the case of Eq. (4.31) because of the second derivative terms.

We can obtain an approximate form for r_V and ω_V by performing an expansion in $k_{||}d_i$. It is more difficult to find an expression for Δ and $\delta\omega_{Vs}$ for finite $k_{||}d_i$ because higher derivatives such as $V_{\text{eff}}^{(3)}$ appear in the expansion. However, to find the lowest order mode frequency and localization we need only consider

$$\begin{aligned} 0 &= V_0 + \frac{m^2 k_{||}^2 d_i^2}{r^2} \qquad (5.9) \\ &\simeq \frac{m^2 k_{||}^2 d_i^2}{r^2} + (r_V - r_0)\frac{\partial}{\partial r}\left(\frac{m^2 k_{||}^2 d_i^2}{r^2}\right) + \frac{1}{2}(r_V - r_0)^2 V_0'' + (\omega_V - \omega_0)\left.\frac{\partial V_0}{\partial \omega}\right|_{r_0,\omega_0} \end{aligned}$$

$$\begin{aligned} 0 &= V_0' + \frac{\partial}{\partial r}\left(\frac{m^2 k_{||}^2 d_i^2}{r^2}\right) \qquad (5.10) \\ &\simeq \frac{\partial}{\partial r}\left(\frac{m^2 k_{||}^2 d_i^2}{r^2}\right) + (r_V - r_0)\left[V_0'' + \frac{\partial^2}{\partial r^2}\left(\frac{m^2 k_{||}^2 d_i^2}{r^2}\right)\right] + (\omega_V - \omega_0)\left.\frac{\partial^2 V_0}{\partial\omega\partial r}\right|_{r_0,\omega_0} \end{aligned}$$

Note that

$$k_{||}' = \frac{m\hat{s}}{rR_0 q(r)} = -k_{||}\frac{\hat{s}}{r}\left[1 - \frac{n^0 q(r)}{m}\right]^{-1}.$$

Thus for modes that satisfy $|1 - n^0 q(r_0)/m| \ll 1$, which we define as "quasi-flute" modes, $(k_{||}d_i)' \simeq k_{||}' d_i \gg k_{||}d_i/r$ and so the frequency shift is second order compared to the shift in the localization of the mode.

Then the approximate values for r_V and ω_V are given by

$$r_V - r_0 \simeq -k_{||}\left.\frac{d_i^2 m^3 \hat{s}\Delta_0^4}{r^3 R_0 q(r)}\right|_{r_0} \sim r_0 \frac{k_{||}}{k_\perp} m^2 \qquad (5.11)$$

$$\omega_V - \omega_0 \simeq k_{||}^2 d_i^2 \frac{v_A|m|}{2r}\left[1 + \left(\frac{D_H'}{2v_A}\right)^2\right]^{-1/2} \times \left.\left[1 + \left(\frac{m^2\Delta_0^2 \hat{s} d_i}{q(r)r^2 R_0}\right)^2\right]\right|_{r_0} \sim \omega_0 \left(\frac{k_{||}}{k_\perp}\right)^2 m^2 \qquad (5.12)$$

$$k_{||} \equiv k_{||}(r_V) \simeq k_{||}(r_0)\left.\left[1 + \left(\frac{m^2\Delta_0^2 \hat{s} d_i}{q(r)r^2 R_0}\right)^2\right]^{-1}\right|_{r=r_0} \qquad (5.13)$$

These expressions characterize the mode solution for quasi-flute modes, for which $n^0 \simeq m/q(r_0)$. Different signs of $k_{||}$ push the mode localization in different directions, although this effect saturates for larger $k_{||}$, i.e., when the mode is no longer quasi-flute. In fact, in the regime where $|1 - n^0 q(r)/m| > 1$, the mode localization asymptotically approaches a fixed value, as shown in Fig. 5-11. The frequency, however, keeps increasing with $k_{||}$ and $k_\perp$ in analogy with the magnetosonic-whistler mode. To summarize our results, we find that there is a strong dependence of mode characteristics on $k_{||}$ and shear for quasi-flute modes. Given that we consider only $k_{||}/k_\perp \ll 1$ our analysis can be compared with the results of Ref. [19] only in the limit of $1/q(r)^2 \lesssim (n^0/m)^2 \ll 1/\epsilon^2$.

Chapter 6

Ion cyclotron emission driven by alpha-particles

Enhanced ion cyclotron emission (ICE) has been observed in various experiments with fusing plasmas. The parameters chosen for the subsequent analysis are based on ICE observations on JET[1, 3]. Key features of the observations are described here along with observations on TFTR[2] which display significantly different behavior.

There are four main fusion reactions which can occur in current experiments:

$$\mathrm{D} + \mathrm{D} \rightarrow {}^{3}\mathrm{He}(0.82\ \mathrm{MeV}) + \mathrm{n}(2.45\ \mathrm{MeV}) \tag{6.1}$$

$$\mathrm{D} + \mathrm{D} \rightarrow \mathrm{T}(1.0\ \mathrm{MeV}) + \mathrm{p}(3.0\ \mathrm{MeV}) \tag{6.2}$$

$$\mathrm{D} + {}^{3}\mathrm{He} \rightarrow \mathrm{p}(14.6\ \mathrm{MeV}) + {}^{4}\mathrm{He}(3.7\ \mathrm{MeV}) \tag{6.3}$$

$$\mathrm{D} + \mathrm{T} \rightarrow {}^{4}\mathrm{He}(3.6\ \mathrm{MeV}) + \mathrm{n}(14.0\ \mathrm{MeV}) \tag{6.4}$$

We focus primarily on α-particles (^{4}He) produced by reaction (6.4), because the much larger cross-section for D-T reactions for current plasma temperatures less than 20 keV leads to a greater reaction rate than D-D fusion even when the fraction of tritium in the plasma is of the order of a few percent.

One interpretation for ICE, adopted in this work, is that the enhanced radiation is the result of interactions between the energetic particles with modes having magnetosonic characteristics[21, 4]. Two features of the charged fusion products are central

to this analysis. First, the velocity of the ions produced by fusion is comparable to the Alfvén velocity v_A of the background plasma, and as has been indicated in Chapter 4 the mode-particle interaction is modified by the particle energy through finite Larmor radius effects when the particle velocity is greater than v_A. In addition, the radial drifts incurred by the particles, combined with the fact that fusion reactions are concentrated in the plasma core, lead to a very anisotropic distribution function outside of the plasma core, as seen in Chapter 3.

After describing the experimental observations, we examine the magnetosonic-cyclotron instability in the homogeneous case. The chapter concludes with a description of the new features of the ICE model expounded in this work, reviewing the significance of contained modes. Further assumptions and approximations are detailed which allow for a simplified calculation of the growth rate to be performed in Chapter 7.

6.1 ICE observations

ICE has been observed in a wide variety of plasmas undergoing fusion. The emitted power levels are significantly above expected thermal emission. As a function of frequency, the ICE spectrum typically consists of two parts, a series of narrow peaks at lower frequencies and a continuum at the high end of the spectrum. The peaks occur at evenly spaced intervals whose magnitude is comparable to the cyclotron frequencies for hydrogenic ions, ^{3}He, or ^{4}He (α-particles). There is some ambiguity in the harmonics of these frequencies, in particular as $\Omega_D = \Omega_\alpha$. Often, not all harmonics are present. In some experiments, only odd multiples of Ω_α were observed[2]. The peaks may also exhibit features such as a doublet structure. The continuum spectrum extends to frequencies of up to 500 MHz.

Experiments in JET have observed ICE for a wide range of fusion reactivity[3]. The total emitted power of ICE in JET has been roughly proportional to the observed neutron production rate, over a range of six decades. This range of experiments includes D-D and D-T plasmas, with either Ohmic heating or neutral beam injection

(NBI). Experiments on Ohmically heated discharges observed ICE to be correlated with inverted sawteeth[22].

We focus on a series of NBI heated H-mode discharges of D-T plasmas with the plasma configured as a single null X-point. Parameters for numerical calculations were chosen with these experiments in mind, in particular using the plasma parameters as given for pulse number 26148 in Ref. [3]. For this pulse tritium beams were injected at 78 keV. The NBI accounted for a small fraction of the 14.3 MW of total heating. For these discharges the fusion products are predominantly α-particles and neutrons from reaction (6.4). Separate harmonics were observed for the first seven harmonics of Ω_α, with the continuum spectrum beginning at roughly $8\Omega_\alpha$. The peaks corresponded to multiples of the cyclotron frequency Ω_α near the low-field side of the plasma edge, near $R \simeq R_0 + 0.8a$, where $a \simeq 1.05$ m is the minor radius of the plasma column. The width of the individual peaks corresponded to the variation in Ω_α over a region up to 0.2 m wide in major radius. However, mechanisms for frequency broadening other than variations in the cyclotron frequency may also be important. The power spectrum for pulse 26148 as reproduced from Ref. [21] is shown in Fig. 6-1. The time evolution of the neutron emission rate is compared with the integrated ICE power in Fig. 6-2, with the total number of α-particles as determined by transport code shown as well. These results have been interpreted[3] as an indication that changes in the fusion reaction rate affect ICE power only after a delay of approximately 0.5 s, which is comparable to the slowing down time. Time-resolved spectra revealed a strong correlation between increases in the intensity of ICE and edge localized MHD modes (ELMs), as shown in Fig. 6-3 for pulse number 26147. Figs. 6-2 and 6-3 are reproduced from Ref. [3]. Detection of ICE in these spectra was limited to $k_{||} \lesssim 7\ \mathrm{m}^{-1} \ll 1/d_{i0} \simeq 20\ \mathrm{m}^{-1}$, where $d_{i0} = c/\omega_{pi}$ evaluated at the center of the plasma.

Correlations with sawteeth are not observed for these discharges. Large ELMs (with displacements of 10-20 cm) exhibit a different behavior and temporarily quench the ICE. This is interpreted as indicating that the ELM has extended into the region of the plasma where the mode-particle interactions are occurring, and terminated the

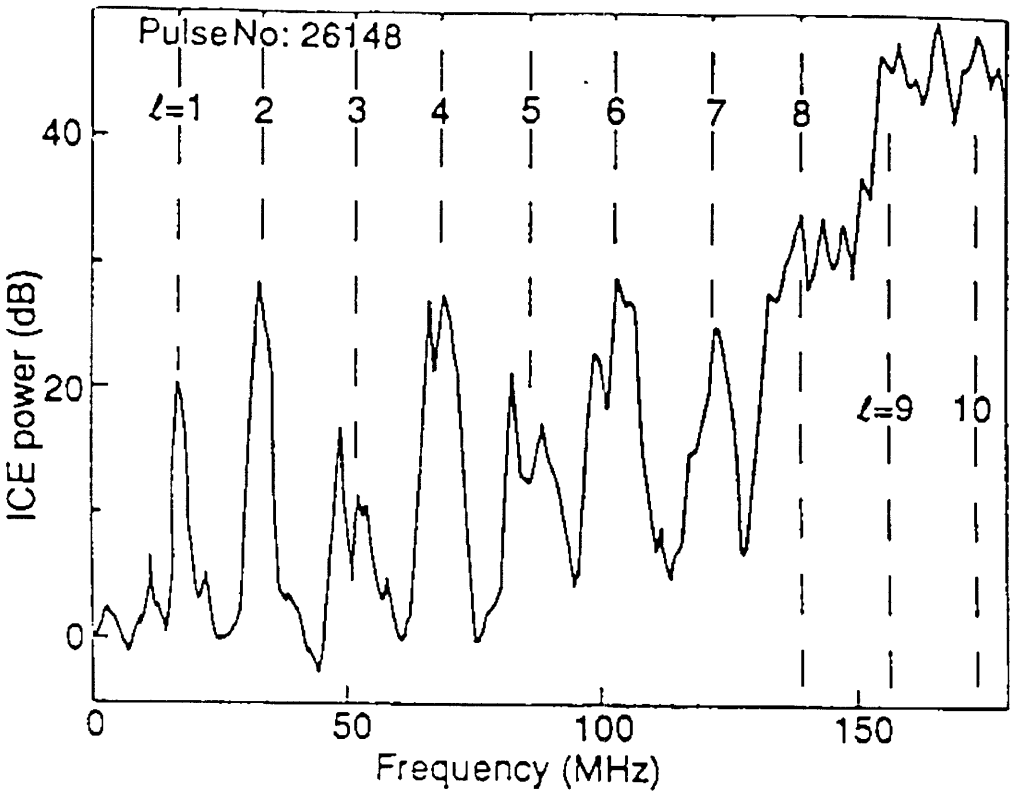

Figure 6-1: Enhanced ion cyclotron emission from D-T fusing plasmas produced by the JET machine. The peaks correspond to harmonics of Ω_α, the cyclotron frequency of the α-particles generated by D-T reactions, evaluated at the outer edge of the torus, specifically for $R \simeq R_0 + 0.8a$, where a is the minor radius of the plasma column and R_0 is the major radius at the magnetic axis. The multiple ℓ of the cyclotron frequency is indicated. Figure reproduced from *Physics Letters A* **172** (6) B. Coppi, "Origin of radiation emission induced by fusion reaction products," pp. 439-442, 1993.

local population of fast ions. Most of the emitted power is in the continuum range; the first seven harmonics account for only 2% of the total power. The total power was of the order of a few watts, as compared with 235 kW of α-particle energy produced by fusion. Simulations indicated that the α-particle density near the low-field side of the plasma edge was 10-20 times smaller than the central density. This figure is consistent with the model distribution function in Eq. (2.9) with $\Sigma = 0.05$, because the peak value of the distribution function is similar to the distribution function in the plasma core, which is only weakly dependent on pitch angle.

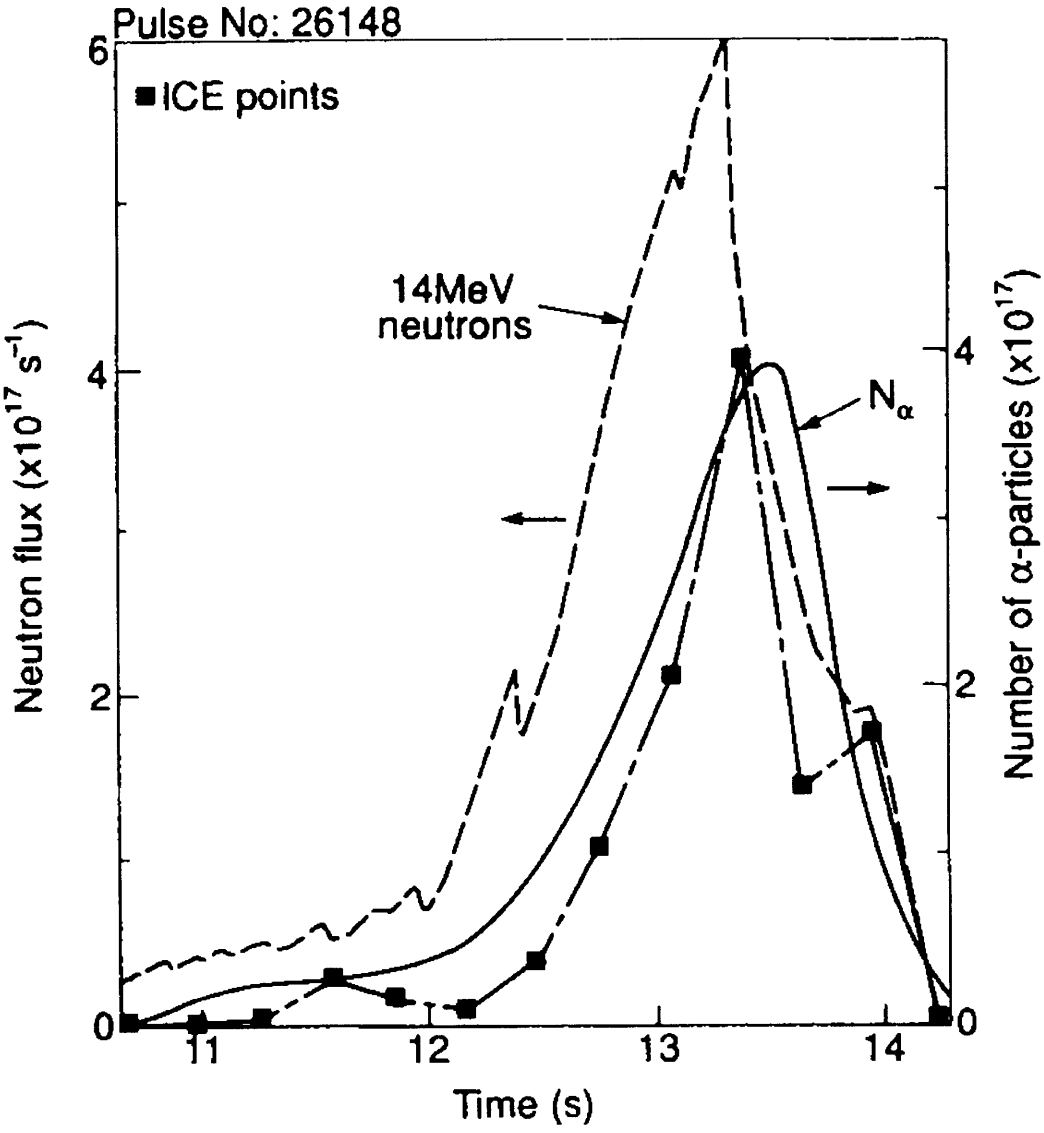

Figure 6-2: Time evolution of 14 MeV neutron emission (dashed line) and total number of α-particles (solid line), compared with the integrated ICE signal (points) for DT pulse number 26148 on the JET machine. The scale on the ICE power is linear and in arbitrary units.

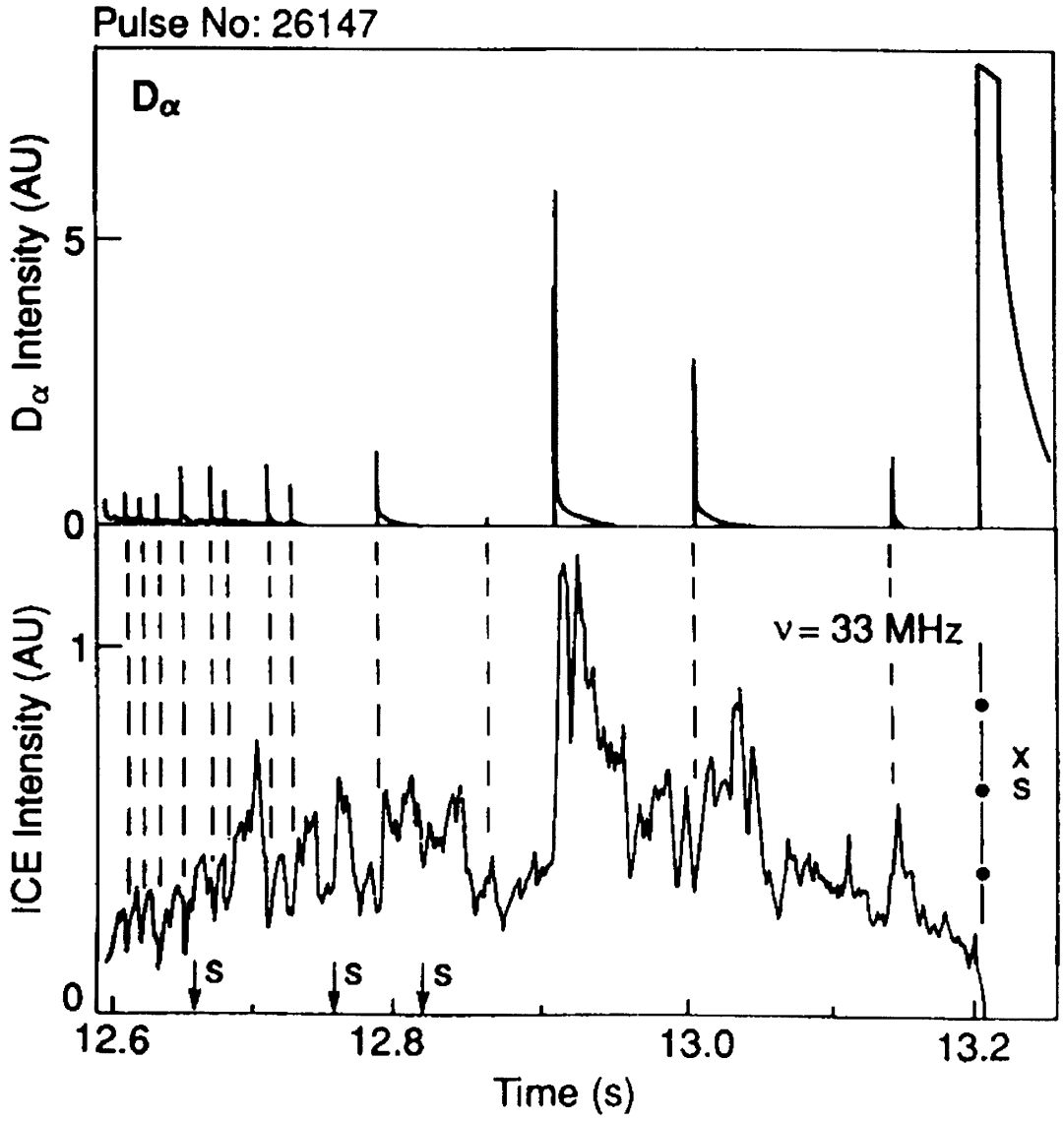

Figure 6-3: Comparison of the ICE signal with ELM events for DT pulse number 26147 on the JET machine. The times of sawtooth collapse are denoted by the symbols "S", and the X event and associated sawtooth collapse by "XS".

Experiments on TFTR have seen significantly different characteristics of ICE in fusing plasmas[2]. Radiation has been observed for frequencies up to 400 MHz, with a continuum spectrum developing late in the discharge in the range $5 - 10\ \Omega_D$. The time behavior of the ICE is complex, without a strict correlation between the neutron flux and total emitted power. We focus on D-T injected beams, such as shot 73255, which is shown in Fig. 6-4 as reproduced from Ref. [2]. Early in the discharge, harmonics of both Ω_α and $\Omega_{^3He}$ are observed, with narrow peaks; however, they correspond to the cyclotron frequency evaluated in different regions of the plasma. Late in the discharge, harmonics of Ω_T and $\Omega_D = \Omega_\alpha$ are observed, having peaks that are much broader. There is no observed correlation between total emitted ICE power and neutron flux rate, although there is a weak (sublinear) dependence of the power emitted at the low harmonics of Ω_α early in the discharge. In these experiments most ($\sim 90\%$) of the plasma heating derives from neutral beam injection and the density profile is strongly peaked at the plasma core[23]. The minor radius is taken to be $a \simeq 0.875$ m, and d_{i0} satisfies $1/d_{i0} \simeq 26\ \mathrm{m}^{-1}$, which leads to a slightly lower ratio of $d_{i0}/a \simeq 0.044$ than for the parameters used to model experiments on JET.

Discharges with neutral beams consisting of pure deuterium or pure tritium exhibit a similar behavior, except that early in D-D discharges there are no Ω_α harmonics, and late in the discharge the harmonics correspond to the cyclotron frequency of the beam ion species only.

6.2 Homogeneous magnetosonic-cyclotron instability

In view of the interpretation that ICE is driven by energetic particles, we examine the instabilities driven by α-particles in a homogeneous, magnetized plasma. We consider electromagnetic waves in a homogeneous plasma having the form

$$\vec{E}_1(y,z,t) = \vec{E}_1 \exp(-i\omega t + ik_\perp y + ik_{||} z)$$

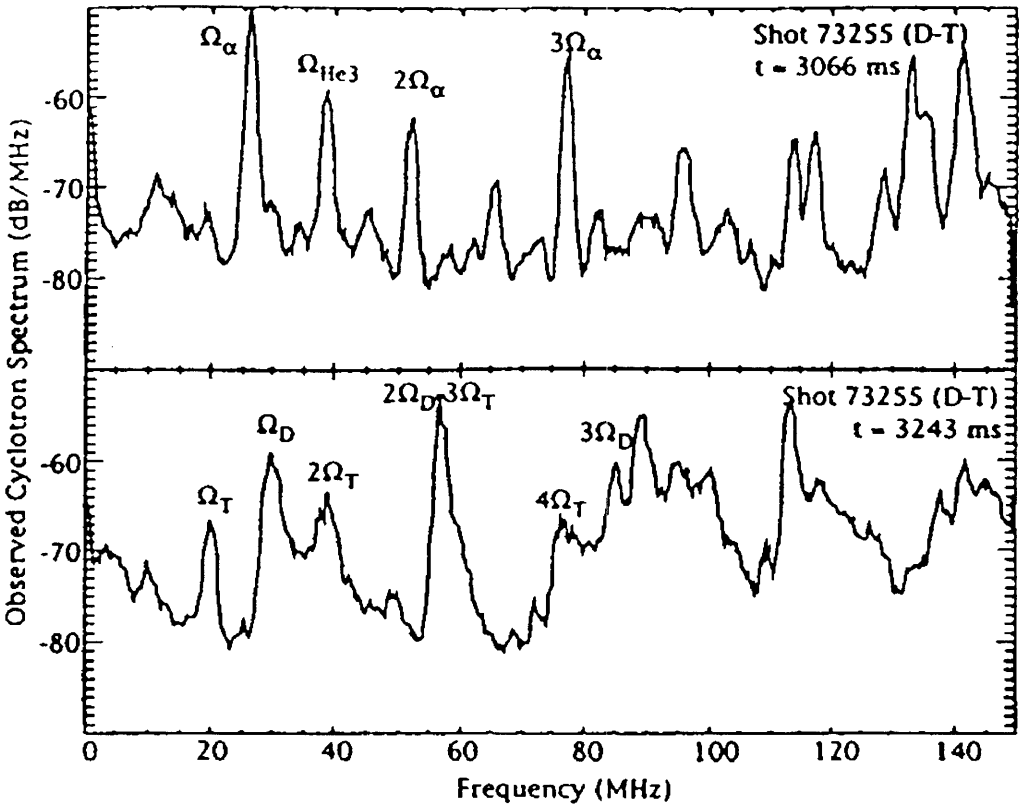

Figure 6-4: ICE spectra during D and T beam injection on the TFTR machine. Spectra correspond to immediately after beam injection (top) and later in the shot (bottom).

where the equilibrium magnetic field is taken to be $\vec{B} = B_0\hat{e}_z$ with $B_0 > 0$. We treat the effect of a small component of α-particles as a perturbation to the wave as supported by the background plasma, and evaluate the resulting growth rate. For these calculations, it is conventional and simplest to define the gyrophase φ such that

$$\vec{v} = v_{\|}\hat{e}_z + v_{\perp}(\cos\varphi\ \hat{e}_y - \sin\varphi\ \hat{e}_x) \tag{6.5}$$

with $v_\perp$ a positive quantity. With this convention, the equation of motion of the gyrophase is

$$\frac{d}{dt}\varphi = -\Omega_\alpha.$$

When $\varphi = 0$, the perpendicular velocity is oriented parallel to the perpendicular component of the wave vector (or anti-parallel, depending on the sign of $k_\perp$).

In the absence of guiding center drifts, the perturbed α-particle distribution function can be evaluated using the method of characteristics to yield

$$\begin{aligned}\delta f_\alpha \;=\; & -iq_\alpha \exp(i\xi\ \sin\varphi)\exp(-i\omega t + ik_\perp y + ik_{\|}z)\sum_p \frac{\exp(-ip\varphi)}{\omega - k_{\|}v_{\|} - p\Omega_\alpha} \\ & \left\{ v_\perp \left[\frac{p}{\xi}J_p(\xi)E_{1y} - iJ_p'(\xi)E_{1x}\right]\left[\frac{\partial}{\partial\mathcal{E}} + \left(1 - \frac{k_{\|}v_{\|}}{\omega}\right)\frac{1}{B}\frac{\partial}{\partial\mu}\right] f_{\alpha 0} \right. \\ & \left. + v_{\|}J_p(\xi)E_{1z}\left[\frac{\partial}{\partial\mathcal{E}} + \frac{p\Omega_\alpha}{\omega}\frac{1}{B}\frac{\partial}{\partial\mu}\right] f_{\alpha 0}\right\}\end{aligned} \tag{6.6}$$

where $\xi \equiv k_\perp v_\perp/\Omega_\alpha$ and J_p is the ordinary Bessel functions with index p. Note that for positively charged ions, ξ has the same sign as $k_\perp$. We shall find that the final growth rate is independent of the sign of $k_\perp$. Here all co-ordinates represent macroscopic variables and not guiding center position. In terms of the actual particle variables, the guiding center position is given by

$$\vec{X}_g = \vec{x} + \frac{1}{\Omega_\alpha}\vec{v}\times\hat{e}_{\|} = \vec{x} + \frac{v_\perp}{\Omega_\alpha}(\cos\varphi\ \hat{e}_x + \sin\varphi\ \hat{e}_y)$$

It has also been assumed that $f_{\alpha 0}$, the unperturbed α-particle distribution function,

is independent of gyrophase. The Bessel functions arise from the identity

$$\exp(-i\xi\sin\varphi) = \sum_p \exp(-ip\varphi)J_p(\xi)$$

Because we are modelling the interaction of α-particles with modes related to the magnetosonic-whistler wave, we set to zero the parallel electric field, $E_{1z} = 0$. Thus to evaluate the growth rate we need only consider the current perpendicular to the equilibrium magnetic field.

The perpendicular components of the perturbed α-particle current are given by

$$\delta\vec{J}_{\alpha\perp} = q_\alpha \int d^3v\ \vec{v}_\perp\ \delta f_\alpha \tag{6.7}$$

The average over gyrophase yields the quantity

$$\frac{1}{2\pi}\int_0^{2\pi} d\varphi\ \exp(-ip\varphi + i\xi\sin\varphi)(\cos\varphi\ \hat{e}_y - \sin\varphi\ \hat{e}_x) = \frac{p}{\xi}J_p(\xi)\hat{e}_y + iJ_p'(\xi)\hat{e}_x$$

The resulting current is

$$\begin{aligned}\delta\vec{J}_{\alpha\perp} &= -i\frac{q_\alpha^2}{m_\alpha^{5/2}}\exp(-i\omega t + ik_\perp y + ik_\| z)\int 4\pi\frac{B^2\mu d\mu d\mathcal{E}}{\sqrt{2(\mathcal{E}-\mu B)}} \\ &\sum_p \frac{1}{\omega - k_\| v_\| - p\Omega_\alpha}\left[\frac{p}{\xi}J_p(\xi)\hat{e}_y + iJ_p'(\xi)\hat{e}_x\right]\left[\frac{p}{\xi}J_p(\xi)E_{1y} - iJ_p'(\xi)E_{1x}\right] \\ &\left[\frac{\partial}{\partial\mathcal{E}} + \left(1 - \frac{k_\| v_\|}{\omega}\right)\frac{1}{B}\frac{\partial}{\partial\mu}\right] f_{\alpha 0}\end{aligned} \tag{6.8}$$

The resonant part of the interaction is given by replacing

$$\frac{1}{\omega - k_\| v_\| - p\Omega_\alpha}$$

with

$$-i\pi\delta(\omega - k_\| v_\| - p\Omega_\alpha).$$

It is this resonant term which is in phase with the electric field and so contributes to the growth rate of the mode. In general only a single harmonic will be resonant, with

harmonic number ℓ given by $\omega \simeq \ell\Omega_\alpha$. The induced growth rate then has the form

$$\begin{aligned}\gamma &= -\Re\mathrm{e}\frac{\vec{E}_1^* \cdot \delta\vec{J}_\alpha}{\omega\epsilon_0 \frac{\partial D_0}{\partial\omega}|\vec{E}_1|^2} \\ &= \frac{1}{\omega\partial D_0/\partial\omega} 2\pi^2 \frac{\omega_{p\alpha}^2}{n_\alpha}\frac{\Omega_\alpha^2}{k_\perp^2} \\ &\quad \int \frac{B d\mu d\mathcal{E}}{m_\alpha^{1/2}\sqrt{2(\mathcal{E}-\mu B)}} \delta(\omega - k_\| v_\| - \ell\Omega_\alpha) W_\ell(\xi) \left[\frac{\partial}{\partial\mathcal{E}} + \left(1 - \frac{k_\| v_\|}{\omega}\right)\frac{1}{B}\frac{\partial}{\partial mu}\right] f_{\alpha 0}\end{aligned} \tag{6.9}$$

with $\omega_{p\alpha}^2 \equiv n_\alpha q_\alpha^2/\epsilon_0 m_\alpha$,

$$W_\ell(\xi) \equiv \frac{\left|\ell J_p(\xi)E_{1y} - i\xi J_p'(\xi)E_{1x}\right|^2}{|E_{1x}|^2 + |E_{1y}|^2} = \frac{\left|\ell J_p(\xi)\Lambda_p + \xi J_p'(\xi)\right|^2}{1+|\Lambda_p|^2},$$

and where D_0 is the determinant of the dispersion matrix. The polarization Λ_p is defined as $\Lambda_p = iE_{1y}/E_{1x}$. Note that W_ℓ is independent of the sign of ξ. For magnetosonic modes having a small parallel wave vector, $\Lambda_p \simeq \omega/\Omega_i$ and

$$\frac{\partial D_0}{\partial\omega} \simeq 2\frac{\omega_{pi}^2}{\omega^3}.$$

Because of the delta-function, the quantity $k_\| v_\|/\omega$ in the differential operator can be replaced with $(\omega - \ell\Omega_\alpha)/\omega$, which is independent of velocity.

Defining $\hat{f} \equiv 2\pi f_{\alpha 0} v_\alpha^3/n_\alpha$, we can perform the integral over μ, which eliminates the delta-function from the resonance, and express the growth rate normalized to the main ion species cyclotron frequency as

$$\frac{\gamma}{\Omega_i} = \frac{n_\alpha}{n_e}\frac{\omega^2}{\Omega_i^2}\frac{q_\alpha\pi}{2}\frac{\Omega_\alpha^2}{k_\perp^2 v_\alpha^2} I \tag{6.10}$$

where the quantity I has the form

$$I \equiv \int d\mathcal{E}\frac{\Omega_\alpha}{|k_\||v_\alpha} W_\ell(\xi)\left[\frac{\partial}{\partial\mathcal{E}} + \left(1 - \frac{k_\| v_\|}{\omega}\right)\frac{1}{B}\frac{\partial}{\partial\mu}\right]\hat{f}\Big|_{v_\| = (\omega - \ell\Omega_\alpha)/k_\|} \tag{6.11}$$

Here the condition $v_{||} = (\omega - \ell\Omega_\alpha)/k_{||}$ corresponds to

$$\mu = \mu_{\rm res}(\mathcal{E}) = \frac{\mathcal{E}}{B} - \frac{m_\alpha}{2B}\left(\frac{\omega - \ell\Omega_\alpha}{k_{||}}\right)^2 .$$

However, the partial derivatives act with respect to general $\mathcal{E}$ and μ.

Taking the normalized distribution function to have the form

$$\hat{f} = C\delta(c(\mathcal{E},\mu) - c_0)g(\mathcal{E},\mu)$$

the factor I reduces to

$$\begin{aligned} I \;=\; & \frac{\Omega_\alpha}{|k_{||}|v_\alpha} W_\ell(\xi) \frac{1}{|\partial c/\partial\mathcal{E} + \partial c/B\partial\mu|} \\ & \left[-\frac{C}{2\mu B} g(\mathcal{E},\mu)\left(1 - \frac{k_{||}v_{||}}{\omega}\frac{\partial c/B\partial\mu}{\partial c/\partial\mathcal{E} + \partial c/B\partial\mu}\right)\xi\frac{d}{d\xi}\ln W_\ell(\xi) \right. \\ & \left. + \frac{k_{||}v_{||}}{\omega}\left(\frac{\partial c}{B\partial\mu}\frac{\partial}{\partial\mathcal{E}} - \frac{\partial c}{\partial\mathcal{E}}\frac{\partial}{B\partial\mu}\right)\left(\frac{Cg(\mathcal{E},\mu)}{\partial c/\partial\mathcal{E} + \partial c/B\partial\mu}\right)\right]\Bigg|_{\substack{c(\mathcal{E},\mu)=c_0 \\ v_{||}=(\omega-\ell\Omega_\alpha)/k_{||}}} \end{aligned} \tag{6.12}$$

For example, choosing $c = \mathcal{E}$, $c_0 = C = \mathcal{E}_\alpha$, and

$$g = \exp\left[-\frac{(\mu B/\mathcal{E} - \Lambda_0)^2}{2\Sigma^2}\right]$$

then

$$I = \frac{\Omega_\alpha}{|k_{||}|v_\alpha} W_\ell(\xi) g(\mathcal{E},\mu)\left[-\frac{\mathcal{E}}{2\mu B}\xi\frac{d}{d\xi}\ln W_\ell(\xi) + \frac{k_{||}v_{||}}{\omega}\left(\frac{\mu B/\mathcal{E} - \Lambda_0}{\Sigma^2}\right)\right]\Bigg|_{\substack{\mathcal{E}=\mathcal{E}_\alpha \\ v_{||}=(\omega-\ell\Omega_\alpha)/k_{||}}}$$

Note, however, that for this choice of distribution function the particle density corresponds to the local particle density at the mode layer, and not the average particle density n_α. In fact, the density is roughly given by $n_\alpha\Sigma[2\pi/(1-\Lambda_0)]^{1/2}$.

Two other simplified distribution functions commonly used in calculations of the growth rate[24, 25, 26] are

$$\hat{f} = v_\alpha\delta(v_\perp - v_\alpha)\exp\left[-(v_{||} - v_d)^2/2v_s^2\right]$$

which yields

$$I = \frac{\Omega_\alpha}{|k_\parallel| v_\alpha} W_\ell(\xi) g(\mathcal{E},\mu) \left[-\left(1 - \frac{k_\parallel v_\parallel}{\omega}\right) \xi \frac{d}{d\xi} \ln W_\ell(\xi) - \frac{k_\parallel v_\parallel}{\omega} \frac{v_\alpha^2}{v_s^2} \frac{v_\parallel - v_d}{v_\parallel} \right] \Bigg|_{\substack{v_\perp = v_\alpha \\ v_\parallel = (\omega - \ell\Omega_\alpha)/k_\parallel}}$$

and

$$\hat{f} = \delta(\Lambda - \Lambda_0) \exp\left[-(v - v_\alpha)^2 / 2v_T^2\right]$$

where $\Lambda \equiv \mu B / \mathcal{E}$, which yields

$$\begin{aligned} I \;=\; & \frac{\Omega_\alpha}{|k_\parallel| v_\alpha} W_\ell(\xi) g(\mathcal{E},\mu) \frac{1}{(1-\Lambda)^2} \\ & \left[-\frac{1}{2\Lambda} \left(1 - \Lambda - \frac{k_\parallel v_\parallel}{\omega}\right) \xi \frac{d}{d\xi} \ln W_\ell(\xi) \; + \frac{k_\parallel v_\parallel}{\omega} \frac{v}{2} \frac{d}{dv} \ln\left[v^2 g(v)\right] \right] \Bigg|_{\substack{\Lambda = \Lambda_0 \\ v_\parallel = (\omega - \ell\Omega_\alpha)/k_\parallel}} \end{aligned}$$

In general, the growth rate consists of two terms, one from finite Larmor radius effects and the other from velocity gradients in the distribution function, such as anisotropy. The anisotropy term becomes larger for distribution functions that are more peaked. The finite Larmor radius term increases inversely with $k_\parallel$; this is compensated for by the fact that the resonance condition becomes more difficult to satisfy, yet one important consequence is that the finite Larmor radius term becomes dominant as $|k_\parallel| \to 0$.

6.3 Interaction of energetic ions with contained modes

The interaction of fusion products with magnetosonic waves corresponding to the homogeneous case will not by themselves explain observations of ICE in a confined plasma. This is because such modes will convect to the plasma edge in a time scale a/v_A. Thus, significant energy deposition by energetic particles is only possible if the initial amplitude of the wave is large and the growth rate is larger than $v_A/a = \Omega_i d_i / a$. This condition is not likely to be satisfied in a conventional plasma experiment with a small subpopulation of energetic ions. The contained modes, however, do not convect

out of the plasma and will couple only weakly to external modes. Thus, these modes can build up to significant amplitudes by absorbing energy from fusion products, at which point they may generate ICE at levels observed in experiments. Thus, we interpret any delay in the generation of ICE from the onset of significant fusion reactivity as the time needed for the contained modes to saturate, and not as being related to the slowing down time.

We recall that the parameters used in numerical calculations of the α-particle distribution function and the contained mode were $B_0 \simeq 2.8$ T, $R_0 \simeq 3.5$ m, $\epsilon \equiv a/R_0 \sim 0.3$, and $n_0 \simeq 3.75 \times 10^{19}$ m^{-3}. The Alfvén velocity at the core is $v_A \simeq 7.08 \times 10^6$ m/s. The deuteron (and α-particle) cyclotron frequency is $\Omega_D \simeq 1.34 \times 10^8$ rad/s. The gyroradius of 3.5 MeV α-particles is given by $\rho_\alpha \simeq 0.0965$ m.

Considering other ions produced by fusion reactions, the gyroradius for tritium and for protons is $\rho_{\rm T} \simeq \rho_{\rm p} \simeq 0.91\rho_\alpha$, so that the orbits of these energetic ions would be almost identical to those of α-particles produced by fusion. Furthermore, the fusion rate for D-D reactions has roughly the same profile as that for D-T reactions, so that the distribution functions would be similar. However, because of the different particle velocities, collisional slowing down times would be different. In the case of ^{3}He, $\rho_{^3{\rm He}} \simeq 0.41\rho_\alpha \simeq 4.0$ cm for the parameters used in this model. Thus a much smaller fraction of such particles reach the mode layer. In addition to anisotropy in velocity space, instabilities are driven by finite Larmor radius effects. For resonant interactions, such that $\omega \simeq \ell\Omega$ where Ω is the cyclotron frequency of the resonating particles, the strength of these effects is determined by the parameter $k_\perp v_\perp/\omega$. For magnetosonic modes this quantity is related to the ratio of the particle velocity to the Alfvén velocity. For the charged fusion products from reactions (6.1), (6.2), and (6.4), the particle velocities are

$$
\begin{aligned}
v_{\rm p} &\simeq 2.40 \times 10^7 \text{ m/s} \\
v_\alpha &\simeq 1.31 \times 10^7 \text{ m/s} \\
v_{\rm T} &\simeq 7.99 \times 10^6 \text{ m/s} \\
v_{^3{\rm He}} &\simeq 7.24 \times 10^6 \text{ m/s}
\end{aligned}
$$

Finite Larmor radius effects are strongest for the protons and α-particles. Tritium produced by fusion is not expected to destabilize the contained mode for the parameters comparable to experiments on JET, because the perpendicular particle velocity is smaller than the Alfvén velocity and finite Larmor radius effects are not a significant driving term. Note that v_A is slightly higher at the mode layer than at the plasma core. By contrast, experiments on TFTR[23] have as a typical set of parameters $B_0 \simeq 5.0$ T and $n_0 \simeq 7 \times 10^{19}$ m^{-3}, so that $v_A \simeq 9.22 \times 10^6$ m/s in the plasma core. In addition, the Alfvén velocity at the mode layer is significantly higher on TFTR because of the much more peaked density profile. Thus, finite Larmor radius effects are much weaker in TFTR than in the corresponding experiments on JET.

The mode width is much smaller than the radial excursion of the energetic α-particles in the outer regions of the plasma, especially for the higher harmonics. Thus, the interaction of the particle with the contained mode can be treated approximately as a localized driving term at the intersection of the particle orbit with the mode layer. Furthermore, if the growth rate is larger than the bounce frequency, correlations between successive intersections can be neglected and the interaction is purely local. Thus the picture for the mode-particle interaction is given as in Fig. 3-1. For particles which intersect the mode layer at $\vartheta \neq 0$, the orbit passes through the mode layer transversely. This model yields results which are quite different from that of a deeply trapped particle immersed in an applied electromagnetic field. In fact, the resulting growth rate is in certain regimes roughly similar to the growth rate as calculated for the homogeneous case. The main difference lies in the selection criteria for the existence of contained modes. As discussed in Chapter 4, these modes tend to be localized about a fixed radial shell and for typical parameters only exist for one orientation of the poloidal phase velocity.

The mode width Δ is assumed to be larger than the α-particle gyroradius; otherwise, the radial structure of the contained mode will modify the Bessel function form factors in the quantity W_ℓ. However, given that $1 \ll k_\perp^2 \Delta^2 \sim |m|$, the corrections involved should be small. For the modes under consideration, this is equivalent to $\ell a/d_i \gg 1$. This effect will be discussed in more detail in Chapter 7.

In this work calculations are performed for plasmas with a cylindrical cross-section. For the JET discharges which are the focus of our comparison with experiments, the ellipticity near the plasma edge is $\kappa \simeq 1.6$. We also assume that the contained mode can be described in terms of a single poloidal harmonic, which for a toroidal plasma is equivalent to consider large aspect ratio. For the JET experiment, the aspect ratio R_0/a is typically only slightly larger than 3.

Chapter 7

Induced growth rate of contained modes

In Chapter 5 we have examined the dispersion equation for the contained modes, considering only the background plasma. We can see how this is modified by the influence of fusion products by using an expansion in the ratio $n_\alpha/n_e \ll 1$. In fact, the presence of n_α will give rise to an additional current contribution $\delta\vec{J}_\alpha$, yielding a new term in the dispersion equation proportional to n_α. In order to calculate the corrections related to the presence of the fusion products, it is convenient to analyze the problem in terms of the perturbed electric fields $\vec{E}_1$.

Beginning with the original mode equation the dispersion relation can be written as $D_0(\omega, m, n^0) = 0$, where D_0 is related to the effective potential, defined in Eq. (4.25), by $D_0 \simeq -V_{\text{eff}}(\omega, r_{\text{mode}})c^2/\omega^2$, correct to order $1/m$. The perturbed fields will have the form of Eq. (4.26)

$$\vec{E}_1(r) \simeq \vec{E}_1 H_s\left(\frac{r - r_{\text{mode}}}{\Delta}\right) \exp\left[-\frac{(r - r_{\text{mode}})^2}{2\Delta^2} - i\omega t - im\vartheta + in^0\zeta\right] \tag{7.1}$$

In terms of components, $\vec{E}_{1\perp} = E_{1r}\hat{e}_r + E_{1\vartheta}\hat{e}_\vartheta = E_{1r}(\hat{e}_r - i\Lambda_p\hat{e}_\vartheta)$ with $\Lambda_p \equiv iE_{1\vartheta}/E_{1r} \simeq \omega/\Omega_i$. This is similar to the result Eq. (4.9) found in Chapter 4 for the polarization of the magnetosonic-whistler wave in a homogeneous plasma. The dispersion relation

with α particles can be written as

$$D_0(\omega, k) + \delta D_\alpha(\omega, k) = 0 \tag{7.2}$$

where

$$\delta D_\alpha(\omega, k) = \frac{i}{\omega \epsilon_0} \frac{< \vec{E}_1^* \cdot \delta \overleftrightarrow{\sigma} \cdot \vec{E}_1 >}{< \left|\vec{E}_1\right|^2 >}$$

with $\delta \overleftrightarrow{\sigma}$ defined by

$$\delta \overleftrightarrow{\sigma} \cdot \vec{E}_1 \equiv \delta \vec{J}_\alpha \equiv q_\alpha \int \vec{v}\, \delta F_\alpha \, d^3\vec{v} \tag{7.3}$$

The brackets indicate spatial averages. We recall that the mode solution given by Equation (7.1) is sharply localized about $r = r_{\text{mode}}$, and the average will later be replaced by the condition that $\delta \overleftrightarrow{\sigma}$ is evaluated at $r = r_{\text{mode}}$. Corrections to $\vec{E}_1$ do not give any contribution to $\delta \vec{J}_\alpha$ to the order being considered.

Solving perturbatively for the imaginary part of the frequency, γ, yields

$$\gamma = -\Re \text{e} \frac{< \vec{E}_1^* \cdot \delta \overleftrightarrow{\sigma} \cdot \vec{E}_1 >}{\omega \epsilon_0 (\partial D_0 / \partial \omega) < \left|\vec{E}_1\right|^2 >} \tag{7.4}$$

7.1 Magnetic field geometry and drifts

To obtain $\delta \overleftrightarrow{\sigma}$, we begin with a full gyrokinetic calculation of δF_α, the perturbed α-distribution due to the fields from the contained mode, for frequencies above Ω_α[8, 9]. This level of detail is necessary due to the large trapped orbits and Larmor radii of the fusion-produced α-particles. We model the magnetic field as

$$\vec{B} = \frac{B_0}{1 + (r/R_0)\cos\vartheta} \left(\hat{e}_\zeta + \frac{r}{R_0 q(r)} \hat{e}_\vartheta \right)$$

and we consistently neglect effects related to finite $\beta = 2\mu_0 p / B^2$ at the plasma edge. We consider the limit of ω very close to a harmonic resonance with Ω_α, with harmonic number denoted as ℓ, so that only a single harmonic term contributes to each mode-particle interaction. The gyrokinetic calculation applies to systems where the magnetic field varies on a scale length considerably larger than the gyroradius of the

particles. We expand in the parameter $\lambda = \rho_\alpha / L_B$, and keep all terms in the interaction between the mode and the fusion products to first order in λ. For the sake of simplicity we neglect corrections of order $\lambda/q(r)$, which means that we consider only the gradient and curvature drifts due to the toroidal field, which have the combined form

$$\vec{v}_d = -\frac{2\mathcal{E} - \mu B}{m_\alpha R \Omega_\alpha} (\hat{e}_\vartheta \cos\vartheta + \hat{e}_r \sin\vartheta)$$

For the following section, we introduce the notation that the vector $\vec{X}$ refers to the guiding center coordinates, while the relevant coordinates in velocity space are $\mathcal{E}$, μ, and φ, where $\mathcal{E} = m_\alpha v^2/2$, $\mu = m_\alpha v_\perp^2/2B$, and φ is the gyroangle. In the following equations, all spatial coordinates refer to the guiding center location. For functions, the subscript g will indicate that the function dependence is expressed in terms of guiding center variables.

The unperturbed distribution function for the fusion products is approximately given by F_{g0} as obtained in Eq. (2.9). The function F_{g0} does not depend on φ but only on $\mathcal{E}$, μ, and the guiding center coordinates. However, because calculations of the mode-particle interaction are being carried out to first order in λ, the first order correction to F_{g0} must also be included. As in Refs.[8, 9] this correction arises from the more precise form of the adiabatic invariant

$$\mu_1 = \frac{m_\alpha v_\perp^2}{2B} \left[1 - \frac{2\vec{v}_\perp \cdot \vec{v}_d}{v_\perp^2} + \mathcal{O}\left(\frac{\lambda}{q(r)}\right) \right].$$

The first correction to μ as defined above is an order λ quantity and leads to a new form for the distribution function:

$$F_{g\alpha} = F_{g0}(\mu, \mathcal{E}, \vec{X}) - (\vec{v}_\perp \cdot \vec{v}_d) \frac{1}{B} \frac{\partial F_{g0}}{\partial \mu} \tag{7.5}$$

By using the results from the previous section we can take F_{g0} of the form Eq. (2.9).

7.2 Gyrokinetic calculation of linear response

The perturbed distribution function for the α-particles under the effect of the contained mode will be given by the gyrokinetic version of the Vlasov kinetic equation[8, 9]

$$\langle L_g \rangle_\ell \langle \delta F_{g\alpha} \rangle_\ell = - \langle S_g \rangle_\ell \tag{7.6}$$

where

$$\langle L_g \rangle_\ell = (v_\parallel \hat{e}_\parallel + \vec{v}_d) \cdot \nabla_X - i(\omega - \ell \Omega_\alpha(R))$$

For simplicity, in the above formula we neglect corrections to the resonant frequency, of the form $\omega_\varphi = \langle \vec{v} \cdot \nabla_x \varphi \rangle_0$. The quantity $\langle S_g \rangle_\ell$ is related to the perturbed field operating on the unperturbed distribution function and is defined by

$$\begin{aligned} \langle S_g \rangle_\ell \;=\; q_\alpha \Big\langle \Big[(\vec{E}_1 + \vec{v} \times \vec{B}_1) \cdot \Big(\vec{v} \frac{\partial}{\partial \mathcal{E}} + \frac{\vec{v}_\perp}{B} \frac{\partial}{\partial \mu} - \frac{\vec{v} \times \hat{e}_\parallel}{v_\perp^2} \frac{\partial}{\partial \varphi} \Big) \\ + (\vec{E}_1 + \vec{v} \times \vec{B}_1) \times \frac{\hat{e}_\parallel}{\Omega_\alpha} \cdot \nabla_X \Big] F_{g\alpha} \Big\rangle_\ell \end{aligned} \tag{7.7}$$

The harmonic components, which by definition are independent of gyrophase, are defined by the expansion

$$\delta F_{g\alpha} = \sum_\ell \exp(-i\ell\varphi) \langle \delta F_{g\alpha} \rangle_\ell$$

where φ is the gyrophase angle given by $\vec{v}_\perp = v_\perp(\cos\varphi \; \hat{e}_a - \sin\varphi \; \hat{e}_b)$. The unit vectors are chosen so that $\hat{e}_a \simeq \hat{e}_\vartheta$, $\hat{e}_b \simeq \hat{e}_r$ and they form an orthonormal system with $\hat{e}_\parallel = \vec{B}/B$, consistent with the convention used in Section 6.2, Eq. (6.5).

Since we assume that the spatial structure of the mode determines the layer of the interaction, but that the nature of the interaction is determined mainly by the velocity distribution of the α-particles within the interaction layer, we can neglect the spatial derivatives of the unperturbed distribution function represented by the last

term in Eq. (7.7). Thus the relevant terms in Eq. (7.6) are

$$\langle S_g \rangle_\ell = \langle L_{g1} \rangle_\ell F_{g0} - \left\langle \vec{E}_1 \cdot \vec{v}_d - \frac{i}{\omega} \left[\vec{v} \times (\nabla \times \vec{E}_1) \right] \cdot \vec{v}_d \right\rangle_\ell \frac{1}{B} \frac{\partial F_{g0}}{\partial \mu} \tag{7.8}$$

where

$$L_{g1} = q_\alpha \left\{ \vec{E}_{g1\perp} \cdot \vec{v}_\perp \left(\frac{\partial}{\partial \mathcal{E}} + \frac{1}{B} \frac{\partial}{\partial \mu} \right) + \frac{i}{\omega} \left[v_\parallel \left(\hat{e}_\parallel \cdot \nabla_x \vec{E}_1 \right) \cdot \vec{v}_\perp \right]_g \frac{1}{B} \frac{\partial}{\partial \mu} \right\}$$

We have set $E_{1\parallel} = 0$ in the above equation. We define the quantities $\overline{F}_\ell$ for functions of phase space, and $\overline{\overline{A}}$ that is convenient for field functions, as

$$\begin{aligned} \langle F_g \rangle_\ell &= \overline{F}_\ell(r, \vartheta) \exp(-i\omega t - im\vartheta + in^0 \zeta) \\ \left\langle A_g \exp\left(i \frac{k_\perp v_\perp}{\Omega_\alpha} \sin\varphi \right) \right\rangle_0 &= \overline{\overline{A}}(r, \vartheta) \exp(-i\omega t - im\vartheta + in^0 \zeta) \end{aligned}$$

where r, ϑ, ζ are guiding center coordinates and $k_\perp \simeq -m/r$. Both $\overline{F}_\ell$ and $\overline{\overline{A}}$ are functions of guiding center coordinates. Note that the guiding center position $\vec{X}$ is defined by $\vec{X} = \vec{x} + \vec{v} \times \hat{e}_\parallel / \Omega_\alpha$. The quantity $\overline{\overline{A}}$ as a function of $\vec{X}$ is roughly equivalent to the slowly varying amplitude as a function of particle position $\vec{x}$, so that

$$A(\vec{x}, t) = \mathcal{A}(\vec{x}) \exp(i\omega t - i\vec{k} \cdot \vec{x}) \qquad \rightarrow \qquad \overline{\overline{A}}(\vec{X}) \simeq \mathcal{A}(\vec{x})|_{\vec{x}=\vec{X}}$$

By explicitly evaluating the components of $\langle S_g \rangle_\ell$ we find that $\overline{\delta F}_\ell$ must satisfy the following equation[27]:

$$\begin{aligned} &\left[\frac{v_\parallel}{q(r) R} \left(\frac{\partial}{\partial \vartheta} - i \left[m - n^0 q(r) \right] \right) - i \left(\omega - k_\perp v_{d\vartheta} - \ell \Omega_\alpha \right) + v_{dr} \frac{\partial}{\partial r} \right] \overline{\delta F}_\ell \\ &\qquad = -\frac{q_\alpha}{m_\alpha} P_{\ell r}(F_{g0}) \overline{\overline{E_{1r}}} - \frac{q_\alpha}{m_\alpha} P_{\ell\vartheta}(F_{g0}) \overline{\overline{E_{1\vartheta}}} \end{aligned} \tag{7.9}$$

where

$$P_{\ell\vartheta}(F_{g0}) = \frac{\ell}{\xi} J_\ell(\xi) \sqrt{2\mu B m_\alpha} \left[\frac{\partial}{\partial \mathcal{E}} + \left(1 - \frac{k_\parallel v_\parallel}{\ell \Omega_\alpha} - \frac{k_\perp v_{d\vartheta}}{\ell \Omega_\alpha} \right) \frac{1}{B} \frac{\partial}{\partial \mu} \right] F_{g0}$$

$$P_{\ell r}(F_{g0}) = iJ'_\ell(\xi)\sqrt{2\mu B m_\alpha}\left[\frac{\partial}{\partial \mathcal{E}} + \left(1 - \frac{k_{||}v_{||}}{\ell\Omega_\alpha} - \frac{k_\perp v_{d\vartheta}}{\ell\Omega_\alpha}\right)\frac{1}{B}\frac{\partial}{\partial\mu}\right]F_{g0}$$

with $\xi \equiv k_\perp v_\perp/\Omega_\alpha$, $v_\perp = \sqrt{2\mu B/m_\alpha}$ and $k_{||} = -(1/qR)(m - n^0 q)$. The operators $P_{\ell r}$ and $P_{\ell\vartheta}$ were calculated by neglecting the radial variation in the amplitude of the perturbed electric field. These operators also contain corrections of order λ; these corrections are proportional to $\partial/B\partial\mu$, giving no contribution for an isotropic function. Neglecting the radial variation in the electric field as a function of gyrophase (for fixed guiding center) is a valid approximation for the case where $1 \ll k_\perp^2\Delta^2 \sim |m| \sim \ell a/d_i$. Thus, the corrections are small even when $\Delta < \rho_\alpha$, because the poloidal variation still dominates the gyrophase dependence of the electric field.

Equation (7.9) has an integral solution

$$\begin{aligned}\overline{\delta F_\ell} &= -\int^\vartheta d\vartheta' \frac{q_\alpha}{m_\alpha}\frac{q(r)R}{v_{||}}\left[P_{\ell r}(F_{g0})\overline{\overline{E_{1r}}} + P_{\ell\vartheta}(F_{g0})\overline{\overline{E_{1\vartheta}}}\right] \\ &\quad \times \exp\left\{-i\int_\vartheta^{\vartheta'} d\vartheta''\left[\frac{q(r)R}{v_{||}}\left(\omega - k_\perp v_{d\vartheta} - \ell\Omega_\alpha\right) + \left(m - n^0 q(r)\right)\right]\right\}\end{aligned} \tag{7.10}$$

where the terms within the integral are evaluated at the guiding center $\vartheta', r(\vartheta')$, which defines particles orbits through

$$r(\vartheta') = \int^{\vartheta'} \frac{q(r)Rv_{dr}}{v_{||}}\, d\vartheta''.$$

7.3 Radial mode structure effects on gyrokinetic calculations

The equation found above for the perturbed distribution function was derived in the limit that the spatial variation of the mode was of the form $\exp(i\vec{k}\cdot\vec{x})$. Although the perpendicular wave vector is much larger than the spatial derivative of the eigenmode, the radial width of the mode can, at sufficiently high frequencies, be comparable to the α-particle gyroradius. Thus there will be additional terms in addition to the Bessel functions which occur in the α-particle response. We now derive a more general formulation of Eq. (7.9) by examining how the Bessel functions are

modified by the radial variation in the mode amplitude.

With $k_\perp \simeq -m/r$ and the gyrophase φ defined so that $d\varphi/dt = -\Omega$, we have

$$\vec{v}_\perp \simeq v_\perp \left(\cos\varphi\ \hat{e}_\vartheta - \sin\varphi\ \hat{e}_r\right).$$

The guiding center location $\vec{X}$ is given by

$$\vec{X} = \vec{x} + \frac{v_\perp}{\Omega}\left(\cos\varphi\ \hat{e}_r + \sin\varphi\ \hat{e}_\vartheta\right).$$

In this section, we distinguish the guiding center coordinates and corresponding functions with the subscript g. Thus, the poloidal angle can be rewritten in terms of guiding center co-ordinates as

$$\vartheta = \vartheta_g - \frac{v_\perp}{r\Omega}\sin\varphi = \vartheta_g + \frac{\xi}{m}\sin\varphi,$$

where $\xi \equiv k_\perp v_\perp/\Omega$, and the radius is

$$r = r_g - \frac{v_\perp}{\Omega}\cos\varphi.$$

We neglect the difference between ζ and ζ_g. Taking the lowest radial eigenmode for the contained mode, the perturbed electric field can be written in terms of guiding center coordinates as

$$\begin{aligned}
\vec{E}_g &= \vec{E}\exp(-i\omega t - im\vartheta + in^0\zeta)\exp\left[-\frac{(r-r_{\rm mode})^2}{2\Delta^2}\right] \qquad (7.11)\\
&\simeq \vec{E}\exp(-i\omega t - im\vartheta_g + in^0\zeta)\exp\left[-\frac{(r_g-r_{\rm mode})^2}{2\Delta^2}\right]\\
&\qquad \exp\left[-i\xi\sin\varphi + \frac{v_\perp(r_g-r_{\rm mode})}{\Omega\Delta^2}\cos\varphi - \frac{v_\perp^2}{2\Omega^2\Delta^2}\cos^2\varphi\right].
\end{aligned}$$

The integrals over gyrophase which we perform in order to calculate δF_g correspond to evaluating the Fourier components of $\vec{E}_g$ in terms of the gyrophase angle.

The Bessel functions occur from the generating function

$$\exp(-i\xi \sin\phi) = \sum_{p=-\infty}^{\infty} \exp(-ip\phi) J_p(\xi)$$

In the homogeneous case, this leads to the form for the perturbed distribution function already given in Chapter 6.

The radial mode structure thus leads to two terms which can modify the previous result for the perturbed distribution function. We first consider the correction proportional to $r_g - r_{\rm mode}$ and show that its effect is minimal for the physical situation being investigated. The effect of the last term, proportional to $\cos^2\varphi$, will be examined below.

We solve for

$$-i\xi \sin\phi + \frac{v_\perp (r - r_0)}{\Omega \Delta^2} \cos\phi \equiv -i\Xi \sin\Phi$$

The relative weight of these two quantities is given by

$$\Psi \equiv \frac{v_\perp (r - r_0)}{\xi \Omega \Delta^2} = \frac{(r - r_0)}{k_\perp \Delta^2}$$

If we assume that $v_\perp / \Omega\Delta \ll \xi$, which is equivalent to $|k_\perp \Delta| \gg 1$, then we can consider the regime where $|\Psi| < 1$. This limit only breaks down in regions where the mode amplitude is exceedingly small.

Thus we find

$$\Xi = \xi \sqrt{1 - \Psi^2}$$

and

$$\Phi = \phi + i\eta$$

where

$$\tanh\eta \equiv \Psi$$

This is equivalent to

$$\exp\eta = \left(\frac{1 + \Psi}{1 - \Psi}\right)^{1/2},$$

although a more useful expression, valid for $\Psi \ll 1$, is simply

$$\eta = \Psi + \mathcal{O}\left(\Psi^3\right)$$

Thus we can generalize to complex valued coefficients to find

$$\begin{aligned}\exp(-i\Xi\sin\Phi) &= \sum_{p=-\infty}^{\infty} \exp(-ip\Phi) J_p(\Xi) \\ &= \sum_{p=-\infty}^{\infty} \exp(-ip\phi) J_p\left(\xi\sqrt{1-\Psi^2}\right)\exp(p\eta)\end{aligned}$$

Because $\Psi^2 \ll 1$, we can neglect the correction to the argument of the Bessel function. However, the numerical factor, which is independent of velocity and only a function of position, may still be important if

$$\ell^2\Psi^2 \sim \frac{\ell^2}{k_\perp^2\Delta^2} \sim \frac{\ell^2}{|m|} \sim \ell\frac{d_i}{a}$$

is of order unity or larger. This requires that the harmonic number be large. We neglect the cubic terms and approximate $\eta \simeq \Psi$. Then, if we combine the radial eigenfunction with the factor $\exp(p\Psi)$ we find

$$\exp\left[-\frac{(r-r_0)^2}{2\Delta^2}\right]\exp\left[-\frac{p(r-r_0)}{k_\perp\Delta^2}\right] = \exp\left(\frac{r_1^2}{2\Delta^2}\right)\exp\left[-\frac{(r-r_0-r_1)^2}{2\Delta^2}\right]$$

where $r_1 \equiv p/k_\perp$. When $p = \ell \approx \omega/\Omega$ this implies $r_1 \sim -\ell a/m \sim -d_i$, using the conventions that the frequency is positive and noting that contained modes have positive m. In terms of the guiding centers of the resonating particles, the mode is shifted inwards by an amount of order d_i. Thus, since we are interested in $p \approx \ell$, we can approximate

$$\begin{aligned}\exp\left[-i\xi\sin\phi + \frac{v_\perp(r-r_0)}{\Omega\Delta^2}\cos\phi - \frac{(r-r_0)^2}{2\Delta^2}\right] \\ \simeq \exp\left[-i\xi\sin\phi - \frac{(r-r_0-r_1)^2}{2\Delta^2}\right].\exp\left(\frac{\ell^2}{2k_\perp^2\Delta^2}\right)\end{aligned} \tag{7.12}$$

The quantity $\ell^2/k_\perp^2\Delta^2$ which we used to estimate the importance of the velocity-independent correction is equivalent to r_1^2/Δ^2, which depends upon the ratio of the radial shift to the mode width. When $r_1^2 \gg \Delta^2$, we must consider that the typical value for Ψ will not be of order $1/k_\perp\Delta$, but will instead be

$$\frac{(r-r_0)}{k_\perp\Delta^2} \simeq \frac{r_1}{k_\perp\Delta^2} = \frac{\ell}{k_\perp^2\Delta^2} \sim \frac{l}{|m|} \sim \frac{d_i}{a} \ll 1$$

using the properties we have found for the contained modes. However, it turns out that even for cases when $\ell/k_\perp^2\Delta^2$ is of order unity, leading to a violation in our original set of assumptions, the final result is not significantly changed so long as $k_\perp^2\Delta^2 \gg 1$ and $|\xi| \ll |\ell k_\perp \Delta|$. Only the intermediate step combining $\sin\varphi$ and $\cos\varphi$ into a single term must be altered, because there is no real-valued η which satisfies $|\tanh\eta| > 1$.

The physical significance of the apparent radial shift in the mode layer resulting from the transformation to guiding center coordinates is evident from the fact that the shift is in the $\vec{v}_p \times \vec{B}$ direction, where $\vec{v}_p$ is the phase velocity of the mode. We note that particles within the mode layer which move in the same direction as the phase velocity of the mode have guiding centers on this side of the mode layer. It is only these particles which experience a slowly varying electric field in their reference frame, and thus can have a strong interaction with the mode. Although the mode shifts by a length scale of order d_i, and d_i can be larger than the gyroradius, this paradoxical result only occurs for the case when

$$1 > \frac{v_\perp}{\Omega d_i} = \frac{v_\perp}{v_A} \sim \frac{\xi}{\ell}.$$

In this regime, finite Larmor radius effects are negligible and the perturbed particle distribution in resonance with $\ell \neq 0$ is extremely small anyway. It is also interesting that this shift in the mode layer occurs even when the gyroradius is smaller than the mode width, although typically the shift will be smaller than the mode width as well and so is not physically significant.

We shall see below that for $k_\perp^2\Delta^2 \gg 1$, the exponential factor $\exp(\ell^2/2k_\perp^2\Delta^2)$, while it may be significant, is roughly canceled out by the effect of the second correc-

tion to the homogeneous case, proportional to $\cos\varphi^2$. In effect, the proper estimate for the importance of the radial mode structure is not to compare the mode width with the gyroradius, but rather with the section of the gyroorbit within which the particle is approximately moving at the phase velocity of the mode and experiences a constant phase. The size of this section of the orbit scales is comparable to the perpendicular wavelength, so the appropriate condition is $1 \ll k_\perp^2 \Delta^2 \sim |m| \sim \ell d_i/a$.

The growth rate depends upon the integral of $\vec{E}^* \cdot \delta\vec{J}$ over phase space, which can be replaced by the integral of $\vec{E}_g^* \cdot \delta\vec{J}_g$ over $\vec{X}$ and over $\mathcal{E}$, μ, and φ. This includes an integral over r_g, so the apparent mode shift which results from changing to guiding center coordinates has no effect on the growth rate except that the distribution function should be taken at $r = r_{\text{mode}} - \ell/k_\perp$.

We now consider the second correction due to the radial mode structure, and define the velocity-dependent parameter

$$\chi = \frac{v_\perp^2}{4\Omega^2\Delta^2}.$$

The quantity we are interested in is

$$\exp(-i\xi\sin\varphi)\exp\left(-2\chi\cos^2\varphi\right) = \exp(-i\xi\sin\varphi)\exp(-\chi)\exp\left[-\chi\cos(2\varphi)\right]$$

With the substitution $\varphi \to 2\varphi + \pi/2$ and $\xi \to -i\chi$, the generating relationship for the Bessel function can be rewritten as

$$\exp[-\chi\cos(2\varphi)] = \sum_{q=-\infty}^{\infty} \exp(-2iq\varphi)(-1)^q I_q(\chi)$$

where $I_q(x) \equiv i^{-q}J_q(ix)$ is the imaginary Bessel function. Thus the product of these two terms becomes

$$\exp(-i\xi\sin\varphi)\exp\left[-2\chi\cos^2\varphi\right] = \sum_{p,q} \exp[-i(p+2q)\varphi]J_p\xi(-1)^q I_q(\chi)\exp(-\chi)$$

Thus the ℓth harmonic term becomes

$$\sum_q J_{\ell-2q}(\xi)(-1)^q I_q(\chi)\exp(-\chi)$$

This cannot be reduced to a single Bessel function because the index of the first Bessel function shifts twice as much as the index of the second Bessel function, a reflection of the fact that the second term originated from the quantity $\cos^2\varphi$. However, we note that $I_q(\chi)\exp(-\chi)$ rapidly decreases as the index increases. We expect significant corrections when χ becomes comparable to unity; however, this requires that $\xi \sim 4a/\rho_\alpha \simeq 40$, and ξ is comparable to the harmonic number. Note that for the parameters appropriate for current experiments, when $\Delta \sim \rho_\alpha$ we also have $\omega \sim \Omega_{LH}$ and so additional corrections arise because the polarization and dispersion relation of the mode appropriates some of the properties of the lower hybrid mode.

If the Bessel function were relatively independent of the index, then the net effect of the correction would be to multiply $J_\ell(\xi)$ by the factor

$$\sum_q (-1)^q I_q(\chi)\exp(-\chi) = \exp(-2\chi).$$

However, it turns out that this simplification only works if $\xi \simeq \ell$, which requires $v_\alpha/v_A \simeq 1$.

If we examine the zeroes of J_ℓ, denoted as $\{x_{\ell i}\}$, we find that the modified Bessel function should also be close to zero at these points. For $\ell \gg 1$, we can perform a Taylor expansion in the index of the Bessel function to obtain

$$J_{\ell-2q}(x_{\ell i}) = -2q\frac{\partial}{\partial \ell}J_\ell(x_{\ell i}) + q^2\frac{\partial^2}{\partial \ell^2}J_\ell(x_{\ell i}) + \mathcal{O}\left(\frac{q^3}{\ell^3}\right).$$

The modified Bessel function at a zero of J_ℓ can then be approximated as

$$\sum_{q=-\infty}^{\infty} J_{\ell-2q}(x_{\ell i})(-1)^q I_q(\chi)\exp(-\chi)$$
$$= \sum_{q=1}^{\infty}\left[J_{\ell-2q}(x_{\ell i}) + J_{\ell+2q}(x_{\ell i})\right](-1)^q I_q(\chi)\exp(-\chi)$$

$$\simeq \sum_{q=1}^{\infty} 2q^2 \frac{\partial^2}{\partial \ell^2} J_\ell(x_{\ell i})(-1)^q I_q(\chi) \exp(-\chi)$$

which is small because $I_\ell(\chi) \ll 1$ for $\chi \ll \ell$.

We see that the modified Bessel functions which result have a similar functional dependence on ξ; in particular, the nodes occur at roughly the same values of ξ. It turns out that when we take into account the velocity dependence of both ξ and χ, the modified Bessel function is approximately proportional to the original Bessel function so long as $k_\perp \Delta \gg 1$ and $\chi \ll \ell^2$. This second condition can also be expressed as

$$\ell \gg \frac{\xi}{2k_\perp \Delta} = \frac{v_\perp}{2\Omega\Delta} \qquad \Rightarrow \qquad \ell \gg \frac{v_\perp^2}{\ell \Omega^2 \Delta^2} \sim \frac{v_\perp^2}{\Omega^2 d_i a}$$

For realistic parameters, $|\xi/\ell| \sim v_\perp/v_A$ is of order unity or smaller, so both conditions are satisfied whenever the poloidal mode number is large. The proportionality constant is consistent with the fact that at $\xi = \ell$, the modified Bessel function is reduced by a factor $\exp(-2\chi)$ when $1 \ll \xi^2/\chi = 4k_\perp^2 \Delta^2$. The net result is that for large $k_\perp^2 \Delta^2$,

$$\frac{1}{2\pi} \int_0^{2\pi} d\varphi \ \exp(i\ell\varphi) \exp(-i\xi \sin\varphi) \exp\left(-2\chi \cos^2\varphi\right) \tag{7.13}$$
$$\simeq J_\ell(\varphi) \exp\left(-\frac{2\chi\ell^2}{\xi^2}\right) = J_\ell(\varphi) \exp\left(-\frac{\ell^2}{2k_\perp^2\Delta^2}\right)$$

The exponential factor is independent of velocity and cancels out the factor from Eq. (7.12), as stated above.

The approximation that the only effect of the radial mode structure on the perturbed distribution function is to impose a comparable dependence on position compares favorably with numerical computations of the Fourier components of $\vec{E}_g$ as defined by Eq. (7.11). The results are illustrated in Figs. 7-1 and 7-2. For both figures, we take $k_\perp \Delta = -10$, recalling that $k_\perp$ is negative for positive m, and we examine the Fourier component with $\ell = 20$. Fig. 7-1 shows the results as a function of $(r_g - r_{\rm mode})/\Delta$ for $\xi = 24$, and Fig. 7-2 shows the results as a function of ξ for fixed $(r_g - r_{\rm mode})/\Delta = 0$. This somewhat extreme case has a gyroradius equal to more

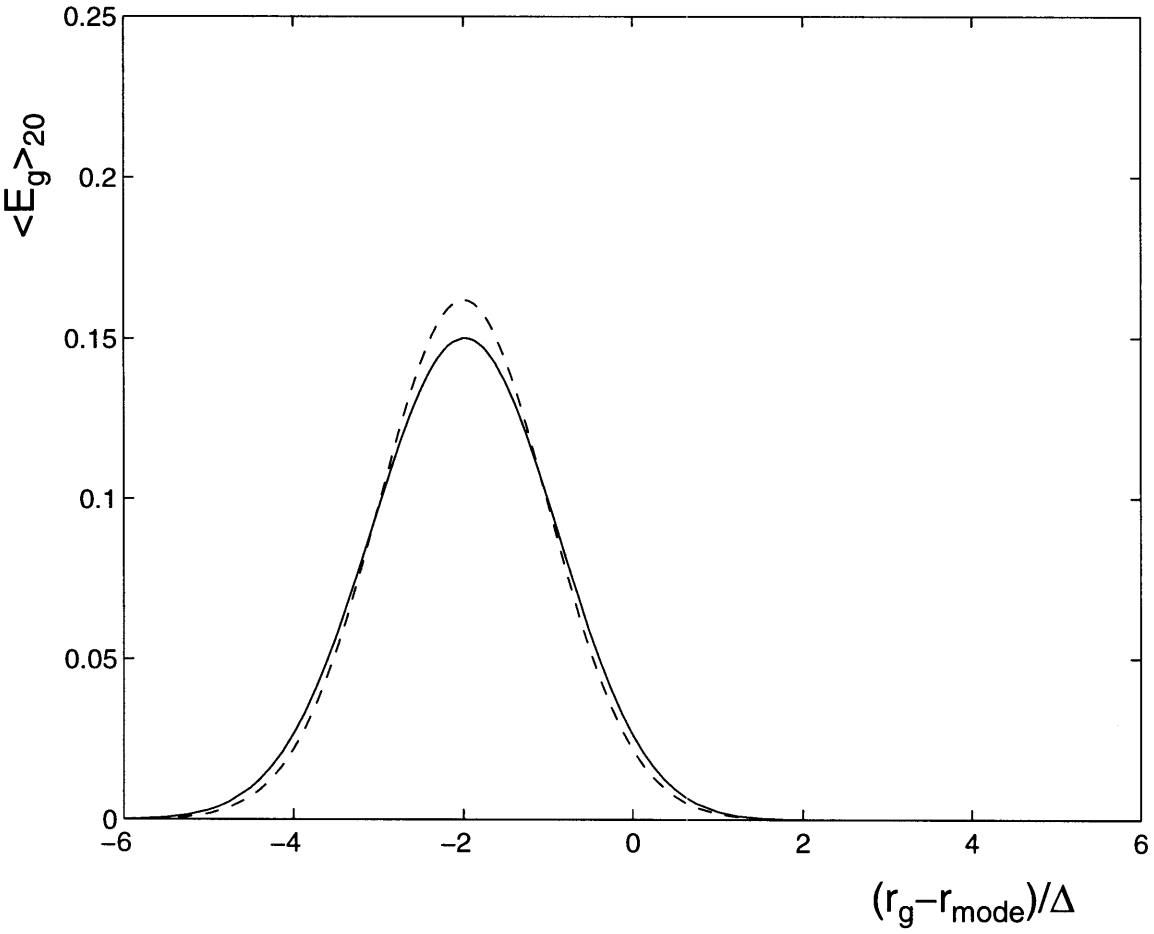

Figure 7-1: Electric field contribution to the resonant particle response considering the radial mode structure in addition to the perpendicular propagation. The resonance with $\ell = 20$ is shown as a function of $(r_g - r_{\text{mode}})/\Delta$ for $\xi = 24$ and with $k_\perp \Delta = -10$. The guiding center particle response is peaked further to the interior of the plasma than the mode itself. Numerical results (solid line) are compared to the approximation that the radial dependence mirrors the mode structure except for the displacement (dashed line).

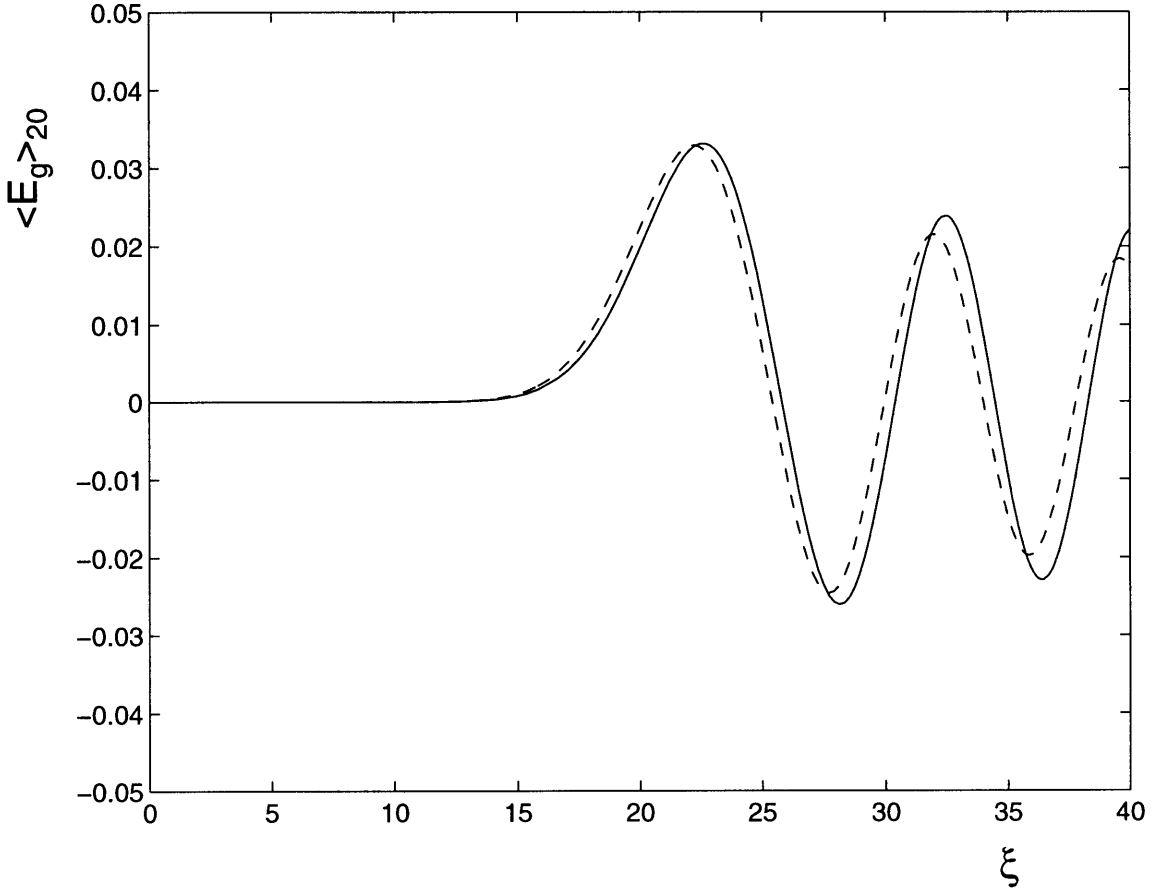

Figure 7-2: Electric field contribution to the resonant particle response considering the radial mode structure in addition to the perpendicular propagation. The resonance with $\ell = 20$ is shown as a function of ξ for $(r_g - r_{\text{mode}})/\Delta = 0$ and with $k_\perp \Delta = -10$. Numerical results (solid line) are compared to the approximation that the velocity dependence is identical to the homogeneous case (dashed line).

than twice the mode width.

In general the term W_ℓ, which contains the Bessel function dependence, will have to be replaced by a more complicated function of $v_\perp$. However, for physically meaningful parameters the correction is small even for Δ comparable to the gyroradius, except for the apparent displacement of the mode layer. In particular, when $k_\perp^2 \Delta^2 \gg 1$, the modified Bessel functions have the same sign as the original Bessel functions, so the sign of the contribution of finite Larmor radius effects to the growth rate should remain the same when the radial mode structure is taken into account. Corrections to the magnitude of the growth rate are small in this limit.

One circumstance in which this estimate does not work well occurs when ξ is near a zero of J_ℓ. In this case, even a small correction to the argument of the Bessel function, which includes replacing ξ with $\xi\sqrt{1-\Psi^2}$, can significantly alter the resonant reaction. Because this correction varies with position, the perturbed distribution function will also have a different dependence on radius. In addition, the errors involved in the above approximation increase with the distance from the shifted mode layer. The figures shown correspond to parameters which push the limits of the approximation, because $\xi = 24$ is somewhat close to the first non-trivial zero of J_{20}, at $\xi \simeq 25.42$, and $r_g = r_{\text{mode}}$ is far from the peak of the perturbed distribution function, which is shifted by two standard deviations away from the mode localization surface.

In addition to modifying the form of the function W_ℓ, the radial structure of the contained mode also introduces additional, small terms to the perturbed distribution function. This occurs because the perturbed distribution function contains quantities proportional to

$$\left\langle \vec{E}_\perp \cdot \vec{v}_d \left(1 - \frac{k_\perp v_\perp}{\ell\Omega}\right)\right\rangle_\ell$$

which vanish for a wave in a homogeneous plasma and were not considered previously. The radial mode structure leads to the inclusion of Bessel functions of order $p \neq \ell$, yielding contributions to the above expression which are proportional to $p - \ell = 2q$. These terms, which are already expected to be small when $k_\perp^2 \Delta^2 \gg 1$, are further

reduced in comparison to $\left\langle \vec{E}_\perp \cdot \vec{v}_\perp \right\rangle_\ell$ by a factor of

$$\frac{k_\perp v_d}{\ell\Omega}\frac{2q}{\ell} I_q(\chi).$$

Note that $v_d/v_\perp$ is of order $\lambda = \rho_\alpha/L_B$.

7.4 Growth rate in the local approximation

In terms of $\overline{\delta F_\ell}$, the slowly varying part of the current from Eq. (7.3) can be expressed as

$$\overline{\overline{\delta J_\alpha}} = \int \overline{\delta F_\ell} \exp\left(-i\vec{k}_\perp \cdot \frac{\vec{v}_\perp \times \hat{e}_{||}}{\Omega_\alpha}\right) \vec{v}\; d^3\vec{v} \tag{7.14}$$

where the exponential factor arises from the difference between the quantities $\vec{k}_\perp \cdot \vec{x}$ and $\vec{k}_\perp \cdot \vec{X}$. For high mode numbers, it is appropriate to neglect coupling between different poloidal harmonics and to look at $< \overline{\overline{E_1}}^* \cdot \overline{\overline{\delta J_\alpha}} >$, the ϑ-average of the energy flow from the particles to the mode, evaluated at $r = r_{\text{mode}}$.

We evaluate this term by adopting the "local approximation" in which the perturbed current does not depend on orbit integrals but only on local parameters and in particular on a spatial dependence that enters into F_{g0} and the resonance terms Ω_α and $v_{d\vartheta}$. In this case the perturbed distribution function has the form

$$\overline{\delta F_\ell} = \frac{-i(q_\alpha/m_\alpha)[P_{\ell r}(F_{g0})\overline{\overline{E_{1r}}} + P_{\ell\vartheta}(F_{g0})\overline{\overline{E_{1\vartheta}}}]}{\omega - k_\perp v_{d\vartheta} - \ell\Omega_\alpha + (v_{||}/q(r)R)\,[m - n^0 q(r)]} \tag{7.15}$$

In the limit of $\gamma \ll |\omega - \ell\Omega_\alpha|$, the resonant particle contribution can be written in the form

$$\Im\mathrm{m}\left(\frac{1}{\omega - k_\perp v_{d\vartheta} - \ell\Omega_\alpha + (v_{||}/q(r)R)\,[m - n^0 q(r)]}\right)$$
$$= -\pi\delta\left(\omega - k_\perp v_{d\vartheta} - \ell\Omega_\alpha + \frac{v_{||}}{q(r)R}\left[m - n^0 q(r)\right]\right)$$

The resonant part of the conductivity tensor, defined by Eq. (7.3) as $\delta\vec{J}_\alpha = \delta\overleftrightarrow{\sigma}\cdot\vec{E}_1$,

takes the form

$$\delta\overleftrightarrow{\sigma} = -\frac{q_\alpha^2}{m_\alpha^{5/2}}\int \frac{4\pi^2\mu B^2\, d\mu\, d\mathcal{E}}{\sqrt{2(\mathcal{E}-\mu B)}}\delta(\omega - k_{||}v_{||} - k_\perp v_{d\vartheta} - \ell\Omega_\alpha) \tag{7.16}$$
$$\times\begin{pmatrix} (\ell J_\ell/\xi)^2 & i(\ell/\xi)J_\ell J_\ell' \\ -i(\ell/\xi)J_\ell J_\ell' & J_\ell'^{\,2}\end{pmatrix}\times\left[\frac{\partial}{\partial\mathcal{E}} + \left(1 - \frac{k_{||}v_{||}+k_\perp v_{d\vartheta}}{\ell\Omega_\alpha}\right)\frac{1}{B}\frac{\partial}{\partial\mu}\right]F_{g0}$$

where the matrix is in the $\{\hat{e}_\perp, \hat{e}_r\}$ basis.

Through the delta function, each mode selects a class of orbits such that a particle can resonate with the mode as it passes through $r = r_{\rm mode}$. The growth rate γ obtained by substituting Eq. (7.16) into (7.4) only has significant contributions from these resonant particles.

The "local approximation" used to obtain Eq. (7.16) is valid when $\gamma > \omega_b$, where $\omega_b/\Omega_\alpha \sim 6\times10^{-4}$. The typical magnitude of γ is $\Omega_\alpha n_\alpha/n_e$, where $n_\alpha/n_e \sim 2\times10^{-3}$ for typical experiments. In some cases the growth rate, which is obtained by taking the integral over ϑ of the local contribution, is comparable with the bounce frequency. When this occurs, the local approximation we have adopted is not valid and an expansion in bounce harmonics of Eq. (7.10) has to be carried out in order to evaluate the growth rate.

In terms of dimensionless variables the resonance condition, which determines the resonant magnetic moment $\mu = \mu_{\rm res}(\mathcal{E},...)$, is given for $v_{||} > 0$ by

$$\frac{\omega}{\Omega_{\alpha 0}} - \frac{\ell}{1+(r/R_0)\cos\vartheta} - K_{||}\sqrt{\mathcal{E}/\mathcal{E}_\alpha - \mu B/\mathcal{E}_\alpha} - K_\perp(\mathcal{E}/\mathcal{E}_\alpha - \mu B/2\mathcal{E}_\alpha) = 0 \tag{7.17}$$

where $K_{||} \equiv k_{||}\sqrt{(2\mathcal{E}_\alpha/m_\alpha)}/\Omega_{\alpha 0}$ and $K_\perp \equiv -(2k_\perp\mathcal{E}_\alpha\cos\vartheta)/(m_\alpha\Omega_{\alpha 0}^2 R_0)$; here $K_\perp$ is defined so as to be a positive quantity for the given magnetic field configuration and for $\Re e\omega > 0$.. The final form for the local contribution to the growth rate is:

$$\frac{\gamma}{\Omega_{i0}} \simeq -\frac{n_\alpha}{n_{e0}}2\pi H(\vartheta_{cr} - |\vartheta|)\frac{\omega_{pi0}^2}{\Omega_{i0}^2}\frac{2}{\omega\partial D_0/\partial\omega}$$
$$\times\left\{\left(\frac{\mu B/\mathcal{E}_\alpha - 0.8}{(0.05)^2}\right)V_\ell\ e^{-\frac{1}{2}\left(\frac{\mu B/\mathcal{E}_\alpha - 0.8}{0.05}\right)^2}\left(1 - \frac{k_{||}v_{||}+k_\perp v_{d\vartheta}}{\ell\Omega_\alpha}\right)\right.$$

$$+e^{-\frac{1}{2}\left(\frac{\mu B/\mathcal{E}_\alpha - 0.8}{0.05}\right)^2}\mathcal{E}_\alpha\frac{\partial V_\ell}{\partial \mathcal{E}}$$
$$+\mathcal{E}_\alpha\frac{d\mu_{\rm res}}{d\mathcal{E}}\frac{\partial}{\partial \mu}\left[V_\ell\ \ e^{-\frac{1}{2}\left(\frac{\mu B/\mathcal{E}_\alpha - 0.8}{0.05}\right)^2}\right]\Bigg\}_{\substack{\mathcal{E}=\mathcal{E}_\alpha \\ \mu=\mu_{\rm res}}} \tag{7.18}$$

where $2(\omega_{pi}^2/\Omega_i^2)[\omega\partial D_0/\partial\omega]^{-1} \sim \mathcal{O}(1)$ is a positive quantity, and

$$V_\ell = \frac{1}{k_\perp^2\rho_\alpha^2}\frac{1}{\left|K_\parallel - K_\perp\left(\sqrt{\mathcal{E}/\mathcal{E}_\alpha - \mu B/\mathcal{E}_\alpha}\right)\right|}W_\ell(\xi)$$

$$W_\ell(\xi) = \frac{1}{1+\Lambda_p^2}\left[\Lambda_p \ell J_\ell(\xi) - \xi J_\ell'(\xi)\right]^2$$

The local contribution to the growth rate given in Eq. (7.18) is evaluated at $r = r_{\rm mode}$. In order to find the growth rate an integral over ϑ of the local contribution has to be performed. This local contribution can be separated into components related to anisotropy, derivatives of the Bessel functions and a remainder term, which when explicitly evaluated leads to the expression

$$\begin{aligned}\frac{\gamma}{\Omega_{i0}} \simeq\ & 2\pi\frac{n_\alpha}{n_{e0}}\frac{\omega_{pi0}^2}{\Omega_{i0}^2}\frac{2}{\omega\partial D_0/\partial\omega}H(\vartheta_{cr}-|\vartheta|)\frac{m_\alpha\Omega_\alpha^2}{2\mathcal{E}_\alpha k_\perp^2} \\ & \times\exp\left[-\frac{(\mu B/\mathcal{E}_\alpha - 0.8)^2}{2(0.05)^2}\right]\left|K_\parallel + K_\perp\sqrt{\mathcal{E}/\mathcal{E}_\alpha - \mu B/\mathcal{E}_\alpha}\right|^{-1}W_\ell(\xi) \\ & \times\Bigg\{\left(1+\frac{k_\parallel v_\parallel + k_\perp v_{d\vartheta}}{\ell\Omega_\alpha} - \frac{K_\parallel}{K_\parallel + K_\perp\sqrt{\mathcal{E}/\mathcal{E}_\alpha - \mu B/\mathcal{E}_\alpha}}\right)\left(\frac{\mu B/\mathcal{E}_\alpha - 0.8}{(0.05)^2}\right) \\ & -\frac{\mathcal{E}_\alpha}{2\mu B}\left(2 - \frac{K_\parallel}{K_\parallel + K_\perp\sqrt{\mathcal{E}/\mathcal{E}_\alpha - \mu B/\mathcal{E}_\alpha}}\right)\xi\frac{\partial}{\partial\xi}\ln W_\ell(\xi) \\ & -\frac{1}{2}\left(\frac{K_\perp}{K_\parallel + K_\perp\sqrt{\mathcal{E}/\mathcal{E}_\alpha - \mu B/\mathcal{E}_\alpha}}\right)^2\Bigg\}_{\substack{\mathcal{E}=\mathcal{E}_\alpha \\ \mu=\mu_{\rm res}}}\end{aligned} \tag{7.19}$$

Note that the last term is always stabilizing, and arises solely from the poloidal guiding center drift, which does not include the poloidal component of the motion along the equilibrium magnetic field. Thus, the interaction is weaker than the equivalent interaction in the homogeneous case which was treated in Chapter 6. We find that both finite Larmor radius effects and anisotropy are required for appreciable instability to occur. The contribution of anisotropy to the growth rate is given in the

first term in the curly brackets. Because of the particle drifts, finite Larmor radius effects do not necessarily dominate over anisotropy as $|k_{||}| \to 0$, in contrast with the homogeneous instability. For $\xi = k_\perp v_\perp / \Omega_\alpha$ comparable with ℓ, which holds when v_α is comparable with v_A, the derivative of W_ℓ is dominated by $\Lambda_p \ell J_\ell(\xi)$ and is always positive so long as $\Lambda_p > 1$; for the contained mode $\Lambda_p \sim \ell$ and therefore $\Lambda_p > 1$ whenever $\ell > 1$. In the case of the first harmonic we need a more detailed analysis as the qualitative behavior of W_ℓ is sensitive to the actual parameters. The derivative of W_ℓ will in fact be such that even when it gives a positive contribution in general it will not be large enough to generate instability by itself unless either ξ is significantly bigger than ℓ, which is not consistent with the considered experimental parameters, or $\xi \ll \ell$, which corresponds to large $v_{||}$ (passing orbits) are is a negligible portion of the distribution function.

7.5 Discussion of the mode-particle resonance

We examine in more detail the physical significance of the resonance conditions given by

$$\omega - k_{||} v_{||} - k_\perp v_{d\vartheta} - \ell \Omega_\alpha .$$

We note that the quantity

$$\omega - k_{||} v_{||} - k_\perp v_{d\vartheta}$$

is just the Doppler shifted frequency of the mode in the frame of the particle guiding center. Thus, the resonance condition with $\ell = 0$ is for particles which are co-moving with the wave front of the mode.

The special nature of the resonant particles is illustrated by the existence of stable and unstable fixed points in the frame moving with the mode. These stationary orbits do not themselves exchange energy with the mode when at exact resonance, but an infinitesimal change in parallel velocity will lead to a particle with strong mode-particle interactions. At stable fixed points, particles with slightly lower $v_{||}$ become accelerated up to the parallel phase velocity $\omega / k_{||}$, performing small oscillations rela-

tive to the wave front. This acceleration of particles up to the phase velocity of the mode results in trapping of the particle by the wave front. Particles with $v_{||} > \omega/k_{||}$ are similarly decelerated by the wave front, leading to the characteristic dependence of the growth rate on $dF/dv_{||}$. The number of trapped particles depends nonlinearly on the amplitude of the mode. The linear growth rate is a more subtle process, because energy transfer between the particles and the mode depends on the distribution of resonating particles. Linear growth rates are soon eliminated by coherent behavior in the response of the particles to the mode, with only a small net effect on mode amplitude, unless collisions or nonlinearities lead to phase mixing of the distribution function. Typically, the "phase memory" which inhibits energy exchange is easily overcome by physical processes, but it complicates the physical picture of the interaction.

There are two basic forms of energy exchange in a magnetized plasma, depending on the polarization of the mode. Landau damping is the more commonly described process, whereby the parallel component of the perturbed electric field accelerates resonating particles. In terms of the electric potential, the mode can be viewed as a series of wells which move with the phase velocity and strongly interact with co-moving particles. When the perturbed electric field lies perpendicular to the equilibrium magnetic field, the interaction is referred to as transit-time damping, although this term is used somewhat loosely to describe other physical processes. The terms Landau and transit-time damping are usually reserved for the case of $\ell = 0$, and generally for the case where the frequency is small smaller than the cyclotron frequency.

In the limit of small $\xi \equiv k_\perp v_\perp/\Omega$, where the distinction between the location of the particle and the guiding center is not very great, transit-time damping can be pictured in terms of the magnetic mirror force described in Chapter 3.1. This force corresponds to an effective potential for a particle with fixed magnetic moment $\mu \equiv mv_\perp^2/2B$, $F_\parallel = -\mu\nabla_\parallel B$. The perturbed magnetic field generates potential wells analogous to the case of Landau damping. However, this force arises from finite Larmor radius effects, and is the result of the curvature in the magnetic field which is necessitated by the condition $\nabla\cdot\vec{B} = 0$ whenever $\nabla_\parallel B \neq 0$. The energy transfer arises from the electromotive force (EMF) around the particle gyroorbit generated by the perturbed electric field. In the $\ell = 0$ case, interactions only arise from the component of the electric field perpendicular to the wave vector of the mode, because this leads to an asymmetry in the force experienced by the particle in different portions of its gyroorbit. The accelerating electric field in the rest frame of the particle guiding center increases the perpendicular velocity, with the EMF given by

$$\text{EMF} = \oint d\vec{s}\cdot\vec{E}' = -\frac{1}{\Omega}\oint d\varphi\ \vec{v}_\perp\cdot\left(\vec{E}_\perp + v_\parallel\hat{e}_\parallel\times\vec{B}_\perp\right) = -\frac{1}{\Omega}\oint d\varphi\ \vec{v}_\perp\cdot\vec{E}_\perp\left(1-\frac{k_\parallel v_\parallel}{\omega}\right)$$

Here the guiding center drift has been neglected. That this term does not vanish depends upon the variation in $\vec{E}_\perp$ along gyroorbits. The physical mechanism for the generation of EMF is illustrated in Fig. 7-3.

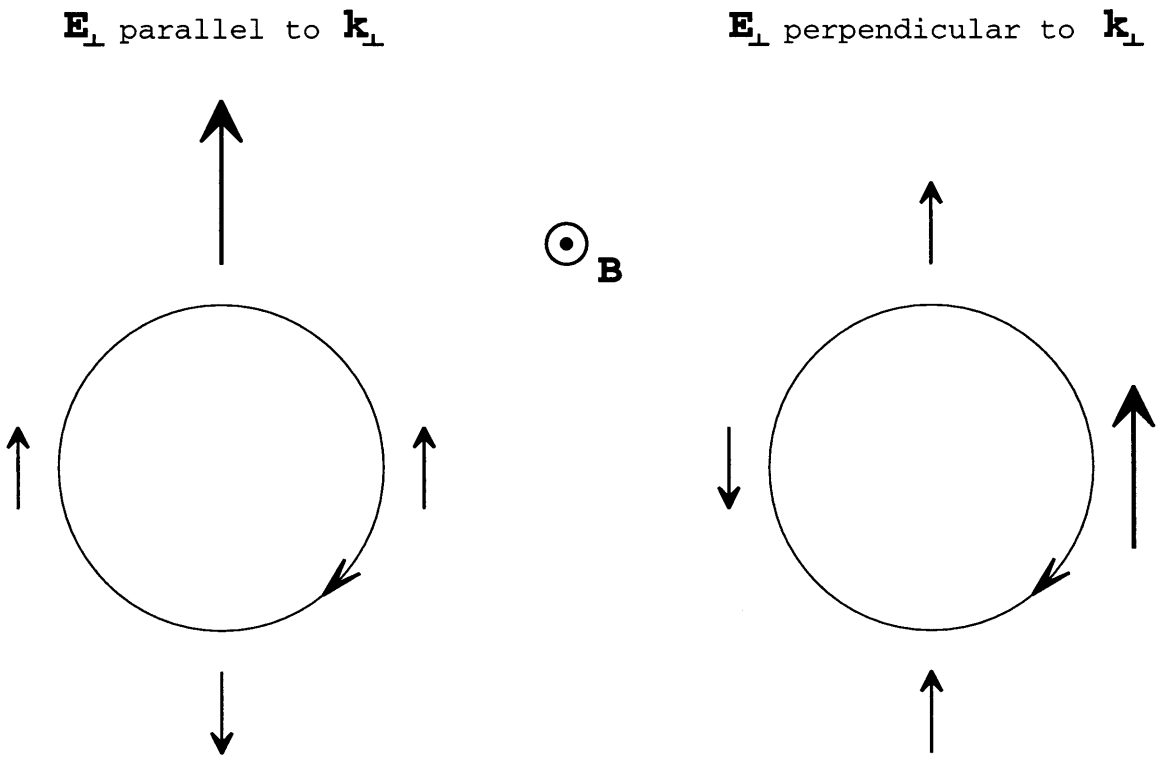

Figure 7-3: Illustration of induced EMF experienced by energetic ions by a perturbed electric field. The variation of the perturbed electric field along the particle gyroorbits (circles) is indicated by the arrows. For the case where the mode frequency is much lower than the cyclotron frequency, the EMF only results from the component of $\vec{E}_\perp$ which is perpendicular to $\vec{k}_\perp$.

The lowest order interaction tends to preserve the magnetic moment and alter the parallel energy of the particles. However, at frequencies greater than or equal to the cyclotron frequency, the perpendicular energy of the particles is mostly affected by the mode, as evidenced by the lowest order dependence of δF on

$$\left(\frac{\partial}{\partial \mathcal{E}} + \frac{1}{B}\frac{\partial}{\partial \mu}\right) F_0 = \frac{1}{m v_\perp}\frac{\partial}{\partial v_\perp} F_0$$

The harmonics of the cyclotron frequency in the resonance condition arise from the variation in the local electric field as perceived by the particle as it travels along its gyroorbit. The gyromotion has a frequency of Ω, and couples the temporal variation of the field seen by the particle with the spatial variation of the mode. The Fourier decomposition in time of the electric field as seen by the particle thus leads to terms which are multiples of the fundamental harmonic Ω. Even when the frequency is too high for Doppler shifting to eliminate the time dependences at the guiding center, the frequency can interact resonantly with specific Fourier components of $\exp[ik_\perp y(t)]$. This leads to terms in the perturbed distribution function which vary as $\exp(i\ell\varphi)$.

Another interpretation of the resonance at $\omega \approx \ell\Omega_\alpha$ is that when the velocity of the ions perpendicular to the equilibrium magnetic field is comparable to the phase velocity of the mode perpendicular to the equilibrium magnetic field, then there is one section of the gyroorbit where the phase velocity of the mode becomes small in the rest frame of the particle. It is only in this region of the gyroorbit in which the particles experience a nearly stationary phase for the collective mode, and so can interact strongly with the mode. This leads to a periodic interaction whose Fourier components yield the cyclotron frequency harmonics. For the case of contained modes, the phase velocity is on the order of the Alfvén velocity and so significant instability driven by α-particles can only occur for $v_\alpha \gtrsim v_A$.

7.6 Numerical calculations

For a fixed value of the frequency ω, Eq. (7.17) defines the acceptable value of $\mu = \mu_{\rm res}$ at $r = r_{\rm mode}$ for which there can be instability at a given poloidal angle ϑ. Here we have used the fact that the energy at birth of the particles is fixed. We find that there is a destabilizing interaction for those frequencies such that $\mu_{\rm res}B < 0.8\,\mathcal{E}_\alpha$, where $\mu_{\rm res}B \sim 0.8\,\mathcal{E}_\alpha$ corresponds to barely trapped particles as discussed in Chapter 3. Therefore, the particles which contribute to the instability are located in those regions of phase space where the α-particle distribution function has a positive slope with respect to magnetic moment.

We study the growth rate considering a fixed set of mode numbers m, n^0 which determine uniquely the frequency of the mode. For a given value of the frequency, the resonance condition corresponds to a narrow range of ϑ for which the resonance condition can hold true, as we see by examining the different terms in the resonance. In Eq. (7.17), the terms which vary with pitch angle are of the order of $K_{||} \simeq \ell k_{||}/k_\perp$ and $K_\perp \simeq \ell\rho_\alpha/R_0$, using $k_\perp\rho_\alpha \sim \ell$, and thus are much smaller than the terms which vary with poloidal angle, which are of the order of $\ell r/R$. Because of these differences in scale within the resonance condition, a wide span in velocity space results in a small poloidal interval for interacting α-particles.

In Fig. 7-4, the local contribution to the growth rate is represented for the contained mode from Eq. (7.18) for $m = 56$ and $n^0 = 21$, which is in resonance with harmonic number $\ell = 6$. The growth rate is normalized to $\Omega_{\alpha a}n_\alpha/n_e$ where $\Omega_{\alpha a} \equiv \Omega_\alpha(r_0, \vartheta = 0)$, that is the cyclotron frequency evaluated at the outer edge of the plasma column. On the abscissa the poloidal angle is normalized to π radians. This mode interacts with α-particles passing through the range $0 < \vartheta < \pi/10$, with almost the entire range of $\mu B/\mathcal{E}_\alpha$ being represented.

From this analysis we can say that the resonance condition is given roughly by $\omega \sim \ell\Omega_\alpha(\vartheta)$, so that each mode can only interact with α-particles whose orbits intersect the modes close to this poloidal angle, which is determined exclusively by the frequency of the mode. In principle, any mode having a resonance within $0 < \vartheta < \pi/3$ can

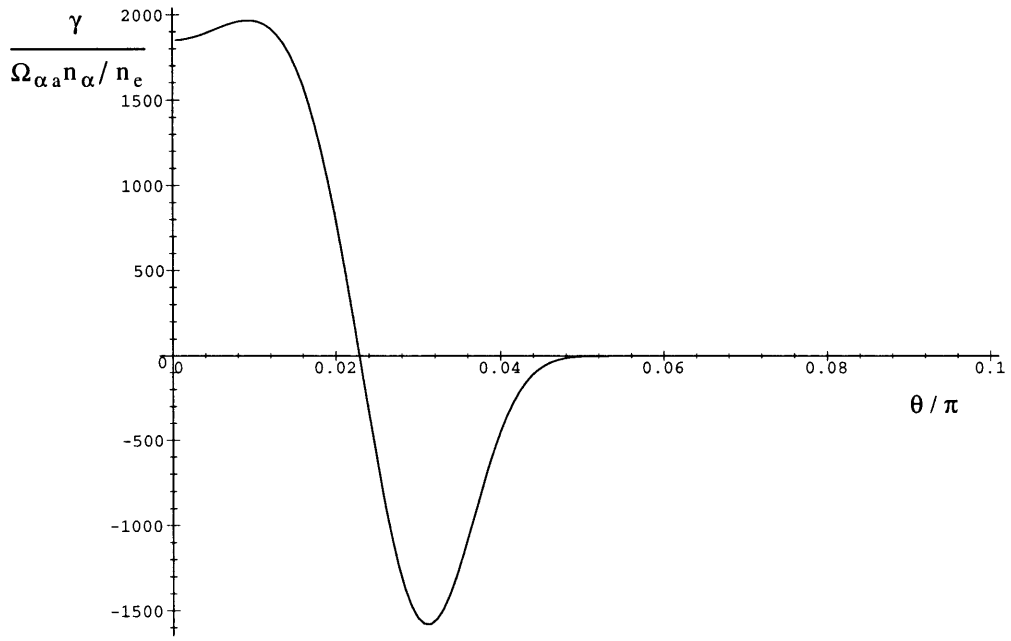

Figure 7-4: Local contribution to the growth rate as a function of poloidal angle for a given mode. Here we represent the case $m = 56$, $n^0 = 21$, that corresponds to resonant interactions with $\ell = 6$ in the interval $0 < \vartheta < \pi/10$. The growth rate is normalized to $\Omega_{\alpha a} n_\alpha / n_e$, where $\Omega_{\alpha a}$ is the α-particles cyclotron frequency evaluated at $\vartheta = 0$ and $r = r_0$, and where r_0 is the mode localization.

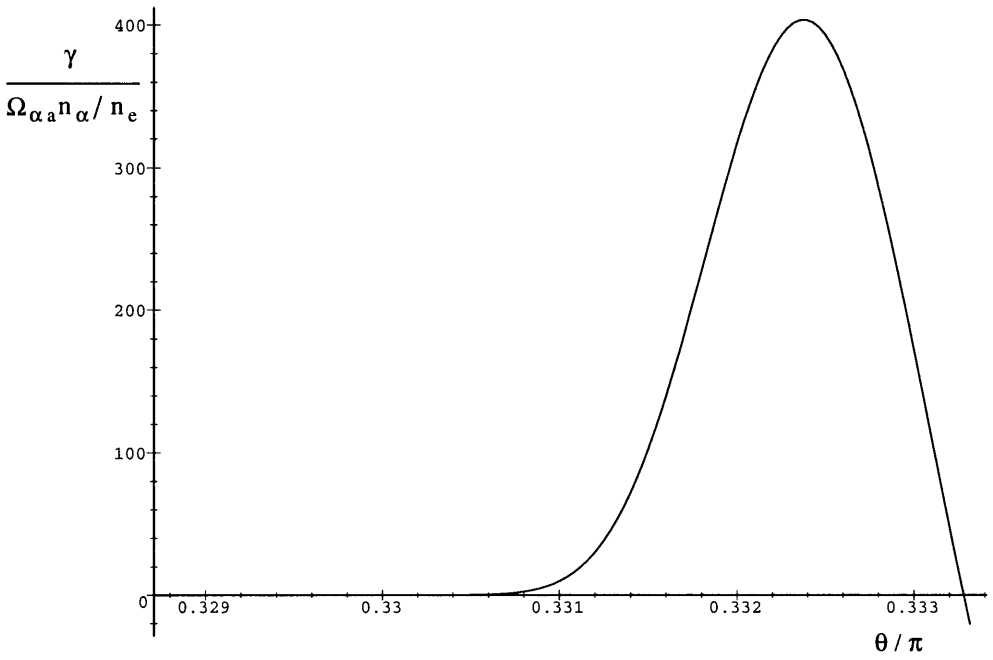

Figure 7-5: Local contribution to the growth rate as a function of poloidal angle for a given mode. Here we represent the case $m = 73$, $n^0 = 25$, that corresponds to resonant interactions with $\ell = 7$ in the interval $0.329\ \pi < \vartheta < \pi/3$. The growth rate is normalized to $\Omega_{\alpha a} n_\alpha / n_e$, where $\Omega_{\alpha a}$ is the α-particles cyclotron frequency evaluated at $\vartheta = 0$ and $r = r_0$, and where r_0 is the mode localization.

be driven unstable; however, upon taking the poloidal average of the growth rate given by Eq. (7.18), we fit instability predominantly for those modes whose region of interaction is close to $\vartheta = 0$, and there is a second class of unstable modes whose region of interaction is adjacent to $\vartheta = \pi/3$, where the α-particles are barely confined in the plasma. An example of this is shown in Fig. 7-5, which is analogous to Fig. 7-4 but for $m = 73$ and $n^0 = 25$ and in resonance for $\ell = 7$.

We find the growth rate resulting from all the local contributions by integrating over poloidal angle; the resulting (positive) growth rates are shown in Fig. 7-6 for the case $\Sigma = 0.05$, where Σ is the variance as defined in Eq. (2.9) and is a measure of the anisotropy. In this figure, the growth rate is normalized to $\Omega_{\alpha a} n_\alpha / n_e$ and is

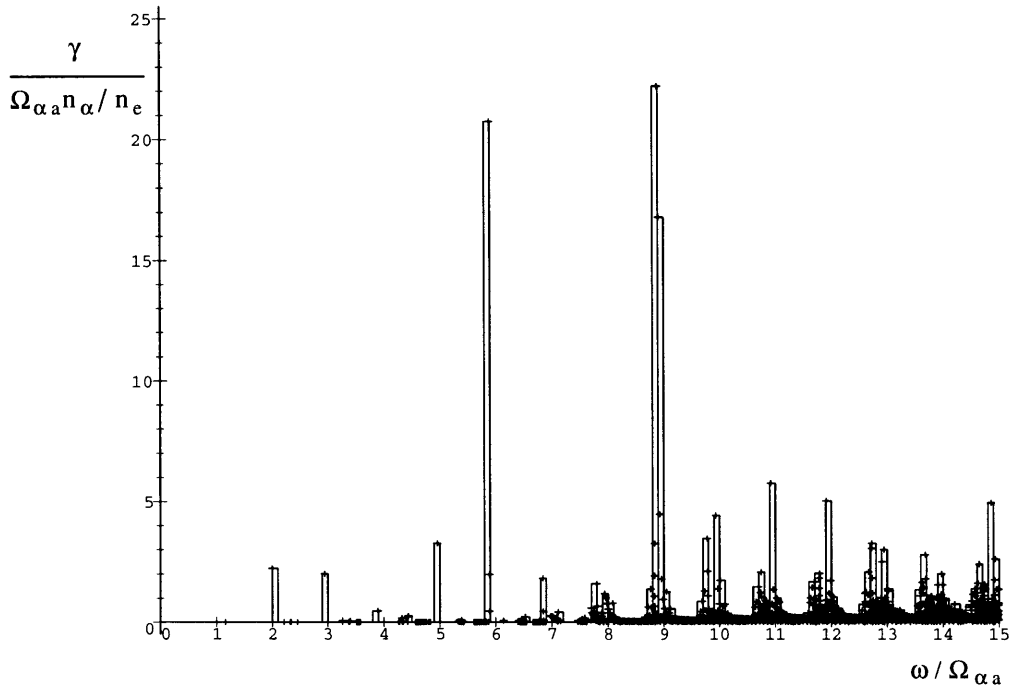

Figure 7-6: Growth rates for contained modes which are driven unstable by the interaction with fusion products. The growth rates (crosses) are shown for different frequencies which correspond to specific choices of the mode numbers m and n^0. The mode frequency is normalized to $\Omega_{\alpha a}$ and the growth rate is normalized to $\Omega_{\alpha a} n_\alpha / n_e$, where $\Omega_{\alpha a}$ is the α-particles cyclotron frequency evaluated at $\vartheta = 0$ and $r = r_0$, and where r_0 is the mode localization. For clarity, the dependence of the growth rate on mode frequency for a finite resolution in frequency of 0.1 $\Omega_{\alpha a}$ is also shown (histogram), where the maximum positive growth rate for modes within each frequency band is indicated.

represented for the contained mode as derived in Chapters 4 and 5. On the abscissa we indicate multiples of $\Omega_{\alpha a}$ to compare with experimental results. Here we consider only modes that have $|k_{||}/k_{\perp}| < 0.1$, and we adopt a simplified model in which $r_{\text{mode}} \simeq r_0$ and $\omega \simeq \omega_0(1+k_{||}^2 d_i^2/2)$. In Fig. 7-6 single modes having similar frequencies are grouped for purposes of clarity and for a visualization of an observed spectrum, assuming that the emitted power associated with the excitation of each mode is related to the growth rate. We note that the results represented are for a simplified model and are sensitive to slight changes in the plasma parameters used in the calculations. For fixed radius the variation in poloidal angle does not give sufficient spread in the frequency of the unstable modes to exhibit the observed transition to a continuum spectrum, therefore the variation in the mode localization should be included to find the width of the peaks and the transition to a continuum spectrum as indicated in Chapter 5.

We do not find a significant growth rate for the first harmonic when $\Sigma = 0.05$; this occurs because when $\ell = 1$ the derivative of W_ℓ, which is related to the Bessel functions which give a weight to the interaction, results in a damping effect on the mode in the range of velocities considered ($v_\perp \lesssim v_\alpha \equiv \sqrt{2\mathcal{E}_\alpha/m_\alpha}$) for the specific parameters considered, in particular because $\xi_{\text{res}} \sim 1$. An analogous situation can be found in the case of the loss-cone instability[28] where Bessel functions which represent finite Larmor radius effects play a fundamental role in determining the possibility of having instability for a given distribution function. Clearly, our theory is not yet complete as it does not justify the excitation of the first harmonic with a growth rate of sufficient magnitude to justify the reduced form of Eq. (7.10) adopted in the local approximation. To obtain a full picture of the interaction other effects should be taken into account in our analysis, such as effects related to inhomogeneity (ω_* effects) that have been neglected. In addition, the effect of nonlinear processes and coupling between the different harmonics should be considered. For the lower harmonics which are excited, we see that there are large gaps between the frequencies of excitation.

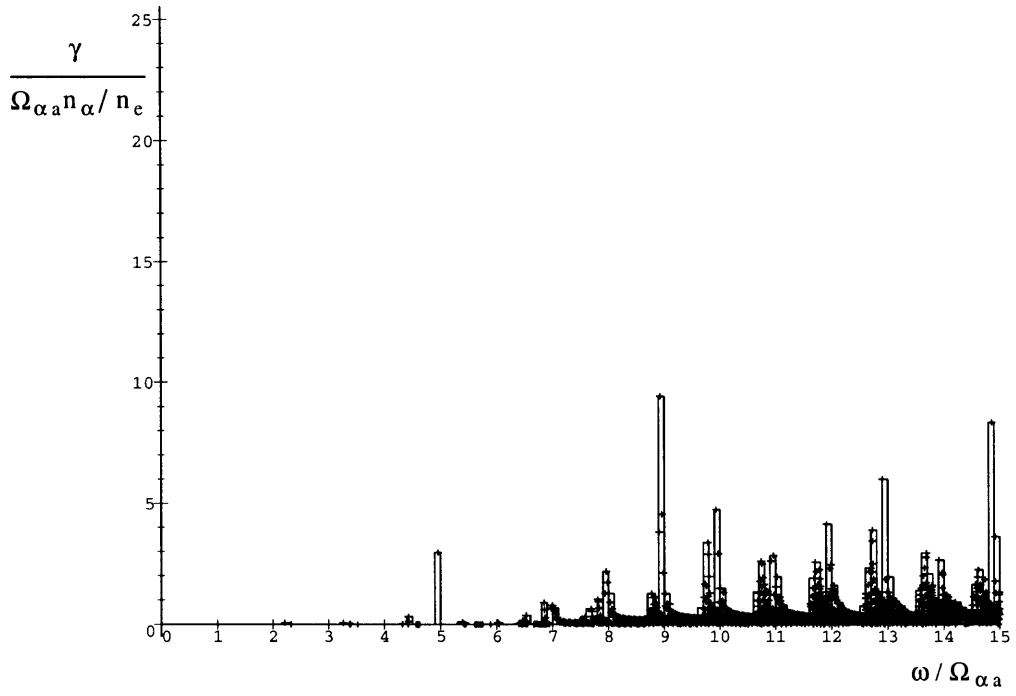

Figure 7-7: Growth rates (crosses) as a function of mode frequency as in the previous figure, but with a reduced anisotropy in the model for the distribution function. For clarity, the dependence of the growth rate on mode frequency for a finite resolution in frequency of 0.1 $\Omega_{\alpha a}$ is also shown (histogram), where the maximum positive growth rate for modes within each frequency band is indicated.

In Fig. 7-7 we show the same graph as in Fig. 7-6 with slightly different values of the parameters, taking $\Sigma = 0.1$ instead of 0.05 to show the dependence of the model on anisotropy. When Σ is increased, that is for a more isotropic distribution function, we see that the peaks of the growth rate become smaller and modes tend to be stabilized. This shows the sensitivity of the growth rate on the model distribution function and highlights the importance of anisotropy as the driving term in the instability.

Taking the limit of a uniform magnetic field and considering the electrostatic component of the mode electric field as the dominant one when $\ell \gg 1$, if we examine the growth rate given by Eq. (7.18) we see that our calculation agrees with the well established instability[29] for the homogeneous magnetosonic wave.

Chapter 8

Comparison of resonant interactions and collisions

The resonant interactions between α-particles at the edge and contained modes competes with the effect of electron collisions to determine changes in the particle orbits. For experiments on current tokamaks, both of these effects may be overshadowed by drift losses due to magnetic field ripple[30]. We have seen in Chapter 2 that collisional slowing down tends to preserve the characteristic ratio between the energy and magnetic moment, $\mathcal{E}/\mathcal{M}$. The effect of pitch angle scatter is mainly to broaden the distribution function around this characteristic value. In addition, the canonical toroidal angular momentum $\mathcal{L}_\zeta$ changes at a slower rate. However, the simplification used in Chapter 2 that the average effect of collisions over an orbit is to preserve $\mathcal{L}_\zeta$ is not accurate. The main reason for this is that for trapped orbits with large radial excursions, which are the focus of this analysis, the portion of the orbit with $v_{||} > 0$ is much larger than that with $v_{||} < 0$. Also, the instantaneous effect of collisions on $\mathcal{L}_\zeta$ is proportional to $Rv_{||}$, which has large positive values towards the edge and small negative values in the core. Thus for these particles collisional slowing down tends to render $\mathcal{L}_\zeta$ more negative over time. The α-particles with large radial excursions are characterized by having a relatively small value of $|\mathcal{L}_\zeta|$ at birth.

The rate of change can be roughly characterized as

$$\dot{\mathcal{L}}_\zeta \approx -\frac{mRv_{||}\Big|_{r=r_{\max}}}{\bar{\tau}_{\rm sl}}$$

Although this seems to denote the maximum rate of change of the angular momentum, the effect of collisions tends to be greater towards the edge of the plasma due to the lower electron temperature. Thus the overestimate from setting the average of $Rv_{||}$ equal to its maximum is roughly made up for by replacing the local collision rate with the average collision rate.

Numerical calculations for the effect of collisional slowing down on $\mathcal{L}_\zeta$ are shown in Fig. 8-1 as a function of $v_{||}/v$ near the plasma edge. The straight, dotted line represents the approximation above. The electron temperature profile is taken to be proportional to that of the ion temperature; for D-T experiments on JET, $T_e \simeq T_i/2$ at the core. Parallel velocities corresponding to unconfined particles are not shown.

Because collisions tend to decrease $\mathcal{L}_\zeta$, the radius of the turning point of the orbit must increase, leading to orbits which are more like deeply trapped orbits in the sense that the radial excursion experience by the particle becomes smaller. This effect, combined with the loss of energy of the α-particle to the electrons, tends to reduce the maximum radius of the particle orbits. However, the particles would have to lose almost all of their energy before their orbits could be described in terms of the banana orbit approximation.

Mode-particle interactions in resonance with multiples of the particle cyclotron frequency predominantly affect the perpendicular energy of the particle. Modes which are driven unstable by α-particles tend to remove perpendicular energy from the particles, eventually taking them into passing orbits which no longer reach into the core of the plasma. Since this is a localized interaction, the canonical angular momentum will be unaffected so long as no parallel energy is absorbed by the mode.

The resonant interactions leading to instability primarily involve α-particles which intersect the mode layer at small poloidal angle (largest distance from the axis of symmetry). This is a small fraction even of the α-particles at the edge. However,

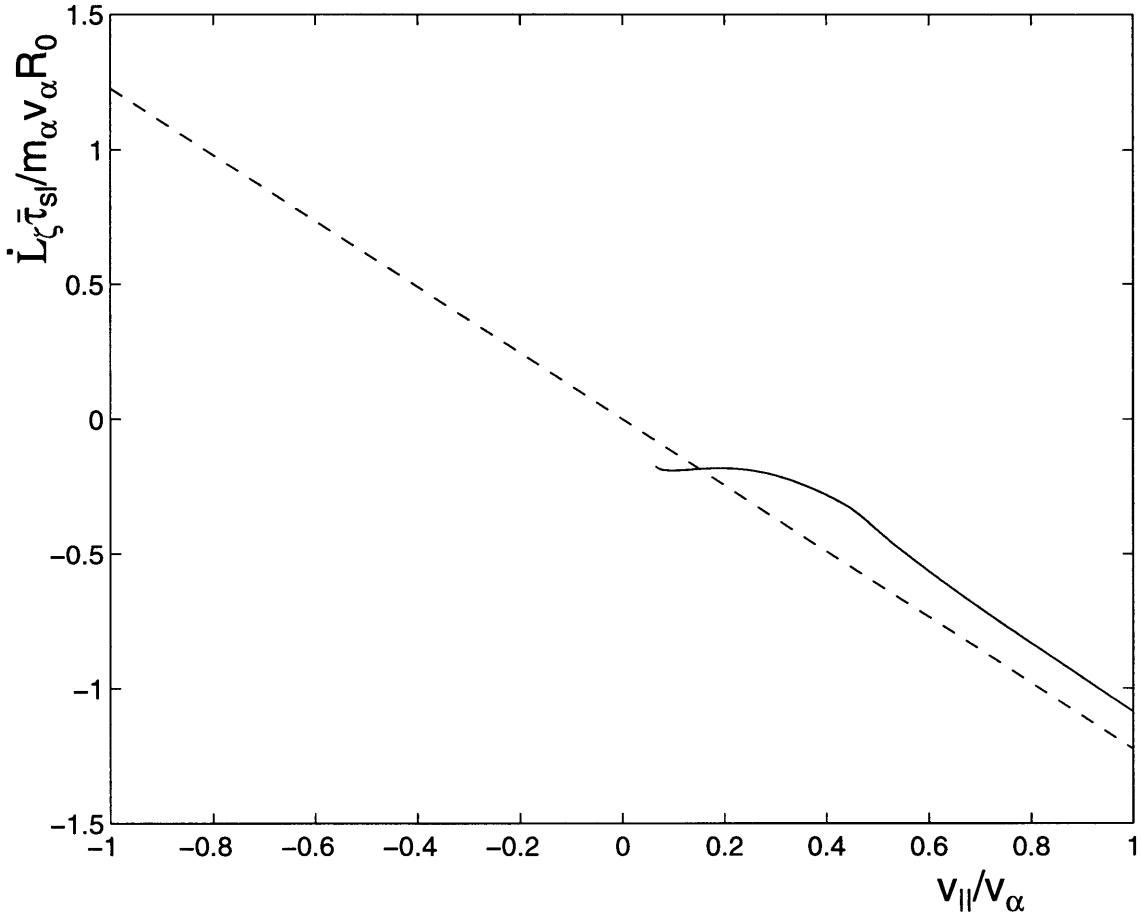

Figure 8-1: Rate of change of canonical angular momentum due to collisions, as a function of $v_{||}/v$ for single particles at $r = r_0 \simeq 0.75\ a$, $\vartheta = 0$. Time derivatives are scaled to $m_\alpha v_\alpha R_0/\bar{\tau}_{sl}$.

if contained modes were externally excited which damp against α-particles, these particles would gain perpendicular energy and eventually lose confinement as their radial drifts carried them out of the plasma. Interactions which damp contained modes can occur over a wide range of poloidal angle, so this process would be able to remove most of the energetic particles whose orbits take them out of the central region of the plasma. As we have seen in Chapter 7, growth rates can be comparable to or larger than the bounce frequency which is itself much larger than $1/\tau_{sl}$. The resulting resonant interactions will affect α-particles much more strongly than collisions, until changes to the local distribution function cause the instability to saturate.

Almost all of the α-particles at the mode layer were produced in the central region of the plasma. The radial excursions are much larger than orbits corresponding to the banana orbit approximation. In particular, trapped particles created near the core drift to the outer regions of the plasma. The largest radius to which α-particles are carried by their orbits is roughly given by 2.6 $(q^2\rho^2R)^{1/3}$, where q is the inverse rotational transform of the magnetic field, ρ is the particle gyroradius, and R is the major radius[15]. T. E. Stringer, in Ref. [15], calculates that for parameters similar to ours ($a = 1$ m, $B_0 = 3.3$ T), 17% of the α-particle distribution occupies the region $r > 0.5\ a$, while less than 5% of the α-particles were produced in this region. Effects which alter the constants of the motion of the particles will change the α-particle distribution function and in particular could lead to radial transport. The two effects considered here, collisions and mode-particle interactions, are illustrated below.

In Fig. 8-2, the orbit of a 3.5 MeV α-particle that interacts with the mode layer at $\vartheta = 0$ is shown for parameters corresponding to experiments on the JET machine. The separate processes acting on these particles are characterized by the two cases of the orbit of a similar particle after losing 50% of its energy to collisions, and after losing 50% of its perpendicular energy through interactions with the contained mode.

Fig. 8-3 shows the analogous case for a particle that interacts with the mode layer at $\vartheta = \pi/4$, except that now the effects of interactions with the contained mode is shown for a particle whose perpendicular energy increases by 50%. Note the loss of confinement due to this energy transfer.

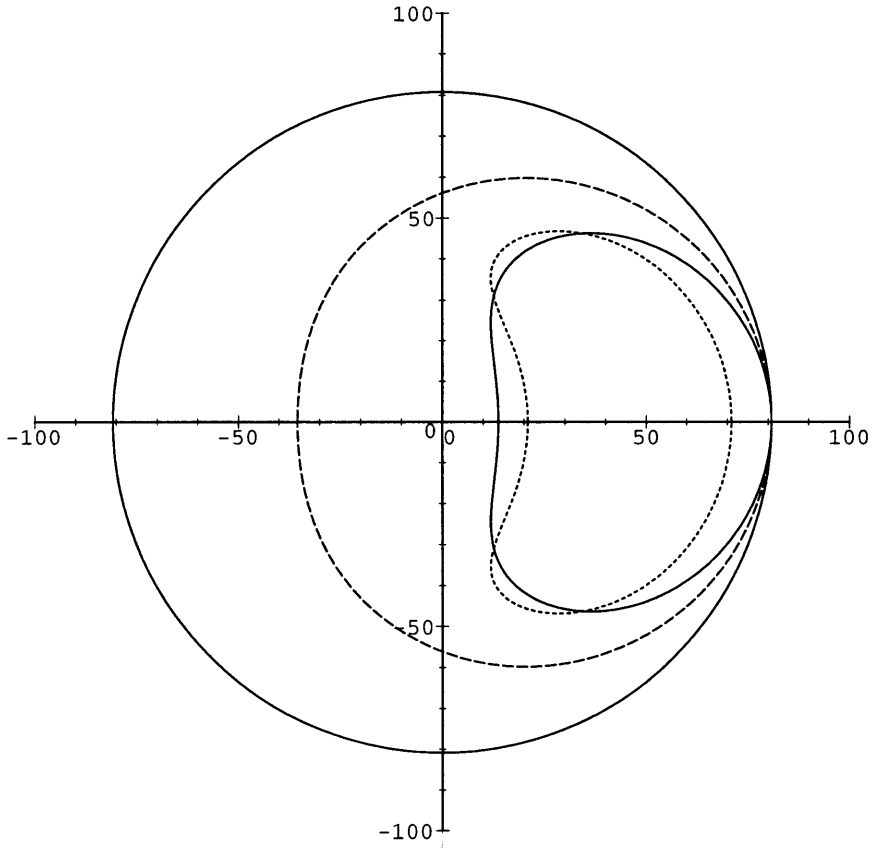

Figure 8-2: Orbit of a 3.5 MeV α-particle which intersects the mode at $\vartheta = 0$ (solid line). Also shown are orbits of a similar particle after losing 50% of its energy to collisions (dotted line) and after losing 50% of its perpendicular energy through interactions with the contained mode (dashed line).

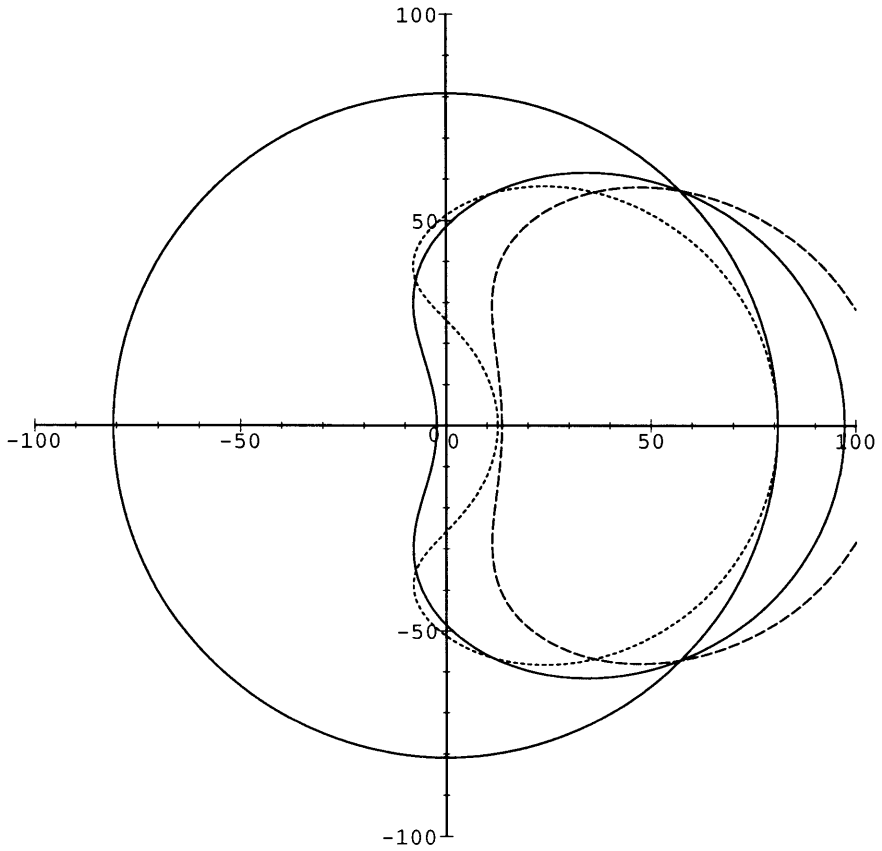

Figure 8-3: Orbit of a 3.5 MeV α-particle which intersects the mode at $\vartheta = \pi/4$ (solid line). Also shown are orbits of a similar particle after losing 50% of its energy to collisions (dotted line) and after gaining 50% of its perpendicular energy through interactions with the contained mode (dashed line). Note that the direction of energy flow is for the mode-particle interaction is reversed from that of the previous figure.

Chapter 9

Model for toroidal rotation generated by ICRF

Significant plasma rotation has been observed to be produced in toroidal plasmas subject to ion cyclotron range of frequencies (ICRF) heating in the absence of any evident direct angular momentum inputs[31, 32]. In Alcator C-Mod, it is characterized by large velocities at the magnetic axis in the direction of the plasma current, with peak velocities of up to 150 km/s when the contribution of the deuteron diamagnetic velocity is added[32]. The induced toroidal rotation is observed in conjunction with the existence of improved confinement conditions compared to the L-mode regime, in particular with the onset of the H-mode regime. Plasmas in the L-mode confinement regime exhibit a greatly reduced rotation, and in the opposite direction.

The onset of this rotation and its decay after the ICRF has been turned off are characterized by similar time scales of less than 100 ms, which is comparable to the energy confinement time and a clear indication of anomalous transport. To explain the observations according to our theoretical model we must consider two issues, one being the source of torque on the plasma and the other being the transport of the resulting angular momentum. Distinct types of collective modes are necessary to model these two features of the experimental observations.

9.1 Torque generated by balanced inputs

We consider the mechanism for the generation of torque on a plasma from balanced ICRF inputs to be related to the existence of a special class of magnetosonic-whistler modes at frequencies of the order of the ion cyclotron frequency and above, that can resonate with the injected waves. This class of modes is characterized by a strong asymmetry in the direction of poloidal propagation in that there are two types of modes, one convective and one standing. The contained modes, which propagate around magnetic flux surfaces but form standing modes in the radial direction, can be confined within a narrow radial layer located in the outer region of the plasma column[4], typically at a radius $r_0 > 0.6\ a$. For the Alcator C-Mod experiment, only modes with a poloidal phase velocity in the ion cyclotron direction relative to the toroidal magnetic field will have radial confinement, around $r_0 \simeq 0.7\ a$. This fixes the sign of the poloidal mode number m.

The origin of the asymmetry in poloidal propagation is the RHS of the equation $\vec{E} + \vec{u}_i \times \vec{B} = \vec{J} \times \vec{B}/en$, which is related to the Hall effect. This corresponds to enforcing the so called frozen-in law $\vec{E} + \vec{u}_e \times \vec{B} = 0$ for the electron population. As shown in Chapter 5, significant propagation along the equilibrium magnetic field tends to reduce the asymmetry between modes with opposite phase velocities. The effect of parallel propagation is to reduce the importance of the parameter d_{i0}/a, where $d_{i0} = c/\omega_{pi}$ evaluated at the center of the plasma, and thus to reduce the role of the Hall effect in shaping the nature of the mode solutions. As a result, the asymmetry in the radial mode structure with respect to the direction of the poloidal phase velocity is greatest for modes which propagate nearly perpendicular to the equilibrium magnetic field. Another motivation to focus on modes with nearly perpendicular propagation is that for large $k_{||}$ it is difficult to find contained modes of the fast magnetosonic type.

Radially confined modes will deposit their angular momentum on the plasma background as they damp against the plasma. In contrast, modes having the opposite phase velocity will travel to the edge of the plasma column and dissipate their

angular momentum to the surrounding environment. Through the magnetic field geometry, the orientation of the toroidal phase velocity is correlated with that of the poloidal phase velocity for modes propagating nearly perpendicular to the equilibrium magnetic field through the condition $n^0 \simeq m/q(r)$. Here $q(r)$ is the inverse rotational transform which in the limit of a cylindrical plasma is given by $q(r) = rB_\zeta/R_0B_\vartheta$. The resulting net torque applied to the plasma is in the direction of the plasma current, consistent with experimental observations. Through the sign of $q(r)$, the toroidal mode number for radially confined modes changes sign if the current is reversed.

The excitation of contained modes by ICRF offers an explanation of experimental observations of plasma rotation being generated by inputs which themselves carry no angular momentum. The angular momentum which is deposited in the plasma has the same direction as the toroidal plasma current, consistent with observations of toroidal flow velocities. To evaluate this mechanism as an explanation for toroidal rotation it is also necessary to investigate the relationship between the flow velocities of the main ion species and the observed impurity species, and to consider processes for the transport of angular momentum to the core of the plasma. We also examine features of this rotation generation which would distinguish its effect from other sources of angular momentum in ICRF-heated plasmas. A sketch of the physical processes involved in the deposition of angular momentum at the mode layer from balanced inputs is shown in Fig. 9-1.

To display the different features of contained modes from those of an unconfined magnetosonic-whistler wave, we consider the form of the effective potential for the two different types of modes. This effective potential determines the radial eigenfunction of the standing modes through the equation

$$\frac{d^2b_1}{dr^2} - V_{\text{eff}}(r,\omega)b_1 = 0 \tag{9.1}$$

where

$$V_{\text{eff}} \simeq -\frac{\omega^2}{v_A^2 + k_{||}^2 D_H^2} - \frac{k_\perp \omega}{r(v_A^2 + k_{||}^2 D_H^2)} \frac{d}{dr}(D_H) + k_\perp^2, \tag{9.2}$$

v_A is the Alfvén velocity, and $D_H = B/\mu_0 ne$. The wave vector components $k_{||}$ and

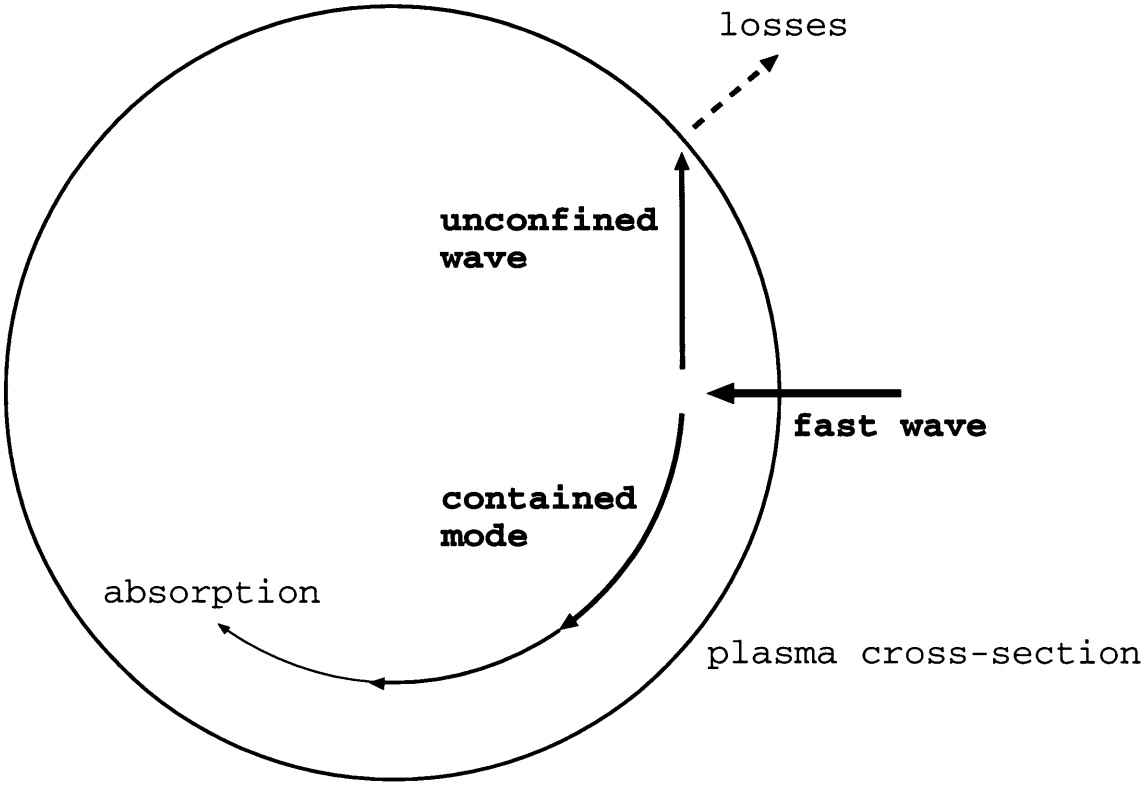

Figure 9-1: Sketch of the separation of the balanced ICRF inputs into two conveyors of angular momentum: a contained mode, which propagates poloidal in the ion cyclotron direction and damps against the plasma; and an unconfined magnetosonic-whistler mode which carries energy and angular momentum out to the plasma edge.

$k_\perp$ can be approximated as

$$k_\perp \simeq k_\vartheta = -m/r$$

and

$$k_\| \simeq -\frac{m}{Rq(r)}\left[1 - \frac{n^0 q(r)}{m}\right],$$

where m and n^0 are the poloidal and toroidal mode numbers, respectively.

The contained mode frequency, if taken to be positive, is roughly

$$\omega \simeq |k_\perp| v_A = |m| v_A / r_0$$

where r_0 is the mode localization radius. For typical experimental parameters contained modes exist only for m positive; the poloidal phase velocity is in the ion cyclotron direction. For plasma parameters typical of those produced by the Alcator C-Mod machine[33], $r_0 \simeq 0.7\ a$. In Fig. 9-2 the effective potential is shown for the two cases $m = 6$, $n^0 = 3$ and $m = -6$, $n^0 = -3$. The corresponding frequencies are 2.03 Ω_i and 1.66 Ω_i respectively.

The derivation of the properties of the contained mode in Chapters 4 and 5 was predicated on the assumption that $k_\|^2 \ll k_\perp^2$. This condition is equivalent to requiring that $(n^0)^2 \ll m^2 R_0^2/a^2$, where R_0 is the major radius and a is the minor radius of the plasma column. It was found that in the limit $k_\| \to 0$, the region within which the contained modes were localized was centered about a fixed value r_0. The characteristics of the radial eigenmodes can be distinguished as having two regimes, for which the component of propagation parallel to the equilibrium magnetic field has different roles.

In the quasi-flute regime, where $|1 - n^0 q(r)/m| \ll 1$, the localization of the mode shifts from the $k_\| \to 0$ limit by an amount which is proportional to $k_\|$. The condition for this regime can be expressed as $k_\|^2 B^2 \ll k_\perp^2 B_\vartheta^2$. In this regime, $k_\zeta B_\zeta$ and $k_\vartheta B_\vartheta$ still roughly cancel each other out. In the oscillatory regime, when $|1 - n^0 q(r)/m| \gtrsim 1$, the shift in the mode layer with $k_\|$ saturates. The variation with $k_\|$ exhibited by the radius of localization of the mode in the quasi-flute regime increases with the poloidal

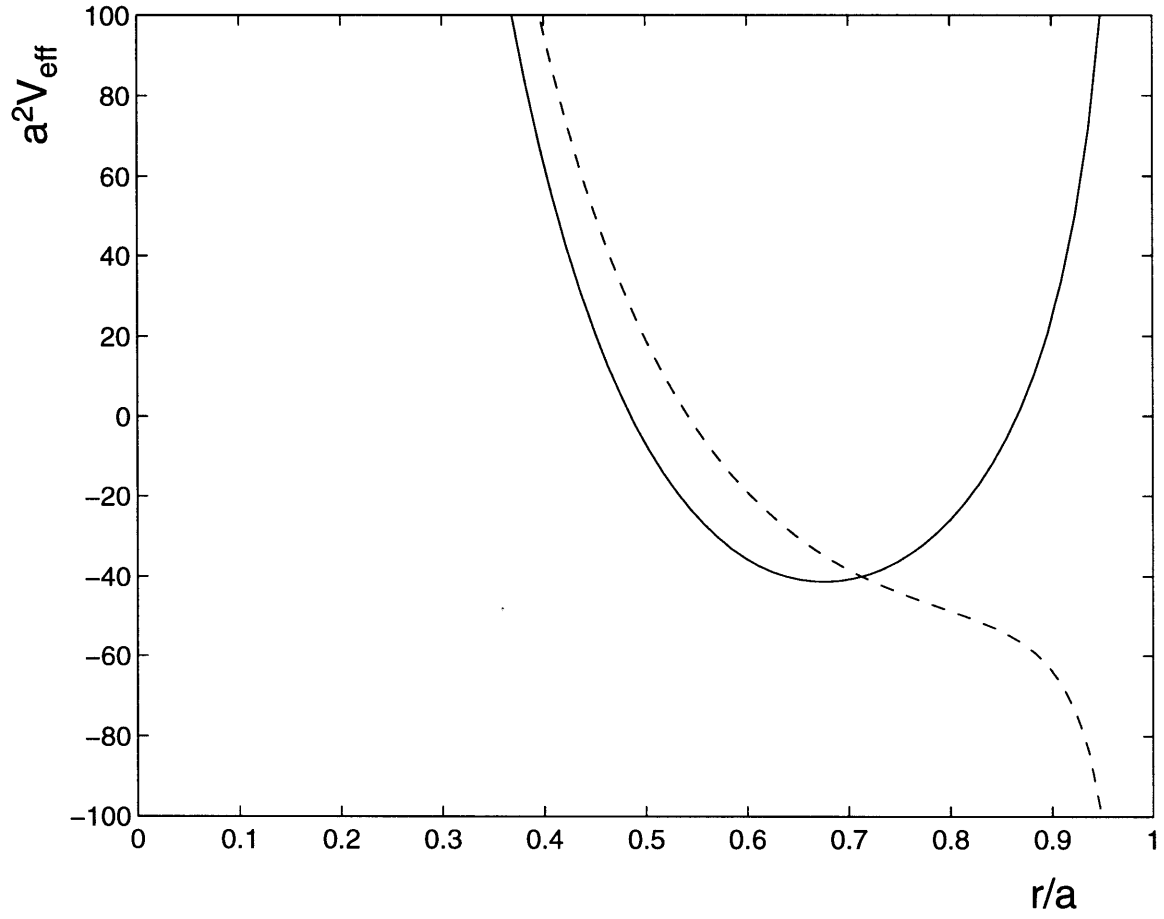

Figure 9-2: Form of the effective potential for the case of modes propagating in the direction of the ion cyclotron ($m > 0$, solid line) and electron cyclotron motion ($m < 0$, dashed line).

mode number. Contained modes in the oscillatory regime can be found in a broad region within the plasma column. For sufficiently high frequencies, this subclass of modes is excluded only from the plasma core, where $r < 0.4\ a$. Quasi-flute modes, on the other hand, are found clustered around an "invariant" radial surface which is determined by the density profile and the ratio of length scales d_i/a.

9.2 Estimate for rotation induced by contained modes in Alcator C-Mod

Consider the global physical quantities

$$\begin{aligned} \mathcal{E} &= \text{RF energy absorbed by contained modes} \\ \mathcal{L}_\zeta &= \text{angular momentum acquired by plasma} \end{aligned}$$

To determine the implications of a significant role for contained modes in the generation of angular momentum, we can argue from basic considerations that a contained mode with energy $\mathcal{E}$ will have toroidal angular momentum

$$\mathcal{L}_\zeta = \mathcal{E} n^0/\omega, \tag{9.3}$$

where n^0 is the toroidal mode number. For a given experiment, n^0 and ω may be determined by the ICRF inputs. Alternatively, we can estimate that the frequency is roughly $\omega \simeq |k_\perp| v_A = |m| v_A/r_0$, where v_A is the Alfvén velocity, and modes with small $k_\parallel$ are characterized by toroidal mode numbers $n^0 \simeq m/q(r_0)$. The quantity r_0 is the radius around which the contained modes are localized. For experimental parameters contained modes exist only for $m > 0$, so that the poloidal phase velocity is in the ion cyclotron direction. For modes with $k_\parallel \simeq 0$ this requires that $n^0 \simeq m/q(r) > 0$, given that $q(r)$ is taken to be a positive quantity ($B_\zeta/B_\vartheta > 0$), and so the toroidal phase velocity is in the same direction as the equilibrium toroidal current.

If we assume that the saturation levels of angular momentum are determined solely

by the net torque applied to the plasma and an independent rate $1/\tau$ of transport out of the plasma, then the steady state balance is given by $\dot{\mathcal{L}}_\zeta \simeq \mathcal{L}_\zeta^{\rm sat}/\tau$. In terms of the toroidal velocity profile $v_\zeta(r)$, the angular momentum is $\mathcal{L}_\zeta = VR_0 m_i \langle n_i v_\zeta \rangle$ where $\langle\ \rangle$ denotes a volume average, R_0 is the major radius, and V is the volume of the plasma column.

Characteristic parameters for the Alcator C-Mod experiments are $a \simeq 0.22$ m, $R_0 \simeq 0.67$ m, $n_0 \simeq 10^{20}$ m^{-3}, $B_0 \simeq 5.3$ T, and $q(r_0) \simeq 2$, where the radius of localization is $r_0 \simeq 0.7\ a$. The ellipticity is $\kappa \leq 1.8$, with typical values of $\kappa \simeq 1.6$ during the sequence of experiments which examined plasma rotation. The elongation of the plasma allows for a larger cross-sectional area with the given minor radius, and thus enables a high total current. During ICRF heating, the core density increases up to 2.5×10^{20} m^{-3}. For a deuterium plasma the Alfvén velocity is $v_A \simeq 8200$ km/s. The peak plasma temperature is about 2 keV and the deuterium thermal velocity is about 450 km/s. For a peak rotation velocity of 100 km/s, excluding the diamagnetic velocity contribution, with a sharply peaked velocity profile as shown in Fig. 9-3, the angular momentum is estimated to be $\mathcal{L}_\zeta \sim 10^{-3}$ J-s. The apparent rate of energy conversion required by Eq. (9.3) seems consistent with the injected power of about 2 MW.

9.3 Angular momentum transport

We explain the fact that the induced rotation is strongest in the H-mode confinement regime by considering two competing effects in the transport of angular momentum: ion temperature gradient driven modes, which leads to diffusion of angular momentum; and velocity gradient driven modes, which can generate active transport of angular momentum into the core of the plasma in addition to diffusive processes.

Combining these effects, we represent the flux of angular momentum by

$$\Gamma_J \simeq -\alpha_J D_i^{\rm th} \frac{dJ}{dr} - \left(D_J \frac{dJ}{dr} + v_J \frac{2r}{a} J \right) \tag{9.4}$$

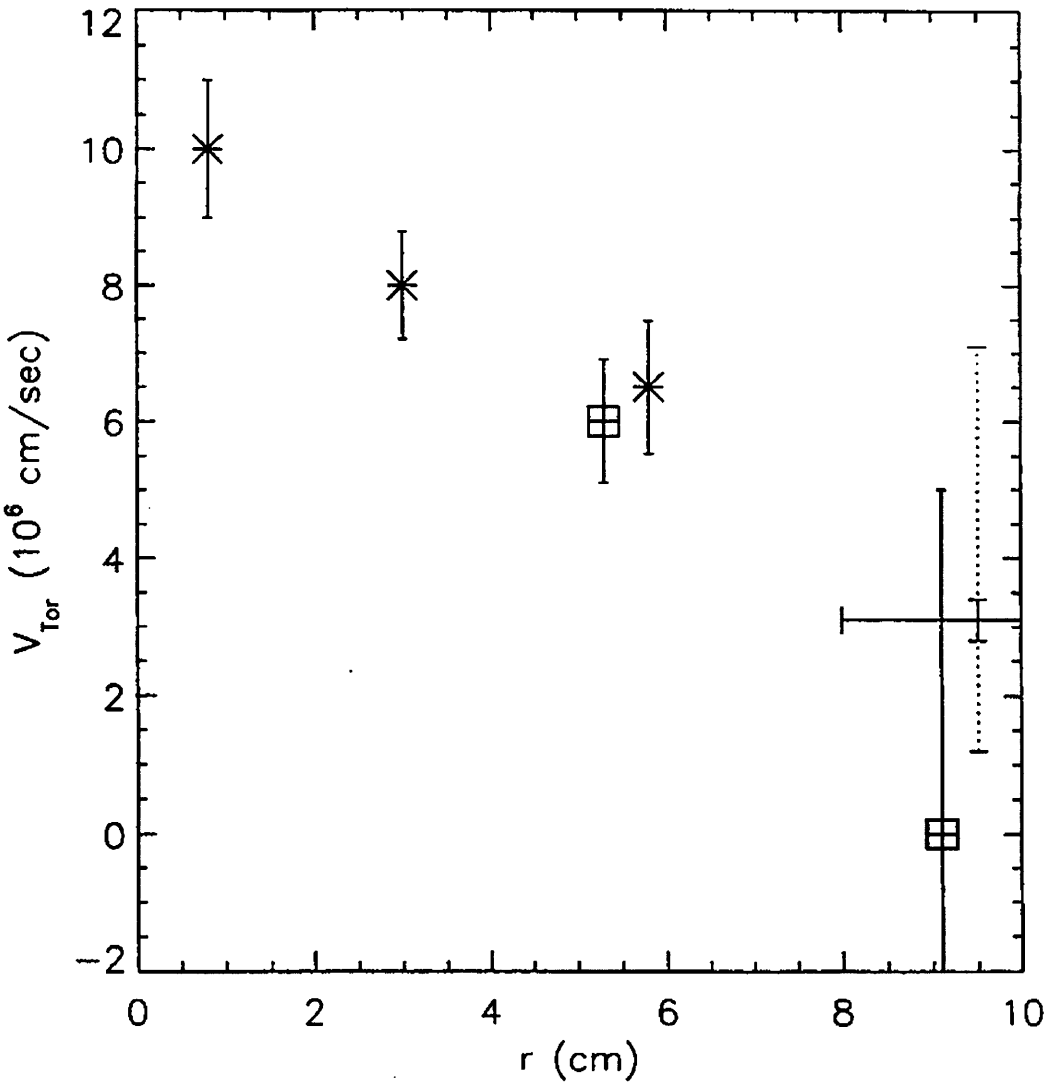

Figure 9-3: Radial profile of toroidal velocities as observed on the Alcator C-Mod machine.

where J is the density of angular momentum, D_i^{th} is the effective diffusion coefficient for the ion thermal energy produced by ion temperature gradient driven modes that also carry angular momentum outwards[34], the term proportional to D_J indicates the transport of angular momentum resulting from velocity gradient driven modes, and α_J is an appropriate dimensionless parameter. When the ion thermal transport is large, angular momentum that is deposited near the plasma periphery induces only a small amount of plasma rotation. When, instead, a thermal transport barrier is formed, as in the case of the H-mode regime, the angular momentum settles into the centrally peaked profile usually observed and given by

$$\frac{dJ}{dr} \simeq -\frac{v_J}{D_J}\frac{2r}{a}J.$$

The higher central rotation is due to a combination of the the reduction in the net diffusion coefficient and of the effect of the inflow term $v_J(2r/a)J$ which is similar to that usually adopted to describe the particle transport[35] in the context of profile consistency. By dimensional analysis, noting that the angular momentum source, diffusion coefficient, and inflow velocity v_J all have an inverse time dependence, we can find a symmetry in the time-independent velocity profile which satisfies Eq. (9.4). Increasing the diffusion coefficient is equivalent to reducing the source of angular momentum and the active transport, which leads to a flatter velocity profile and an overall reduction in toroidal velocities.

We examine the role of ion temperature gradient drive modes in generating transport of angular momentum by evaluating the quasilinear momentum transport in a slab geometry. Assuming that perpendicular dynamics are restricted so that the magnetic moment is unchanged by the perturbation and the perturbed perpendicular velocity is given by

$$\vec{v}_\perp \simeq \vec{v}_E + \vec{v}_P$$

where $\vec{v}_E \simeq c\vec{E} \times \vec{B}/B^2$ is the electric drift and $\vec{v}_P$ is the polarization drift. Then

$$\nabla_\perp \cdot \vec{v}_\perp \simeq 0 \tag{9.5}$$

Thus from mass conservation,

$$\frac{\partial}{\partial t}n + \nabla \cdot (n\vec{v}) = 0, \tag{9.6}$$

the linearized equation becomes

$$-i\omega\hat{n} = -ik_{||}(\hat{n}v_{||} + n\hat{v}_{||}) - \vec{v}_E \cdot \nabla_\perp n.$$

We take a slab configuration with $\vec{B} = B_0\hat{e}_z$ and with gradients only in the x-direction. We consider modes with wave vectors of the form $\vec{k} = k_{||}\hat{e}_z + k_y\hat{e}_y$, and we consider the polarization drift to be negligible. Then the linearized mass conservation equation simplifies to

$$k_{||}\hat{v}_{||} = \bar{\omega}\frac{\hat{n}}{n} + i\hat{v}_{Ex}\frac{1}{n}\frac{dn}{dx} \tag{9.7}$$

where

$$\bar{\omega} \equiv \omega - k_{||}v_{||}$$

is the Doppler shifted frequency.

Focussing on the ions, the parallel force balance equation is

$$m_i n\left(\frac{\partial}{\partial t} + \vec{v}\cdot\nabla\right)v_{||} = -\nabla_{||}p_{i||} + enE_{||} + F_{||} \tag{9.8}$$

where $F_{||}$ could be, for example, the thermal force or the friction force between the ions and electrons. Using mass conservation, this can be expressed as the conservation equation

$$\frac{\partial}{\partial t}(m_i n v_{||}) + \nabla \cdot (m_i n v_{||}\vec{v}) = -\nabla_{||}p_{i||} + enE_{||} + F_{||}$$

The quantity $m_i n v_{||}\vec{v}$ indicates the flow of parallel momentum. We will be considering the quasilinear flow in the $\hat{e}_x$ direction. Because there is no equilibrium flow along the density gradient and the x-component of the perturbed velocity is $\hat{v}_{Ex}$, the momentum flux is determined by

$$\Gamma_{Jx} = \langle m_i n v_{||} v_x \rangle = \frac{1}{2}\Re\mathrm{e}\left(m_i\widehat{nv}_{||}\hat{v}^*_{Ex}\right) \tag{9.9}$$

where

$$\widehat{nv}_{||} \equiv n\hat{v}_{||} + \hat{n}v_{||}.$$

Thus we have two contributions to the momentum flux,

$$\Gamma_1 \equiv \frac{1}{2}\Re\mathrm{e}\left(m_i n\hat{v}_{||}\hat{v}^*_{Ex}\right) \tag{9.10}$$

and

$$\Gamma_2 \equiv \frac{1}{2}\Re\mathrm{e}\left(m_i v_{||}\hat{n}\hat{v}^*_{Ex}\right) = m_i v_{||}\Gamma_n, \tag{9.11}$$

where $\Gamma_n = \langle \hat{n}\hat{v}^*_{Ex}\rangle$ is the particle transport. While the detailed mechanisms for ion transport are not thoroughly understood, there is strong evidence for enhanced particle confinement beyond what can be explained in terms of particle diffusion. The active transport of ions into the core of the plasma is indicated by the observation of profile consistency[35] in well confined plasmas. The inwards particle transport leads to a corresponding inwards flow of angular momentum.

We shall see that Γ_1 leads to diffusion of ion momentum. The physical significance of this term is the transport of momentum due to the exchange of particles with different parallel velocities, and thus the corresponding momentum flux must ultimately be related to velocity gradients. Using Eq. (9.7),

$$\Gamma_1 = \frac{1}{2}\Re\mathrm{e}\left[m_i\left(\frac{\bar{\omega}}{k_{||}}\hat{n} + \frac{i}{k_{||}}\hat{v}_{Ex}\frac{dn}{dx}\right)\hat{v}^*_{Ex}\right] = \frac{1}{2}\Re\mathrm{e}\left(m_i\frac{\bar{\omega}}{k_{||}}\hat{n}\hat{v}^*_{Ex} + m_i\frac{i}{k_{||}}|\hat{v}_{Ex}|^2\frac{dn}{dx}\right)$$

The second term clearly gives no contribution to the momentum flux when $k_{||}$ is real valued, because the perturbed parallel momentum is exactly out of phase with the perturbed drift velocity. Thus

$$\Gamma_1 = \frac{1}{2}\Re\mathrm{e}\left(m_i\frac{\bar{\omega}}{k_{||}}\hat{n}\hat{v}^*_{Ex}\right) \tag{9.12}$$

The net quasilinear momentum flux is

$$\Gamma_1 + m_i v_{||}\Gamma_n = \frac{1}{2}\Re\mathrm{e}\left(m_i\frac{\bar{\omega}}{k_{||}}\hat{n}\hat{v}^*_{Ex}\right) + \frac{1}{2}\Re\mathrm{e}\left(m_i v_{||}\hat{n}\hat{v}^*_{Ex}\right) = \frac{1}{2}\Re\mathrm{e}\left(m_i\frac{\omega}{k_{||}}\hat{n}\hat{v}^*_{Ex}\right)$$

noting that by definition $\omega = \bar{\omega} + k_{||} v_{||}$. It is more convenient to consider these two contributions separately, however, because the dispersion relation is a function of the Doppler shifted frequency $\bar{\omega}$.

Defining the electric potential as $\vec{E} = -\nabla\Phi$, the drift velocity is $\hat{v}_{Ex} = -ik_y c\hat{\Phi}/B$. For an adiabatic electron response

$$\frac{\hat{n}}{n} = \frac{e\hat{\Phi}}{T_e},$$

there is no net particle flow, and so we consider corrections to the electron response. For now, we use as a general notation

$$\frac{\hat{n}}{n} = \frac{e\hat{\Phi}}{T_e}(1 + A). \tag{9.13}$$

where $A = A_r + iA_i$ is a complex-valued coefficient which will depend on the frequency and wave vector. The momentum flux then becomes

$$\Gamma_{Jx} = -\frac{1}{2} m_i n k_y \frac{cT_e}{eB} \left|\frac{e\hat{\Phi}}{T_e}\right|^2 \frac{1}{k_{||}} \Im\mathrm{m}[\bar{\omega}(1 + A)] - \frac{1}{2} m_i n k_y \frac{cT_e}{eB} v_{||} \left|\frac{e\hat{\Phi}}{T_e}\right|^2 A_i \tag{9.14}$$

We note that the total flow of momentum will be due to the combined total of quasilinear flows from different modes; in particular, we consider different parities of the wave vector, in particular the net flow of momentum from modes having the opposite sign of $k_{||}$. The momentum flux driven by Γ_n can depend upon the sign of $k_{||}$ only through the quantity A_i. We assume that A_i has a significant component which is even with respect to the sign of $k_{||}$. The contribution to the momentum flux represented by Γ_1 has an explicit dependence on $k_{||}$, so the flows arising from two modes having parallel wave vectors $\pm k_{||}$ tend to cancel each other out unless $\Im\mathrm{m}[\bar{\omega}(1+A)]$ also varies with the sign of $k_{||}$. Thus, we look for terms in the dispersion equation which have odd parity in $k_{||}$. We note from Eq. (9.7) that the relationship between $k_{||}\hat{v}_{||}$, $\hat{n}$, and $\hat{v}_{Ex}$ only depends on the sign of $k_{||}$ through the quantity $\bar{\omega}$.

We then evaluate the perturbed force balance equation using that fact that for

any physical quantity F, the linearized form of

$$\left(\frac{\partial}{\partial t} + \vec{v} \cdot \nabla\right) F$$

is

$$-i\bar{\omega}\hat{F} + \hat{v}_{Ex}\frac{dF}{dx}.$$

Thus Eq. (9.8) becomes

$$m_i n \left(-i\bar{\omega}\hat{v}_{||} + \hat{v}_{Ex}\frac{dv_{||}}{dx}\right) = -ik_{||}(\hat{n}T_{i||} + n\hat{T}_{i||} + en\hat{\Phi}) + \hat{F}_{||}$$

which can be rewritten as

$$\bar{\omega}k_{||}\hat{v}_{||} = \frac{k_{||}^2}{m_i}\left(\frac{\hat{n}}{n}T_{i||} + \hat{T}_{i||} + e\hat{\Phi}\right) + \frac{i}{m_i n}k_{||}\hat{F}_{||} - ik_{||}\hat{v}_{Ex}\frac{dv_{||}}{dx} \tag{9.15}$$

The force represented by $\hat{F}_{||}$ should change sign with $k_{||}$, so the only quantity which violates parity with $k_{||}$ is the term proportional to $dv_{||}/dx$. Thus, we expect that without a gradient in $v_{||}$, there would be no net contribution tom the momentum flux from the term $\langle\hat{v}_{||}\hat{v}_{Ex}\rangle$.

To find the specific wave equation which leads to transport, we also consider the parallel energy conservation equation for the ions,

$$\frac{N}{2}\frac{\partial}{\partial t}(nT_{i||}) + \frac{N}{2}\nabla \cdot (nT_{i||}\vec{v}) = -nT_{i||}\nabla \cdot \vec{v} + q_{||}$$

where N is the number of degrees of freedom, and $q_{||}$ represents, for example, energy transfer between the electrons and ions. We set $N = 1$, which reflects the fact that perpendicular energy is not affected by low frequency modes. Using the mass conservation equation, we rewrite the energy equation as

$$\frac{1}{2}n\left(\frac{\partial}{\partial t} + \vec{v} \cdot \nabla\right) T_{i||} - T_{i||}\left(\frac{\partial}{\partial t} + \vec{v} \cdot \nabla\right) n = q_{||} \tag{9.16}$$

which is equivalent to the adiabatic equation of state

$$\frac{d}{dt}\left(\frac{p_{i\|}}{n^\gamma}\right) = \frac{(\gamma-1)q_\|}{n^\gamma}$$

with $d/dt \equiv \partial/\partial t + \vec{v}\cdot\nabla$ and $\gamma \equiv 1 + (2/N) = 2$.

The perturbed energy balance equation is then

$$\frac{n}{2}\left(-i\bar{\omega}\hat{T}_{i\|} + \hat{v}_{Ex}\frac{dT_{i\|}}{dx}\right) - T_{i\|}\left(-i\bar{\omega}\hat{n} + \hat{v}_{Ex}\frac{dn}{dx}\right) = \hat{q}_\| \tag{9.17}$$

The energy flow $q_\|$ should be independent of the sign of $k_\|$, so the energy balance equation does not introduce explicit dependence on the sign of $k_\|$. Thus we can conclude that in the limit $dv_\|/dx \to 0$, $\bar{\omega}$ is independent of the sign of $k_\|$ and the momentum flux due to Γ_1 vanishes when summed over wave vectors.

In light of this, we treat $dv_\|/dx$ as a small perturbation to the wave equation, which is an appropriate limit when $v_\| \ll v_{\mathrm{th}i}$. We then neglect the quantities $\hat{F}_\|$ and $\hat{q}_\|$, which introduce only minor corrections to the mode equation when there are no velocity gradients and do not yield an independent contribution to the net momentum flux.

By combining the linearized equations, Eqs. (9.7), (9.15), and (9.17), we can eliminate most of the perturbed fields to find the following condition on the ions:

$$\frac{\hat{n}}{n}\left(1 - 3\frac{k_\|^2}{\bar{\omega}^2}\frac{T_{i\|}}{m_i}\right) = -\frac{i}{\bar{\omega}}\hat{v}_{Ex}\left[\frac{1}{n}\frac{dn}{dx}\left(1 - 2\frac{k_\|^2}{\bar{\omega}^2}\frac{T_{i\|}}{m_i}\right) + \frac{k_\|^2}{\bar{\omega}^2}\frac{1}{m_i}\frac{dT_{i\|}}{dx} - \frac{k_\|^2}{k_y\bar{\omega}}\Omega_i + \frac{k_\|}{\bar{\omega}}\frac{dv_\|}{dx}\right] \tag{9.18}$$

where $\Omega_i \equiv eB/m_i c$.

If we consider the superthermal limit where $|\bar{\omega}^2| \gg k_\|^2 T_i/m_i$, then the second term on both the right and left side of the equation can be neglected. This corresponds to neglecting the contribution of density fluctuations to the perturbed pressure in the force balance equation, and the density gradient term in the energy balance equation. Using the definition of $\hat{v}_{Ex}$ and the model for the electron dynamics of Eq. (9.13), we

then find the dispersion relation

$$\bar{\omega}(1+A) \simeq -k_y \frac{cT_e}{eB}\left(\frac{1}{n}\frac{dn}{dx} + \frac{k_{||}^2}{\bar{\omega}^2}\frac{1}{m_i}\frac{dT_{i||}}{dx} + \frac{k_{||}}{\bar{\omega}}\frac{dv_{||}}{dx} - \frac{k_{||}^2}{k_y\bar{\omega}}\Omega_i\right) \tag{9.19}$$

If we define the sound velocity as $c_s^2 \equiv T_e/m_i$, the electron drift frequency

$$\omega_{*e} \equiv -k_y \frac{cT_e}{eB}\frac{1}{n}\frac{dn}{dx},$$

the ion temperature drift frequency

$$\omega_{Ti} \equiv k_y \frac{c}{eB}\frac{dT_{i||}}{dx},$$

and the ion velocity drift frequency

$$\omega_v \equiv k_y \frac{cT_{i||}}{eB}\frac{1}{v_{||}}\frac{dv_{||}}{dx},$$

then the dispersion equation becomes

$$1 + A - \frac{\omega_{*e}}{\bar{\omega}} + \frac{k_{||}v_{||}\omega_v}{\bar{\omega}^2} + \frac{k_{||}^2 c_s^2 \omega_{Ti}}{\bar{\omega}^3} - \frac{k_{||}^2 c_s^2}{\bar{\omega}^2} = 0 \tag{9.20}$$

Because we are in the superthermal ion regime, and typically $T_i \gtrsim T_e$, we can neglect the last term in Eq. (9.20), which originated from the electric force term in the momentum balance equation. Furthermore, because $v_{||} \ll v_{\mathrm{th}i}$, the term proportional to the velocity gradient is small compared to unity. However, this term is important because it is the only quantity which depends upon the sign of $k_{||}$.

We first solve for the lowest-order frequency by neglecting the parameter A as well as the term proportional to $dv_{||}/dx$. We assume that

$$\left(\frac{\omega_{*e}}{\omega_{Ti}}\right)^2 = \left(\frac{T_{i||}}{T_e}\eta_i\right)^2 \gg 1$$

where

$$\eta_i \equiv \frac{n}{T_{i\|}} \frac{dT_{i\|}/dx}{dn/dx} = \frac{r_n}{r_T},$$

$$r_n = -\frac{1}{n}\frac{dn}{dx},$$

and

$$r_T = -\frac{1}{T_{i\|}}\frac{dT_{i\|}}{dx}.$$

For simplicity we take the limit where $|\bar{\omega}| \gg |\omega_{*e}|$, in which case the lowest order form of the dispersion equation is

$$\bar{\omega}^3 \simeq -k_\|^2 c_s^2 \omega_{Ti} \tag{9.21}$$

which has one real root and a pair of complex conjugate roots. Consistency requires that

$$\frac{T_{i\|}}{T_e}\eta_i \gg \frac{k_y \rho_s^2}{k_\|^2 r_n^2} \gg \left(\frac{T_{i\|}}{T_e}\eta_i\right)^{-2} \tag{9.22}$$

where $\rho_s \equiv c_s/\Omega_i$. Note that $|k_y \rho_i / k_\| r_T|^2 \gg 2T_e/T_{i\|}$ but $|k_y \rho_s / k_\| r_n|^2$ does not have to be larger than unity.

The unstable root is then, to lowest order,

$$\bar{\omega} \simeq \omega_0 \equiv |k_\|^2 c_s^2 \omega_{Ti}|^{1/3} \left(\frac{\sigma}{2} + i\frac{\sqrt{3}}{2}\right) \tag{9.23}$$

where $\sigma \equiv \mathrm{sgn}(k_y dT_{i\|}/dx)$. The growth rate is comparable to the real part of the frequency, so terms which have been neglected in the dispersion equation should introduce only a small correction to the growth rate, and hence to the momentum transport. The lowest order quasilinear momentum flux is given by

$$\Gamma = -\frac{1}{2} m_i n k_y \frac{cT_e}{eB} \left|\frac{e\hat{\Phi}}{T_e}\right|^2 \left[\frac{1}{k_\|}|k_\|^2 c_s^2 \omega_{Ti}|^{1/3} \left(\frac{\sigma}{2}A_i + \frac{\sqrt{3}}{2}A_r\right) + v_\| A_i\right] \tag{9.24}$$

Assuming that A is independent of the sign of $k_\|$, the first term in the above expression yields an equal and opposite contribution to the momentum flux for pairs of modes

having equal k_y and $\pm k_{||}$. If A_i depends on the sign of k_y, then the last term will yield an overall contribution to the momentum flux even after combining pairs of modes having $\pm k_{||}$ and $\pm k_y$. Thus, by symmetry in the parallel direction, to lowest order the only net momentum flux arises from the particle transport, and is given by

$$m_i v_{||} \Gamma_n = -\frac{1}{2} m_i n k_y \frac{cT_e}{eB} \left| \frac{e\hat{\Phi}}{T_e} \right|^2 v_{||} A_i \tag{9.25}$$

This yields an active transport in parallel momentum across field lines, and further corrections will not significantly alter the corresponding momentum flux. However, to evaluate the diffusive transport it is clear that the term related to $dv_{||}/dx$ is the only correction to the dispersion equation which will yield a net flux of momentum corresponding to the term Γ_1.

To evaluate the effect of the velocity gradient on the mode frequency, we expand the frequency as

$$\bar{\omega} = \omega_0 + \delta\omega$$

and only keep terms to first order in $\delta\omega$. We also neglect the parameter A both in the dispersion equation and in Eq. (9.14), given that $|A|^2 \ll 1$.

The resulting first order correction to the frequency is

$$\delta\omega = -\frac{1}{3}\frac{k_{||} v_{||} \omega_v}{\omega_0} = \frac{1}{3}\mathrm{sgn}(k_{||}) \left| \frac{k_{||} c_s}{\omega_{Ti}} \right|^{1/3} \frac{k_y}{c_s} \frac{cT_{i||}}{eB} \frac{dv_{||}}{dx} \left(-\frac{\sigma}{2} + i\frac{\sqrt{3}}{2} \right) \tag{9.26}$$

Following Eq. (9.14), the correction to the growth rate yields a contribution to the momentum flux of

$$\Gamma_{1v} = -\frac{1}{2} m_i n k_y \frac{cT_e}{eB} \left| \frac{e\hat{\Phi}}{T_e} \right|^2 \frac{\sqrt{3}}{6} \frac{k_y}{|k_{||}|} \left| \frac{k_{||} c_s}{\omega_{Ti}} \right|^{1/3} \frac{T_{i||}}{T_e} \rho_s \frac{dv_{||}}{dx} \tag{9.27}$$

As mentioned above, this results in diffusive transport and is independent of the sign of both k_y and $k_{||}$.

We proceed to evaluate the electron dynamics and obtain an expression for the parameter A. Although the parameter A will in general include a frequency depen-

dence, we set $\bar{\omega} \simeq \omega_0$ as A is expected to be a small parameter. We consider a collisional regime for the electrons, $\bar{\omega} \leq k_{\|}^2 v_{the}^2/\nu_e$ where ν_e is the electron collision frequency, and examine modes which are subthermal compared to the electron velocity. Alternatively, we could consider kinetic effects which also contribute to the phase shift between the perturbed density and electric potential. Any model leading to inwards particle transport, however, will result in the fundamental result of directed momentum transport. In the force balance equation the electrons can then be approximated as massless, yielding

$$\frac{\hat{n}}{n} \simeq \frac{e\hat{\Phi}}{T_e} - (1+\alpha_T)\frac{\hat{T}_e}{T_e} \tag{9.28}$$

where α_T is the thermal force coefficient. The electron energy balance equation is then[36]

$$\frac{3}{2}n\left(\frac{\partial}{\partial t} + \vec{v}\cdot\nabla\right)T_e - T_e\left(\frac{\partial}{\partial t} + \vec{v}\cdot\nabla\right)n = q_e = \nabla_{\|}\left(\hat{\chi}_e \frac{nT_e}{m_e\nu_e}\nabla_{\|}T_e\right)$$

where $\hat{\chi}_e$ is the thermal conductivity coefficient. Here we have set $N = 3$ for the electrons because collisions alter perpendicular as well as parallel energy. The resulting perturbed equation yields

$$\frac{\hat{T}_e}{T_e} = \frac{-i}{\omega_\chi - 3i\bar{\omega}/2}\left[\omega_{*e}\left(\frac{3}{2}\eta_e - 1\right)\frac{e\hat{\Phi}}{T_e} + \bar{\omega}\frac{\hat{n}}{n}\right] \tag{9.29}$$

where

$$\omega_\chi \equiv \hat{\chi}_e \frac{k_{\|}^2 T_e}{m_e\nu_e}$$

and

$$\eta_e \equiv \frac{n}{T_e}\frac{dT_e/dx}{dn/dx}.$$

Using $|\bar{\omega}|^2 \ll \omega_\chi^2$, we find that

$$\frac{\hat{n}}{n} \simeq \frac{e\hat{\Phi}}{T_e}\left[1 + i\frac{1+\alpha_T}{\omega_\chi}\left(\bar{\omega} - \omega_{*e} + \frac{3}{2}\eta_e\omega_{*e}\right)\right]$$

so that

$$A \simeq i\frac{1+\alpha_T}{\omega_\chi}\left[\bar{\omega} + \left(\frac{3}{2}\eta_e - 1\right)\omega_{*e}\right] \tag{9.30}$$

Note that only the second term is odd in k_y, so in Eq. (9.25) the only contribution which does not cancel out with modes having the opposite sign of k_y is

$$\begin{aligned}\Gamma_{nA} &= -\frac{1}{2}nk_y\frac{cT_e}{eB}\left|\frac{e\hat{\Phi}}{T_e}\right|^2\frac{1+\alpha_T}{\omega_\chi}\left(\frac{3}{2}\eta_e - 1\right)\omega_{*e} \\ &= -\frac{1}{2}nk_y\frac{cT_e}{eB}\left|\frac{e\hat{\Phi}}{T_e}\right|^2\frac{k_y}{|k_\parallel|}\frac{1+\alpha_T}{\hat{\chi}_e}\frac{\nu_e}{|\Omega_e|}\frac{1}{|k_\parallel|}\left(-\frac{3}{2T_e}\frac{dT_e}{dx} + \frac{1}{n}\frac{dn}{dx}\right)\end{aligned}$$

Typically $dT_e/dx < 0$ and $\eta_e \geq 2/3$ so the particle transport is inwards and the momentum transport goes like $-v_\parallel$.

The combination of these two transport terms is

$$\begin{aligned}\Gamma_{1v} + m_i v_\parallel \Gamma_{nA} &= -\frac{1}{2}m_i n\frac{k_y^2}{|k_\parallel|}\frac{cT_e}{eB}\left|\frac{e\hat{\Phi}}{T_e}\right|^2\left[\frac{\sqrt{3}}{6}\frac{T_{i\parallel}}{T_e}\left|\frac{k_\parallel c_s}{\omega_{Ti}}\right|^{1/3}\rho_s\frac{dv_\parallel}{dx}\right. \\ &\qquad \left. + v_\parallel\frac{1+\alpha_T}{\hat{\chi}_e}\frac{\nu_e}{|\Omega_e|}\frac{1}{|k_\parallel|}\left(-\frac{3}{2T_e}\frac{dT_e}{dx} + \frac{1}{n}\frac{dn}{dx}\right)\right]\end{aligned}$$

We note that the second term arose by using electron-electron collisions as a heuristic model for the physical processes leading to particle transport. In the regimes typical of the plasma core for current experiments on ICRF heating, kinetic effects are expected to be the dominant effect. In addition, this model presents difficulties in the context of experiments which observe plasmas in the H-mode regime to have an extremely flat density profile. It is possible, for example, that the inward particle flux which carries in angular momentum is associated through mass conservation with the rise in core density that results from improved confinement, without there being a peaked density profile. However, in this case the velocity profile would tend to flatten out after the core density saturates, which in some experiments occurs soon after the ICRF power is set to a maximum. We conclude that other processes such as toroidal effects may be responsible for the concentration of angular momentum at the plasma core.

9.4 Experimental considerations

Consideration of flows driven by diamagnetic effects is important for a proper interpretation of the experiments because the velocities are measured for impurity ions which are not affected by diamagnetic drifts as significantly as are the main ion species. Effects of ICRF on particle orbits have also been proposed as a mechanism for the onset of toroidal rotation, an effect which is related to the changes in particle magnetic moment induced by ICRF.

The force balance condition for each ion species relates the fluid velocities to diamagnetic effects through the radial electric field, which must have a consistent value for each species. The force balance equation is[32]

$$E_r = \nabla p_s / n_s e Z_s + v_{s\zeta} B_\vartheta - v_{s\vartheta} B_\zeta \tag{9.31}$$

where s is the ion species, p_s is the pressure, and $\vec{v}_s$ is the fluid velocity. The observed poloidal velocities are below the threshold for observation and yield a negligible contribution to the radial electric field. For the impurities, the diamagnetic contribution to the radial electric field is small because of the large value of Z_s. Thus, the toroidal fluid velocity of the main ion species is expected to be related to the experimentally observed velocity of the impurities by

$$v_{i\zeta} \simeq v_{I\zeta} + v_i^{\text{dia}} \tag{9.32}$$

where

$$v_i^{\text{dia}} = -\frac{1}{neB_\vartheta}\frac{dp_i}{dr}$$

is the diamagnetic velocity. This represents an increase in velocity in the direction of the plasma current. For experiments on the Alcator C-Mod machine, the impurities measured are argon ions and the diamagnetic flows suggest that the deuterium ions rotate about 50% faster than the argon ions. Fig. 9-4 shows the contribution to the radial electric field, and thus to the toroidal ion flow velocity, from the argon impurities term and the pressure gradient term. In Fig. 9-5 experimental observations

of the generation of toroidal flows during ICRF are shown.

Similar experiments have been performed on the JET machine[31], with observations of induced rotation in the direction of the plasma current. The radial profile of the velocities was not measured, however a line average of the fluid flow 20-30 cm below the magnetic axis indicated a toroidal velocity of up to 50 km/s. During ICRF and while H-mode confinement was maintained, the toroidal flow of the plasma was observed to accelerate at a uniform rate of 15 km/s^2. The plasma parameters for these experiments were $a \simeq 0.95$ m, $R_0 \simeq 2.95$ m, $B_0 \simeq 2.8$ T, $I \simeq 3$ MA and $Z_{eff} \simeq 2.5$.

Experimental results are shown in Fig. 9-6, reproduced from Ref. [31], where up to 7 MW of ICRF power was injected into the plasma and core densities reached 3×10^{19} m^{-3}. The ICRF spectrum was symmetric in the sign of the toroidal mode number n^0, and was peaked at the values $n^0 \simeq \pm 30$. In these experiments the diamagnetic flows are significantly smaller than the observed toroidal velocity of the nickel impurities, and so within experimental errors the figure reflects the velocity of the deuterium ions. In experiments on both the Alcator C-Mod and JET machines, higher rotation rates in the direction of the plasma current are associated with improved energy confinement. The time scales for plasma spin-up and decay of toroidal rotation were in both cases comparable to the energy confinement time.

A possible additional source of angular momentum is the small but nonvanishing change in the parallel velocity of individual ions as they are heated by ICRF. This direct heating effect induces plasma rotation directed opposite to the plasma current, and may explain the observed rotation in the L-mode regime. Experiments on the Alcator C-Mod machine use ICRF at 80 MHz, which corresponds to the hydrogen cyclotron frequency and thus heating of the minority hydrogen species.

One feature of our model for induced plasma rotation is that plasma heating is not a necessary element in this mechanism. In particular, momentum is deposited in the region of localization for the contained modes and not at a mode conversion layer. The response of the contained modes to ICRF is characterized by intervals of roughly $0.3\ \Omega_i$, rather than the spacing of the cyclotron frequency harmonics. As a result,

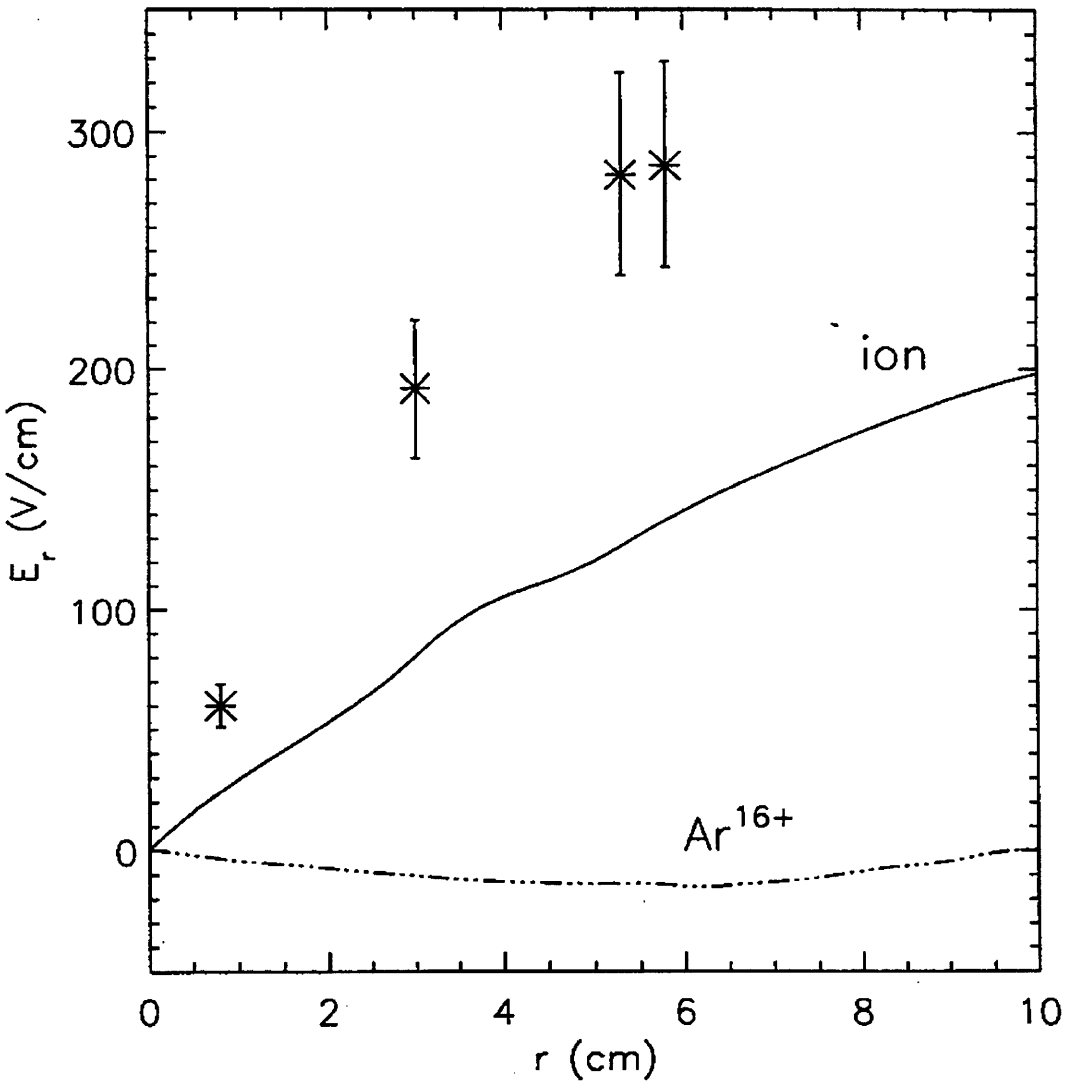

Figure 9-4: Observed contributions to the toroidal ion velocity in terms of equivalent radial electric field from experiments on the Alcator C-Mod machine. Quantities corresponding to Argon impurity velocities and diamagnetic flows for the ions are given.

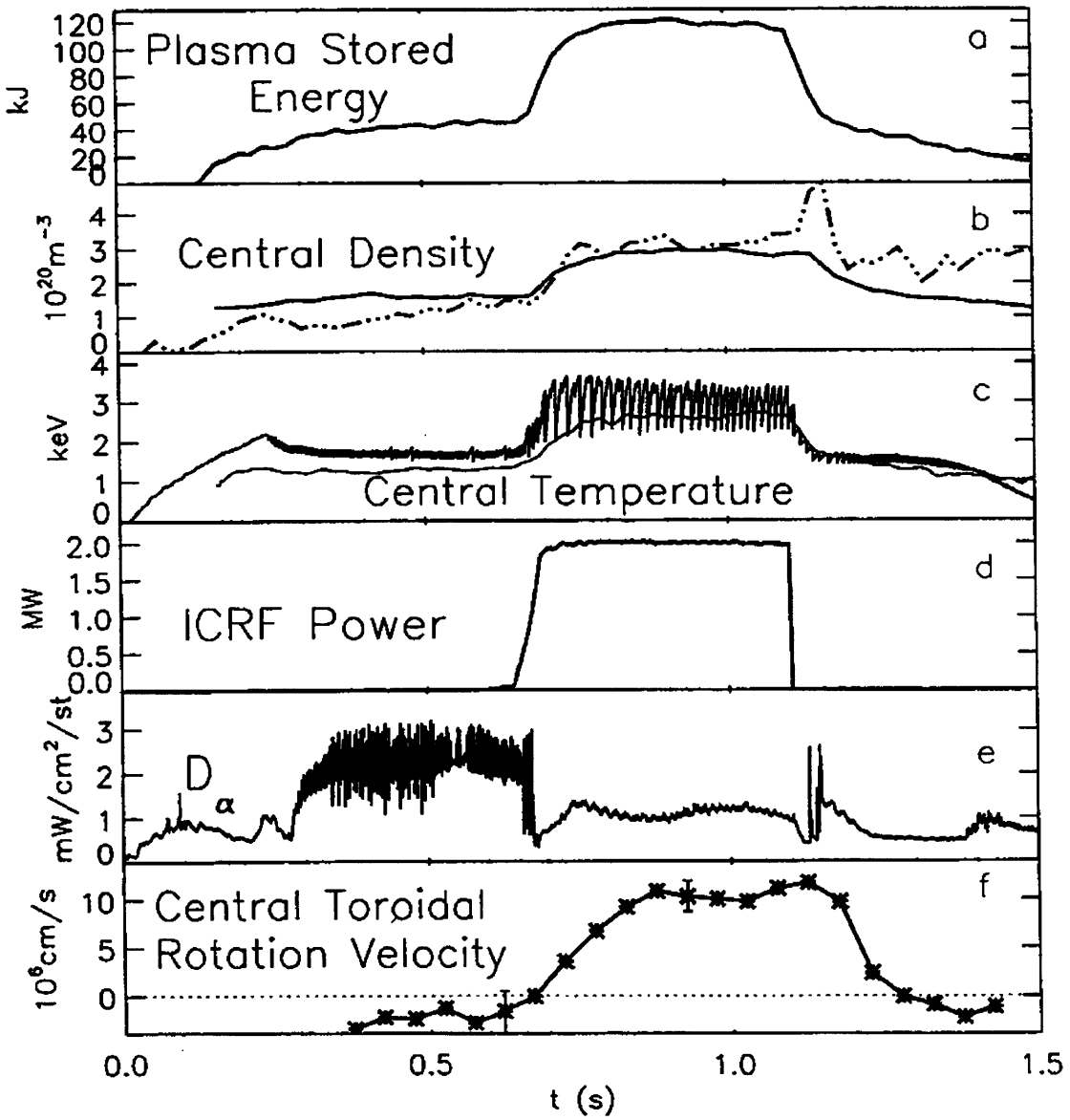

Figure 9-5: Experimental observations of the generation of toroidal flows during ICRF on Alcator C-Mod.

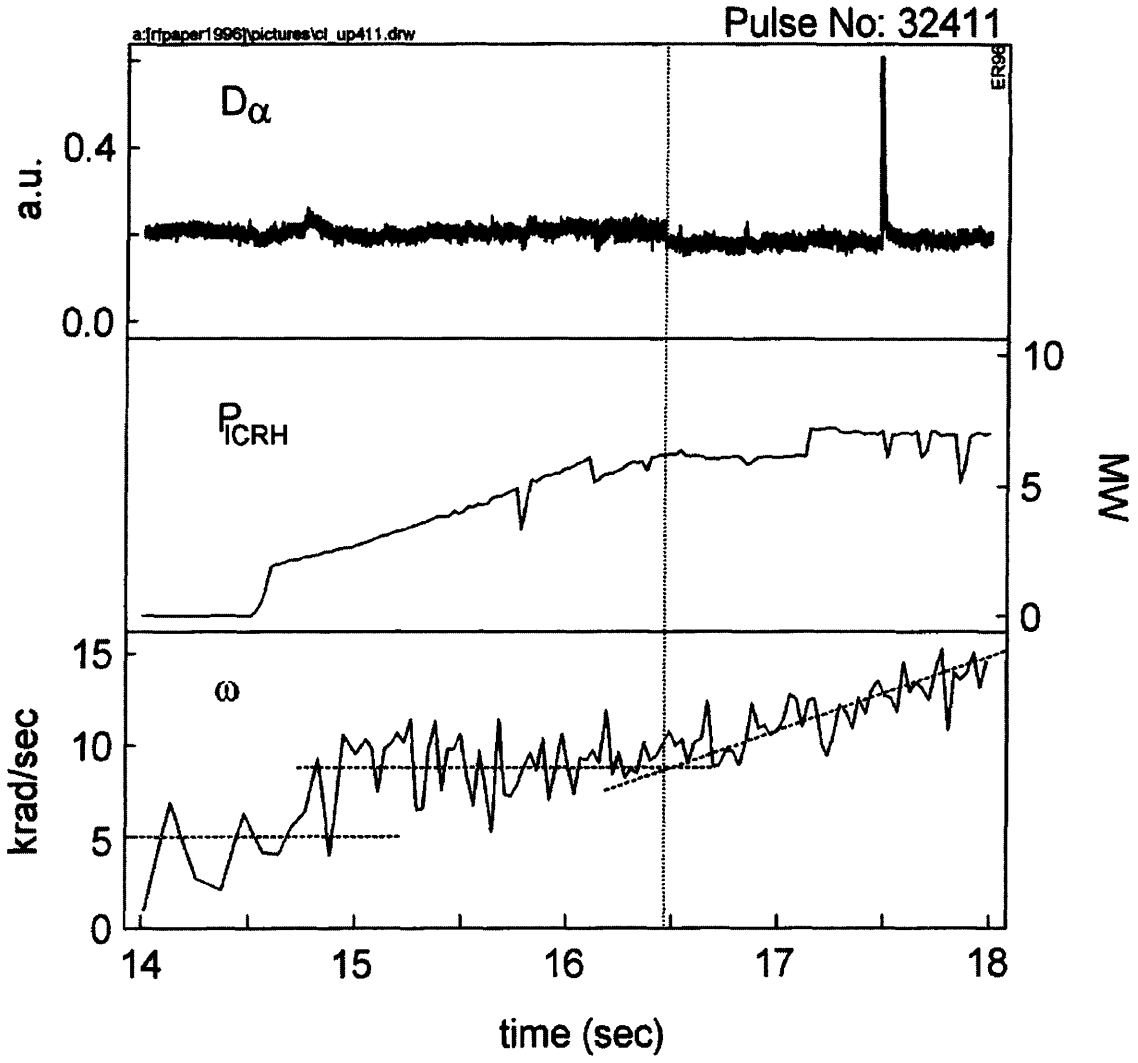

Figure 9-6: Time evolution of plasma rotation during ICRF heating on the JET machine, for pulse number 32411. After ICRF input reaches a maximum, the plasma undergoes a constant toroidal acceleration in the direction of the plasma current.

plasma rotation should be observed even when the ICRF is not tuned to a cyclotron resonance. However, the strong confinement regimes in which angular momentum deposition can overcome diffusive losses may be difficult to achieve without the aid of efficient ICRF heating. In addition, for plasmas with a tight aspect ratio, frequencies significantly above the ion cyclotron frequency typically correspond to a harmonic of the cyclotron frequency somewhere within the plasma. Measurements of the plasma response to ICRF requires that some of the heating antennas be reserved for use as passive detectors, which presents difficulties in the attempt to detect resonances with contained modes during ICRF heating at full power.

Another possible signature of the importance of contained modes in the generation of plasma rotation is that significant production of torque would require that much of the energy be deposited in the contained modes, which lie in the outer region of the plasma. This could lead to a change in the temperature profile. In addition, the unconfined magnetosonic-whistler type of modes would be reflected in increased activity in edge modes or in external modes. These modes would carry a net angular momentum in the direction opposite to the toroidal rotation.

9.5 ICRF heating and mode conversion

Antennas operating at the ion cyclotron range of frequencies (ICRF) excite magnetosonic modes within the plasma. One method for using these modes to heat an inhomogeneous plasma is to tune the frequency so that there is a mode conversion layer in which the injected energy is funneled into ion Bernstein waves (IBW). The IBW then damps against the electrons because $\omega/k_{||}v_{\mathrm{the}}$ is of order unity[37]. The mode conversion layer is characterized by special values of the plasma parameters such that distinct types of modes have the identical frequencies and wave numbers, but different plasma dynamics.

Typically, the mode conversion layer is found near the resonance for the incoming mode and the cutoff for the outgoing mode[38]. For example, in the case of fast magnetosonic waves in a two ion species plasma, there is a resonance at the ion-ion

hybrid frequency, given in high density plasmas by[39]

$$\Omega_{iI}^2 \simeq \Omega_i \Omega_I \frac{x_i \Omega_I + x_I \Omega_i}{x_i \Omega_i + x_I \Omega_I} \tag{9.33}$$

where x_i and x_I are the relative concentrations of the two ion species. This is approximately the cutoff of the IBW when $k_\perp^2 \rho_i^2 \ll 1$. For a given frequency, the value of the equilibrium magnetic field at which this resonance occurs is typically close to the cutoff value for fast waves. The mode conversion layer thus occurs in a region containing a decaying mode solution to the fast wave. However, the two layers are close enough so that a significant amount of the wave energy is converted into IBW, although there is also some reflection and transmission of the fast wave. This mechanism for mode conversion is characterized by rapid changes in the wave vector as a function of major radius, dominated by the $|k_\perp| \to \infty$ resonance of the fast wave.

Another model for mode conversion is an adiabatic process in which, because of changes in the plasma parameters, the mode gradually changes its dynamics until its physical characteristics are quite different than its original form. These schemes, while of some practical and theoretical interest, have not been developed into heating schemes for toroidal plasmas.

In addition to mode conversion, injected energy can change its form through nonlinear mode coupling, in which a single wave couples to a combination of waves of different types. The selection rule for mode coupling is that the sum of the frequencies and the sum of the wave vectors must vanish in the region in which coupling takes place. For a toroidal geometry with a plasma having a large aspect ratio, so that normal modes can be described as having a single poloidal mode number m, this requires that the poloidal and toroidal mode numbers m and n^0 sum to zero.

In Alcator C-Mode, ICRF heating uses mode conversion of fast magnetosonic waves into IBW to heat the plasma[37]. The location of the mode conversion layer depends on the frequency of the waves launched by the antennas, the magnetic field strength, and the components of the plasma. For a hydrogen plasma with ^{3}He impurities, mode conversion occurs close to $R = R_0$, where R is the major radius of the

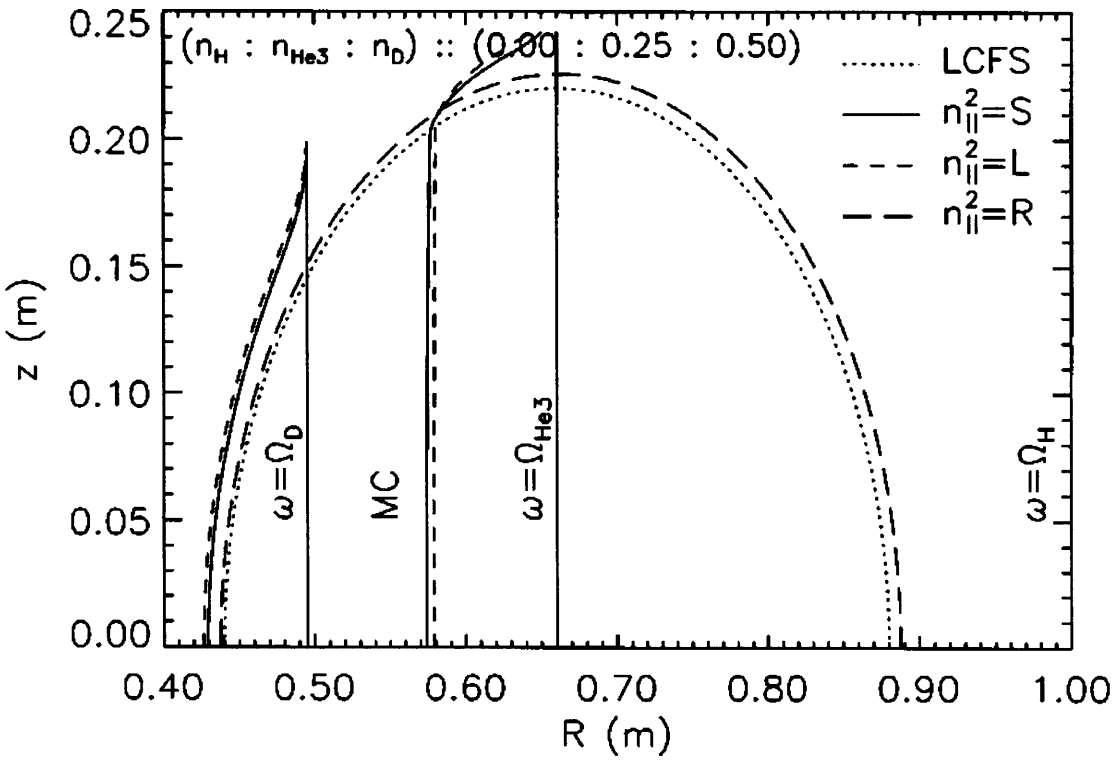

Figure 9-7: Resonances, cutoffs, and mode conversion layer for ICRF waves for a D(^{3}He) plasma on the Alcator C-Mod experiment.

plasma and R_0 passes through the magnetic axis. Most of the heating is found to occur near the plasma of the center, predominantly in the region $r \leq 0.3\ a$, where a is the minor radius of the plasma column. This configuration is expected to be similar to that of a deuterium-tritium plasma because the ratio of the cyclotron frequencies is the same in both cases. Heating off-axis was observed in deuterium plasmas with ^{3}He impurities, where the mode conversion layer is shifted towards the high-field side of the plasma column. Over half of the energy from ICRF was found to be deposited into the electrons, and modelling indicated that over one third of the injected energy was absorbed by electrons after mode conversion to IBW. The various resonances and cutoffs for this case are shown in Fig. 9-7, taken from Ref. [37].

In ICRF experiments on Alcator C-Mod, the antenna has a height h of approximately 0.25 m and is located at $R_{\rm ANT} \simeq 0.92$ m. The magnetic axis is located at $R_0 \simeq 0.66$ m, so $r_{\rm ANT} \simeq 0.26$ is about 4 cm beyond the edge of the plasma. The

characteristic poloidal mode number is given by $\pi/2 \sim |m|\vartheta_{\rm ANT} \simeq |m|h/r_{\rm ANT} \simeq |m|$. This implies that the most significant poloidal components are $m = \pm 2$. For balanced inputs, the antennas are phased so that the spectrum is symmetric about $n^0 = 0$. Because of the geometry and phasing of the antennas, the toroidal spectrum is peaked about $n^0 = \pm 10$, with a standard deviation of approximately 3. At $n^0 = 0$ the spectrum vanishes exactly because there is no net loop voltage induced by the antennas.

The processes through which the fast waves generated by ICRF might excite contained modes, and the similar magnetosonic waves which are not confined, are still not well characterized. In particular, the differences in mode numbers present difficulties in explaining the direct conversion of fast waves into contained modes. The contained modes at 80 MHz $\simeq 5 \times 10^8$ rad/s have $m \simeq 6$, and for small $k_{||}$, implying that $m \simeq n^0 q(r)$, the modes should have $n^0 \simeq 3$. From Eq. (4.34), noting that $\Delta \propto |m|^{-1/2}$, we find that the inverse scale length for the radial mode structure is $1/\Delta \simeq 5/a$. This is consistent with the large m expansion for the mode frequency in Chapter 4 in the limit $k_{||} \to 0$,

$$|\omega| \simeq \omega_0 + \delta\omega_{0s},$$

where ω_0 and $\delta\omega_{0s}$ are given by Eqs. (4.32) and (4.35); ω_0 is proportional to $|m|$ and $\delta\omega_{0s}$ is proportional to $1 + 2s$, where s, a non-negative integer, is the radial eigennumber. We note that in this section the mode frequency is no longer assumed to be positive. We can use the mode equations for the limit $k_{||} \to 0$ because at such low harmonics the mode frequency and radial width depend very weakly on $k_{||}$. This approximation for the frequency can be rewritten as

$$\omega^2 \simeq \left(k_\perp^2 + \frac{1+2s}{\Delta^2}\right)\tilde{v}_A^2, \tag{9.34}$$

where $\tilde{v}_A$ is slightly modified from the true Alfvén velocity at the radius r_0 because of the Hall term in the effective potential. The fast waves, on the other hand, have $m \simeq \pm 2$ and $n^0 \simeq \pm 10$. The inverse radial scale lenght of these fast waves change rapidly as they propagate inwards. Taking the dispersion relation to be analogous to

Eq. (9.34), where ω^2 has separate contributions from $k_\perp^2$ and from the radial variation, we estimate for a frequency of 80 MHz that at $r = r_0$ the radial inverse scale length is of the order of $10/a$.

9.5.1 Linear mode conversion

The simplest possibility for exciting contained modes is a direct conversion of the injected fast wave energy to the contained modes having a comparable frequency. This requires that the contained modes have the same toroidal mode numbers as the injected fast waves. For a cylindrical plasma the poloidal mode numbers would also have to be the same. Whereas the ICRF inputs have $|m|$ close to 2, the contained modes at 80 MHz have m close to 6. However, due to the toroidicity of the plasma, the difference in the poloidal mode number between the ICRF inputs and the contained modes can be bridged through linear coupling of poloidal harmonics, both for the injected fast waves and the contained modes. Thus, the two contained modes which are most likely to be excited by the fast waves in this picture have $m = 6$ and $n^0 = \pm 10$. If both In addition, the rapid radial variation of the fast waves may enhance the linear coupling to larger poloidal harmonics through the geometry of the plasma. As the toroidal mode numbers should remain unchanged from the ICRF inputs at $n^0 \simeq \pm 10$, we must consider contained modes having significant propagation parallel to the equilibrium magnetic field.

If both of these modes were driven equally, there would be no net torque on the plasma as the angular momentum of these modes are equal and opposite. Thus, any torque on the plasma must be a result of the difference in parallel propagation of these two modes. In particular, taking $q(r_0) \simeq 2$ and $r_0/R_0 q(r_0) \simeq 0.13$, the mode moving in the direction of the plasma current, which has $n^0/\omega > 0$, is characterized by $k_\parallel/k_\perp \simeq -0.3$, while the mode moving in the counter-current direction has $k_\parallel/k_\perp \simeq 0.55$. In fact, the mode moving in the counter-current direction has an even larger parallel wave vector than the original fast wave. The corresponding angles that the wave vectors make with the equilibrium magnetic field are roughly 75 and 60 degrees, respectively. The wave equation which led to contained mode solutions was

predicated on the assumption that $k_{\|}^2 \ll k_{\perp}^2$, in other words that the angle of the wave vector with the equilibrium magnetic field is close to 90 degrees. For the modes propagating in the counter-current direction this is not a good approximation. Thus, it is reasonable to consider the possibility that the contained modes moving in the co-current direction receive significant pumping from the ICRF-induced fast waves at the same time that the counter-current modes are not radially confined and instead convect out of the plasma. Alternatively, the counter-current contained modes may be too strongly damped by the ions. One advantage to this model is that n^0 is much larger than $m/q(r_0) \simeq 3$, which corresponds to modes with near-zero $k_{\|}$. Since the angular momentum carried by the contained modes for a fixed energy is proportional to n^0, the expected rotation which can be driven by this process is more than three times larger than the generic estimate of Section 9.2 for modes which propagate nearly perpendicular to the equilibrium magnetic field.

9.5.2 Nonlinear mode coupling

Given the likelihood that the linear excitation of contained modes by ICRF will not prove to be an efficient mechanism, then we must in turn consider nonlinear mode coupling. By this process, fast waves driven by ICRF would couple into two modes, at least one of which would be the contained mode. We first consider the possibility that the fast waves branch into two contained modes, or one contained mode and the analogous unconfined mode, at least one of which has a frequency larger than 80 MHz. The poloidal mode numbers much also be larger than the typical fast wave values, which have $|m| = 2$ or 3. Thus the summation rule for nonlinear coupling, that the frequencies and wave vectors must both add to zero, requires that the two resultant modes, which we denote as mode 1 and mode 2, must have frequencies of opposite signs, as well as poloidal mode numbers of opposite signs. Thus,

$$\begin{aligned} \omega + \omega_1 + \omega_2 &= 0 \\ m + m_1 + m_2 &= 0 \end{aligned}$$

$$n^0 + n_1^0 + n_2^0 \;=\; 0 \tag{9.35}$$

However, this implies that the poloidal phase velocities $-r\omega_1/m_1$ and $-r\omega_2/m_2$ must have the same sign. Thus, either the fast wave couples to two contained modes, or to two of the unconfined magnetosonic waves.

We recall that 80 MHz corresponds to the second harmonic of the deuterium cyclotron frequency. For parameters typical of experiments on Alcator C-Mod, the frequency of the contained modes is roughly $|\omega| \simeq \omega_0 + \delta\omega_{0s}$ where, as determined by Eqs. (4.32) and (4.35),

$$\omega_0 \simeq \frac{|m|\Omega_D}{3.6}, \qquad \delta\omega_{0s} \simeq 0.3\ (1+2s)\Omega_D, \tag{9.36}$$

and s is the radial eigennumber, which is a non-negative integer. Thus modes with a frequency difference of $2\Omega_D$ should have a difference in poloidal mode numbers of roughly 7, and not 2 or 3 as required if they are to couple to the ICRF-driven modes. However, if we consider modes with different radial eigenfunctions, part of the difference in frequency can be accounted for by the factor $\delta\omega_{0s} \propto 1 + 2s$ rather than by differences in poloidal mode number. We can use the above approximation to the dispersion relation and selection criteria for mode coupling to find required combinations of modes. For example, taking $m = 3$ for the fast waves, we have

$$\begin{aligned} 3 &= |m| = |m_2| - |m_1| \\ |\omega_1| &\simeq \frac{|m_1|}{3.6}\Omega + 0.3\ (1+2s_1)\Omega \\ |\omega_2| &\simeq \frac{|m_2|}{3.6}\Omega + 0.3\ (1+2s_2)\Omega \end{aligned} \tag{9.37}$$

For consistency we must also have

$$\begin{aligned} 2\Omega &\simeq |\omega| = |\omega_2| - |\omega_1| \\ &\simeq \frac{|m_2| - |m_1|}{3.6}\Omega + 0.6\ (s_2 - s_1)\Omega \\ &\simeq 0.8\ \Omega + 0.6\ (s_2 - s_1)\Omega \end{aligned} \tag{9.38}$$

This implies that $s_2 - s_1 = 2$ is a good candidate for effective mode coupling. One set of possibilities for non-linear coupling to contained modes is

$$\begin{array}{llll} \omega \simeq 2\Omega_D, & m = 3, & n^0 = 10 & \\ \omega_1 \simeq 3\Omega_D, & m_1 = 10, & n_1^0 = 1, & s_1 = 0 \\ \omega_2 \simeq -5\Omega_D, & m_2 = -13, & n_2^0 = -11, & s_2 = 2. \end{array} \tag{9.39}$$

A similar coupling scheme would drive unconfined magnetosonic waves, which could be carried out of the plasma without reaching the mode conversion layer.

Another possibility is that the second mode which couples to the ICRF-induced fast waves is not a magnetosonic type of wave at all, which we label as X for "unknown". As an example, in order to couple fast waves with $\omega \simeq -2\Omega_D$, $m = -2$, and $n^0 = -10$, to the contained mode similar to mode 1 as above but having purely perpendicular propagation, we find the properties of mode X by

$$\begin{array}{llll} \omega \simeq -2\Omega_D, & m = -2, & n^0 = -10 & \\ \omega_1 \simeq 3\Omega_D, & m_1 = 10, & n_1^0 = 5 & s_1 = 0 \\ \omega_X \simeq -\Omega_D, & m_X = -8, & n_X^0 = 5. & \end{array} \tag{9.40}$$

This mode carries all of the original wave vector component parallel to the equilibrium magnetic field, but still has a much larger perpendicular propagation than parallel propagation. Although the ratio of the rate of energy deposition into these two modes is undetermined, the energy which is converted into mode X could also experience nonlinear coupling into another mode of a similar type and a contained mode. Such a cascading effect would eventually carry most of the energy into contained modes irregardless of the branching ratios of individual coupling processes. We note that the overall fraction of energy which can reasonably be drawn from the ICRF antennas is difficult to determine with any precision. The two cases above are sketched in Fig. 9-8. The component of propagation parallel to the equilibrium magnetic field of a fast wave induced by ICRF must be balanced by the combination of the two modes with which the fast wave couples. In the first case, both contained modes have roughly

negative one-half of the parallel wave vector of the initial wave, whereas in the second case the contained mode propagates perpendicular to the equilibrium magnetic field and the parallel wave vector is completely cancelled by mode X.

Finally, in the special case of off-axis heating where mode conversion to IBW occurs in the outer regions of the plasma, some of the IBW wave energy may be converted into contained modes before being absorbed by the electrons. An advantage to this model is that ion Bernstein waves typically have large poloidal mode numbers. However, this only applies in the heating scheme used for D(^{3}He) plasmas.

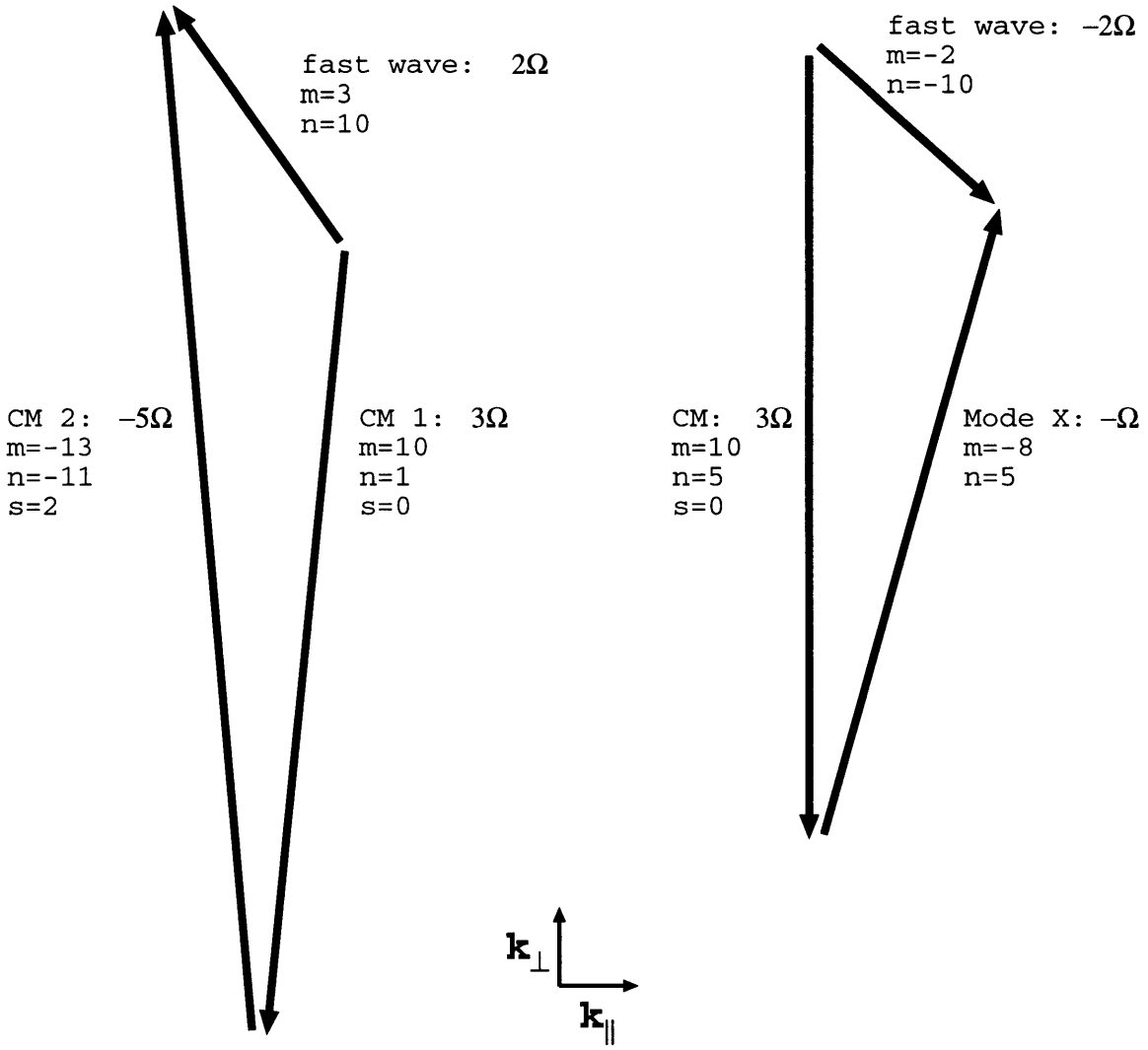

Figure 9-8: Examples of nonlinear mode coupling from fast waves to two contained modes (left) or to one contained mode and a second wave of a different type (right). The vectors correspond to the wave vectors in the $\hat{e}_{||}$–$\hat{e}_{\perp}$ plane, where $\hat{e}_{\perp} \simeq \hat{e}_{\vartheta}$. The radial variation of the modes are not indicated in this figure. For clarity and following convention, the arrow for the incident fast wave is shown reversed relative to the two outgoing waves to which it couples, so that the two vectors representing outgoing waves add up to the vector for the incident wave. Here, we take $r/R_0 \simeq 0.25$ and $q(r) \simeq 2$.

Chapter 10

Conclusions

Plasmas under fusion burn conditions are characterized by the presence of a considerable population of high energy particles produced by the fusion reactions. These particles can significantly affect the plasma behavior through their interactions with the background thermal particles, both by collisions and by collective modes. The main distinguishing feature of the fusion products is their high energy, even compared to injected particle beams. Ion velocities may be greater than electron thermal velocities, and experimental configurations which adequately confine background ions may not strongly confine fusion products. In particular, fusion products are susceptible to much larger radial excursions and even losses out of the plasma than the background plasma. Because of these effects and the non-thermal distribution of fusion products, these energetic ions exhibit qualitatively different behavior from that of energetic ions in non-fusing plasmas. For example, the distribution function in velocity space of energetic ions from neutral beam injection (NBI) does not have the strong anisotropy and dependence on position within the plasma which is found for fusion products.

To analyze these effects, we first consider the production of α-particles from fusion and their single particle motion. The distribution function of fusion products results from the combination of these dynamic effects. We model the α-particle distribution function under the hypothesis that the mode growth time is shorter than the alpha-particle slowing down time due to electron collisions. The effect of collisions can then be treated as a perturbation to the particles orbits. From physical considerations and

numerical calculations, a simplified model is obtained for the distribution function in the outer region of the plasma, where the local fusion reaction rate is low.

The process of electron cyclotron emission is well known for both astrophysical and laboratory plasmas. Recent experimental results have shown a new feature, that there can be enhanced radiation emission over a range of harmonics of the cyclotron frequency of the particles produced by fusion reactions. This emission can be attributed to the interaction of these high-energy particles with collective modes.

We have identified a class of modes, herein referred to as the "contained" modes, which propagate nearly perpendicular to the equilibrium magnetic field and have a considerable poloidal mode number m. These modes are localized within a relatively narrow radial layer towards the outer regions of the plasma and can be excited by resonant interactions with fusion products. We have studied such characteristics as the localization point of the mode, the radial width, the direction of propagation, the relevant mode-particle interaction and the induced growth rates. At frequencies significantly higher than the ion cyclotron frequency, the localization of the mode is found to vary significantly with the component of propagation parallel to the equilibrium magnetic field.

On the basis of these properties we argue that these modes can be responsible for the observed spectrum of enhanced radiation emission. In particular, the fact that contained modes are radially confined and thus do not convect out of the plasma makes this class of modes a good candidate for absorbing significant power from the fusion products. Furthermore, the contained modes can convey information about the distribution of fusion products. This is related to the fact that as the poloidal mode number increases, mode solutions can be found which are localized further within the plasma column. At sufficiently high frequencies, radial eigenmodes can be found which are centered close to $r = a/2$, where a is the minor radius of the plasma column. Thus the lower frequency spectrum can be interpreted as yielding information exclusively about a subset of energetic particle with the largest radial excursion, while the higher frequency spectrum can be related to a broader class of energetic particles.

An understanding of this phenomenon suggests the possibility of influencing α-particle transport through coupling with externally applied modes having frequencies in the range we have considered. The α-particle distribution and perpendicular energy may be manipulated through appropriately chosen injected waves. Moreover, modes of this kind can serve the purpose of transferring energy from the fusion products to the reacting nuclei, thus bypassing the need to deposit the energy first on the electrons and then to the fusing nuclei through collisional processes.

Referring to a toroidal configuration, the properties of the contained mode are discussed in the limit of large poloidal number m. For a given pair of poloidal and toroidal mode numbers m and n^0, there exists a single radius about which the mode is localized. We have shown that for frequencies of the order of or above the ion cyclotron frequency, the Hall term in Ohm's law plays a crucial role in determining the nature of the mode solutions. The significance of this term is characterized by the quantity $d_{i0}/a = c/a\omega_{pi}$ evaluated at the center of the plasma, where a is the minor radius of the plasma, ω_{pi} is the plasma frequency and c is the speed of light. The minimum m for which frequencies are comparable to the ion cyclotron frequency is of the order of a/d_{i0}. This quantity times $R_0 q/a$, where q is the inverse rotational transform of the magnetic field, also gives an estimate of the value of m for which the parallel propagation can significantly affect the mode solution within the limit $|k_{||}/k_{\perp}| \ll 1$, where $k_{||}$ and $k_{\perp}$ are the components of the wave vector parallel and perpendicular to the equilibrium magnetic field, respectively. In addition, the quantity d_{i0}/a together with the density profile determines the radius of localization of the mode.

To summarize the behavior of the contained mode, the mode eigenfunctions approximate the solutions for a harmonic oscillator, and are characterized by a poloidal mode number m, a toroidal mode number n^0 and in addition a radial eigennumber s that corresponds to the number of nodes in the radial eigenfunction and gives a first order correction in $1/m$ to the frequency. We find that for a fixed value of m the frequency is minimized at n^0 such that $k_{||} = 0$, and in this limit the flux surface around which the mode is localized approaches a fixed radius r_0, that depends on the density profile and lies towards the edge of the plasma column. In particular,

more peaked density profiles result in localization points further to the interior of the plasma. The width of the mode scales as $m^{-1/2}$.

Since the Hall effect breaks the symmetry in the poloidal direction we find that even when $k_{||}$ is set to zero, the localization point changes with the sign of the poloidal phase velocity. In particular, for a given density profile and restricting our attention to positive frequencies, we can define a critical value that we denote by d_i^{crit} such that for $d_{i0} > d_i^{\text{crit}}$ contained solutions only exist for $m > 0$, while below we have solutions for both $m > 0$ and $m < 0$. When solutions only exist for one sign of m, this corresponds to a poloidal phase velocity in the ion cyclotron direction relative to the toroidal magnetic field. The value of d_i^{crit} is roughly the same for a broad class of typical density profiles. In the limit of nearly perpendicular propagation, $k_{||} = 0$, the mode is localized about a fixed radius r_0. By studying influence of finite propagation parallel to the equilibrium magnetic field, we find that the radius about which the mode is localized deviates from the $k_{||} \to 0$ limit by an amount proportional to $k_{||}$ for small values of $k_{||}$, such that

$$k_{||}^2 B^2 \ll k_{\perp}^2 B_{\vartheta}^2.$$

This is equivalent to the condition $|1 - n^0 q/m| \ll 1$. The shifting of the mode layer saturates for larger values of $k_{||}$. We have found analytical expressions for the eigenfunctions and frequencies which depend on plasma parameters and the density profile. For large m, we have found very good agreement between these analytical calculations and numerical results.

The enhanced radiation emission above the ion cyclotron frequency observed on the JET machine in experiments with fusing plasmas is found to correlate strongly with the fusion reaction rate. This leads us to consider the interaction of α-particles with the contained mode at resonances of the cyclotron frequency Ω_α. The magnetic field varies roughly in inverse proportion to the distance R from the symmetry axis, so that the resonance condition is roughly $\omega \simeq \ell\Omega_\alpha(R)$, where R is partially determined by the mode localization and ℓ is the harmonic number. This suggests that the transition to a continuum spectrum as experimentally observed, which occurs around

7 Ω_α in Fig. 6-1, is caused by the change in location of the mode-particle interactions, in part dictated by the shift in localization of the mode as described above.

We find that the particles that can interact with the contained mode are trapped particles with large radial excursions in their orbits; the distribution of these particles is strongly anisotropic in velocity space, and is weighted towards the outermost edge. This correlates with the experimental observation that the emission peaks are measured at multiples of the cyclotron frequency corresponding to the magnetic field strength at the outer edge[1, 2, 3]. The poloidal extent of the region of interaction between the energetic particles and the contained modes is determined by the distribution function which is concentrated at the outermost edge of the plasma column, as modelled by the maximum poloidal angle ϑ_{cr}. The radial extent of this region is delimited by the range of mode localizations allowed by the mode equation. Mode-particle resonances can lead to the instability of these contained modes, driven by the strong velocity-space anisotropy of the energetic particle distribution function at the mode layer.

Using a linear gyrokinetic calculation, we obtain a positive growth rate induced by the energetic particles that is linear in n_α/n_e. This calculation is performed in the "local approximation" that is valid when the growth rate is larger than the bounce frequency, because in this case separate passes of a particle through the mode layer are uncorrelated. A full calculation would involve a second integral over particle orbits of a rapidly phase related to the gyrophase. The resulting growth rate is sufficient to justify the local approximation and to maintain instability even including the various mechanisms for damping that affect the unperturbed mode, such as thermal damping. We note that for higher frequencies, there is a greater density in frequency of unstable modes, which is consistent with the observation that the emitted power in the continuum part of the spectrum is greater than that for the discrete spectrum at lower frequencies. In a configuration where the anisotropy is reduced, the growth rates decrease and some harmonics are completely stabilized, making it clear that the anisotropy drives the mode unstable.

The significant growth rates found for the contained modes reflect a strong in-

teraction between α-particles and the contained modes, which could potentially have significant effects on the confinement and energy deposition of energetic α-particles. In particular, these results suggest that any form of injected power used for fusing plasmas should be investigated for the possible excitation of contained modes, which could alter the deposition profile of fusion energy, and even scatter α-particles out of the plasma. Contained modes at large multiples of the cyclotron frequency exist which are positioned far from the plasma edge, with a radius of localization approaching 0.5 a. Thus, these effects can be influential not only for the fraction of *alpha*-particles whose orbits reach close to the plasma edge, but also for the bulk of α-particles which remain near the plasma core. The experimental observations of plasma rotation driven by balanced inputs at the ion cyclotron range of frequencies (ICRF), discussed below, may be an example of contained modes being driven by a technique to achieve external heating. Currently, these effects are not seriously considered when analyzing schemes which involve the injection of power into the plasma for heating the plasma or improving confinement.

We have seen that through the Hall effect, which yields an up-down asymmetry in the poloidal phase velocity for the contained mode, the twist in the equilibrium magnetic field can lead to torque being generated by wave injection at the ion cyclotron range of frequencies (ICRF) even when the inputs are balanced. Our model is that this torque leads to toroidal rotation in the direction of the plasma current as seen in experiments[31, 32]. This is in contrast to other observed manifestations of the Hall effect which induce a much slower plasma rotation aligned opposite to the plasma current. An example of this effect is energetic ion losses during NBI, for which counter-current rotation has been detected[31]. Other investigations of asymmetries in the plasma behavior rely on a similar physical picture, with the Hall effect leading to a disparity in the properties of plasma waves having opposite phase velocities. For example, the fast magnetosonic waves launched by the antennas during ICRF are found to be unbalanced despite the symmetric loading of the antennas because of an asymmetry in the coupling coefficients between the antennas and the plasma[40]. However, this effect is not sufficiently strong to be applicable to the issue of plasma

rotation observed in the experiments. Asymmetries with respect to the sign of the toroidal velocity also exist for the ion Bernstein waves generated through mode conversion at the major radius where the ion-ion hybrid frequency is in resonance with the ICRF frequency[39].

Our model was the first to consider the role of contained modes in generating plasma rotation as a mechanism for enhancing the physical consequences of the asymmetries related to the Hall effect. The plasma rotation is considered to be a result of differences in the radial evolution of comparable plasma modes having opposite toroidal phase velocities. Fast magnetosonic waves and IBW are not radially confined, and so are not suitable candidates for this type of model without an additional mechanism to prevent convection of wave energy and angular momentum out of the plasma in order to allow the modes to build up over time.

The magnitude and direction of the plasma rotation as evaluated in our model, using contained modes, is consistent with experimental results and is thus a good candidate for explaining the rotation induced by ICRF. The additional hypothesis of angular momentum transport is indicated by the rapid spin up and slowing down of plasma rotation after the onset and termination of peak ICRF power. The interpretation is that most of the angular momentum from ICRF is initially deposited in the outer regions of the plasma column, with the centrally peaked rotation profile as observed in experiments being a manifestation of profile consistency[35]. The enhanced radial transport is the result of separate collective processes within the plasma.

This interpretation is supported by the fact that the rotation velocity is correlated with plasma confinement and is not observable during poor confinement regimes such as the L-mode[32]. The presence of anomalous transport processes in the disposition of angular momentum is confirmed by the observed rate of angular momentum dissipation after ICRF is turned off. The time scale for the decay of plasma rotation is comparable to the energy confinement time. The underlying mechanism for the enhanced transport of angular momentum are still not well understood, although quasilinear calculations of ion temperature gradient driven modes indicated that these can generate diffusion of angular momentum.

Another issue considered is the required power deposited into contained modes in order to generated the observed torque on the plasma. This power is typically a fraction of the total power injected by ICRF antennas. Several processes have been proposed for the excitation of contained modes by the fast waves produced by ICRF. The relative importance of these processes is still an open problem, as is the total fraction of ICRF power which can reasonably be expected to be channeled through contained modes.

A significant feature of our model is that contained modes are internal modes of the plasma and thus can be excited to significantly larger amplitudes than unconfined waves. As discussed in reference to ion cyclotron emission, the result is stronger physical effects on the plasma dynamics which lead to enhancement of phenomena such as plasma rotation and the slowing down of energetic ions. The sharp radial localization of the modes also leads to significant changes in the dynamics of mode-particle interactions compared with interactions involving unconfined magnetosonic waves.

Bibliography

[1] JET Team. Fusion energy production from a Deuterium-Tritium plasma in the JET tokamak. *Nuclear Fusion*, 32(2):187–203, 1992.

[2] S. Cauffman and R. Majeski. Ion cyclotron emission on the Tokamak Fusion Test Reactor. *Review of Scientific Instruments*, 66(1):817–819, January 1995.

[3] G. A. Cottrell, V. P. Bhatnagar, O. Da Costa, R. O. Dendy, J. Jacquinot, K. G. McClements, D. C. McCune, M. F. F. Nave, P. Smeulders, and D. F. H. Start. Ion cyclotron emission measurements during JET Deuterium-Tritium experiments. *Nuclear Fusion*, 33(9):1365–1387, 1993.

[4] B. Coppi, G. Penn, and C. Riconda. Excitation of contained modes by high energy nuclei and correlated cyclotron emission. *Annals of Physics*, 261(2):117–162, December 1997.

[5] B. Coppi. Collective modes in igniting plasmas. In T. Tajima and M. Okamoto, editors, *Physics of high energy particles in toroidal systems*, number 311 in AIP Conference Proceedings, pages 47–62, New York, 1993. American Institute of Physics, American Institute of Physics.

[6] B. Coppi. Confinement of fusion reaction products and radiation emission induced by them. *Fusion Technology*, 25:326–329, May 1994.

[7] B. Balet and G. Cottrell. Private communication, 1997.

[8] L. Chen and S. T. Tsai. Linear oscillations in general magnetically confined plasmas. *Plasma Physics*, 25(4):349–359, 1983.

[9] X. S. Lee, J. R. Myra, and P. J. Catto. General frequency gyrokinetics. *Physics of Fluids*, 26(1):223–229, January 1983.

[10] S. Glasstone and R. Lovberg. *Controlled Thermonuclear Reactions.* D. van Nostrand Co., Princeton NJ, 1960.

[11] Ya. I. Kolesnichenko. Review paper: the role of alpha particles in tokamak reactors. *Nuclear Fusion*, 20(6):727–780, 1980.

[12] A. Nocentini, M. Tessarotto, and F. Engelmann. Neoclassical theory of collisional transport in the presence of fusion α-particles. *Nuclear Fusion*, 15:359–370, 1975.

[13] P. J. Catto. Course 22.616: Plasma Transport Theory. Class notes, Massachusetts Institute of Technology, 1994.

[14] D. Pfirsch. α-particles in tokamaks. In B. Coppi, G. G. Leotta, D. Pfirsch, R. Pozzoli, and E. Sindoni, editors, *Physics of plasmas close to thermonuclear conditions*, volume 1, pages 237–269. Commission of the European Communities, Brussels, 1980.

[15] T. E. Stringer. Radial profile of α-particle heating in a tokamak. *Plasma Physics*, 16:651–659, 1974.

[16] B. Coppi, S. Cowley, R. Kulsrud, P. Detragiache, and F. Pegoraro. High-energy components and collective modes in thermonuclear plasmas. *Physics of Fluids*, 29(12):4060–4072, December 1986.

[17] Franklin F. Chen. *Introduction to Plasma Physics and Confined Fusion*, volume 1: Plasma Physics. Plenum Press, New York and London, second edition, 1984.

[18] D. A. McPherson and D. C. Pridmore-Brown. Density gradient effects on Alfvén wave propagation in a cylindrical plasma. *Physics of Fluids*, 9(10):2033+, October 1966.

[19] G. Kamelander and Ya. I. Kolesnichenko. Localized whistler eigenmodes in tokamaks. *Physics of Plasmas*, 3(11):4102–4105, November 1996.

[20] G. Penn, C. Riconda, and F. Rubini. Description of contained mode solutions to the relevant magnetosonic-whistler wave equations. *Physics of Plasmas*, 5(7):2513–2524, July 1998.

[21] B. Coppi. Origin of radiation emission induced by fusion reaction products. *Physics Letters A*, 172(6):439–442, 1993.

[22] P. Schild, G. A. Cottrell, and R. O. Dendy. Sawtooth oscillations in ion cyclotron emission from JET. *Nuclear Fusion*, 29:834–839, 1989.

[23] D. Ernst. Private communication, 1998.

[24] N. N. Gorelenkov and C. Z. Cheng. Excitation of Alfvén cyclotron instability by charged fusion products in tokamaks. *Physics of Plasmas*, 2(6):1961–1971, June 1995.

[25] R. O. Dendy, C. N. Lashmore-Davies, K. G. McClements, and G. A. Cottrell. The excitation of obliquely propagating fast Alfvén waves at fusion ion cyclotron harmonics. *Physics of Plasmas*, 1(6):1918–1928, June 1994.

[26] T. Fulop, Ya. I. Kolesnichenko, M. Lisak, and D. Anderson. Origin of superthermal ion cyclotron emission in tokamaks. *Nuclear Fusion*, 37(9):1281–1293, 1997.

[27] Caterina Riconda. *Contained modes in inhomogeneous plasmas and their interaction with high energy particles.* PhD dissertation, Massachusetts Institute of Technology, Cambridge MA 02139, February 1997.

[28] M. N. Rosenbluth and R. F. Post. High-frequency electrostatic plasma instability inherent to "loss-cone" particle distributions. *Physics of Fluids*, 8:547–550, 1965.

[29] A. B. Mikhailovskii. Collective processes in a tokamak with high-energy particles. In M. A. Leontovich, editor, *Reviews of Plasma Physics*, volume 9, pages 103–264. Consultants Bureau, New York, 1986.

[30] Y. Koide, T. Tude, K. Ushigusa, N. Asakura, A. Sakasai, S. Ide, S. Ishida, M. Kikuchi, M. Azumi, A. Funahashi, and JT-60 Team. Spontaneous plasma

rotation of near-perpendicular neutral beam injection and lower hybrid current drive plasmas in JT-60U. In *Plasma Physics and Controlled Nuclear Fusion Research 1992*, volume 1, pages 777–789, Vienna, 1992. International Atomic Energy Agency, International Atomic Energy Agency.

[31] L.-G. Eriksson, E. Righi, and K.-D. Zastrow. Toroidal rotation in ICRF-heated H-modes on JET. *Plasma Physics and Controlled Fusion*, 39:27–42, 1997.

[32] J. E. Rice, M. J. Greenwald, I. H. Hutchinson, E. S. Marmar, Y. Takase, S. M. Wolfe, and F. Bombarda. Observations of central toroidal rotation in ICRF heated Alcator C-Mod plasmas. *Nuclear Fusion*, 38(1):75–85, 1998.

[33] I. H. Hutchinson, R. Boivin, F. Bombarda, P. Bonoli, S. Fairfax, C. Fiore, J. Goetz, S. Golovato, and et al. First results from Alcator-C-MOD. *Physics of Plasmas*, 1(5):1511–1518, 1994.

[34] B. Coppi. Astrophysical and laboratory experiments and theories on high energy plasmas. *Plasma Physics and Controlled Fusion*, 36:B107–B121, 1994.

[35] B. Coppi and N. Sharky. Model for particle transport in high-density plasmas. *Nuclear Fusion*, 21(11):1363–1382, 1981.

[36] B. Coppi and C. Spight. Ion-mixing mode and model for density rise in confined plasmas. *Physical Review Letters*, 41(8):551–554, 1978.

[37] P. T. Bonoli, P. O'Shea, M. Brambilla, S. N. Golovato, A. E. Hubbard, M. Porkolab, Y. Takase, R. L. Boivin, and et al. Electron heating via mode converted ion Bernstein waves in the Alcator C-Mod tokamak. *Physics of Plasmas*, 4(5):1774–1782, May 1997.

[38] F. W. Perkins. Heating Tokamaks via the ion-cyclotron and ion-ion hybrid resonances. *Nuclear Fusion*, 17:1197–1224, 1977.

[39] T. H. Stix and D. G. Swanson. Propagation and mode-conversion for waves in nonuniform plasmas. In A. A. Galeev and R. N. Sudan, editors, *Basic Plasma*

Physics I, volume 1 of *Handbook of Plasma Physics*, Section 2.4, pages 335–366. North-Holland, Amsterdam, 1983.

[40] E. F. Jaeger, M. D. Carter, L. A. Berry, D. B. Batchelor, C. B. Forest, and H. Weitzner. Co-counter asymmetry in fast wave heating and current drive. *Nuclear Fusion*, 38(1):1–12, 1998.